Aus dem Deutschen Zentrum für Neurodegenerative Erkrankungen München
und dem Adolf-Butenandt-Institut
(im Biomedizinischen Centrum München, BMC)

Lehrstuhl: Stoffwechselbiochemie
Vorstand: Prof. Dr. rer. nat. Dr. h.c. Christian Haass

# Generation and Functional Analysis of ALS associated HNRNPA Zebrafish Mutants

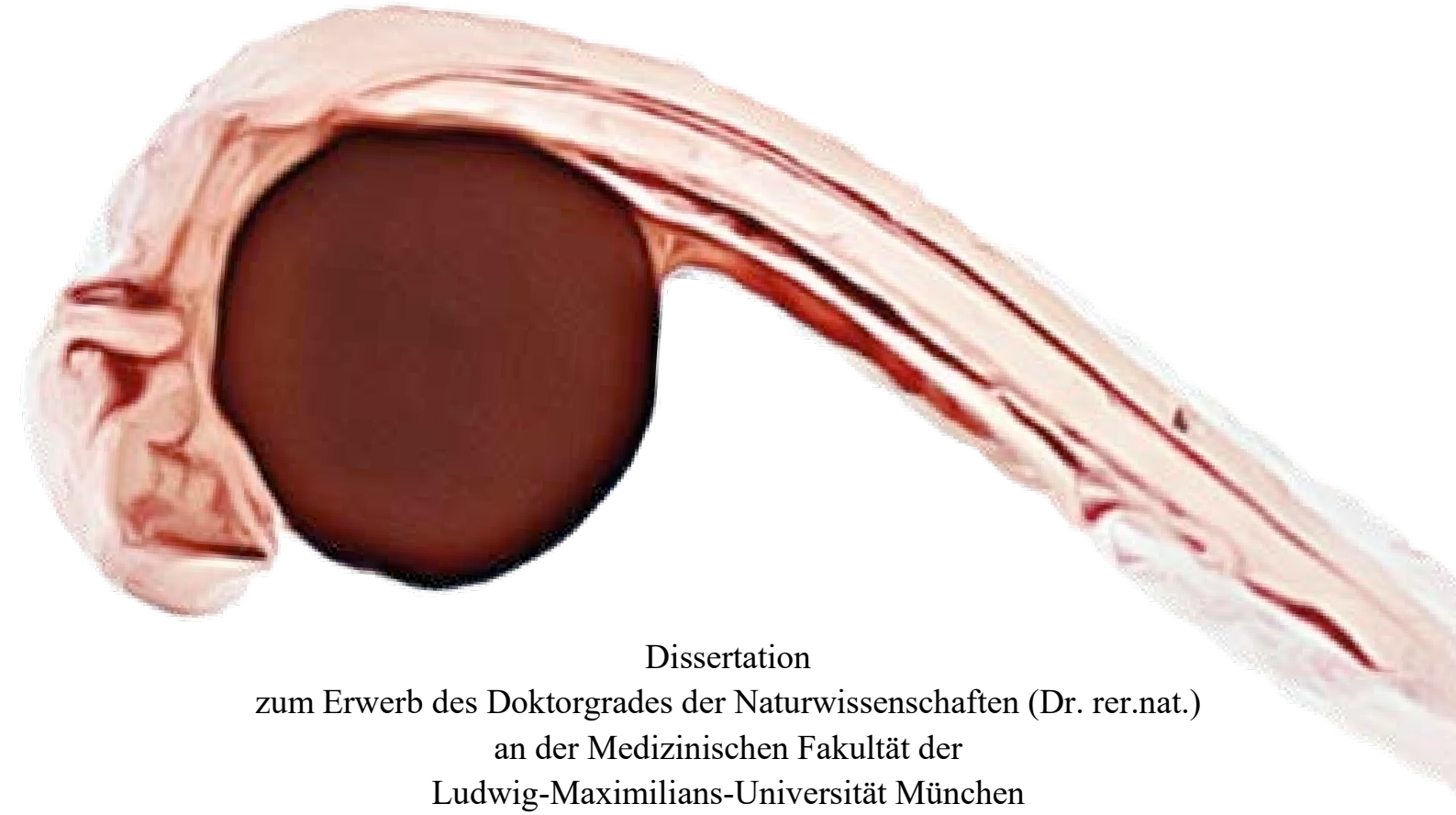

Dissertation
zum Erwerb des Doktorgrades der Naturwissenschaften (Dr. rer.nat.)
an der Medizinischen Fakultät der
Ludwig-Maximilians-Universität München

Vorgelegt von
Lara Jansen
aus Austin/Texas

2019

Gedruckt mit Genehmigung der Medizinischen Fakultät
der Ludwig-Maximilians-Universität München

| | |
|---|---|
| Betreuer: | Prof. Dr. rer. nat. Dr. h.c. Christian Haass |
| Zweitgutachter: | Prof. Dr. Jürgen Bernhagen |
| Dekan: | Prof. Dr. med. dent. Reinhard Hickel |
| Tag der mündlichen Prüfung: | 21.11.2019 |

# Eidesstattliche Versicherung

München, den 12.12.2019

Ich, Lara Jansen, erkläre hiermit an Eides statt, dass ich die vorliegende Dissertation mit dem Titel

**Generation and Functional Analysis of the ALS associated HNRNPA Zebrafish Mutants**

selbstständig verfasst, mich außer der angegebenen keiner weiteren Hilfsmittel bedient und alle Erkenntnisse, die aus dem Schrifttum ganz oder annähernd übernommen sind, als solche kenntlich gemacht und nach ihrer Herkunft unter Bezeichnung der Fundstelle einzeln nachgewiesen habe.

Ich erkläre des Weiteren, dass die hier vorgelegte Dissertation nicht in gleicher oder ähnlicher Form bei einer anderen Stelle zur Erlangung eines akademischen Grades eingereicht wurde.

Lara Jansen
München, den 12.12.2019

*And those who were seen dancing were thought to be insane*
*by those who could not hear the music*

– F. Nietzsche

# Abstract

The neurodegenerative disease amyotrophic lateral sclerosis (ALS) is clinically characterized by the progressive loss of upper and lower motoneurons and pathologically by the presence of Tar DNA-binding protein of 43 kDa (TDP-43) positive aggregates. The cause of this fatal and rapidly progressing disease, for which effective treatments are lacking, remains still unknown. Increasing evidence points to altered RNA metabolism as a potential pathomechanism due to the high percentage of RNA binding proteins (RBP) encoded by disease causing genes and their aggregation in ALS patients. Mutations in the RBPs *Heterogeneous nuclear ribonucleoproteins A1* (*HNRNPA1)* and *HNRNPA2B1* were identified in ALS and Multisystem proteinopathy (MSP) patients. Another member of the HNRNPA family, HNRNPA3, was also linked to ALS due to its ability to bind *Chromosome 9 open reading frame 72* (*C9ORF72)* repeats, and its localization to p62 positive TDP-43 negative C9ORF72 inclusions. The structural similarity of HNRNPA proteins to TDP-43, their ability to bind one another, and the presence of TDP-43 aggregates in *HNRNPA1* and *HNRNPA2* mutation carriers, suggest common pathomechanisms of these proteins. To unravel the physiological function of HNRNPA1, HNRNA2B1, and HNRNPA3, and their association to ALS, this study aims to establish zebrafish loss of function mutants lacking the orthologues of the corresponding genes. Genetic analysis revealed that due to the teleost specific genome duplication zebrafish possess two *HNRNPA1* orthologues named *hnrnpa1a* and *hnrnpa1b*, but no *HNRNPA2B1* orthologue. In this thesis *hnrnpa1a*, *hnrnpa1b*, and *hnrnpa3* zebrafish mutants were generated and characterized, and compared to the *tardbp*$^{-/-}$*; tardbpl*$^{-/-}$ mutant, which lacks the zebrafish TDP-43 orthologues.

While single *hnrnpa1a, hnrnpa1b, and hnrnpa3* knockout (KO) zebrafish are viable and fertile, double *hnrnpa1a* and *hnrnpa1b* KO mutants are embryonically lethal. Moreover, the double mutants are developmentally delayed, have shortened motoneuron axons, muscle defects, show vascular mispatterning with reduced or absent blood flow, have a thinned yolk extension and increased neutral lipid uptake from the yolk. Some of these phenotypic alterations, such as shortened motoneurons and degenerated muscles, are also present in *tardbp*$^{-/-}$*; tardbpl*$^{-/-}$ mutants and are presumably a general phenomena preceeding the embryonic lethality. The impaired intersomitic vessels observed in both mutants show distinct characteristics, since *hnrnpa1a*$^{-/-}$*; hnrnpa1b*$^{-/-}$ mutants only develop dorsal lateral lamellopodia, diverting from their physiological migration path and misconnect, whereas *tardbp*$^{-/-}$*; tardbpl*$^{-/-}$ mutants additionally have ectopic endothelial sprouts from the dorsal aorta.

RNA sequencing of *hnrnpa1a*$^{-/-}$*; hnrnpa1b*$^{-/-}$ embryos revealed *apolipoprotein (apoda.1)* as one of the top downregulated genes. APOD is a lipid transporter and was previously shown to be

neuroprotective. Upon knockdown of *apoda.1* in wildtype embryos we could mimic the lipid phenotype observed in *hnrnpa1a*$^{-/-}$*; hnrnpa1b*$^{-/-}$ mutants. This finding points to a direct link between HNRNPA1 loss of function and downregulation of APOD. We hypothesize that HNRNPA1 ALS patients lack the neuroprotective upregulation of APOD, which contributes to disease progression and neurodegeneration.

# Zusammenfassung

Die neurodegenerative Erkrankung Amyotrophe Lateralsklerose (ALS) ist klinisch durch den Verlust der oberen und unteren Motorneuronen und pathologisch durch die Präsenz von Tar DNA-binding protein of 43 kDa (TDP-43) positiven Aggregaten gekennzeichnet. Die Ursache dieser unheilbaren und schnell fortschreitenden Krankheit ist bisher nicht bekannt. Mehrere Forschungsergebnisse, wie zum Beispiel der große Anteil an aggregierenden RNA bindenden Proteinen (RBPs) und Mutationen in den entsprechenden Genen als Krankheitsursache in ALS Patienten, deuten darauf hin, dass veränderter RNA Metabolismus eine große Rolle in der Krankheitspathogenese spielt. Mutationen in den RBPs *Heterogeneous nuklear ribonukleoprotein A1 (HNRNPA1)* und *HNRNPA2B1* wurden in Multisystem Proteinopathy (MSP) und ALS Patienten identifiziert. Ein weiteres Mitglied der HNRNPA Protein Familie, HNRNPA3, wurde zudem mit ALS assoziiert, da es an *Chromosome 9 open reading frame 72 (C9ORF72)* Wiederholungssequenzen bindet und mit p62 positiven TDP-43 negativen C9ORF72 Aggregaten kolokalisiert. Die strukturelle Ähnlichkeit der HNRNPA Proteine zu TDP-43, deren direkte Interaktion miteinander, sowie TDP-43 Aggregate in HNRNPA1 Patienten, suggerieren gemeinsame Pathomechanismen dieser Proteine.

Zur Studie der physiologischen Funktion von HNRNPA1, HNRNPA2B1 und HNRNPA3, und deren Beitrag zu ALS, wurden Zebrafischmutanten generiert, in welcher die jeweiligen orthologen Gene defekt sind. Die genetische Analyse ergab, dass durch die Teleost spezifische Genomduplikation im Zebrafish zwei *HNRNPA1* Orthologe existieren: *hnrnpa1a* und *hnrnpa1b,* jedoch kein HNRNPA2B1 Ortholog. Diese Dissertation widmet sich der Erstellung und Charakterisierung der *hnrnpa1a, hnrnpa1b* und *hnrnpa3* Mutanten, sowie deren Gegenüberstellung mit der *tardbp*$^{-/-}$*; tardbpl*$^{-/-}$ Mutante, in welcher die Zebrafisch TDP-43 Orthologe defekt sind.

Während die Einzelmutanten von *hnrnpa1a, hnrnpa1b,* und *hnrnpa3* keine Auffälligkeiten zeigen, ist die Doppelmutante von *hnrnpa1a* und *hnrnpa1b* embryonal letal. Die Doppelmutante ist zudem entwicklungsverzögert, hat kürzere Motoneurone und degenerierte Muskeln, fehlentwickelte Gefäße mit stark verminderter oder fehlender Durchblutung, sowie eine dünnere Dottersackverlängerung und erhöhte Aufnahme von neutralen Lipiden aus dem Dottersack. Einige dieser phenotypischen Veränderungen, wie zum Beispiel die verkürzten Motoneurone und degenerierten Muskeln, sind auch in *tardbp*$^{-/-}$*; tardbpl*$^{-/-}$ Mutanten präsent. Allerdings, kann man davon ausgehen, dass diese Veränderungen eine unspezifische Folge des sterbenden Embryos darstellen. Die in beiden Mutanten beobachtete Fehlbildung der Gefäße unterscheidet sich zudem, da *hnrnpa1a*$^{-/-}$*; hnrnpa1b*$^{-/-}$ Mutanten laterale Lamellopodien dorsal

ausbilden, welche ihren physiologischen Migrationsweg verlassen und fehlerhafte Verbindungen bilden, wohingegen zusätzliche ektopische Endothelzellprozesse aus der dorsalen Aorta charakteristisch für *tardbp*$^{-/-}$*; tardbpl*$^{-/-}$ Mutanten sind.

RNA Sequenzierung der *hnrnpa1a*$^{-/-}$*; hnrnpa1b*$^{-/-}$ Doppelmutante identifizierte *apolipoprotein (apoda.1)* als eines der Gene, dessen Expression am meisten reduziert ist. APOD ist ein Lipidtransporter und besitzt neuroprotektive Eigenschaften zu besitzen. *apoda.1* knockdown in Wildtyp-Embryonen führte zu dem gleichen Lipidphenotyp, welcher in *hnrnpa1a*$^{-/-}$*; hnrnpa1b*$^{-/-}$ Mutanten beobachtet wurde. Diese Erkenntnis stellt eine direkte Verbindung zwischen HNRNPA1 Funktionsverlust und reduzierter APOD Expression dar. Wir nehmen an, dass HNRNPA1 ALS Patienten die neuroprotektiv wirkende vermehrte Expression von APOD fehlt, was zur Krankheitheitsenticklung und Neurodegeneration beisteuert.

# Table of contents

# 1 Introduction

According to a report by the United Nations in 2015, the world's population age increased so drastically that the number of people aged 60 and over is predicted to more than double in the next 35 years [1]. This aging society is accompanied by an increased number of people suffering from neurodegenerative diseases, as aging represents the main risk factor for neurodegeneration. While Alzheimer's disease (AD) is the most prevalent neurodegenerative disease, Parkinson's disease (PD), Huntington's disease (HD), prion disorders, tauopathies, Amyotrophic lateral sclerosis (ALS) and frontotemporal lobar dementia (FTLD) are also becoming more common [2]. Interestingly, in all these neurodegenerative diseases a subset of neurons becomes particularly susceptible to neurodegeneration, and most of them share the presence of distinct proteins aggregates [3] [4].

Thanks to enormous progress in the past years in identifying genetic variants, which modify or cause various diseases, exon sequencing and genome-wide association studies (GWAS) led to the discovery of thousands of phenotype-associated loci. Although several pathways, such as protein degradation or RNA metabolism could be associated with neurodegenerative diseases, little is known about the involved proteins' role in disease and their physiological functions. Investigating the disease genes' physiological functions and the impact of patient-associated mutations in cell culture and animal models will help us to better understand the pathomechanisms in the future.

Although many advances were made in the field, effective therapies are currently lacking, and drug development remains slow as clinicians and researchers are still challenged by the diversity of potential underlying disease mechanisms and overlapping clinical symptoms of different neurodegenerative diseases. While only 10% of the cases are familial, also in sporadic cases susceptibility genes are occasionally affected. In addition, there is evidence that not only single gene mutations cause neurodegeneration, but that environmental risk factors can also play a role in disease development [5]. Risk factor genes and environmental factors can for example act on a local level by affecting cell adhesion or neurotransmission; or influence the broader system by altering, for example, inflammation or metabolism [6] [7]. New approaches aim to specify patient subgroups and to identify the pathological mechanisms that are upstream and causative for pathology and clinical symptoms. Thereby individually tailored therapeutics depending on the underlying genetic causes and aggregated disease proteins may be established [8]. The identification of disease-related genes' function

and their involvement in disease mechanisms allows for successful implementation of this goal.

## 1.1 Aim of the project

The aim of this PhD thesis is to characterize the functions and downstream targets of the ALS-associated proteins Heterogeneous nuclear ribonucleoprotein (HNRNP) HNRNPA1 and HNRNPA2B1 and HNRNPA3 *in vivo*. Mutations in HNRNPA1 and HNRNPA2B1 were found to be causative for ALS. Moreover, these two proteins mislocalize to the cytoplasm in muscle biopsies of Multisystem proteinopathy (MSP) patients and colocalize with the main ALS-associated protein Tar DNA-binding protein of 43 kDa (TDP-43) [9]. HNRNPA3 is linked to ALS due to its ability to bind *Chromosome 9 open reading frame 72* (*C9ORF72)* repeats, the most common genetic cause of ALS, and the identification of HNRNPA3 pathology in ALS patients with *C9ORF72* repeat expansions [10] [11]. It is not clear yet whether the mutations and/or the mislocalization of these predominantly nuclear proteins to the cytoplasm resemble a gain or loss of function, or both. By generating loss of function zebrafish of the HNRNPA1 orthologues *hnrnpa1a* and *hnrnpa1b,* and the HNRNPA3 orthologue *hnrnpa3*, I aim to generate an animal model that mimics the potential HNRNPA1, HNRNPA2B1 or HNRNPA3 loss of function scenario in ALS.

First, general tools were established, such as zebrafish Hnrnpa1a, Hnrnpa1b, and Hnrnpa3 specific antibodies, to provide the basis for this study. Next, I generate single *hnrnpa1a*, *hnrnpa1b*, and *hnrnpa3* knockout (KO) zebrafish by genome editing, using the Clustered regularly interspaced short palindromic repeats (CRISPR)/CRISPR-associated (Cas)9/Cas9 system. As these genes are highly similar in sequence and overlapping functions for the respective proteins were described, I incross the single KO to generate double or triple loss of function mutants. Zebrafish Hnrnpa1a, Hnrnpa1b, and Hnrnpa3 specific antibodies will demonstrate if the mutants are full loss of function alleles. After successful generation of these lines, I analyze them for phenotypical, biochemical and molecular alterations. My focus will be to thoroughly describe the obtained phenotype, analyze molecular changes, and correlate these findings with previously established Hnrnpa animal models. HNRNPA and TDP-43 are both members of the HNRNP protein family, are involved in ALS, and are structurally and functionally very similar. For successful comparison of molecular changes associated with Hnrnpa1a, Hnrnpa1b, Hnrnpa3 or TDP-43 loss of function in zebrafish, RNA sequencing is performed on the corresponding KO mutants. By determining the similarities between the Hnrnpa1 KO zebrafish and the previously generated Tdp-43 loss of function

zebrafish I aim to identify disease related commonalities [12]. These might be ultimately used to design novel treatment options.

## 1.2 Amyotrophic lateral sclerosis

ALS, also known as Lou Gehrig disease, is an adult-onset neurodegenerative disease, which is characterized by the loss of upper (UMN) and lower motoneurons (LMN). The name derives from both the degeneration of corticospinal motoneurons, of which the descending axons in the lateral spinal cord are scarred (lateral sclerosis), and the loss of spinal motoneurons with secondary denervation and muscle wasting (amyotrophy) [13]. With an incidence varying from 0.3 to 2.5 cases per 100.000 people per year, ALS represents the most frequent motoneuron disease (MND) [14].

### 1.2.1 ALS and closely associated diseases

Neurodegenerative diseases are often characterized by the aggregation of proteins. This feature also helps to differentiate among other diseases, which is hardly possible according to clinical symptoms. Besides clinically pure forms of ALS, patients are often diagnosed with additional symptoms and there is significant clinical and pathological overlap to other disease entities. With advancing genome sequencing, clinical and pathological examination of ALS and other diseases it became clear, that ALS patients most frequently show additional features of FTLD and MSP.

#### 1.2.1.1 Frontotemporal lobar degeneration

Historically, ALS and FTLD were thought two represent two distinct neurodegenerative disorders. With the discovery of common clinical, genetic, and pathological characteristics ALS and FTLD are now considered to be two extreme ends of a disease spectrum [15, 16]. FLTD describes a heterogenous group of diseases, which all primarily affect the frontal and temporal lobes of the brain, but are divers on a clinical, pathological, and genetic level. There are three major associated disorders including semantic dementia (SD), progressive non-fluent aphasia (PNFA), and behavioral variant frontotemporal dementia (bvFTD), which is the most frequent variant accounting for 50% of FTLD patients. FTLD represents the second most common dementia after AD in patients under 65 years of age and has an incidence of 3.5-4.1 per 100.000 people per year [17]. Next to FTLD related clinical features, neurological imaging obtained from magnetic resonance imaging (MRI), computed tomography (CT), and

positron-emission tomography (PET) allows FTLD diagnosis[18]. FTLD is characterized by behavioral changes such as neuropsychological, speech, and language deficits typical of frontotemporal dysfunction, and neuropathologically by deposits of mostly TDP-43 or Tau [19]. In few cases other proteins aggregate in FTLD patients leading to the establishment of FTLD subtypes according to the main deposited protein. Patients with Tau positive inclusions are referred to as FTLD-TAU, which make up 45% of all FTLD cases. Tau pathology negative cases include FTLD-TDP patients (45%), who show TDP-43 positive inclusions, and FTLD-FUS patients (9%) with Fused in Sarcoma (FUS) positive inclusions. Approximately 1% of FTLD cases show inclusions for proteins of the ubiquitin-proteasome pathway, lacking TDP-43, FUS, or Tau pathology and are referred to as FTLD-UPS [20]. Patients with *C9ORF72* mutations show apart from TDP-43 inclusions also aggregation of dipeptide repeat proteins (DPR) proteins [21] [22]. As TDP-43, DPRs, and FUS aggregates are likewise found in ALS cases, ALS and FTLD were pathologically connected [20]. This connection is further supported by the patients' symptom overlap, as around 14% of ALS patients exhibit FTLD like symptoms and 30-50% of FTLD patients suffer from ALS associated movement disorders. Symptomatic subclasses reflecting ALS or FLTD or mixed forms were defined, such as ALS with cognitive and behavioral impairment (ALS-Ci/Bi), FTLD-MND for FTLD with motoneuron dysfunction, and ALS-FTLD for patients with similar portions of ALS or FLT related symptoms [23] [24] [25] [26]. The genetic overlap of ALS and FTLD is further supported by genetic studies, which revealed diseases causing mutations in the same genes, such as TDP-43 and FUS. The ultimate link is provided by *C9ORF72* mutations, which cause ALS, FTLD, or ALS-FTLD in a similar frequent manner [21] [22]. Despite overlapping characteristics regarding ALS and FTLD genetics and pathology, some disease mutations and proteins exist that can be uniquely assigned to one of the diseases. Mutations in the *microtubule-associated protein tau* (*MAPT*) encoding the microtubule-associated protein Tau result in FTLD characterized by Tau positive aggregates, while mutations in *SOD1* encoding the copper/zinc superoxide dismutase 1 are associated with pure ALS [29].

#### 1.2.1.2 Multisystem proteinopathy

MSP is an inherited pleiotropic degenerative disorder that affects multiple tissues and organs, such as the muscle, bone, or the nervous system. The phenotype is highly variable and shares symptoms with inclusion body myopathy (IBM), FTLD, ALS or Paget's disease of bone (PDB). Clinically, MSP is defined to include the diagnosis of at least two of the diseases IBM, PDB, and ALS/FTLD [30]. GWAS studies have for the first time linked ALS/FTLD to

MSP by the identification of Valosin-containing-protein (*VCP)* mutations in MSP and ALS patients [31] [32] [33]. Additionally, mutations in *p62* were described for patients suffering from PDB, ALS, or FTLD providing another gene that links these diseases together [34]. Recently, rare mutations in *HNRNPA1* and *HNRNPA2B1* were identified in MSP families, which are also present in sporadic (sALS) and familial (fALS) cases of ALS. Postmortem tissues obtained from MSP patients show ubiquitin-positive inclusions that contain RBPs, such as TDP-43, HNRNPA1, or HNRNPA2B1 [35] [36]. Additionally, aggregates of proteins involved in ubiquitin-dependent autophagy, including P62/SQSTM1, VCP, OPTINEURIN, and UBIQUILIN-2 were found in these patients [37]. These findings support the involvement of disturbed RNA metabolism and autophagy as key contributors to pathogenesis related to HNRNPA1 or HNRNPA2B1 mutations.

The common genetic mutations together with the overlapping clinical symptoms, and aggregated proteins among the disease spectra point to shared molecular mechanisms in ALS, FTLD and MSP. The phenomenon of ALS and its overlap to other diseases raises fundamental questions for seemingly distinct diseases, but also presents important opportunities for developing therapeutics for a broad spectrum of degenerative diseases.

### 1.2.2 ALS clinical classification

ALS belongs to the group of MNDs. Apart from ALS this category comprises several other diseases all sharing the characteristic of sequential degeneration of LMNs or UPMs. In contrast to ALS, in Primary lateral sclerosis (PLS) and Pseudobulbar palsy only UMN are affected, whereas Progressive muscular atrophy (PMA) and Progressive bulbar palsy (PBP) result only in LMN loss. ALS is a heterogeneous disease from a clinical point of view and subsets of the disease are classified by the degeneration of different sets of motoneurons and impairment of different body regions [38]. Most of the patients' (approximately 70%) disease starts as degeneration of UMNs and LMNs in the limbs, resulting in limb muscle weakness and locomotion deficits. Around 25% of the patients present bulbar onset including UMNs and LMNs dysfunction of cranial nerve nuclei, causing in dysarthria and dysphagia. The remaining 5% of the patients show initial trunk or respiratory dysfunction [39]. Although, the clinical presentation and the disease course of ALS vary among patients, the mean onset is at 55 years of age and the symptoms progressively spread to other parts of the body ultimately resulting in dysfunction of all voluntary muscle control. At late disease stage wasting of

respiratory muscles leads to patients death approximately three years after symptom onset due to respiratory failure [40].

In order to diagnose a disease as ALS the *El Escorial World Federation of Neurology Criteria of the Diagnosis of Amyotrophic Lateral Sclerosis* developed standard criteria that have to be fullfilled [41]. The core of these criteria are the degeneration of LMN and UMN and the exclusion of other underlying diseases [42] [43]. The involvement of LMN is depicted by increasing muscle atrophy, muscle failing or muscle twitching (fasciculations) caused by spontaneous discharges of motor neurons. Fasciculations are often initially present at hand muscles, but electromyography (EMG) analysis is indispensable for final diagnosis. Signs of UMN degeneration are spasticity and degeneration in the motor cortex, which can be assessed by MRI and PET. Exclusion of other diseases via electrophysiology and cognitive testing leads to final ALS diagnosis [44].

After the first description of ALS in 1869 by Jean Martin Charcot, nowadays there is still no cure for ALS and the majority of patients are treated with the FDA approved drug Riluzole (Rilutek, Sanofi-Aventis) or by symptomatic orientated therapy. Riluzol is a sodium channel blocker lowering glutamate effects and acts as a neuroprotector by decreasing glutamate mediated excitotoxicity. Upon Riluzole treatment the disease course of ALS is slightly modified and achieves only a modest improvement in survival of 3-6 months [45].

#### 1.2.2.1 Molecular pathology and genetics in ALS

Over the past years ALS research lead to better understanding of disease mechanism by characterization of protein inclusions and the identification of their key components. While ubiquitin immunoreactive inclusions are found in all ALS cases [46, 47], pathological subtypes were established according to the major aggregating protein. TDP-43, which is found in inclusions in 97% of ALS, represents the most abundant aggregated protein (ALS-TDP), while SOD-1 inclusion pathology is only seen in approximately 2% of ALS cases (ALS-SOD1). Approximately 1% of ALS cases (ALS-FUS) show inclusions of FUS protein [48] [19] (reviewed in [49]).

Genetic studies further contributed to identify mutations in several genes that cause ALS. fALS is inherited by a dominant trait with high penetrance, while the remaining 90% are sALS patients who do not show a family history. Even though a high number of ALS genes was identified, understanding the precise mechanisms causing the disease remains a challenge.

The first genetic mutations, which were found to cause ALS, were identified in the *SOD1* gene in 1993 and account for about 12-20% of fALS cases and 1-2% of sALS cases [50]. *SOD1* mutations cause pure ALS with SOD1 and ubiquitin aggregates, devoid of TDP-43 and FUS inclusions [51] [52]. The discovery of mutations in *TARDBP* (which encodes TDP-43) in autosomal dominant ALS and FTLD families identified the pathological hallmark of FTLD and ALS and make up to ~4% of fALS cases, which show TDP-43 positive inclusions [19]. FUS mutations account for 4% of fALS and 1% of sALS cases, which show FUS positive inclusions [53].

As protein aggregates are the major hallmark of ALS pathology, defects in protein homeostasis were early suggested as a potential pathomechanism. Indeed, many mutations that cause ALS are involved in the protein degradation pathway. These mutations are thought to lead to a loss of function resulting in impaired protein degradation, which ultimately leads to pathological protein aggregates. Examples are mutations in the genes *Sequestosome* (*SQSTM1), Optineurin (OPTN)*, *Ubiquilin* (*UBQLN2*), *Valosin-containing protein* (*VCP)* and *Cyclin-F* (*CCNF) [54] [55] [56] [31] [57]*. All these ALS cases share a common pathology characterized by inclusions of ubiquitinated proteins and TDP-43 aggregates.

With the recent discovery of a *GGGGCC* ($G_4C_2$) hexanucleotide repeat expansion in the noncoding region of the *C9ORF72* the most common genetic cause of ALS could be identified being responsible for 40%-50% of fALS cases and 8%-10% of sALS cases [21] [22]. While healthy individuals have 2 to 30 repeats, the repeat number expands to hundreds and thousands in C9ORF72 patients (C9-ALS) [58] [59]. C9ORF72 protein has been proposed to be a DENN (differentially expressed in normal and neoplastic cells) protein with a guanine exchange factor function for small GTPases based on sequence homology. Moreover, recent studies suggested a function for C9ORF72 in autophagy and stress granule (SG) formation [60] [61] [62] [63]. Loss of C9ORF72 function was early suggested as an underlying pathomechanism. While the repeat expansion suppresses the production of C9ORF72 protein by inhibiting transcription, several disease models could not identify a direct correlation between reduced C9ORF72 levels and neurodegeneration [21] [22], e.g. C9ORF72 deficient mice do not display neurodegenerative phenotypes [64] [65]. Moreover, no study could so far identify a pathway that links C9ORF72 activity to neuronal survival. Apart from C9ORF72 loss of function in ALS, two other disease mechanisms are under debate to cause C9-ALS. First, the repeat expansion generates DPRs that arise from non-ATG translation (RAN translation). Hereby all possible reading frames of the sense and anti-sense strand are translated giving rise to five different DPRs: GA, GR, GP, PR and PA [66] [67]

[68] [62]. The accumulation of transcripts with the long repeat sequence in RNA foci suggests toxic RNA gain-of-function pathomechanisms as these RNA foci are suggested to disrupt RNA metabolism and sequester RBPs. This is supported by the finding that RBPs, with the biggest group being HNRNPs including HNRNPA1, HNRNPA2/B1 and HNRNPA3, bind to $G_4C_2$ repeats and are sequestered in RNA foci in the spinal cord of ALS/FTLD patients, resulting in their cellular depletion and perturbed cellular RNA metabolism [21] [69] [70] [71]. Second, the DPR proteins are found in protein deposits, which are p62 positive and TDP-43 negative [62] [72] and are to different extents neurotoxic (reviewed in [73]). Poly GA aggregates, for example were found to recruit 26S proteasome complexes, providing a link of C9ORF72 repeats and protein aggregation due to an impaired proteasome function [72]. Additionally, in all C9-ALS cases pathological aggregation of TDP-43 can be found in the cortex and cerebellum [74]. So far only HNRNPA3 was identified to be contained in some p62 positive TDP-43 negative C9ORF72 specific inclusions [67]. Further evidence for a relationship between HNRNPA3 and C9ORF72 comes from *in vitro* studies. These showed that knockdown (KD) of HNRNPA3 in cell culture and primary fibroblasts from C9-ALS patients lead to DPR accumulation and an increase of repeat RNA foci [11]. Most likely all the C9 associated pathomechanisms are not mutually exclusive.

#### 1.2.2.2 The role of RBPs in ALS

Apart from mutations in TDP-43 and FUS, mutations in other RBPs were identified, including TATA box-binding protein associated factor 15 (TAF15) [75], Ewing sarcoma breakpoint region 1 (EWSR1) [76], Matrin-3 (MATR3) [77], HNRNPA1, HNRNPA2B1 [9], and T-cell intracytoplasmic antigen (TIA1) [78]. In most of the cases these mutations cause aggregates of the respective protein in ALS patients' brains. Motoneurons are the main affected cells in ALS and with their axons reaching lengths up to 1m they are dependent on transport of mRNAs along the cytoskeleton and local translation. Moreover, due to their non-dividing nature they are dependent on tight mRNA homeostasis regulation [79]. These features make motoneurons especially vulnerable to dysfunctional RNA metabolism and potentially link the selective motoneuron degeneration observed in ALS to mutated and aggregated RBPs.

1.2.2.2.1 TDP-43

TDP-43 is able to shuttle between the nucleus and the cytoplasm and has a variety of important functions in RNA metabolism ranging from transcription regulation, splicing, to microRNA (miRNA) processing [80]. TDP-43 was found to bind thousands of mRNAs by which it regulates their splicing and RNA stability suggesting potential impact on RNA metabolism on a broad scale [81] [82]. Additionally, TDP-43 regulates its own transcript levels through an autoregulatory feedback loop by binding to its own 3' UTR [81] [83] [84]. Cytoplasmic mislocalized TDP-43 as observed in ALS, is heavily post-translationally modified via cleavage, phosphorylation, acetylation, and ubiquitination, and forms granular pathology that assembles to large inclusions [85]. These pathogenic variants are mostly located in the C-terminus of the protein, which allows ribonucleoprotein binding and is involved in splicing. At the C-terminus a prion like domain (PrLD) is present, which is enriched in uncharged polar amino acids and drives protein aggregation. The nuclear clearance of TDP-43 and its accumulation into aggregates suggests that loss of nuclear TDP-43 function may lead to deleterious abnormal RNA metabolism [86]. Alternatively, toxic gain of function from increased normal TDP-43 activity or from a novel toxic cytoplasmic function may be culprit [87].

1.2.2.2.2 TIA1

TIA1 is structurally very similar to TDP-43 and HNRNPAs. Under normal conditions TIA1 is predominantly localized in the nucleus and functions in RNA metabolism including RNA splicing, and mRNA silencing [88]. Upon stress TIA1 translocates to the cytoplasm, where it suppresses RNA translation and functions in SG formation through self-association of its PrLD [89] [90]. Mutations in TIA1 were recently found in ALS patients, whereby all the mutations are found in the PrLD domain and cause impaired SG disassembly and promote accumulation of non-dynamic SGs that sequester TDP-43 [91] [92]. Patients with TIA1 mutations do also show TDP-43 positive cytoplasmic inclusions in the CNS, however no aberrant accumulation was reported for TIA1 [93].

1.2.2.2.3 FET proteins

Based on their similar structure - a zinc finger domain, a RNA recognition motif (RRM), and a N-terminal low complexity PrLD - **F**US, **E**WSR1, and **T**AF15 proteins are grouped together and termed FET family [94]. The FUS protein is also a member of the HNRNP protein family

(sometimes referred to as HNRNP P2) and mutations in FUS are therefore hypothesized to lead to neuronal death via disturbed RNA metabolism. The majority of FUS mutations cluster at the C-terminus of the protein in the PY-NLS domain [95] and these mutations are thought to impair transport mediated nuclear import leading to redistribution of FUS to the cytosol [96] [97] where it accumulates together with other FET proteins in SG as a cellular stress response [98]. Eventually, accumulated FUS transitions to stable inclusions, which represent the pathological hallmark in patients [95]. As FUS acts as a transcriptional regulator and controls RNA splicing of many genes, nuclear loss of function due to redistribution may lead to impaired RNA metabolism and detrimental effects in neurons. Due to the high similarity of its genomic sequence and protein structure to the previously identified FUS gene in ALS, EWSR1 was considered as a potential disease gene, of which two mutations were subsequently identified in sALS cases [78]. Moreover, mutations in sALS and fALS associated mutations were identified in TAF15, which functions in DNA repair, alternative splicing, transcription and RNA transport [75].

1.2.2.2.4 HNRNPA proteins

The latest discovery of mutations in RBPs was in 2013 in two other members of the HNRNP family – HNRNPA1 and HNRNPA2B1. Three *HNRNPA1* mutations were linked to ALS (D262N; P288S) or MSP (D262V). Only one mutation in *HNRNPA2B1* (D290V) was reported in a family with MSP, which is surprisingly homologue to the ALS associated HNRNPA1$^{D262V}$ mutation [9] [99]. Mutations in *HNRNPA1* and *HNRNPA2B1* show an autosomal dominant mode of inheritance in fALS and account for <1% of fALS and sALS cases, while they are also associated with the broader disease spectrum MSP [100]. The underlying disease mechanism connecting *HNRNPA1* or *HNRNPA2B1* mutations to neurodegeneration is not clear yet, but loss of function by mislocalization and/or aggregation or gain of function due to toxic aggregates or a combination of both was suggested. A loss of function mechanism was suggested by a group, which reported increased aggregation and localization of mutant HNRNPA2B1 to SGs in a cell-based system [101]. Evidence for only partial loss of function is supported by a study from Martinez et al., which revealed that the HNRNPA2B1$^{D290V}$ mutation is not equivalent to loss of HNRNPA2B1 protein in regard to alternative splicing changes [102].

Evidence for a functional link between HNRNPA1 or HNRNPA2B1 and the main ALS associated protein TDP-43 comes from a study showing that the expression of HNRNPA1 and HNRNPA2/B1 is altered in patients with FTLD-TDP, suggesting that perturbations in

RNA metabolism are not exclusively driven by TDP-43 loss of function [103]. Moreover, a direct interaction between HNRNPA1 and UBQLN1 was determined, which is dependent on the HNRNPA1 PrLD domain and reduced by HNRNPA1$^{D262V}$ mutations [104]. Lastly, HNRNPA1 and HNRNPA2 were linked to the ALS gene *VCP* as they were identified as VCP-associated phenotype suppressors when knocked down in a Drosophila *VCP* mutant model [105].

The majority of the so far identified mutations in HNRNPA1 and HNRNPA2/B1 are localized in the PrLD. Under physiological conditions these HNRNPs were shown to self-aggregate and this behavior is increased by the disease-causing mutations. The mutated HNRNPA1 and HNRNPA2B1 form self-seeding fibrils that can recruit wildtype protein, which suggests prion-like properties [9]. RNA binding to HNRNPA1 further enhances fibrillization and formation of protein-rich droplets suggesting that HNRNPA1 interacts with RNA to mediate phase transition and that mutations promote fibrillization and alter the dynamics of membraneless organelles ultimately leading to SG formation [106]. An exception to these mutations is the P288S mutation, which was identified in a Chinese family with "Flail arm ALS", an atypical ALS subtype with severe wasting and weakness of the arms without significant functional involvement of other regions [107]. The mutation localizes to the PY-domain at the C-terminus of the protein [99]. It can be concluded that HNRNPA1 and HNRNPA2/B1 were clearly linked to ALS, while their genetic mutation frequency is low [108].

Disease causing mutations in the TDP-43, FUS, HNRNPA1, HNRNPA2B1, EWSR1, TAF15 and TIA1 suggest that disturbed biology of RBPs plays a central role in ALS pathology (reviewed in [109]). The RBPs TDP-43, FUS, HNRNPA1, HNRNPA2B1, MATR3, and TIA1 in particular share common features. They are ubiquitously expressed and contain multiple RNA binding domains and a PrLD, which makes them aggregation prone. The majority of disease causing mutations is localized in the PrLD and impacts the domain's aggregation potential inducing liquid-liquid phase transition and leading to altered SG kinetics [110]. By phase separation the local protein concentration is quickly increased, which causes recruitment of other proteins, and promotes their interaction within the SG. This process is very dynamic and can return into resting state quickly. Interestingly, disease-causing mutations clustered in the PrLDs of TDP-43, FUS, HNRNPA1, and HNRNPA2B1 enhance the prion like state of the protein, which promotes assembly into SG under stressors. During this process the prion domains form an abnormally strong interaction, which persists

after stress relieve [111] [112] [113]. This leads to persistent sequestration of mRNA and impedes their translation [114]. Interestingly, increased formation of aggregates by liquid-liquid phase transition was also observed by elevated protein concentrations due to cytoplasmic mislocalization linking nuclear loss of function and prion like behavior of the ALS associated proteins [115] [111].

In conclusion, under physiological conditions the RBPs are found in RNA granules in the nucleus, but they mislocalize to the cytoplasm in disease state where they form inclusions [116] [117]. Due to their common nature and their similar behavior in disease state, researchers suggested a common pathogenic mechanism for these proteins in ALS, which causes loss or gain of function or a combination of both (reviewed in [109] [118].

## 1.3 HNRNP proteins

HNRNP proteins are nuclear proteins that bind to nascent transcripts produced by RNA polymerase II and are mostly associated in RNA-protein complexes [119]. Historically,

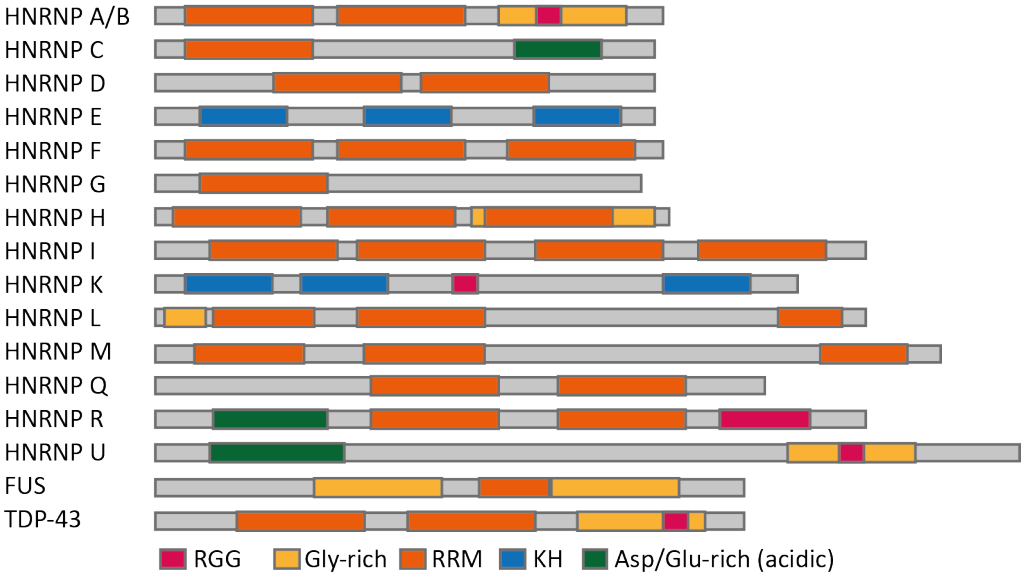


**Figure 1.1 - Schematic illustration of the HNRNP family.** Except of hnRNP E, K and U all members possess one or more RRM domains, which are involved for RNA/ssDNA binding. Glycine rich domains, which are found in HNRNPA/B, HNRNP H, HNRNP L, HNRNP U, FUS and TDP-43 and are highly aggregation prone. (Adapted from [120])

HNRNP proteins were grouped according to their RNA binding domains (RBD) composition [119]. The first list of HNRNPs was ultimately generated by co-immunopurification with monoclonal antibodies against HNRNPC, followed by two-dimensional gel electrophoresis, generating a group of 20 proteins that were named HNRNPs A-U (see Figure 1.1) [121]. Apart from various structural differences, all HNRNPs contain RBDs, many contain RGG boxes, consisting of repeats of Arg-Gly-Gly tripeptides, and most HNRNPs contain auxiliary

domains, such as proline-, glycine- or acid-rich domains [119] [122]. HNRNPs participate in many steps of nucleic acid processing, such as telomere maintenance, chromatin remodeling and DNA repair. Overall, HNRNPs can have overlapping functions, but some also have very specialized roles that are dependent on specific RNA-protein or protein-protein interactions [120]. As their function highly depends on their cellular localization, mechanisms that regulate their nucleo-cytoplasmic shuttling are of extreme importance [123].

### 1.3.1 Physiological function of HNRNPA proteins

The HNRNPA/B subfamily consists of the proteins HNRNPA0, HNRNPA1, HNRNPA2B1 and HNRNPA3. HNRNPA1, HNRNPA2B1, and HNRNPA3 (all three together are herein referred to as HNRNPA) proteins contain two N-terminal RRMs followed by a C-terminal Gly-rich domain (see Figure 1.1) [124] [125]. The RRM allows HNRNPA proteins to interact with single stranded nucleic acids, including RNA and single stranded DNA (ssDNA) to regulate transcription and splicing [126]. The RGG domain has a distinctive amino acid (aa) composition and allows protein-protein interactions. HNRNPA/Bs are present in molar excess over their high affinity binding targets and have multiple roles in RNA processes such as alternative pre-mRNA splicing, nuclear import, cytoplasmic trafficking of mRNA, mRNA stability and turnover, and translation [120]. They package nascent transcript in a non-sequence specific manner, but have also distinct preferences for RNA sequences [119] [127, 119]. HNRNPA1 and HNRNPA2/B1 have been well characterized as splicing repressors and promote distal splice site selection to regulate splicing of many mRNAs [128]. Like many other HNRNP proteins, HNRNPA proteins are predominantly located in the nucleus at steady-state but can shuttle between the nucleus and cytoplasm, which is controlled by the M9 nuclear localization signal near the Gly-rich domain [129] [130]. Most studies have investigated the functions of HNRNPA1 and HNRNPA2/B1, while less is known about HNRNPA3. HNRNPA1 is one of the most abundant nuclear proteins and two gene variants generated by alternative splicing were so far experimentally validated: A1-B, which represents the full-length isoform and encodes a protein of 372 aa, and A1-A, the shorter variant, translates into a protein that lacks exon 8 resulting in a 320 aa protein. The shorter isoform was found to be 20-fold more abundant than the full-length transcript [120]. HNRNPA1 is able to negatively modulate its own pre-mRNA alternative splicing by inhibiting splicing of intron 10 [131]. It also has a role in stress response as it was shown to accumulate in cytoplasmic SG, in stress-activated cell, and is required for recovery from stress [132] [133].

HNRNPA2B1 is present in two distinct isoforms, A2 (341 aa) and B1 (353aa), which are both transcribed from the *HNRNPA2B1* gene. Apart from its shared functions with HNRNPA1 and HNRNPA3 in RNA metabolism, HNRNPA2B1 has a role in trafficking mRNAs to neuronal dendrites, where HNRNPA2/B1 recognizes a 21-nucleotide A2 response element (A2RE) in target transcripts [134] [135]. HNRNPA3 and HNRNPA2/B1, but not HNRNPA1 act as mRNA trafficking trans-acting factors in neurons [136]. All three HNRNPAs bind to single stranded telomere DNA and telomerase RNA, and interact with telomere-binding factors, which suggests that they regulate access to telomeres to protect telomeres from degradation and thereby maintain genome stability [137] [138] [139] [140].

### 1.3.2 Clinical significance of HNRNPAs

Given their central role in gene expression and their multiple functions, it is not surprising that HNRNPAs were associated with a variety of diseases apart from ALS or MSP, such as cancer, Multiple Sclerosis (MS) [141] [141], and AD [142]. Sporadic AD (sAD) patients for example show a reduced expression of HNRNPA1 and HNRNPA2B1 in the entorhinal cortex and in an AD mouse model loss of HNRNPA1 or HNRNPA2B1 was associated with reduced cognitive function [143]. Additionally, HNRNPA1 was discovered to modulate alternative splicing of the APP gene, promoting the generation of toxic amyloid beta peptide, which is the core protein of amyloid plaques in AD brains [144].
HNRNPAs were associated with cancer as they show aberrant expression in certain cancer types, e.g. HNRNPA1 expression is highly increased in lung cancer samples and is associated with tumor proliferation [145] [146]. Moreover, several oncogenes were identified as direct targets of HNRNPA1 [147]. Also HNRNPA2B1 was associated with cancer, as its KD in breast cancer cells induces apoptosis [148]. This data links HNRNPA mutations and protein levels to multiple diseases and hence implies a strong connection between HNRNPA homeostasis, neurological dysfunction, and cell proliferation.

### 1.3.3 The interaction of HNRNPAs and TDP-43 in health and disease state

TDP-43 and HNRNPA proteins belong to the large and complex HNRNP protein family and were both associated with ALS. While it is not yet understood how misfunction of these proteins causes the same disease, several lines of evidence point to cross-regulation among these proteins and suggest common disease pathways. The most striking finding is the similarity in structure of HNRNPAs and TDP-43 (see Figure 1.1). Buratti et al. could show

that HNRNPA proteins interact directly with TDP-43, and function cooperatively to regulate RNA metabolism. Moreover, an unbiased screen for disease modifiers of VCP-related degeneration in a Drosophila model of MSP identified the fly homologues of TDP-43, HNRNPA1, and HNRNPA2B1, pointing to a common physiological requirement in VCP associated neurodegeneration [149]. Functional interaction between HNRNPA1 and TDP-43 was shown by Deshaies et al., who demonstrated that TDP-43 binds HNRNPA1 pre-mRNA and controls HNRNPA1 splicing. TDP-43 depletion thereby results in a longer *HNRNPA1* isoform, named *HNRNPA1-B,* which includes exon 8 and is hence aggregation-prone and negatively impacts cell survival [150]. The specific interaction between TDP-43 with HNRNPA1 and HNRNPA2B1 is further supported by the finding that pathological aggregation of these proteins was found in a MSP patient with the $HNRNPA1^{D262V}$ mutation, in the absence of FUS pathology. Double staining revealed that muscle tissue with TDP-43 pathology typically also shows HNRNPA1 and HNRNPA2B1 pathology. In most instances the proteins were also colocalizing [101]. This is further evidenced by the finding that TDP-43 redistribution to the cytoplasm and aggregation in spinal motor neurons (SpMN) from ALS patients was accompanied by loss of nuclear HNRNPA1 [151]. Interestingly, the majority of mutations so far identified in HNRNPA1, HNRNPA2B1, and TDP-43 locate within the C-terminal glycine-rich domain that has previously been found to be the site of HNRNP protein interaction [149] [152].
These findings further demonstrate cross-regulation between these ALS/FTLD relevant RBPs and supports the concept of impaired RNA metabolism in ALS/FTLD.

### 1.3.4 The role of HNRNPA1 in the cell cycle

The cell cycle is a highly regulated process, which involves complex feedback mechanisms and regulations of many proteins in order to control chromosome replication. The cell cycle control is highly conserved among eukaryotes [153] and its deregulation results in severe consequences for the cell resulting in hypoproliferation and apoptosis upon cell cycle arrest or in hyperproliferation ultimately leading to tumor formation. The somatic cell cycle is divided into two main phases: S-phase, during which DNA replication takes place and M-phase, during which mitosis occurs. These two main phases are separated by two so-called gap phases ($G_1$ and $G_2$), respectively. Another gap phase is assigned to non-dividing cells, such as neurons, known as $G_0$. Cells that have entered $G_0$ are terminally differentiated and are not re-entering the cell cycle [154]. The crucial proteins that regulate the cell cycle are the cyclins and their associated cyclin-dependent kinases (CDK), whose expression and activity fluctuate

as the cell transitions from one cell cycle stage to the other [155]. For example, the activation of CyclinD-CDK4/6 complex is triggered by the presence of mitotic growth factors and controls the re-entry of resting cells into the $G_1$ cell cycle phase. In order to transit from $G_1$ to S-phase the CyclinE-CDK2 complex needs to be activated to phosphorylate Retinoblastoma-like 2 (RBL2) upon which it dissociates from the transcription factor E2F2. The freed E2F2 shuttles to the nucleus where it binds promoters that initiate transcription of S-phase genes [156]. The $G_1$/S transition is tightly controlled by the CDK inhibitors p21 and p27, which inactivate the CyclinE-CDK2 and whose accumulation results in $G_1$ arrest. In the presence of CyclinA, the cell divides and progresses to $G_2$, whereas the cell goes down an apoptotic pathway in the absence of CyclinA [157]. Ultimately, the CyclinB-CDK1 complex initiates mitosis (see Figure 1.2).

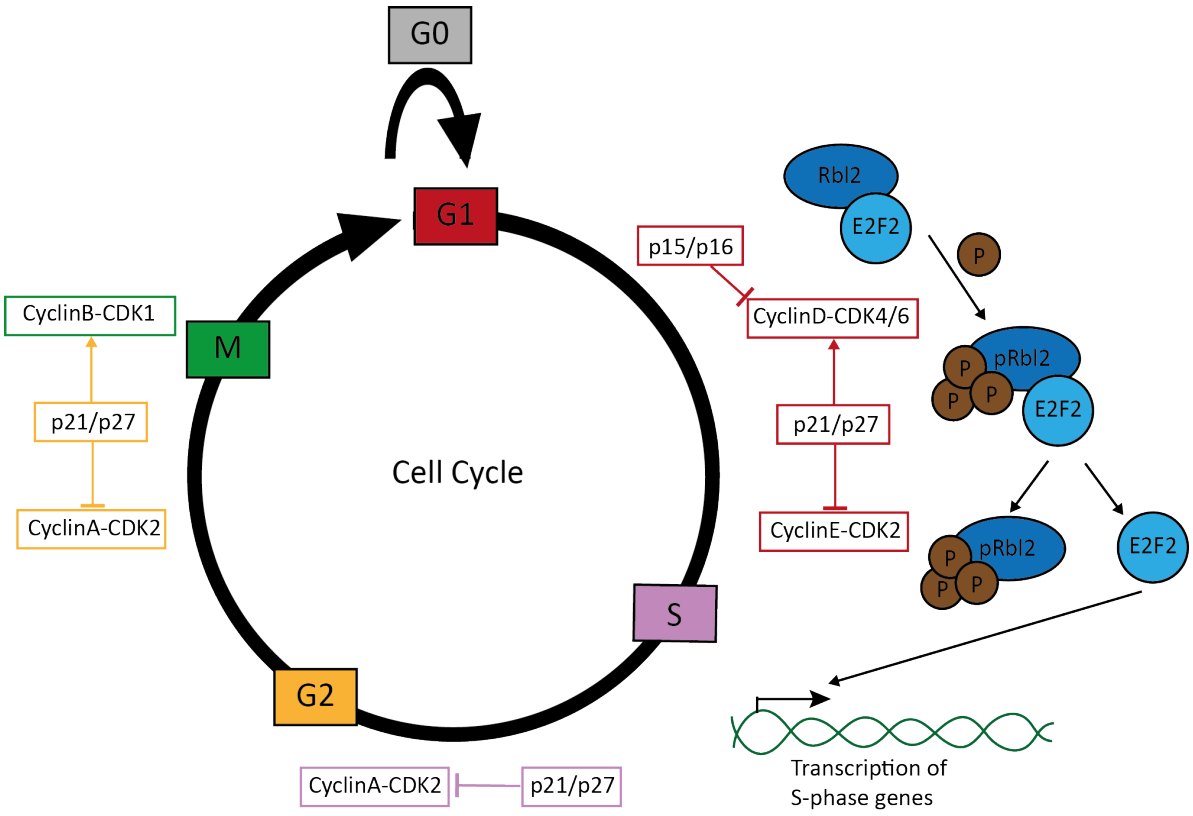


**Figure 1.2 - Schematic illustration of the cell cycle.** For explanation see text.

HNRNPAs are associated with cell cycle abnormalities due to their role in cancer development (see section 1.3.2). It was shown that HNRNPA1 and HNRNPA2B1 but not HNRNPA3 are modulated during cell cycle progression with the most abundant expression of HNRNPA2B1 in $G_1$ and S-phase and a high expression of HNRNPA1 during $G_2$/M phase

transition [120]. Further evidence for a vital role of HNRNPA1 in cell cycle derives from studies demonstrating that KD of HNRNPA1 results in cell cycle arrest [146] [158].
Several pathways are considered to mediate the arrest in cell cycle progression upon HNRNPA1 depletion. HNRNPA1 interacts with telomerase RNA and maintains length of telomeres, which is important for cell cycle progression [159]. Additionally, HNRNPA1 reduction may inactivate the NF-κB pathway, which has been linked to cancer [160].

### 1.3.5 Animal models of HNRNPA1 and HNRNPA2B1

Some animal models of HNRNPA1 were so far generated to better understand the physiological function of HNRNPA1 and to thereby gain insights of molecular pathomechanisms that underlie HNRNPA associated ALS and MSP. The experimental approach and associated phenotypes of these models are summarized in Table 1.1. Drosophila null mutants for the HNRNPA1 orthologues Hrp36 and Hrp38 show slowed development with significant reduction in adult life span, decreased female fecundity, and high sensitivity to starvation [161]. So far no genetic zebrafish model lacking the HNRNPA orthologues was established, but two studies are published using *hnrnpa1b* specific morpholinos (MOs) that lead to phenotypic abnormalities in zebrafish upon *hnrnpa1b* KD [162, 163]. Chang et al. described vascular mispatterning and dorsal axis abnormalities, while Cartealy et al. report small and undeveloped embryos, which lack the midbrain-hindbrain boundary. The zebrafish KD models target only one *hnrnpa1* orthologue and show conflicting results. This might potentially be due to off target effects, which are often seen with MO experiments. Also, so far no double KD or double KO has been generated. The generation of stable genetic loss of HNRNPA1 mutants lacking Hnrnpa1a and Hnrnpa1b will better capitulate full loss of HNRNPA1 *in vivo*. Chang et al. also established a mouse HNRNPA1 KO model by deletion of exon 2-7 with the Cre-loxP system. The majority of the homozygous HNRNPA1 KO mice are embryonically lethal. Further investigation of HNRNPA1 KO mice shows shortened body length, irregular tongue muscles, myofibril hypoplasia, and urinary bladder defects [162]. A mouse KD model for HNRNPA2B1 was published by Martinez et al., which lacks 75% HNRNPA2B1 protein after targeting of the *HNRNPA2B1* transcript with antisense oligo nucleotides (ASO). Subsequent RNA sequencing revealed alterations in alternative splicing, including the skipping of an exon in the ALS-associated D-amino acid oxidase (DAO) that reduces D-serine metabolism [102]. Altogether, the lethality of HNRNPA1 KO mice points to an essential role of HNRNPA1 in embryonic development. This is further supported by the two independent zebrafish studies revealing severe phenotypes upon *hnrnpa1b* KD and

reduction in lifespan of drosophila upon KO of the two HNRNPA1 orthologues. Concluding, the animal models suggest a vital role of HNRNPA1 in embryonic development and so far no stable HNRNPA1 KO zebrafish model has been established.

| **Publication** | **Modification** | **Phenotype** |
|---|---|---|
| Liu et al., 2017 [162] | Zebrafish:<br>ATG MO<br>*hnrnpa1b* KD; 0.15 mM | - abnormal dorsal axis<br>- heart edema<br>- lateral asymmetry<br>- intersegmental vessel defects |
| Cartealy, 2008 [163] | Zebrafish:<br>ATG MO<br>*hnrnpa1b* KD; 3.5, 5, and 7 ng | - I: small and underdeveloped embryos<br>- II: kinked body axis and disorganized somite<br>- III: lack of midbrain-hindbrain boundary |
| Liu et al., 2017 [162] | Mouse:<br>HNRNPA1 KO Cre-loxP deletion of exon 2-7 | - embryonically lethal (62%)<br>- shorter body length<br>- hypoplasia of tongue muscles<br>- dilation of ventricles<br>- urinary bladder defects |
| Martinez et al., 2016 [102] | Mouse:<br>HNRNPA2B1 KD ASOs in lateral ventricles of mice | - alternative splicing changes<br>- skipping of a DAO exon<br>- limited changes in gene expression |
| Singh et al., 2012 [161] | Drosophila:<br>P-element insertion<br>*hrp36* and *hrp38* KO | - delay in development<br>- reduction in life span<br>- decreased female fecundity<br>- high sensitivity to starvation and thermal stress |

**Table 1.1 - Overview of HNRNPA KD and KO animal models**

## 1.4 Zebrafish as a model organism

Starting in the 1930s zebrafish (*Danio rerio*) as a small vertebrate has emerged to a classical developmental and embryological model in biomedical research [164]. The most important breakthrough in the 1980s was the production of clones of homozygous diploid zebrafish, which was the beginning of using this vertebrate model in genetics research [165]. In 2013 sequencing of the zebrafish genome by the UK Sanger Institute was completed revealing

homology of approximately 70% in functionality of human and zebrafish genes [166]. Most importantly, about 80% of risk genes that are associated with human disorders have zebrafish orthologues [167]. These findings validate the approach of modeling human disease pathogenesis in zebrafish.

The rapid development of zebrafish paired with high fecundity giving hundreds of eggs per spawning, promoted the rise of the zebrafish to an attractive research model. A zebrafish embryo completes its gastrulation within ten hours after fertilization and the heart beat starts at the end of one day post fertilization (dpf). Most organs are functionally developed within the first five days of development and zebrafish are fertile within three months. Apart from its advantages shared with invertebrates, such as inexpensive husbandry and the possibility of high-throughput drug screens, the zebrafish can be used for imaging studies due to the possibility to obtain transparent embryos and larvae by treating them with phenylthiourea (PTU). The existence of several fluorescent reporter lines labeling a specific cell type or subcellular structure via a fluorescent tag makes it possible to perform live imaging experiments and investigate cellular and subcellular processes *in vivo* [168]. Moreover, chemical screens can be easily performed by adding compounds to the water. Hereby, compounds of clinical relevance can be identified and their potential toxicity and teratogenicity can be determined [169]. The external development and thereby easy accessibility of the embryos allows minimally invasive manipulations, such as targeted mutagenesis and introduction of exogenic DNA or RNA. To date, zebrafish models for a variety of human diseases have been established, including cancer, inflammation, wound healing and regeneration, metabolic disorders, muscle diseases, and neurodegeneration (reviewed in [170]).

Taken together, zebrafish have emerged to a great model system for studying vertebrate development, to examine the effect of mutagenesis, to investigate disease aspects, and to perform high-throughput chemical screens, due to zebrafish' ease of genetic manipulation and its biological features.

### 1.4.1 Genome editing in zebrafish

In the past years a variety of genome editing tools were applied in fish mutagenesis with Zinc-finger nucleases (ZFNs), Transcription activator-like effector nucleases (TALENs) and CRISPR/Cas9 being the most successful ones for gene inactivation [171] [172] [173]. All these approaches share the feature of being nuclease-based genome editing tools as a nuclease is guided to a specific genomic region using different recognition modules where it then

induces a double strand break (DSB). Due to error-prone DNA repair at the site of interest by non-homologous end joining (NHEJ), insertion or deletion (indel) mutations are introduced, which can lead to frameshift mutations generating a KO allele. For knockin (KI) approaches, sequence templates, that carry homology arms and the desired genetic sequence (e.g. a patient mutation) can be co-injected and inserted at the targeted genomic site by the process of homology directed repair (HDR) [174] [175].

As part of the CRISPR system, first a conserved set of genes adjacent to the spacers and repeats, named Cas genes, were identified, which serve as an antiviral defense mechanism in prokaryotes [176] [177] [178, 179]. Later, the last key component in CRISPR activation was identified, a non-coding trans-activating complementary RNA (tracRNA) allowing RNA-guided binding to the nuclease Cas9 by base pairing to mature tracRNA [180]. Following research has further simplified the system for genome editing purposes to a single RNA system (instead of the two RNA system consisting of tracRNA and crRNA by identifying key components and thereby solely used an engineered 20 nucleotide (nt) long single guide RNA (gRNA), for sequence specific DSB by Cas9 [181]. The only sequence requirement for the gRNA target site is a three nucleotide NGG motif (for the *Streptococcus pyogenes* Cas9 (SpCas9) protein), called protospacer adjacent motif (PAM) adjacent to the 20 nt target sequence (see Figure 1.3) [182]. The CRISPR/Cas9 system is a highly effective genome editing system, which differs from previous genome editing approaches since it uses an RNA entity to bind to the DNA. By specificity of the Watson and Crick base pairing the gRNA specifically directs the most widely used SpCas9 nuclease to the targeted genetic locus where it induces a DSB.

The most common technique used in zebrafish for genome editing is microinjection of the Cas9 protein and a gRNA into the embryonic cell at the one cell stage. Upon injection into zebrafish embryos Cas9 and the gRNA form a complex with the targeted DNA site and Cas9 protein induces a DSB at the targeted genomic site. In the past years generating specific KOs by NHEJ or KIs by HDR were successfully carried out in zebrafish (see section 1.4.2 for ALS related examples). Due to the ease of programmability of the gRNAs and the low workload, the CRISPR/Cas9 system is the most preferable genome editing system. Many websites give additional support for the design of sgRNAs with minimized off-target effects and closely located restriction endonuclease (RE) for easy analysis of successful genome editing. Suitable design websites include CHOPCHOP (www.chopchop.cbu.uib.no/), CRISPR Multitargeter (www.multicrispr.net/), and CRISPRdirect (www.crispr.dbcls.jp). The concern of a high probability of off target effects has been often raised due to the short target sequence.

However, the zebrafish model allows to eliminate unspecific side effects caused by off-target genomic modifications by outcrossing the mutated fish.

In conclusion, the use of CRISPR/Cas9 in zebrafish allows fast, cheap, and high throughput genotype-phenotype correlations for candidate genes obtained from clinical genetics.

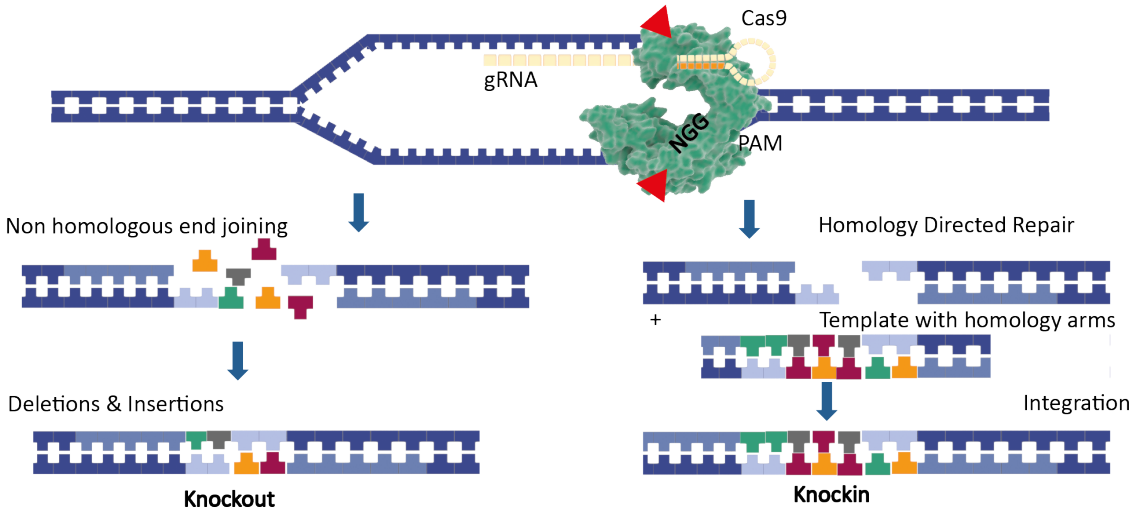


**Figure 1.3 - Schematic illustration of the CRISPR/Cas9 system.** The Cas9 nuclease (green) is recruited to the genomic site via binding to a 20 nt long target sequence containing gRNA (yellow) next to the PAM. The red arrowheads indicate the approximate position of the induced double strand break. Upon creation of a DSB at the targeted site the site can be either repaired through NHEJ sometimes producing indel mutations leading to frame-shift and loss of function mutants. Alternatively the double strand break can be repaired by HDR. For precise KI approaches sequence templates with homology arms can be co-injected and inserted at the targeted genomic site by the process of HDR.

### 1.4.2 Modeling ALS in zebrafish

Apart from the intensive research on ALS associated genes over the past years and the great advances in characterizing the pathological signature of the proteins derived from mutated genes, the physiological function of the encoded proteins remains largely unknown. Up to now a variety of model organisms were used in order to study genetic risk and disease-causing genes *in vivo* by applying three main strategies. First, the gene of interest can be overexpressed in its wildtype or mutated form via RNA or DNA expression. However, this approach is highly critical due to the associated toxicity effects that may arise from abnormally high expression of proteins and protein mislocalization by ubiquitous expression of a protein that is normally only present in specific cellular compartments or cell types. Alternatively, the gene of interest can be transiently knocked down using MOs or stably knocked out using targeted mutagenesis (see section 1.4.1) in order to create a loss of function situation and hence determine the encoded protein's physiological function. Lastly, the gene

of interest can be edited in such a way that it carries a specific patient mutation, to address the function of the encoded mutant protein in *vivo*.

So far several studies have been performed in zebrafish that specifically address ALS associated genes and aim to recapitulate hallmarks of ALS. An overexpression (OE) model of SOD1 protein shows ALS like phenotypes, such as motoneuron loss, muscle atrophy, paralysis, and premature death [183]. A targeted induced local lesions in genomes (TILLING) zebrafish mutant expressing mutant Sod1 (T70I) protein at physiological levels, confirmed this finding, as it also showed key features of ALS: early neuromuscular junction (NMJ) phenotype, susceptibility to oxidative stress (OS), and an adult-onset MND phenotype [184]. In contrast to SOD1, many ALS associated genetic KD and KO models were established over the past years that lead to non-identical phenotypes upon KD or KO of the same gene. For example, KD of zebrafish Fus resulted in a motor phenotype that could be rescued by OE of wildtype human *FUS* but not with *FUS* carrying ALS-related mutations [185]. However, KO of Fus using ZFN mediated genome editing did not cause shortened motoneuron axons or related pathology [186]. KO of the two *TARDBP* orthologues *tarbp* and *tardbpl* in zebrafish by CRISPR/Cas9 resulted in lethality and embryos show shortened motoneurons, vascular mispatterning, and muscle defects [12]. While single *tardbp* or *tardbpl* KO zebrafish show no phenotypic abnormalities [12], MO-mediated KD of zebrafish *tardbp* only performed by another group, was shown to result in shortened SpMN axons [187]. Injection of wildtype and mutant *TDP-43* mRNA into zebrafish embryos elicits similar motoneuron effects, with mutant *TDP-43* causing more severe phenotypes [188]. A mutant zebrafish model carrying three ALS patient mutations (M337V, G348C, G290A) in the *tardbp* gene was recently generated in our laboratory. The zebrafish embryos are vital and elicit no motoneuron defects contrasting the severe phenotype observed in $tardbp^{-/-}$; $tardbpl^{-/-}$ KO mutants. These preliminary results suggest that TDP-43 patient mutations do not cause a full Tdp-43 loss of function in zebrafish (personal communication, Özge Burhan and A. Hruscha and A. Gierson). Also, C9orf72 deficient zebrafish were generated using CRISPR/Cas9 system. The C9orf72 KO embryos show no difference in axon outgrowth length, but swimming behavior analysis revealed a higher locomotor activity upon darkness induced stimulation indicating a physiological requirement of C9orf72 for neuronal function [189] and (personal communication A.Hruscha). Another study established a Granulin (GRN) loss of function model in zebrafish by knocking out the zebrafish *GRN* orthologues *grna* and *grnb* using ZFNs. These fish contrast the phenotype of a previously MO induced *grna* and *grnb* KD embryos that shows SpMN axonopathies and a reduced number of myogenic progenitor cells

number. The phenotype discrepancy may probably be caused by unspecific toxicity of MOs [190] [191].

Overall, many zebrafish models for ALS associated genes were generated, including OE, KO, KD, and KI models. However, as described, transient KD or OE studies often display distinct phenotypes from persistent KO of the same gene. These discrepancies may arise from unspecific toxicity, due to off-target effects or global degradation machinery breakdown upon MO KD [192]. Rossi et al. revealed by KD or KO of two different genes that compensatory network are activated to buffer against deleterious mutations upon KO, but not KD. If this is the case in the ALS models, KD versus KO discrepancies remain to be resolved. Potentially, these discrepancies can also be eliminated by correct experiment design and using proper controls. Stanier et al have written a manual for MO usage that illustrates recommended guidelines for MO usage [193].

# 2 Material and Methods

## 2.1 Material

### 2.1.1 Zebrafish lines

The following zebrafish lines were used in this study:

| Zebrafish line | Origin (Reference) |
|---|---|
| wildtype-line AB | G. Streisinger, Institute of Neuroscience, University of Oregon, Eugene, USA |
| wildtype-line TLF | C. Nüsslein-Vollhard, MPI for Developmental Biology, Tübingen, Germany |
| $Tardbp^{mde159-/-}$ (tardbp-/- in this thesis) | B. Schmid & Hruscha, DZNE and LMU Munich, Germany [12] |
| $Tardbpl^{mde222-/-}$ (tardbpl-/- in this thesis) | B. Schmid & Hruscha, DZNE and LMU Munich, Germany [12] |
| $Tg(fli1a:EGFP)^{y1}Tg$ | J. Bussmann, MPI for Molecular Biomedicine, Münster, Germany [194] |

### 2.1.2 Cell lines

| Cell line | Origin |
|---|---|
| HeLa cells | DSMZ, #ACC 57 |

### 2.1.3 Morpholinos

MOs were purchased from GeneTools. Sequences are given in 5'-3' orientation; e: exon; i: intron.

| | |
|---|---|
| apoda.1-e2i2 | TCCATTGACTTGGTACTCACAGAAT |

### 2.1.4 Vectors and plasmids

| Vector | Insert | Origin | Schmid laboratory database # |
|---|---|---|---|
| pCS2+GW-GFP | Apoda.1 | L.Jansen | N31 |

| | | | |
|---|---|---|---|
| pcr8/GW/TOPO | - | Invitrogen | - |
| pCS2+GW-GFP | HNRNPA1 | L. Jansen | N32 |
| pCS2+GW-GFP | HNRNPA1$^{D262V}$ | L. Jansen | N33 |
| pCS2+ hnrnpa1a | hnrnpa1a | L. Jansen | N34 |
| pCS2+ hnrnpa1+HA | HA+hnrnpa1a | L. Jansen | N35 |
| pCS2+hnrnpa1b | Hnrnpa1b | L. Jansen | N36 |
| pCS2+hnrnpa1b+HA | HA+hnrnpa1b | L. Jansen | N37 |
| pCS2+ hnrnpa3 | hnrnpa3 | L. Jansen | N38 |
| pCS2+ hnrnpa3+HA | HA+hnrnpa3 | L. Jansen | N39 |

### 2.1.5 Oligonucleotides

Oligonucleotides were synthesized by Thermo Scientific. The sequences are shown in 5'-3' orientation. The abbreviation letters and numbers in the oligonucleotide name refer to the Schmid laboratory database.

**Primer for cloning**

| | |
|---|---|
| LJ-A01 hnrnpa1b F | GTCGGTAGGATGTCCAAAGAG |
| LJ-A02 hnrnpa1b STOP R | TTAAAACCGTCTACCGCCAGAG |
| LJ-A03 HA+hnrnpa1b F | TACCCATACGATGTTCCAGATTACGCTGCT GGTAGGATGTCCAAAG |
| LJ-A04 hnrnpa1b noStop R | GCTCTGGCGGTAGACGGTTT |
| LJ-A05 hnrnpa1a F | CGTGACCGCCATGTCCAAAG |
| LJ-A06 hnrnpa1a STOP R | ATCTAAAACCTCCGTCCGCC |
| LJ-A07 HA+hnrnpa1a F | ATGTACCCATACGATGTTCCAGATTACGC TGTGACCGCCATGTCCAAAGA |
| LJ-A08 hnrnpa1a noStop R | GCTCTGGCGGACGGAGGTTT |
| LJ-A09 hnrnpa3 F | GCGCAAAAGCTACAGCATGG |
| LJ-A10 hnrnpa3 STOP R | ACTTACCACTCCAATTAATCTGCT |
| LJ-A11 HA+hnrnpa3 F | ATGTACCCATACGATGTTCCAGATTACGC TCGCAAAAGCTACAGCATGGA |
| LJ-A12 hnrnpa3 noStop R | GTTACGGCTCCAGGAGATAT |
| LJ-A13 apoda.1 F | ATGAAGGTGTTTCTGGTCGTG |
| LJ-A14 apoda.1 R | TCAAAGTTTTTGGTCGCATC |

**Primer for Sequencing**

| | |
|---|---|
| GATC M13-FP | TGTAAAACGACGGCCAGT |
| GATC M13-RP | CAGGAAACAGCTATGACC |
| GATC SP6 | ATTTAGGTGACACTATAGAA |
| GATC T7 | TAATACGACTCACTATAG |

**Primer for Genotyping**

| | |
|---|---|
| LJ-B01 hnrnpa1b.ex2.KO.F – gRNA 1 | CCTTGGTTTGATCTCCGTTACC |
| LJ-B02 hnrnpa1b.ex2.KO.R – gRNA 1 | TGTGTTTGGATCTTTCATCACCT |
| LJ-B03 hnrnpa1b.ex9.KO.F – gRNA 2 | GGCAATGGAAACTTTGGAGGT |
| LJ-B04 hnrnpa1b.ex9.KO.R – gRNA 2 | TCACGTCATTTATGCCTTTAGGA |
| LJ-B05 hnrnpa1a.ex1.KO.F – gRNA 3 | CCTTATTTGGGGGTAAAAACGTA |
| LJ-B06 hnrnpa1a.ex1.KO.R – gRNA 3 | CCTTATTTGGGGGTAAAAACGTA |
| LJ-B07 hnrnpa1a.ex8.KO.F gRNA 4 | GGCGGCGGCTATGATAACT |
| LJ-B08 hnrnpa1a.ex8.KO.R gRNA 4 | GCATTGCTCTGAATAAACCACTACA |
| LJ-B09 hnrnpa3.ex2.F – gRNA 5 | AGCATTATGCAACACATGGAGC |
| LJ-B10 hnrnpa3.ex2.R – gRNA 5 | CACGCAGTCTGTGAGTTTGC |
| LJ-B11 hnrnpa3.Sanger.F | CTGCAACAGGCTTCCATACA |
| LJ-B12 hnrnpa3.Sanger.Wt.R | TCCTCTCTTCTTCCCAGTCG |
| LJ-B13 hnrnpa3.Sanger.Mu.R | TCCTCTCTTCTTCCCAGTCT |

**Primer for semiquantitative polymerase chain reaction (PCR)**

| | |
|---|---|
| LJ-D01 pkma.exon203 F | CGGAGAGACCGCTAAAGGAGAT |
| LJ-D02 pkma.exon203.R | CCGGACCCAGTGAGCACTATAA |
| LJ-D03 pkma.exon202.F | AGTGATGTGGCCAATGCAGTTC |
| LJ-D04 pkma.exon202.R | CAGCATTTGAAGGAAGCCTCGAC |

**Primer for quantitative realtime-PCR (qRT-PCR)**

| | |
|---|---|
| KS-A11 Rpl13a_E3-4a_F | ATTGTGGTGGTGAGGTGTGA |
| KS-A12 Rpl13a_E3-4a_R | CATTCTCTTGCGGAGGAAG |
| KS-A13 Elf1a_2F | AGCAGCAGCTGAGGAGTGAT |
| KS-A14 Elf1a_2R | GTGGTGGACTTTCCGGAGT |
| KS A42 dr-vcam1 ex9-10 F | CAAACGACCTGGGTTACGAA |
| KS A43 dr-vcam1 ex9-10 R | CAGCAGAACCTCCCAAGAAA |

| | |
|---|---|
| KS A45 dr-itga4-ex2-3 F | TGCAGTATGTTGAACAGCCAG |
| KS A46 dr-itga4-ex2-3 R | CAAACTCACACCCAGCCAC |
| KS A47 dr-fn1a-ex3-4 F | TGTACTTGCATTGGCTCTGC |
| KS A48 dr-fn1a-ex3-4 R | GTCTCTGCCATGTGTCTCCA |
| KS A49 dr-fn1b-ex39-40 F | CATTGCCCTTCTGAATAACCA |
| KS A50 dr-fn1b-ex39-40 R | ATGACTGGGCAGGCTAGGTA |
| LJ-C01 hnrnpa1b.F | CCGTGTCTAGAGAGGATTCCAG |
| LJ-C02 hnrnpa1b.R | GTGACGAAGGCAAAGCCTCT |
| LJ-C03 hnrnpa1a.F | AAAGAGCAACAGACCCCTCG |
| LJ-C04 hnrnpa1a.R | TGACGAAGCCAAATCCCCTC |
| LJ-C05 hnrnpa3.F | TGGAGAGTCGCGACAGTAAG |
| LJ-C06 hnrnpa3.R | GAGTCCTCTCTGGAAACGGC |
| LJ-C07 cdkn2a/b-F | CAGCAGCCACCGGAAACATT |
| LJ-C08 cdkn2a/b-R | TCATCACCTGTATAGGCGTTCTTCT |
| LJ-C09 rbl-F | CCGCTTCTACAACCACGTCT |
| LJ-C10 rbl-R | GGAGTTTCAGCCTGCCCATT |
| LJ-C11 cdkn1a-F | TCCCGAAAACACCAGAACGA |
| LJ-C12 cdkn1a-R | TGGTAGAAATCTGTGATGTTGGTCT |
| LJ-C13 gadd45-F | ACTCGGTGATTAAGGCTCTGG |
| LJ-C14 gadd45-R | TCAGGGTCCACATTGAGGGA |
| LJ-C15 ccne-F | ACTTGCAGCTTCAGCACTCT |
| LJ-C16 ccne-R | ACCACTTCAGCCCTGAAACTT |
| LJ-C17 gpnmb-F | ACTTCATTACAGATAAGATTCCACT |
| LJ-C18 gpnmb-R | CCCTCTGACAAAGATGTTTCTG |
| LJ-C19 p53-F | ACTCAGGAAGGTCAGTTGCTG |
| LJ-C20 p53-F | TACGTTTGGTCCCAGTGGTG |
| LJ-C21 apod-F | AAAACAATTGACGGGACGGC |
| LJ-C22 apod-R | GCGTGTAGGGCAAAACATAGG |
| LJ-C23 nampt-F | TCAGCGACAGCTACGACATC |
| LJ-C24 nampt-R | TCCAGGACCTTGAGCACG |

**Primer for gRNA synthesis**

| | |
|---|---|
| M64 | GCGTAATACGACTCACTATAG |

| **gRNA oligo** | |
|---|---|
| *hnrnpa1a* gRNA 3 | ATGGCGGGTGGCATTGCTGC**TGG** |
| *hnrnpa1a* gRNA 4 | GCAGGAAACTTCGGAGGTGG**CGG** |
| *hnrnpa1b* gRNA 1 | CACGTGAGCCAGAGCAGCTG**CGG** |
| *hnrnpa1b* gRNA 2 | GGTGGTGGTGGCGGCAACAG**TGG** |
| *hnrnpa3* gRNA 5 | GAGTCGCGACAGTAAGGAGC**CGG** |

$N_{20}$: targeting oligo, bold letters indicate the PAM motif

### 2.1.6 Bacteria

| **Name** | **Company** |
|---|---|
| One Shot TOP10 Chemically competent *E. coli*, C4040 | Invitrogen |

### 2.1.7 Antibodies

For Western blotting (WB) and whole mount immunofluorescence stainings (IF) the following antibodies were used:

**Primary antibodies:**

| **Antibody (Species)** | **Dilution** | **Origin (Reference)** |
|---|---|---|
| α-Actinin | IHC: 1:100 | Sigma-Aldrich |
| α-tubulin, T6199 (mouse) | WB: 1:10.000 | Sigma-Aldrich |
| Calnexin, SPA-860 (rabbit) | WB: 1:7000 | Stressgen |
| HA (mouse), MMS-101R | WB: 1:200 | Covance |
| HNRNPA1 (rabbit),HA1-CT (VM) AN351 | WB: 1:1000 | Gift from Douglas Black lab |
| Myosin (ZE-BO-1F4) | IHC: 1:1 | Kremmer [195] |
| Pcna (mouse) | WB: 1:1000<br>IHC: 1:100 | Santa Cruz |
| TDP-43 N-term, SAB4200006 (rabbit) | WB: 1:10.000 | Sigma-Aldrich |
| znp-1 (mouse) | 1:100 | DSHB [196] |

**Primary peptide antibodies** generated by the IMI, Helmholtz Center Munich:

| **Antibody (Species)** | **Dilution** | **Epitope** |
|---|---|---|

| | | |
|---|---|---|
| Hnrnpa1b Z1A1-2A7 (rat IgR2a) | WB: 1:1<br>IHC: 1:50 | MSKEGQPREPEQLR |
| Tardbp antibody, 4A12-111 (rat IgR2a) | WB: 1:1<br>IHC: 1:300 | TSTSGTSSSRDQAQTY |
| Tarbpl antibody, 5F5-11 (rat IgR2a) | WB: 1:1 | FERSQYQFPSSHV |
| Tardbpl_tv1 antibody, 16C8-11 (rat IgR2a) | WB: 1:1 | SRQMMDRGRFGGYG |
| Anti-rat (IgG2a), HRP conjugated | WB: 1:10.000 | |

**Secondary antibodies:**

| **Antibody** | **Dilution** | **Origin** |
|---|---|---|
| Alexa Fluor 488 anti-mouse A-11029 | IHC: 1:500 | Invitrogen |
| Alexa Fluor 488 anti-rabbit A-11034 | IHC: 1:10.000 | Invitrogen |
| Alexa Fluor 488 anti-rat A11006 | IHC: 1:10.000 | Invitrogen |
| Anti-mouse-HRP, W4021 | WB: 1:10.000 | Promega |
| Anti-rabbit-HRP, W4011 | WB: 1:10.000 | Promega |

### 2.1.8 Chemicals

#### 2.1.8.1 Chemicals and reagents

| | |
|---|---|
| Acridine Orange, 235474 | Merck |
| Acrylamide / bis solution, 10681.03 | Serva |
| Agarose, 15510-027 | Invitrogen |
| Ammonium persulfate (APS), 9592.2 | Roth |
| Ampicillin, K029.2 | Roth |
| β-Mercaptoethanol, 4227.1 | Roth |
| Boric acid, 100165.1000 | Merck |
| Bromo phenol blue, 18030 | Fluga |
| Calcium chloride (CaCl2), 102382.0500 | Merck |
| Chloroform | RothRoth |

| | |
|---|---|
| Citric acid monohydrate | Sigma-Alrich |
| Collagenase, C9891 | Sigma-Aldrich |
| DanKlorix | Colgate-Palmolive |
| Deoxynucleoside triphosphates (dATP, dCTP, dGTP, dTTP) | Thermo Fisher Scientific |
| Diethylpyrocarbonate (DEPC), D5758 | Sigma-Aldrich |
| Dimethyl sulfoxide (DMSO), 317275 | Merck |
| Disodium hydrogen phosphate ($Na_2HPO_4$), 106580.5000 | Merck |
| Dithiothreitol (DTT) (100mM), Y00147 | Invitrogen |
| 6x DNA loading dye, R0611 | Thermo Fisher Scientific |
| Dry ice | - |
| ECLplus (RPN2132) | Amersham |
| Ethylenediaminetetraactic acid (EDTA), 108418.1000 | Merck |
| 80% Ethanol, UN1170 | CLN |
| Ethanol p.a., 100989.1011 | Merck |
| Fetal bovine serum (FBS), F7524 | Sigma-Aldrich |
| Formamide, F9037 | Sigma-Aldrich |
| Gelatin, 104080.0100 | Merck |
| GelRed, 41003 | Biotium |
| GeneRuler DNA ladder mix, SM0331 | Thermo Fisher Scientific |
| Glycerol p.a., 3783.2 | Roth |
| Glycine p.a., 04943 | Roth |
| 5x GoTaq buffer | Promega |
| GoTaq DNA Polymerase, M830B | Sigma-Aldrich |
| I-Block (T2015) | Thermo Fisher Scientific |
| Isopropanol p.a., 109634.2511 | Invitrogen |
| Liquid nitrogen (liq. $N_2$) | Linde |
| Magnesium chloride ($MgCl_2$), 105833.1000 | Merck |
| Methanol p.a., 106059.2511 | Merck |
| MethaPhor agarose, 50185 | Lonza |
| Methyl cellulose, M0387 | Sigma-Aldrich |
| Milk powder, T145.2 | Roth |
| M-MLV reverse transcriptase, 28025013 | Thermo Fisher Scientific |
| 5x M-MLV reverse transcriptase buffer, 18057018 | Thermo Fisher Scientific |

| | |
|---|---|
| Monopotassium phosphate ($KH_2PO_4$), 104877.1000 | Merck |
| Natrium Chloride | Roth |
| Natriumhydrogencarbonat, S5761 | Sigma-Aldrich |
| Newborn calf serum (NCS), N4762 | Sigma-Aldrich |
| Oil Red O, O1391 | Merck |
| Oligo$(dT)_{12\text{-}18}$ Primer, 18418012 | Thermo Fisher Scientific |
| Opti-MEM, 51985-026 | Gibco |
| Paraformaldehyde (PFA), P6148 | Sigma-Aldrich |
| PCR nucleotide Mix, 11581295001 | Sigma-Aldrich |
| Phenol/chloroform/isoamylalcoohol, A156.1 | Roth |
| Potassium Chloride (KCl), 104936.1000 | Merck |
| Protease Inhibitor (PI) mix, 05056489001 | Roche |
| Pronase, 11459643001 | Roche |
| Proteinase K (PK), 03115852001 | Roche |
| Precision Plus Protein All Blue Standard, 161-0373 | Bio-Rad |
| PTU, P7629 | Sigma-Aldrich |
| Random hexamer primer, S0142 | Thermo Fisher Scientific |
| Random primer mix, S1330S | NEB |
| RiboLock RNase inhibitor (40U/µl), EO0382 | Thermo Fisher Scientific |
| RNAsecure, AM7010 | Thermo Fisher Scientific |
| RNase H, 18021071 | Invitrogen |
| SeeBlu Plu2 pre-stained standard, LC5925 | Invitrogen |
| SOC-Medium, 15544-034 | Invitrogen |
| Sodium chloride (NaCl), 3975.2 | Roth |
| Sodium dodecyl sulfate (SDS), 20765.03 | Serva |
| SP6 Polymerase, EP0131 | Fermentas |
| Spectinomycin, 85555 | Fluka |
| T7 Polymerase, EP0111 | Fermentas |
| Tetramethylethylenediamine (TEMED), 2367.3 | Roth |
| Tricaine, A5040 | Sigma-Aldrich |
| Tris, 08003 | AppliChem |
| Trisodium citrate | Sigma-Aldrich |
| Trizol Reagent, 15596026 | Thermo Fisher Scientific |
| Tropix I-block, T2015 | Applied Biosytems |

| | |
|---|---|
| Turbo DNAse | Thermo Fisher Scientific |
| Tween 20, 822184.0500 | Merck |
| Xylene, 108681.1000 | Merck |

### 2.1.8.2 Solutions and buffer

All solutions and buffers were prepared by using $H_2O$ that was purified and desalted by a Milli-Q system (electric resistance 18.2Ωcm at 25°C).

| | |
|---|---|
| 1-2% agarose | 1%-2% agarose |
| | 1xTBE |
| Acridine Orange stock solution | 3 mg/ml in $dH_2O$ |
| Ampicillin stock | 100 mg/ml dissolved in $dH_2O$ and sterile filtered |
| 10% APS (stock | 10% APS in $dH_2O$ stored at -20°C |
| Bleaching solution | 600 ml tap water, |
| | 280 µl DanKlorix |
| 10x BSA stock | 0.1 g/ml |
| DEPC-$dH_2O$ | 200 µl DEPC per 100ml $dH_2O$ |
| | incubate overnight (o/n) at 37°C and autoclave |
| Deyolking buffer | 55 mM NaCl |
| | 1.8 mM KCl |
| | 1.25 mM NaHCO3 |
| DMEM Glutamax, 61965 | Gibco |
| I-Block | 0.2% Tropix I-Block |
| | 0.1% Tween |
| | in 1xPBS |
| 4x Lämmli sample buffer | 4 ml 20% SDS |
| | 4 ml glycerol |
| | 1 ml β-mercaptoethanol |
| | 1.25 ml 1M Tris, pH 7.6 |
| | 1 pinch bromophenol blue |
| 0.2-1% low melting agarose (LMA) | 1%-2% MethaPhor agarose |
| | 1xTBE |
| Lysis buffer | 10% PK stock in TE, pH 8.0 |

| | |
|---|---|
| 3% methyl cellulose | 3% methyl cellulose in prewarmed $H_2O$ 70°C<br>shake o/n at 4°C and centrifuge until every bubble is gone |
| NCST | 10% NCS stock<br>0.1% Tween in 1xPBS |
| PBS | 0.14 M NaCl<br>10 mM $Na2HPO_4$<br>2.8 mM $KH2PO_4$<br>2.7 mM KCl<br>pH 7.4 |
| 10x PBS | 80 g NaCl<br>17.8 g $Na_2HPO_4x2H_2O$<br>2.4 g $KH_2PO_4$<br>2g KCl<br>add $dH_2O$ up to 1l |
| PBST | 0.1% Tween in 1x PBS |
| PBST milk | 3% milk powder<br>0.1% Tween in 1x PBS |
| 10x PCR buffer | 100 mM Tris, pH8.3<br>500 mM KCl<br>15 mM $MgCl_2$<br>0.1% (w/v) gelatin<br>in $dH_2O$ |
| PCR mix | 60 µl 100mM dATP<br>60 µl 100mM dCTP<br>60 µl 100mM dGTP<br>60 µl 100mM dTTP<br>6 ml 10x PCR buffer<br>36.3 ml $dH_2O$ |
| 4% PFA | 4% PFA in 1x PBS<br>incubate approx. 5min at 80°C until PFA is dissolved<br>cool to 4°C prior to usage or store at -20°C |
| Proteinase K stock | 17 mg/ml Proteinase K in $dH_2O$ |

| | |
|---|---|
| Pronase stock | 30 mg/ml pronase in $dH_2O$ |
| 10x PTU | 0.3 mg/ml in E3 |
| Ringer solution | 55 mM NaCl |
| | 1.8 mM KCl |
| | 1.25 mM NaHCO3 |
| RIPA | 50 mM Tris-HCL, pH 8.0 |
| | 150 mM NaCl |
| | 5 mM EDTA 1% NP-40 |
| | 0.5% Deoxycholat |
| | 0.1% SDS |
| 10x running buffer | 29 g Tris |
| | 144 g glycine |
| | add $dH_2O$ up to 1l |
| | and autoclave |
| SDS running buffer | 0.1% SDS in 1x running buffer |
| Spectinomycin stock | 30 mg/ml dissolved in $dH_2O$ and sterile filtered |
| Stacking gel buffer | 1M Tris, pH6.8 |
| Stripping buffer | 62.5 mM Tris |
| | 2% SDS |
| | 350 µl β-Mercaptoethanol |
| | adjust to pH6.7 |
| 10x TBE | 1080 g Tris |
| | 550 g Boric acid |
| | 400 ml 0.5M EDTA, pH8.0 |
| | add 10l $dH_2O$ |
| TE pH8.0 | 10 mM Tris |
| | 1 mM EDTA |
| | adjust to pH 8.0 and autoclave |
| 10x transfer buffer | 30.3 g Tris |
| | 144 g glycine |
| | add $dH_2O$ up to 1l |
| | adjust to pH8.3 and autoclave |
| 50x tricain | 2 g tricain |
| | 10.5 ml 1M Tris pH9.0 |

| | |
|---|---|
| | Add 500 ml with $dH_2O$ |
| | Adjust to pH 7.0 |
| Wash Buffer | 110 mM NaCl |
| | 3.5 mM KCl |
| | 2.7 mM CaCl2 |
| | 10 mM Tris/Cl |
| | Adjust to pH 8.5 |

#### 2.1.8.3 Media

Bacteria cultivation media was autoclaved before usage to prevent growth of undesired organisms. Sterile filtered antibiotics were added in the indicated concentration to the medium after cooling.

| | |
|---|---|
| Cell culture medium | DMEM |
| | 10% FBS |
| | 1% Penicillin-Streptomycin |
| E3 | 5 mM NaCl |
| | 0.17 mM KCl |
| | 0.33 mM $CaCl_2$ |
| LB-Agar | 1.5% Bacto Agar |
| | 1% Bacto Trypton |
| | 0.5% Yeast extract |
| | 17.25 mM NaCl |
| | in $dH_2O$ |
| | Ampicillin 100 µg/ml or Spectinomycin |
| | 100 µg/ml |
| LB-Medium | 1% Bacto Trypton |
| | 0.5% Yeast |
| | 17.25 mM NaCl |
| | in $dH_2O$ |
| | Ampicillin 100 µg/ml or Spectinomycin |
| | 100 µg/ml |
| Opti-MEM, 51985-026 | Gibco |
| SOC-Medium, 15544-034 | Invitrogen |

### 2.1.9 Kits

| | |
|---|---|
| BC Assay Protein Quantitation Kit, UP40840A | Uptima |
| Gateway LR Clonase II Enzyme Mix, 11791100 | Invitrogen |
| GoTaq DNA Polymerase, M3001 | Promega |
| iQ SYBR Green supermix, 170-8891 | BioRad |
| M-MLV Reverse Transcriptase, 28025-013 | Invitrogen |
| MEGAshortscript T7 Transcription Kit | Ambion |
| mMESSAGE Machine SP6 Kit, AM1340 | Ambion |
| mMESSAGE Machine T7 Kit, AM1344 | Ambion |
| NucleoBond Xtra Midi, 740410 | Macherey-Nagel |
| NucleoSpin Gel and PCR Clean-up, 740609 | Macherey-Nagel |
| NucleoSpin Plasmid, 740588 | Macherey-Nagel |
| pCR8/GW/TOPO TA Cloning Kit | Invitrogen |
| Pierce ECL Plus Western Blotting Substrate, 32132 | Thermo Scientific |
| RNAse-free DNase Set, 79254 | Quiagen |
| RNeasy Mini Kit, 74104 | Quiagen |
| SsoFast Eva Green Supermix, 172-5204 | BioRad |
| TRIzol Plus RNA Purification Kit, 12183555 | Thermo Scientific |

### 2.1.10 Consumables

| | |
|---|---|
| 0.2 ml Strip tubes, AB-0266 | Thermo Fisher Scientific |
| 96-Well PCR Plate, AB-0600 | Thermo Fisher Scientific |
| Blotting Paper, MN 218 B | Macherey-Nagel |
| Borosilicate glass capillaries, 1B100F-4 | World Precision Instruments |
| Centrifuge tubes 15 ml, 50 ml | Sarstedt |
| Combitips Plus 0.5 ml, 5 ml | Eppendorf |
| Cover slip | Thermo Fisher Scientific |
| Hard-Shell 384-Well PCR Plates, HSP-3805 | BioRad |
| Microcentrifuge tubes 1.5 ml, 2.0 ml | Sarstedt |
| Microscope slide | Thermo Fisher Scientific |
| Microscope slide with wells | Thermo Fisher Scientific |
| Multi-well plates (12, 24, 48) | Thermo Fisher Scientific |
| PCR Film, AB-0558 | Thermo Fisher Scientific |

| | |
|---|---|
| Petri dishes (60 mm, 100 mm) | Sarstedt |
| Pipette tips (10 µl, 10 µl long, 200 µl, 1000 µl) | Sarstedt |
| Pipette tips with filter (10 µl, 20 µl, 100 µl, 300 µl, 1000 µl) | Sarstedt |
| Polyvinylidenfluorid (PVDF) Membrane, Immobilon-P, IPVH00010IPVH00010 | Millipore |
| Sterile serological pipettes (5 ml, 10 ml, 25 ml) | Sarstedt |
| Transfer pipettes | Sarstedt |
| X-ray films Super RX, 47410 19236 | Fujifilm |

### 2.1.11 Equipment

| | |
|---|---|
| Accu jet pro | Brand |
| Agarose gel documentation device | Intas |
| Agarose gel systems | Peqlab |
| Benchtop centrifuge Biofuge pico | Heraeus |
| Benchtop cool centrifuge 5427 R | Eppendorf |
| Benchtop cool centrifuge 5430 R | Eppendorf |
| C1000 Thermal Cycler | Bio-Rad |
| Cassette for x-ray film exposure | Radiographic Products |
| Casting stands | Bio-Rad |
| Casting frames | Bio-Rad |
| DMZ-Universal (needle) Puller | Zeitz Instrumente |
| Forceps | Fine Science Tools FST |
| Foam Pads | Bio-Rad |
| Freezer -20°C | Liebherr |
| Freezer -80°C | Heraeus |
| Fridge | Liebherr |
| Incubator 37°C, 55°C | Binder or B. Braun Biotech International |
| Kontes Pellet Pestle, 1.5 ml | Thermo Fisher Scientific |
| Kontes Pellet Pestle Cordless Motor, K749540-0000 | Thermo Fisher Scientific |
| Microwave | Sharp |

| | |
|---|---|
| Microinjector (Femto Jet) | Eppendorf |
| Microinjection molds | Eppendorf |
| Micro scales BP2215 | Sartorius |
| MilliQ academics | Millipore |
| Mini gel holder cassette, 180-3931 | Bio-Rad |
| Mini-PROTEAN Comb, 10-well | Bio-Rad |
| Mini-PROTEAN 3 cell | Bio-Rad |
| Mini-PROTEAN Tetra cell | Bio-Rad |
| Mini trans-blot central core, 170-3812 | Bio-Rad |
| Multipipette plus | Eppendorf |
| NanoDrop | IMPLEN |
| PCR Plate Sealer | Eppendorf |
| PCR Thermocycler, nexus GSX1 | Eppendorf |
| pH Meter | WTW |
| Pipette 2.5 µl, 10 µl, 100 µl, 200 µl, 1000 µl | Eppendorf |
| Plate reader PowerWaveXS | BioTek |
| Rotors (A-2-MTP, Fa-45-48-11, F-35-6-30) | Eppendorf |
| Scales BP3100S | Sartorius |
| Schott bottles | Schott |
| Shaker cold room | Bachofer |
| Shaker RT Duomax 1030 | Heidolph |
| Short plates, 165-3308 | Bio-Rad |
| Spacer plates 1.5 mm 165-3312 | Bio-Rad |
| Stereo Microscope Stemi 2000 | Zeiss |
| Tea nets | - |
| Thermomixer comfort | Eppendorf |
| Thermomixer compact | Eppendorf |
| UV Detectionsystem | Intas |
| Vortexgenie2 | Scientific Industries |
| Waterbath | GFL |

### 2.1.12 Microscopes

| | |
|---|---|
| Cell Observer CSU-X1 Yokogawa Spinning Disc AxioCam MRm | Zeiss |

| | |
|---|---|
| Confocal laser scanning microscope LSM 710 | Zeiss |
| Fluorescence-Stereomicroscope Discovery V8 Aciocam 503 color/ Aciocam 506 mono | Zeiss |
| Stereomicroscope Zeiss Stemi 2000-C | Zeiss |
| Light microscope Axioscope A1 | Zeiss |

### 2.1.13 Hardware and software

| | |
|---|---|
| Adobe Illustrator CS5 | Adobe Systems Software |
| Axiovision 4.0 | Zeiss |
| Bio-Rad CFX Manager 2.0 | Bio-Rad |
| CLC Main Workbench 6 | CLC bio |
| FileMaker Pro | FileMaker |
| GraphPad Prism 7 | GraphPad Software |
| ImageJ/Fiji | NIH, USA |
| LAS 400 Image Reader | GE Healthcare Bio-Sciences AB |
| iMac | Apple |
| Microsoft Office for Mac 2011 | Microsoft |
| ReadCube | Labtiva |
| EndNote | Clarivate Analytics |
| Zen Blue 2011 | Carl Zeiss Microimaging |

## 2.2 Methods

### 2.2.1 Zebrafish specific methods

The following methods were mostly performed according to the Schmid laboratory methods manual.

#### 2.2.1.1 Zebrafish husbandry and handling of embryos

Zebrafish husbandry, breeding, and mating were performed as described by Mullins et al. [197]. Until 5 dpf embryos and larvae were kept in an incubator holding 28.5°C in petri dishes containing E3 medium and no more than 30 embryos/larvae per dish. Zebrafish development stages were assigned as described previously by Kimmel et al. [198]. For *in vivo*

imaging and whole mount immunofluorescence experiments, zebrafish larvae and embryos were treated with 1xPTU before 24 hpf to prevent pigmentation [199].

#### 2.2.1.2 Bleaching of fertilized zebrafish eggs

Bleaching of zebrafish eggs destroys pathogens, which may reside on the outer side of the chorion, to prevent contamination of the fish facility. Bleaching can be performed without harming the embryo in the time frame after epiboly until 1.5 dpf. The fertilized eggs were placed in a tea net and were held in bleaching solution for 5 min followed by a 5 min wash in tap water. This procedure was repeated once and bleaching solution was replaced every four runs. Afterwards the embryos were placed in a petri dish containing E3 medium with 10 µl pronase stock solution, which allows the embryos to hatch from the denatured chorion.

#### 2.2.1.3 Mating of adult zebrafish

In the evening pairs of one female and one male adult zebrafish were transferred from tanks to mating boxes containing dividers to separate males and females overnight. In the following morning dividers were removed in parallel allowing simultaneous spawning of several pairs yielding age matched zebrafish embryos. Eggs were transferred to a petridish containing E3 medium. In the afternoon unfertilized and debris eggs were removed and the fertilized eggs were kept in the incubator at 28.5°C until further analysis or raising.

#### 2.2.1.4 Microinjection into zebrafish eggs

Injection needles were pulled using a needle puller with the program P(A)60. By filling a petri dish with 1.5% agarose in E3 and placing the microinjection molds into the drying agarose, injection dishes with agarose rills were generated. In the morning freshly laid eggs were placed into the agarose rills and were injected at a 1-cell stage with a mix of each 1.5 µl Cas9 protein (0.5 µg/µl) and 1.5 µl gRNA (1-3 µg/µl). Alternatively a plasmid or a MO was injected. The rest of the spawned eggs was placed in a separate petri dish containing E3 medium and served as a control for proper development. DNA and RNA with Cas9 protein were injected into the cell, while RNA only was injected into the yolk. After injection the eggs were kept in the incubator at 28.5°C in E3 medium. In the afternoon the eggs were screened for normal development and unfertilized eggs and debris were removed.

### 2.2.1.5 KD of genes in zebrafish embryos using morpholinos

**Establishment of *apolipoprotein d* (*apoda.1) KD*** A MO targeting the exon 2-intron 2 junction was ordered at GeneTools. 1 mM stocks were prepared by solubilizing the lyophilized solid in sterile $dH_2O$. 10 µl aliquots were prepared and stored at RT for immediate injection or at -20°C for later injections. 1 mM, 0.5 mM or 0.25 mM concentrations were injected into 1-cell stage AB embryos as described in section 2.2.1.4 The MO was designed to block the exon-intron boundary. Thereby three scenarios are possible depending on the sequence: Intron retention, skipping of an exon, or usage of a cryptic splice site resulting in either intron retention or partial intron inclusion. The altered transcripts are in most cases degraded by nonsense-mediated decay. Alternative, the transcripts are transcribed and result in the synthesis of a truncated protein [200]. The injected embryos were observed for phenotypic abnormalities from 1 dpf to 5 dpf and KD efficiency represented by exon exclusion or intron retention was evaluated by PCR. RNA was extracted from a pool of 10 embryos and transcribed into cDNA, which was amplified by *apoda.1* full length spanning primer. The obtained PCR product was separated by gel electrophoresis, bands were excised and DNA was purified, followed by sequencing. Injection of 1 mM led to the greatest KD efficiency, without causing unspecific toxicity, and was thereby chosen for conduction of the following experiments.

### 2.2.1.6 Quantification of rescue capacity of Apoda.1 and KD of Apoda.1 to mimic the Hnrnpa1 loss of function phenotype

1 mM *apoda.1* MO was injected into AB embryos for KD of *apoda.1*. After 30 hpf, the timepoint when *hnrnpa1a*$^{-/-}$; *hnrnpa1b*$^{-/-}$ embryos can be firstly distinguished from their wildtype looking siblings, images were taken using the Axioscope. To address the previously observed lipid phenotype the yolk extension area of injected embryos and their uninjected siblings was measured using Fiji. The average area size was calculated and subjected to statistical analysis.

### 2.2.1.7 Fin biopsies of adult zebrafish

Fin biopsies are taken from adult zebrafish to genotype single fish. Adult zebrafish were individually anesthetized in fish facility water containing 3% tricaine stock solution. After confirming successful anesthetization, which can be tested by touching of the fish gently and confirmation of lack of movement, the fish was placed on a cutting board and a small piece

from the most caudal part of the tail fin was cut and fixed in 100% methanol. Immediately after the zebrafish was transferred into a labeled single box allowing to specifically attribute the fish to its fin until completion of genomic analysis. The fish was observed until full recovery.

#### 2.2.1.8 Fixation and storage of zebrafish samples

For protein analysis or mRNA isolation embryos, larvae and dissected tissue were placed in a microcentrifuge tube and after having removed all liquid they were quickly frozen in liq. $N_2$. Snap frozen samples were stored at -80°C until usage.
For whole-mount immunohistochemistry 30 hpf anesthetized PTU treated and dechorionated embryos were transferred to 4% PFA in microcentrifuge tubes and were fixed o/n at 4°C. The PFA solution was then removed and samples were washed four times for 5 min with PBST at room temperature (RT). For immunofluorescence stainings samples were serially washed for 10 min in increasing concentrations of methanol (25% methanol in PBST, 50% methanol in PBST, 75% methanol in PBST, 100% methanol) followed by two additional washes for 10 min in 100% methanol prior to being stored in 100% methanol at -20°C until usage. Embryos, larvae and fin tissue biopsies for individual genotyping were stored at -20°C in 100% methanol until usage.

#### 2.2.1.9 Lämmli lysis of zebrafish samples

For protein isolation from embryos or zebrafish brains, shock frozen samples were homogenized in 4x Lämmli Buffer using a tissue homogenizer. Brains were lysed in 250 µl, one embryo was lysed in 15 µl and more embryos in an equivalent volume. Samples were then boiled for 5 min at 95°C and centrifuged for 15 min at 13000 rpm to pellet debris. Samples were stored at -20°C and were reused after 5 min boiling at 95°C and followed centrifugation of 1 min at 13000 rpm.

#### 2.2.1.10 *In vivo* imaging of zebrafish embryos

For live imaging PTU treated anesthetized embryos were embedded in 0.8% LMA in E3 containing 1x tricaine. To prevent drying out the agarose was covered with 1x PBST containing 1x tricaine. For long term imaging 24 hpf old embryos were then imaged with the spinning disc cell observer for 20 h. Acridine Orange stained embryos were imaged with the confocal laser scanning microscope using the 488 nm laser.

#### 2.2.1.11 Whole mount immunofluorescence staining

For whole mount immunofluorescence (IF) stainings PFA fixed embryos stored in methanol were used. Samples were washed 2x 10 min in PBST and were serially rehydrated by washing them 5 min at RT in decreasing methanol concentrations (75% methanol in PBST, 50% methanol in PBST, 25% methanol in PBST, 100% PBST). The samples were then washed 3x5 min in PBST at RT. 30 hpf embryos used for caudal primary (CaP) motoneuron staining with Znp-1 antibody were permealized for 10 min with 1 mg/ml collagenase in PBST at RT. Collagenase was removed by washing in PBST for 3x5 min at RT. For Proliferating cell nuclear antigen (Pcna) staining, embryos were kept in 100% aceton for 20 min at -20°C instead of collagenase treatment. After the samples were blocked for 1 h in NCST on a shaker at RT. Then the primary antibodies were added in NCST followed by an overnight incubation step on a shaker at 4°C. The next day the primary antibodies were removed and kept for further usage at 4°C. Samples were then washed for 3x40 min with PBST on a shaker at RT followed by a blocking step with NCST for 2x30 min at RT. Afterwards the secondary antibody diluted in NCST was added and incubated at 4°C on a shaker o/n. After removal of the secondary antibody samples were washed with PBST for 3x40 min. The samples were imaged with the spinning disc cell observer microscope using the 488 nm laser.

#### 2.2.1.12 Motoneuron analysis

After whole mount IF stainings with Znp-1 antibody, which detects CaP motoneurons, SpMN axons were analyzed. To correlate genotypes of the embryos to the motoneuron analysis, the heads of 30 hpf embryos were biopsied after the IF staining and individually collected in microcentrifuge tubes containing TE/Proteinase K buffer to lyse them. The extracted DNA was subject for genotyping procedure using allele specific primers or restriction digest. Immunostained tails of the embryos were stored in PBST until completion of the genotyping. 10 embryos per genotype in 3 different clutches were imaged and morphology and length analysis were done for motoneuron axons.

#### 2.2.1.13 Lysis of zebrafish samples

For the extraction of protein RIPA lysis was used. After shock freezing embryos, larvae or adult tissue in microcentrifuge tubes, these were kept on ice until radioimmunoprecipitation assay buffer (RIPA) buffer containing 1x Proteinase and Phosphatase Inhibitor (PI) was added to the samples and tissues. They were immediately homogenized using a pestle mixer

and centrifuged for 15 min at 4°C at 13.000 rpm. The supernatant containing the protein was transferred to a microcentrifuge tube and was used in a BCA assay to determine the protein concentration. As a next step ½ volume of 2x Lämmli buffer was added prior to incubation for 5 min at 95°C and centrifuged for 15 min at 13.000 rpm to pellet debris. 5-20 mg sample was used for SDS-page. Samples were stored at -20°C and reused after incubating them for 5 min at 95°C and centrifuging for 1 min at 13.000 rpm.

#### 2.2.1.14 Deyolking of zebrafish embryos and sample preparation for mass spectrometry

For the proteomic analysis the yolk was removed from the embryos to prevent that the abundant yolk proteins mask the detection of proteins. 30 hpf embryos were dechorionated and pools of 10 embryos were transferred to a microcentrifuge tube filled with deyolking buffer. By pipetting up and down with a 200 µl pipette the yolk was mechanically removed. Deyolked embryos were then transferred to a new microcentrifuge tube containing 200 µl deyolking buffer. The embryos were shaken at 1100 rpm for 5 min at 4°C on a thermoblock followed by a 30 sec centrifugation at 300 g. The supernatant was discarded and 1 ml washing buffer was added. The washing and centrifugation steps were repeated three times before transferring the embryos to a Protein LoBind tube. Embryos were then frozen in liq. $N_2$ and stored for further usage at -80°C.
Sample preparation for mass spectrometry was performed as described by Sielaff et al. [201]. An amount of 20 µg of protein per sample was subjected to proteolytic digestions using a modified protocol with an additional benzonase digest step in the beginning for single-pot solid-phase enhanced sample preparation (SP3). The protein lysate was diluted 1:2 with water. A volume of 10 µL 100 mM $MgCl_2$, and 25 units Benzonase (Sigma Aldrich, US) were added followed by an incubation for 30 min at 37°C at 1400 rpm in a Thermomixer (Eppendorf, Germany).

#### 2.2.1.15 Acridine Orange staining

To estimate the number of cells undergoing cell death in the zebrafish embryos Acridine Orange staining was performed [202]. Dechorionated anaesthetized 30 hpf PTU treated embryos were incubated for 30 min in 3 µg/ml Acridine Orange in E3 containing 1x tricaine. After 3 washes for 5 min in E3 1x tricaine the embryos were embedded in 0.8% LMA and imaged immediately by the confocal laser-scanning microscope using a 488 nm laser.

#### 2.2.1.16 Oil-Red-O staining

For staining of lipids in zebrafish, PTU treated embryos at 30 hpf were fixed by placing them in a microcentrifuge tube containing 4% PFA at 4°C o/n. On the next day the embryos were rinsed 3x10 min in PBST. Afterwards 0.5% oil red O (ORO) solution (diluted in 100% isopropanol) was diluted to 0.3% in sterile $H_20$ and centrifuged for 5 min at 11.000 rpm. Subsequently, 500 µl Osolution taken from the top of the microcentrigue tube were added to stain the embryos for 1 h at RT on a shaker. The embryos were then washed 3x10 min with 1xPBST before they were embedded in in 1.5% LMA in PBST and imaged using the Axio Scope A1 microscope.

### 2.2.2 Cellbiological methods

The following methods were mostly performed according to the Schmid laboratory methods manual.

#### 2.2.2.1 Cell cultivation

Human cervical carcinoma cells (HeLa) were cultured in Dulbecco's modified Eagle's medium (DMEM) with Glutamax supplemented with 10% fetal calf serum (FCS) and 1% penicillin/streptomycin at 37°C and 5% $CO_2$.

#### 2.2.2.2 Transfection of cells

After plating the cells they were kept for 24 h before they were transfected. The cells were seeded in 12 well cell culture dishes and transfected by inverse transfection. Per well, 2 µl lipofectamin 2000 and 125 µl optiMEM were incubated for 5 min before the mix was combined with 0.8 µg of DNA mixed with 125 µl optiMEM. Next, the DNA/lipofectamin transfection mix was transferred to a new 12 well plate prior splitting cells to 150000 cells in 500 µl per well. Cells were incubated in transfection mix o/n followed by an exchange of media by DMEM/Glutamax/FCS/penicillin/streptomycin the next day. Cells were culture and harvested 48 hpf later (see section 2.2.2.3)

#### 2.2.2.3 Harvesting of HeLa cells and whole cell lysis

Cells were washed 2x in PBS prior to being detached from the dish using a cell culture spatula. Cells were then centrifuged at 3500 x g and the pellet was lysed in 250 µl ice-cold

RIPA lysis buffer containing 1x Proteinase and PI by incubation on ice for 10 min. Afterwards the DNA was sheared by vortexing and after a centrifugation step for 15 min at 13000 rpm at 4°C the remaining debris was pelleted. The supernatant was transferred to a new microcentrifuge tube and protein concentration was determined by BCA assay measurement. Next, cell lysates were mixed with 4x Lämmli sample buffer, boiled at 95°C for 5 min and centrifuged for 1 min at 11000 rpm. Until usage for immunoblotting, cell samples were stored at -20°C.

### 2.2.3 Molecular biological methods

The following methods were mostly performed according to the Schmid laboratory methods manual.

#### 2.2.3.1 Isolation of genomic DNA

For genotyping of individual embryos or adult fish, genomic DNA from embryos or fin biopsies was isolated (for fin biopsies see section 2.2.1.7). The methanol from fin biopsies was removed and the remaining methanol evaporated by incubating the samples at 55°C. Embryos were anesthetized in 1x tricaine. Fin biopsies or embryos were then lysed in each 50 µl lysis buffer containing 10% PK. Samples were first digested at 55°C at 750 rpm for 1 h before inactivating PK at 95°C for 10 min. To pellet remaining tissue debris the samples were centrifuged for 5 min at 13.000 rpm. The genomic DNA containing supernatant was used for further analysis by PCR.

#### 2.2.3.2 Isolation of RNA

**Isolation of RNA using RNeasy Mini Kit** For isolation of RNA from zebrafish embryos or adult brain the RNeasy Mini Kit including on column DNase treatment (RNase-free DNase Set) was used according to the technical handbook. 30 embryos were pooled or one brain was placed in one microcentrigue tube. For RNA sequencing of *hnrnpa1a*$^{-/-}$*; hnrnpa1b*$^{-/-}$ and their wildtype siblings 20 embryos were pooled respectively. After removal of the water, 2x 350 µl RLT buffer containing 10% β- mercaptoethanol was added and embryos were disrupted with a tissue homogenizer. RNA was eluted in 30 µl RNase free water, and RNA quality was evaluated by gel electrophoresis (2 µl loaded), and the concentration was measured with a NanoDrop device. RNA was then stored at -80°C.

**Isolation of RNA using Trizol** RNA from zebrafish adult brains derived from *hnrnpa1a*$^{-/-}$, *hnrnpa1b*$^{-/-}$ or *hnrnpa3*$^{-/-}$ mutant fish that was sent for RNA sequencing was isolated according to the TRIzol Plus RNA Purification Kit. This method allows the extraction of a variety of RNA species of large and small molecular size. Each brain was homogenized in 1 ml TRIzol. RNA was eluted in 30 µl RNAse free water, RNA integrity was checked by gel electrophoresis (2µl loaded), and RNA concentration was determined with a NanoDrop device. RNA was stored at -80°C.

### 2.2.3.3 cDNA synthesis

cDNA was synthetized as described in the M-MLV Reverse Transcriptase Kit. Additionally RiboLock RNase Inhibiter was used for RNase inhibition. For cDNA, which is later used in qRT-PCRs 0.5 µg of total RNA was mixed with 2.5 µl random hexamer primers and 1 µl 10 mM dNTPs in a volume of 12 µl $H_2O$. For cDNA used for cloning of *hnrnpa* constructs 5 µg of total RNA were mixed with 2.5 µl of oligo (dT) primers instead that selectively enrich for mature mRNAs. The cDNA transcription was followed by 20 min RNase H digest at 37°C to remove RNA-DNA hybrids. Efficient cDNA transcription was determined by performing a β-actin PCR according to section 2.2.3.4.1 on the samples.

### 2.2.3.4 PCR

Oligonucleotides used for PCR are listed in section 2.1.5. Pairs of oligonucleotides were designed to have a similar annealing temperature not differing more than 2°C in the range of 50°C to 70°C to allow successful amplification of the spanned genomic region. The following components were mixed in a PCR tube:

| | |
|---|---|
| PCR mastermix / reaction | 17.5 µl PCR mix |
| | 0.5 µl forward primer (10 µM) |
| | 0.5 µl reverse primer (10 µM) |
| | 0.1 µl GoTag DNA Polymerase |

1 µl DNA or cDNA was added to 17.5 µl mastermix and the following PCR program was used after identifying the optimal oligonucleotide annealing temperature using a gradient PCR (see section 2.2.3.4.5). The number of cycles was initially set to 34 and adjusted depending on the band intensity:

| Cycle Step | Temperature | Time | No. of cycles |
|---|---|---|---|
| Initial Denaturation | 95°C | 2 min | 1 |
| Denaturation | 95°C | 30 s | xz |
| Annealing | 50-70 °C | 30 s | xz |
| Extension | 72°C | xy min | xz |
| Final extension | 72°C | 5 min | 1 |

PCR products were analyzed by agarose gel electrophoresis.

2.2.3.4.1 Control PCR

To proof efficient synthesis of cDNA a β-actin PCR was performed. The PCR mix was used in combination with primers oA03 β-actin F and oA04 β-actin R, which specifically amplify β-actin. In one reaction 1 µl of cDNA and 17.5 µl of mastermix were used in the following PCR program:

| Cycle Step | Temperature | Time | No. of cycles |
|---|---|---|---|
| Initial Denaturation | 95°C | 2 min | 1 |
| Denaturation | 95°C | 30 s | 34 |
| Annealing | 65.3 °C | 30 s | 34 |
| Extension | 72°C | 1 min | 34 |
| Final extension | 72°C | 5 min | 1 |

PCR products were analyzed by agarose gel electrophoresis.

2.2.3.4.2 PCRs for sequencing *hnrnpa1a*, *hnrnpa1b*, and *hnrnpa3*

To verify published *hnrnpa1a, hnrnpa1b, and hnrnpa3* sequences in our AB fish line and to identify naturally occurring single nucleotide polymorphisms (SNPs) in our fish population, *hnrnpa1a, hnrnpa1b, and hnrnpa3* genes were sequenced from 2 dpf AB cDNA. For amplification of full-length *hnrnpa* genes the following primer combinations were used:

| Amplicon | F Primer | R-Primer | Annealing Temp |
|---|---|---|---|
| *hnrnpa1a* | LJ-A05 | LJ-A06 | 70.0 |
| *hnrnpa1b* | LJ-A01 | LJ-A02 | 66.4 |
| *hnrnpa3* | LJ-A09 | LJ-A10 | 63.8 |

The primer pairs listed in the table were used in combination with the PCR mix whereby each reaction contained 1 µl genomic cDNA and 17.5 µl mastermix. The annealing temperature was specifically selected for each primer pair as shown in the above table. The extension time was 1 min and 30 sec and the number of cycles was 34. PCR products were analyzed by agarose gel electrophoresis prior to purification and being sent for sequencing to GATC.

2.2.3.4.3 Screening/ genotyping PCR for *hnrnpa* CRISPR/Cas9 mutants

For screening/genotyping PCRs the PCR mastermix was used with the respective primer pairs listed in the table below. The annealing temperature and number of cycles for each primer pair are listed in the table below. For sequencing of the mutant allele the PCR product was digested by RE digest and separated on an agarose gel. The mutant band was cut out from the gel, purified according to the NucleoSpin Gel Clean-up protocol and sent for GATC sequencing.

| Amplicon | F-Primer | R-Primer | Annealing Temp (°C) | Cycle # | RE | T (°C) | Buffer |
|---|---|---|---|---|---|---|---|
| *hnrnpa1a* ex2 | LJ-B05 | LJ-B06 | 58.0 | 32 | Fnu4HI | 37.0 | Cutsmart (CS) |
| *hnrnpa1a* ex8 | LJ-B07 | LJ-B08 | 64.0 | 36 | MnlI | 37.0 | CS |
| *hnrnpa1b* ex2 | LJ-B01 | LJ-B02 | 68.3 | 34 | PvuII | 37.0 | CS |
| *hnrnpa1b* ex9 | LJ-B03 | LJ-B04 | 68.3 | 34 | | | |
| *hnrnpa3* ex2 | LJ-B09 | LJ-B10 | 58.8 | 34 | Fnu4HI | 37.0 | CS |
| *hnrnpa3* Sa | LJ-B11 | LJ-B12 /LJ-B13 | 68.8 | 30 | | | |

2.2.3.4.4 PCRs for cloning HA tagged wildtype *hnrnpa1a*, *hnrnpa1b*, and *hnrnpa3*

For amplification of wildtype *HA*-tagged *hnrnpas,* referred to as *HA+hnrnpa1a*, *HA+hnrnpa1b*, *HA+hnrnpa3*, the primer pairs listed in the table were used in combination with the general mastermix. The annealing temperature was specifically selected for each primer pair as shown in the table below. The extension time was 1 min and 30 sec and the number of cycles was 34. PCR products were analyzed by agarose gel electrophoresis prior to purification and being sent for sequencing to GATC.

| **Amplicon** | **F Primer** | **R-Primer** | **Annealing Temp** |
|---|---|---|---|
| *HA+hnrnpa1a* | LJ-A03 | LJ-A06 | 66.2 |
| *HA+hnrnpa1b* | LJ-A07 | LJ-A02 | 78.3 |
| *HA+hnrnpa3* | LJ-A11 | LJ-A10 | 60.0 |

2.2.3.4.5 Gradient PCR

In order to determine the optimal annealing temperature of a primer pair gradient PCRs were performed using the general mastermix. Thereby a temperature gradient for the annealing temperature with a range from 50-70°C was tested. The extension time was adjusted according to the expected PCR product size. As a last step the PCR products were analyzed by agarose gel electrophoresis.

2.2.3.4.6 Colony PCR

Single clones from a previously plated agar plate were picked with pipette tips and inoculated with 30 µl LB medium containing the appropriate antibiotic. Bacterial colonies were then incubated at RT for 30 min and stored at 4°C. Appropriate primers, which allow the verification of the successful integration of the insert in the plasmid and its orientation, were selected for the PCR. For one reaction 1 µl colony LB culture and 17,5 µl mastermix were used. Annealing temperature and extension time were adjusted according to the temperatures of the primers used and the expected PCR fragment size. PCR products were analyzed by agarose gel electrophoresis.

2.2.3.4.7 qRT-PCR

The primers used for qRT-PCR all spanned an exon-exon junction with an intron longer than 1 kb to exclude amplification of genomic DNA and had an amplicon size of 80-150 bp. To

test the specificity of the primers they were analyzed on wildtype cDNA and validated by the presence of a single band of the predicted size upon agarose gel electrophoresis. The obtained PCR products were additionally sent for sequencing and aligned to their target sequence. qPCR was performed in 384-well format on a C1000 Thermal Cycler. One reaction contained 2 ng cDNA, 2.5 µl SYBR Green, 0.25 µl 10 µM forward primer, and 0.25 µl 10 µM reverse primer. To establish a standard curve total cDNA of all samples were pooled and a dilution series of 1:1, 1:10, 1:100, 1:1000 was set up. Each reaction was conducted as a technical triplicate and for each primer pair a no reverse transcriptase and no template control were included. The PCR program was run on a C1000 Thermal Cycler with the following steps: 30 s at 95°C, 55 cycles of 5 s at 95°C and 10 s at 60°C and a melting curve from 60°C to 95°C with an increase of 0.5°C every 5 s. Relative gene expression of each gene was calculated by ΔΔCT-method and the normalized fold expression was determined by normalizing individual gene expression to the reference genes *rflp13a* and *elf1a2*.

2.2.3.4.8 Semiquantitative PCR

Semiquantitative PCR was performed for *pkma*. 1 µl cDNA, 17.5 µl PCR mix, 0.5 µl 10 µM forward primer, and 0.5 µl 10 µM reverse primer were subjected to the following PCR program:

| **Cycle Step** | **Temperature** | **Time** | **No. of cycles** |
|---|---|---|---|
| Initial Denaturation | 95°C | 2 min | 1 |
| Denaturation | 95°C | 30 s | |
| Annealing | 63.8 °C | 30 s | 25/29/33/27 |
| Extension | 72°C | xy min | |

Four PCRs were set up with different cycle numbers (25, 29, 33, 37) to identify the number of cycles that leads to accumulation of the PCR product just below saturation level so that linearity is fullfilled. For all PCR products the same volume was analyzed via agarose gel electrophoresis.

### 2.2.3.5 Cloning of zebrafish *hnrnpa1a*, *hnrnpa1b*, and *hnrnpa3* constructs

A variety of *hnrnpa1a, hnrnpa1b, and hnrnpa3* constructs were cloned using TOPO cloning (see section 2.2.3.8) and Gateway technology (see section 2.2.3.9). For cloning full-length *hnrnpa1a*, *hnrnpa1b*, and *hnrnpa3*, primers were designed that specifically amplify the full-length gene. After amplification of the genes via PCR from 2 dpf AB zebrafish cDNA pools, the genes were cloned into pCR8/GW/TOPO vectors, which serve as entry vectors. The sequence of the vector insert was verified via GATC sequencing. Subsequently, expression vectors were generated via gateway reaction with pCS2+ plasmids, which contain pCS2+ cytomegalovirus (CMV) promoter as an expression control. Also, destination vectors with a GFP tag 5' of the gateway sites allow for N-terminal fusion of the gene of interest with GFP. These vectors were utilized to N-terminally tag HNRNPA1 and HNRNPA1$^{D262V}$ with GFP. These plasmids were used to analyze the localization of HNRNPA1 protein in zebrafish in wildtype form or when carrying the D262V patient mutation *in vivo*.

### 2.2.3.6 Agarose gel electrophoresis

For separation of PCR products by their size to analyze restriction enzyme digests for genotyping, or to determine RNA quality, agarose gel electrophoresis was performed. A 1-2% agarose gel (agarose in 1xTBE buffer) depending on the size of the PCR product analyzed was poured containing Gel Red (1:20000) to visualize the DNA. The samples were mixed with 5 µl loading dye and 1 µl DNA-ladder was placed next to the samples. Electrophoresis was run in 1xTBE buffer until PCR bands of interest were fully separated. The gel was then documented using a UV detection system.

### 2.2.3.7 DNA gel extraction and PCR purification

DNA extraction from an agarose gel was performed according to the NucleoSpin Gel Clean-up protocol. Purified DNA was eluted in 30 µl water and was either used for cloning into TOPO vector or analyzed by sequencing.

### 2.2.3.8 TOPO cloning

Entry clones were cloned using the pCR8/GW/TOPO TA Cloning Kit. The topoisomerase reaction in the kit requires the existence of sticky ends on the PCR product. Freshly generated

PCR products can be directly used for further cloning when kept on ice whereas stored PCR or cut out PCR bands from agarose gels need addition of adenosines at the ends. Adenosine overhangs were added in the following reaction: 20 µl PCR product, 5 µl 5x GoTaq Buffer, 0.5 µl 10 mM dATP, 0.3 µl GoTaq DNA Polymerase were incubated for 15 min at 72 °C. 1-4 µl of this fresh PCR product were then used in a TOPO cloning reaction according to the cloning kit's manual. The TOPO cloning reaction was incubated at RT before being transformed in chemically competent *E. coli* cells (see 2.2.5.10).

#### 2.2.3.9 Gateway cloning

For transfer of DNA fragments from entry clones to expression clones the Gateway cloning system was used. 150-500 ng pCR8/GW/TOPO vector containing the DNA insert was used as an entry clone and 150 ng of pCS2+GW vector containing a Gateway cassette served as a destination vector. The Gateway cloning reaction was performed according to the user manual of the Gateway LR clonase II Enzyme Mix. Subsequently 2 µl LR Clonase reaction were utilized for transformation to chemically competent *E. coli* cells (see section 2.2.3.10).

#### 2.2.3.10 Chemical transformation of bacteria

For transformation of plasmid DNA into bacteria, chemically competent TOP10 *E.coli* cells were used. *E. coli* cells were thawed on ice prior to adding 2-4 µl of TOPO cloning reactions, 2 µl of LR Gateway cloning reactions, or 10 pg- 100 ng plasmid DNA. In the next step, the cells were incubated on ice for 30 min, heat-shocked at 42°C for 30 s and then quickly chilled on ice for 3 min. To allow growth of bacteria, 250 µl SOC medium were added and bacteria were incubated at 37°C for 1 h at 200 rpm. Then 10-200 µl of the transformed cells were plated out on a pre-warmed LB agar plate containing the appropriate antibiotic to allow growth of cell clones expressing resistance genes due to successful integration of the desired DNA fragment. LB agar plates were incubated o/n at 37°C. The following day bacteria colonies were selected if present and analyzed for correct plasmid integration by colony PCR (see section 2.2.3.4.6).

#### 2.2.3.11 Cultivation of bacteria and plasmid DNA isolation

For plasmid isolation bacteria carrying the plasmid of interest were cultivated in different scales depending on the subsequent usage. For miniprep plasmid isolation single clones were picked from an LB-agar plate and individually transferred to 3-5 ml LB medium containing

the appropriate antibiotic. The bacteria culture was then incubated o/n at 37°C at 200 rpm. The next day plasmid DNA was isolated according to the NucleoSpinPlasmid protocol.
For midiprep plasmid isolation a single clone from an LB agar plate was inoculated in 200 ml LB medium containing the appropriate antibiotic and incubated o/n at 37°C at 200 rpm. On the following day plasmid DNA extraction was performed as described by the NucleoBond Xtra midi protocol. The concentration was measured with a NanoDrop device and stored for later usage at -20°C. Plasmids were sent for sequencing at GATC and entered to the Schmid laboratory plasmid database.

#### 2.2.3.12 RE digest

RE digest is a useful tool for plasmid linearization, screening and genotyping. The optimal buffer and temperature were chosen according to the manufacturers protocol.
For plasmid linearization 10 µg of DNA were digested in 50 µl $H_2O$ reaction containing 5 µl buffer and 1 µl RE. For screening and genotyping 3 µl PCR product were added to 7 µl of the following RE mastermix:

| | |
|---|---|
| RE mastermix / reaction | 1.0 µl buffer |
| | 0.1 µl RE |
| | 6.0 µl sterile $dH_2O$ |

The digestion reaction for any of the above applications was incubated for at least 2 h at the optimal temperature and was subsequently analyzed by agarose gel electrophoresis. Linearized plasmids were purified with Nucleospin PCR clean up, eluted in 25 µl $H_2O$, treated with RNA secure, and the concentration determined by NanoDrop.

#### 2.2.3.13 *In vitro* mRNA synthesis and purification

gRNAs for injection were transcribed from a gRNA template oligonucleotide. First, the gRNA oligonucleotide (oligo) was annealed to the T7 oligo by setting up the following reaction in a microcentrifuge tube: 4.3 µl of 100 mM T7 oligo, 1 µl 10x Annealing Buffer, 0.4 µl RNA secure and 4.3 µl gRNA oligo. After RNA secure treatment of the reaction for 10 min at 60°C the oligos were denatured in a 95°C waterbath for 5 min. The waterbath was slowly cooled down over three hours. In the next step the *in vitro* transcription was set up in a microcentrifuge tube containing the following reagents: 2 µl T7 10x reaction Buffer, 4 µl $H_2O$, 2 µl ATP, 2 µl CTP, 2 µl GTP, 2 µl UTP, 4 µl annealed oligos and 2 µl T7 enzyme mix. The reaction was mixed and spun down before being incubated for 4 hours at 37°C.

RNA that was used for OE of human HNRNPA1$^{D262V}$ and H2B1 was transcribed from a linearized template pCS2+ plasmid containing a CMV promoter. 1 µg linearized plasmid was mixed in a microcentrifuge tube with 10 µl 2xNTP/CAP, 2 µl 10x reaction buffer, filled up with nuclease free $H_2O$ to 20 µl, and 2 µl enzyme mix (SP6/T7). The reaction was then incubated for 2h at 37°C.

For degradation of remaining DNA 2 µl TURBO DNAse were added to the reaction followed by another incubation step for 15 min at 37°C. Next, for gRNAs used for injection, 115 µl nuclease-free $H_2O$ and 15 µl ammonium acetate stop solution were added before RNA was precipitated by the addition of 300 µl 100% ethanol. In the case of RNAs used for OE, the reaction was stoped by adding 30 µl nuclease free $H_2O$ and 30 µl lithium chloride. For better RNA yields RNA was precipitated overnight at -20°C. On the next day, the reaction was centrifuged for 30 min at 4°C at 14.000 xg and the supernatant was discarded. The remaining RNA pellet was washed with 800 µl 70% ethanol and centrifuged for another 30 min at 4°C at 14.000 x g. Next, the supernatant was discarded and the remaining ethanol was removed by evaporation. The RNA was then resuspended in 10 µl RNAse-free $H_2O$ and RNA concentration was measured using a NanoDrop. Additionally, RNA integrity was analyzed by agarose gel electrophoresis. RNA was immediately divided to 1.5 µl aliquots and kept for later use at -80°C.

#### 2.2.3.14 Determination of protein concentration

Protein concentration of zebrafish brain lysates was measured by a BC assay according to the user manual of the BC Assay Protein Quantification Kit. To set up a standard curve BSA was taken. The reaction was measured with a plate reader at 562 nm.

#### 2.2.3.15 SDS-polyacrylamide gel electrophoresis

Proteins were separated on a SDS-polyacrylamide gel according to their molecular weight (MW). The percentage of the gel was chosen according to the expected MW of the studied protein (https://www.thermofisher.com/content/dam/LifeTech/global/Forms/PDF/protein-gel-electrophoresis-technical-handbook.pdf).

Gels were prepared according to the following recipe (calculated for three separating gels and three stacking gels):

| | **10%** | **12%** | **Stacking gel** |
|---|---|---|---|
| 40% acrylamide | 6.3 ml | 7.6 ml | 560 µl |

| | | | |
|---|---|---|---|
| 1M Tris pH 8.8 | 12.5 ml | 12.5 ml | - |
| 1M Tris pH 6.8 | | - | 750 µl |
| 10% SDS | 0.25 ml | 0.25 ml | 60 µl |
| $dH_2O$ | 5.7 ml | 4.4 ml | 4,54 ml |
| 10% APS | 67.5 µl | 67.5 µl | 22.5 µl |
| TEMED | 67.5 µl | 67.5 µl | 22.5 µl |

The polyacrylamide gel electrophoresis (PAGE) equipment was assembled according to the manufacturer's instruction (Mini Protean Tetra Cell System, BioRad) and SDS running buffer was added to the chamber. Before loading the protein samples gel wells were rinsed with SDS running buffer. For determination of protein molecular weight Precision Plus Protein™ All Blue Standard was loaded. Electrophoresis was started at 80 V until proteins started to separate and continued at 120 V until the proteins of interest were separated sufficiently. Gels were subsequently used for Western blotting (see section 2.2.3.16).

#### 2.2.3.16 Protein transfer to PVDF-membrane (Western blotting)

For transfer immobilization of proteins on a PVDF membrane wet Western blotting was performed. Prior to blotting, the PVDF membrane was activated by pre-wetting the membrane in methanol. The membrane was then washed in $dH_20$ before being incubated in 1x transfer buffer. The gel together with the membrane was assembled between Whatman paper and foam pads in a holder cassette. Transformation of proteins from the gel to the membrane was performed in 1x transfer buffer at 400 mA for 60 min before membranes were used for immunodetection.

#### 2.2.3.17 Immunodetection of proteins

After successful transfer of proteins to the membrane, the Western blotting membranes were incubated at RT for 1 h on an orbital shaker in I-Block. The membrane was then incubated in primary antibody undiluted or diluted in I-Block on a shaker at 4°C o/n. On the next day, the primary antibody was removed and kept for further use at 4°C. Remaining antibody was removed by washing 4x15 min in PBST. The secondary antibody was applied diluted in PBST for 1 h at RT. After removal of the secondary antibody the membrane was washed 6x for 15 min with PBST. Immunodetection was performed using ECL Plus as indicated in the manual. Hereby ECL Plus substrate reacts with the HRP conjugate of the secondary antibody

and produces a strong chemiluminescent signal that can be detected upon exposure of X-ray films. After immunodetection the membrane was washed 3x5 min with PBST and dried for storage or later reusage between Whatman papers. Before immunodetection of a previously used and stored membrane the membrane was reactivated in methanol. The membrane was then incubated in 50 ml stripping buffer containing 350 µl β-mercaptoethanol in a shaking water bath at 50°C for 30 min. After rinsing the membrane 4x5 min in PBST on a shaker at RT the membrane was ready for another round of immunodetection, which was performed as described above.

### 2.2.4 General methods

#### 2.2.4.1 Generation of zebrafish specific Hnrnpa specific monoclonal antibodies

Zebrafish specific monoclonal antibodies detecting Hnrnpa1a, Hnrnpa1b and Hnrnpa3 proteins were generated by the service unit monoclonal antibodies at the Core Facility Monoclonal Antibodies, Institute for Molecular Immunology, Helmholtz Center Munich. Rats and mice were immunized using peptides that are N- or C-terminally conjugated with ovalbumin by the Specialty Laboratories GmbH. The screening process for monoclonal antibodies (mAbs) is described in further detail in the result section.

#### 2.2.4.2 Databases, alignments and primer design

The Ensembl Genome Browser (http://www.ensembl.org/index.html) or NCBI (http://ncbi.nlm.nih.gov/) was used for genome and transcript analysis. Sequence alignments, mapping of restriction enzymes. and construction of plasmids maps and knockin constructs were performed using the CLC Main Workbench. For primer design, Primer 3 (http://primer3.ut.ee/) was applied followed by a specificity analysis by Primer-BLAST (http://www.ncbi.nlm.nih.gov/tools/primer-blast/). Blast searches of unknown gene and transcript sequences were performed on NCBI (https://blast.ncbi.nlm.nih.gov/Blast.cgi).

#### 2.2.4.3 gRNA design

For successful generation of KO lines a suitable gRNA sequence, which specifically targets the genomic region of interest, is suitable for CRISPR/Cas9 genome editing and which allows genotyping by restriction fragment length polymorphism (RFLP) needs to be designed. A 20 nucleotide long sequence followed by a NGG PAM motif for Cas9 recognition was chosen,

which lies close the genomic locus of interest. Additionally, a RE site should be present close to the NGG motif for convenient genotyping purposes. Ultimately, the chosen gRNA sequence was blasted against the zebrafish genome on the NCBI website (https://blast.ncbi.nlm.nih.gov/) to identify potential off targets. gRNAs with a low number of off targets were then in vitro transcribed as stated in section 2.2.3.13 and used for zebrafish zygote injection. The results section depicts further evaluation of gRNAs and their usage for mutant generation *in vivo*.

#### 2.2.4.4 Image acquisition, processing and analysis

Images were taken by Zeiss spinning disc cell observer, Zeiss Axio Scope A1 microscope, Zeiss Stereo discoveryV8, and Zeiss confocal laser scanning microscope. Zebrafish embryos were embedded in 1.5% (for fixed embryos) or 0.8% (for live imaging) LMA in PBST for immobilization and imaged on glass bottom microscope dishes.
Images were processed using ZEN blue and Fiji to linearly adjust image brightness, contrast, and size. For quantification of Western blots, the LAS 400 image reader was used to depict band intensities in a linear manner for later analysis in Fiji.

#### 2.2.4.5 Statistics

GraphPad Prism was used for calculations and for generating the graphs, which are shown in this thesis. The statistical tests used in specific experiments are indicated in the respective figure legend. The level of significance shown in the graphs is depicted by asterisks: *$p<0.05$; **$p<0.01$; ***$p<0.001$. In case no significant difference was observed, the abbreviation n.s. is used.

**Western Blot analysis:**
In order to quantify western blot bands, all protein levels to be quantified were adjusted to the corresponding control protein levels (Calnexin or Tubulin). To be able to compare different blots to each other the mean of all wildtype values on a blot was set on the same level with a specific multiplication factor for each blot as these are considered to be the same in each experiment. According to the calculated factor all loaded KO values on the blot were multiplied to obtain comparable values from one blot to the other. As a next step the means of wildtype and KO samples from technical replicates were taken. Ultimately, all values were divided by the wildtype mean, to obtain the change from wildtype to KO values.

# 3 Results

## 3.1 Characterization of zebrafish Hnrnpas

### 3.1.1 HNRNPA orthologues and their expression in zebrafish

Zebrafish has become a popular organism for genetic studies of vertebrate gene function due to its short generation time, transparency and other features that facilitate and accelerate genetic studies. However, for effective modeling of the human gene function, it is important to understand the extent to which orthologues zebrafish genes are related to human genes. Zebrafish belong to the teleostei class, which underwent an additional round of whole genome duplication (WGD) called the teleost-specific genome duplication (TSD) [203]. According to Ensembl Compara 71.4% of human genes have at least one zebrafish orthologue and reciprocally 69% of zebrafish genes have at least one human orthologue [204].

The Ensembl database (http://www.ensembl.org/index.html) indicates that the Hnrnpa/b family in zebrafish consists of several proteins: two Hnrnpa0, two Hnrnpab, two Hnrnpa1, and one Hnrnpa3. The two Hnrnpa1, referred to as Hnrnpa1a and Hnrnpa1b, are both the orthologues of human HNRNPA1 and the orthologue of human HNRNPA3 is Hnrnpa3. There is no zebrafish orthologue for HNRNPA2. Zebrafish Hnrnpa1a, Hnrnpa1b, and one Hnrnpa3 share the main protein domains, such as two RRM domains followed by a RGG domain, with HNRNPA1 and HNRNPA3 (see Figure 3.1).

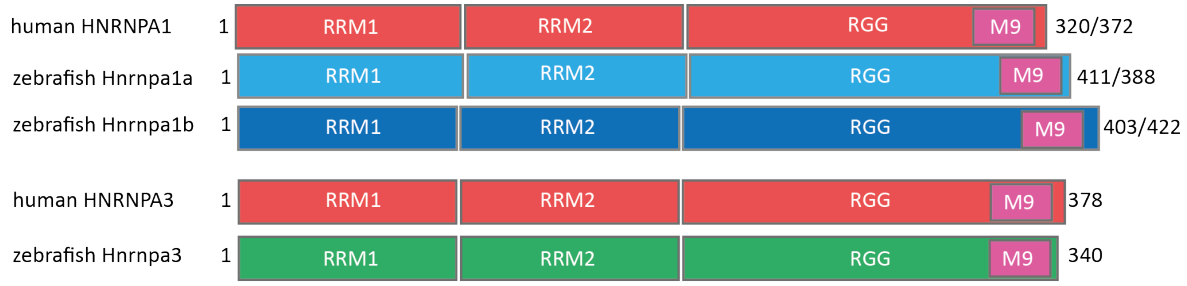


**Figure 3.1 - Schematic illustration of the human HNRNPA and zebrafish Hnrnpa domain structures.** Black numbers: amino acids. RRM: RNA recognition motif 1 and 2. RGG: Arginine-Glycine-Glycine rich domain. The M9 domain, which is required for nuclear shuttling is indicated in pink.

I amplified *hnrnpa1a*, *hnrnpa1b*, and *hnrnpa3* from cDNA of 2 dpf embryos to verify the genetic sequence of respective genes and to identify SNPs in our zebrafish population. *Hnrnpa1a* is located on chromosome 11 and consists of 10 exons with an open reading frame

(ORF) of 1167 bp that encodes a 388 aa protein with a theoretical molecular weight of 38.5 kDa. The longer *hnrnpa1a* isoform encoding 411 aa (with additional 23 aa at the N-terminus) with an ORF of 1236 bp and a theoretical MW of 41.02 kDa could also be amplified. *hnrnpa1b* is located on chromosome 23 and consists of 11 exons with an ORF of 1269 bp coding for 422 aa protein with a calculated MW of 42.6 kDa. A shorter isoform that lacks 19 aa at the N-terminal part was also amplified and has a calculated MW of 40.5 kDa. *Hnrnpa3* is located on chromosome 9 and consists of 11 exons with an ORF of 1023 bp, and is translated into a 340 aa protein with a theoretical molecular weight of 35.6 kDa. *Hnrnpa1a*, *hnrnpa1b and HNRNPA1* share a conserved genome environment, a phenomenon described as synteny [205]. The shared synteny between *hnrnpa1a* and *hnrnpa1b* with *HNRNPA1* is depicted in Figure 3.2. indicates that *hnrnpa1a* and *hnrnpa1b* are orthologues of *HNRNPA1*. Additionally, the shared synteny between *hnrnpa3* and *HNRNPA3* is

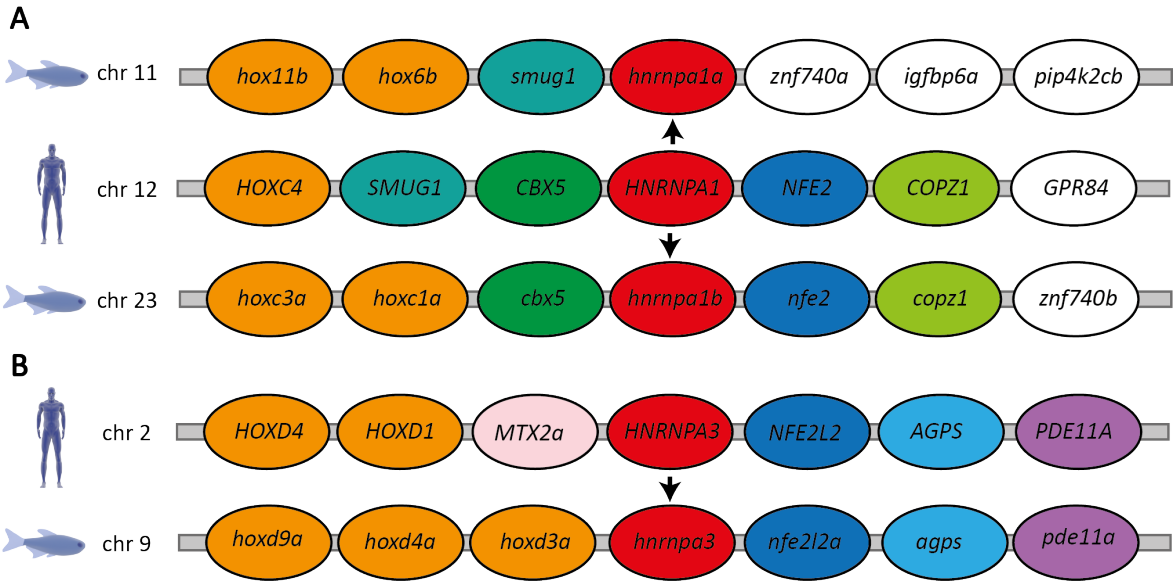


**Figure 3.2 - Synteny between human and zebrafish *HNRNPA1 and HNRNPA3*. A:** Human HNRNPA1 is located on chromosome 12. In zebrafish two *hnrnpa1* genes have evolved by genome duplication: *hnrnpa1a* and *hnrnpa1b* that are located on chromosome 11 and chromosome 23, respectively. The neighbouring genes of human *HNRNPA1* are *SMUG1* and *CBX5* at the 5' site and *NFE2* and *COPZ1* at the 3' site. In zebrafish smug1 is located 5' of *hnrnpa1a*, *cbx5* is located 5' of *hnrnpa1b*, and *nfe2* is located 3' of *hnrnpa1b*. **B:** Human *HNRNPA3* is located on chromosome 2 and zebrafish *hnrnpa3* is located on chromosome 9. The genes situated 5' and 3' of *HNRNPA3* and *hnrnpa3* are highly similar (*HOXD* and *hoxd*, *NFE2l2* and *nfe2l2a*, *AGPS* and *agps*) indicating shared synteny.

shown, providing the evidence that *hnrnpa3* is the *HNRNPA3* orthologue (see Figure 3.2). Sequence analysis revealed 67% sequence identity between human HNRNPA3 and zebrafish Hnrnpa3. In human two HNRNPA1 forms exist, which are generated by alternative splicing:

A1-B, which represents the full-length isoform of 372 aa, and A1-A, the shorter variant, which lacks exon 8 resulting in a 320 aa long portein. Alignment of Hnrnpa1a and Hnrnpa1b to HNRNPA1-A or HNRNPA1-B using the UniProt alignment tool (www.uniprot.org/align) gave sequence identity percentages. The analysis revealed the highest sequence identity between *hnrnpa1a* (63-66 %) and *hnrnpa1b* (61-65 %) when compared to HNRNPA1-B. Comparison of zebrafish *hnrnpa1a* and *hnrnpa1b* to HNRNPA1-A revealed only 55-58 % and 53-57 % sequence identity, respectively. Based on sequence comparison, the zebrafish *hnrnpa1s* are more similar to human Human HNRNPA1-B.

### 3.1.2 Screening for zf-Hnrnpa antibodies

In order to detect Hnrnpa proteins by Western blotting and to thereby confirm the absence of protein in our mutants and to analyze changes in protein expression levels, monoclonal antibodies were generated. Hnrnpa proteins are similar in their amino acid sequence, especially Hnrnpa1a and Hnrnpa1b. To reduce the likelihood of cross-reactivity of these antibodies I selected unique sequences as specific epitopes for immunization (see Figure 3.3).

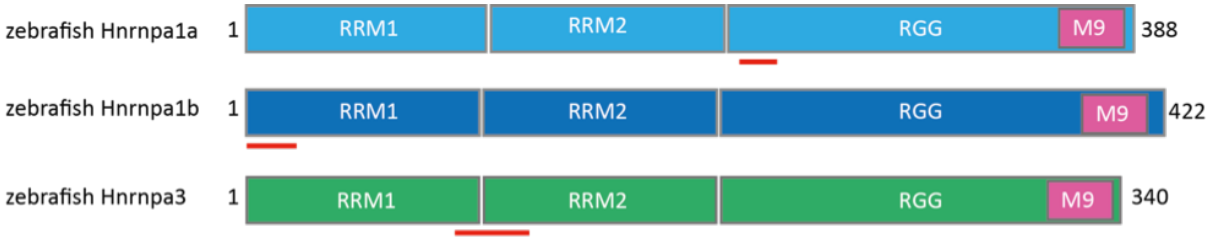


**Figure 3.3 - Schematic illustration of the Hnrnpa1a, Hnrnpa1b, and Hnrnpa3 antibody epitope.** The location of the antibody epitopes are indicated by a red line.

The monoclonal antibody (mAb) unit (IMI, Helmholtz Center Munich) used conjugated peptides to immunize mice and rats (peptides and their conjugates are listed in table 3.1). Subsequently, lymphocytes were taken from these animals and fused with myeloma cells to hybridomas to generate mAbs [206]. Pooled supernatants of the hybridoma cells were screened by an enzyme-linked immunosorbent Assay (Elisa) using bovine serum albumin (BSA) or biotin-conjugated peptides for positive mAbs.

I then tested positive pools by Western blotting of HA-tagged zf-Hnrnpa proteins, which were derived from OE in HeLa cells. Successful OE of these constructs was confirmed by Western blot with the HA antibody and I found HA-Hnrnpa1a migrating on a SDS-PAGE at a MW of approximately 40 kDa, HA-Hnrnpa1b migrating on a SDS-PAGE at a MW of approximately

40 kDa and HA-Hnrnpa3 at a MW of approximately 38 kDa (see Figure 3.4). All three proteins run at a slightly higher MW than expected probably due to the HA tag (3.56 kDa) or/ and posttranslational modifications. The different splice variants of Hnrnpa1a and Hnrnpa1b could not be detected as they run at similar molecular heights, which require greater separation by a higher percentage gel.

| **Peptide name** | **Peptide sequence** | **No. of positive / No. of all hybridoma tested** |
|---|---|---|
| Z1A2 (Hnrnpa1a) | OVA-C- MTEKNSDKRRGF | 0/16 |
| Z1A1 (Hnrnpa1b) | MSKEGQPREPEQLR-C-OVA | 24/151 |
| Z1A3 (Hnrnpa3) | OVA-C-KALPKQEMQSSSNQRYRGG | 31/44 |

**Table 3.1 - Peptides for mAb generation and summary of hybridoma pools tested.** Peptides for immunization were conjugated to OVA N- or C-terminally via an added cysteine (-C-).

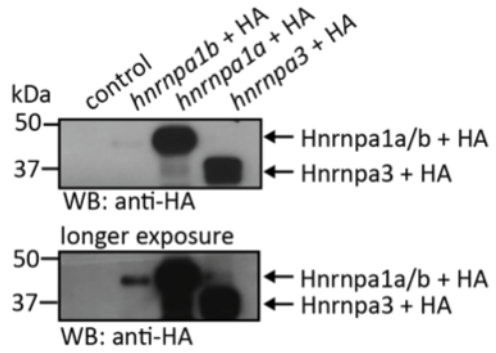


**Figure 3.4 - HA-tagged Hnrnpa1a, Hnrnpa1b and Hnrnpa3 are successfully overexpressed in HeLa cells.** Hnrnpa1a, Hnrnpa1b, and Hnrnpa3 run at a slightly higher MW than expected probably due to the HA tag and/or posttranslational modification. Hnrnpa1a is detected at approximately 40 kDa and Hnrnpa3 runs at approximately 38 kDa. Hnrnpa1b is lower expressed and can be only detected after longer exposure time at approximately 40 kDa.

As a next step, the hybridoma supernatant pools were tested on their ability to detect overexpressed zf-*Hnrnpa1a*, zf-*Hnrnpa1b*, or zf-*Hnrnpa3*. 24 out of 151 tested pools directed to Hnrnpa1b and 31 out of 44 pools directed to Hnrnpa3 detect Hnrnpa1b or Hnrnpa3 in cell culture, respectively (see Figure 3.5 and Table 3.1). Unfortunately, none of the Hnrnpa1a antibodies was positive for Western Blotting

Taken together, zebrafish specific mAbs detecting overexpressed Hnrnpa1b and Hnrnpa3 in HeLa cells were successfully generated, while no mAb could be established that specifically detects Hnrnpa1a.

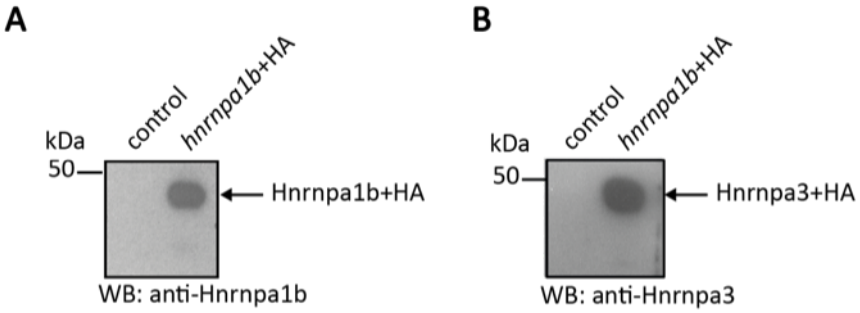


**Figure 3.5 - Overexpressed HA tagged Hnrnpa1b and Hnrnpa3 are specifically detected on Western Blot.** Hnrnpa1b is detected at approximately 40 kDa and Hnrnpa3 runs at approximately 38 kDa. Absence of a band in the control untransfected cells show specificity of the antibodies.

## Hnrnpa3 antibody

While an antibody was identified that detects overexpressed Hnrnpa3 protein, none of the positive mAbs directed to Hnrnpa3 detected endogenous zebrafish Hnrnpa3. However, I identified an antibody (Tardbpl_tv1 16C8-11), which next to its targeted protein Tardbpl_tv1 also seemed to detect Hnrnpa3. To further confirm this initial observation I conducted several control experiments. First the cross-specificity of the antibody was tested on adult Hnrnpa3 KO brains compared to wildtype brains. While in Western blots a band was present at the expected height of 35.6 kDa in samples obtained from wildtype brains, this band was absent

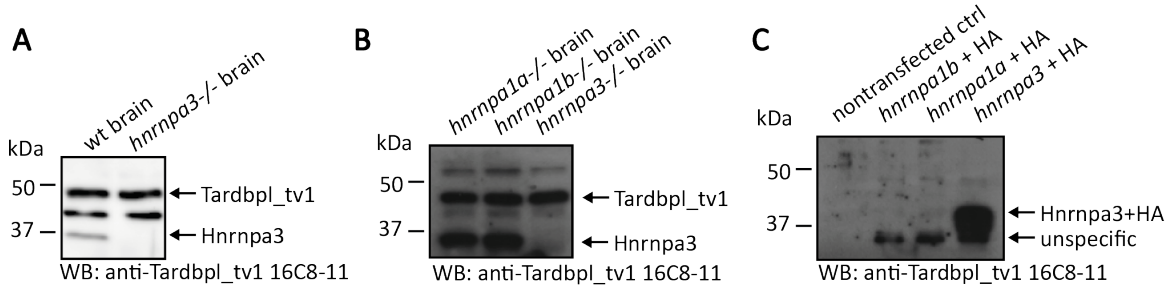


**Figure 3.6 - The monoclonal antibody raised against Tardbpl_tv1 detects also Hnrnpa3 but not Hnrnpa1a or Hnrnpa1b A:** anti-Tardbpl_tv1 16C8-11 detects a band at the expected size of Hnrnpa3 at 35.6 kDa in the zebrafish wildtype brain but not in the brain of *hnrnpa3*$^{-/-}$ fish. **B:** No crossreactivity of the antibody with Hnrnpa1a or Hnrnpa1b on *hnrnpa1a*$^{-/-}$ and *hnrnpa1b*$^{-/-}$ brains. No band at the expected size for Hnrnpa3 was detected in *hnrnpa3*$^{-/-}$ brains, while this band was unchanged in *hnrnpa1a*$^{-/-}$ and *hnrnpa1b*$^{-/-}$ brains. **C:** Hnrnpa3 was detected in *hnrnpa3* transfected HeLa cells at a higher molecular weight (38 kDa) due to HA tag. No band was detected in *hnrnpa1a* or *hnrnpa1b* transfected HeLa cells.

in samples derived from Hnrnpa3 KO brains (see Figure 3.6A). No cross-reactivity with Hnrnpa1a or Hnrnpa1b was further confirmed by the presence of this band in *hnrnpa1a*$^{-/-}$ and *hnrnpa1b*$^{-/-}$ mutant brains (see Figure 3.6B). Moreover, the antibody was tested on HeLa cells overexpressing *HA* tagged *hnrnpa3*, which was clearly detected at the expected size. No

bands at the expected height were detected in HeLa cells overexpressing HA tagged Hnrnpa1a or Hnrnpa1b (see Figure 3.6C). It can be concluded that the antibody directed to Tardbpl_tv1 (16C8-11) also specifically detects zebrafish Hnrnpa3 but not Hnrnpa1a or Hnrnpa1b.

### 3.1.3 Hnrnpa1b and Hnrnpa3 expression throughout development

Having identified Hnrnpa1b and Hnrnpa3 specific mAbs, these were used to determine Hnrnpa1b and Hnrnpa3 protein expression throughout development by immunoblotting. A distinct Hnrnpa1b band was clearly visible above 37 kDa at all developmental stages that were analyzed upon immunoblotting with the Hnrnpa1b antibody.

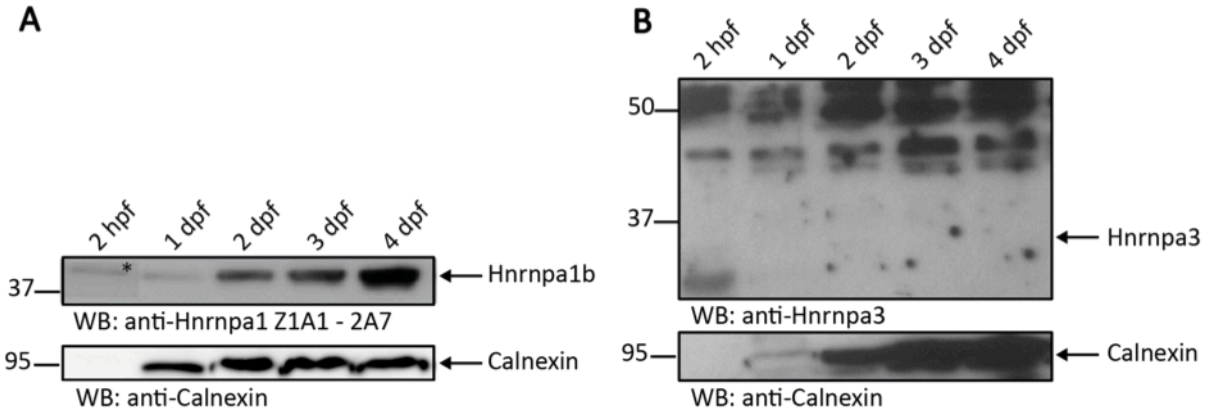


**Figure 3.7 - Hnrnpa1b and Hnrnpa3 protein expression during development. A:** Hnrnpa1b protein is expressed at 2 hpf to 4 dpf visualized by Hnrnpa1b mAb marked by a black arrow **B:** Hnrnpa3 protein levels were below the detection limit from 2 hpf to 4 dpf. Calnexin served as a loading control. Note that the Calnexin band was masked by huge amounts of yolk proteins at 1 dpf. One embryo per lane was loaded. Asterisk marks longer exposure time.

Hnrnpa3, which runs at approximately 37.5 kDa could not be detected at any analyzed developmental stage from 2 hpf to 4 dpf. This may be due to low expression of Hnrnpa3 during development, which is below detection limit of the antibody. The protein expression levels of Calnexin served as a loading control.

Concluding one can say that Hnrnpa1b protein is expressed at all developmental stages analyzed (2 hpf, 1 dpf, 2 dpf, 3 dpf, and 4 dpf). Hnrnpa3 is not detectable by Western blot in early developmental stages pointing to either low Hnrnpa3 expression, absence of Hnrnpa3 during early developmental stages or masking of the epitope during development due to posttranslational modifications.

## 3.2 HNRNPA1$^{D262V}$ protein localization

HNRNPA1 shuttles between the nucleus and cytoplasm under normal conditions with a predominant nuclear localization [207]. In healthy muscles, HNRNPA1 is predominantly localized to the nucleus. In contrast, mutations in HNRNPA1, including the D262V patient mutation, cause depletion from nuclei and are found in sarcoplasmic inclusions of HNRNPA1 in degenerating muscle of sporadic IBM and MSP patients [208]. Moreover, the

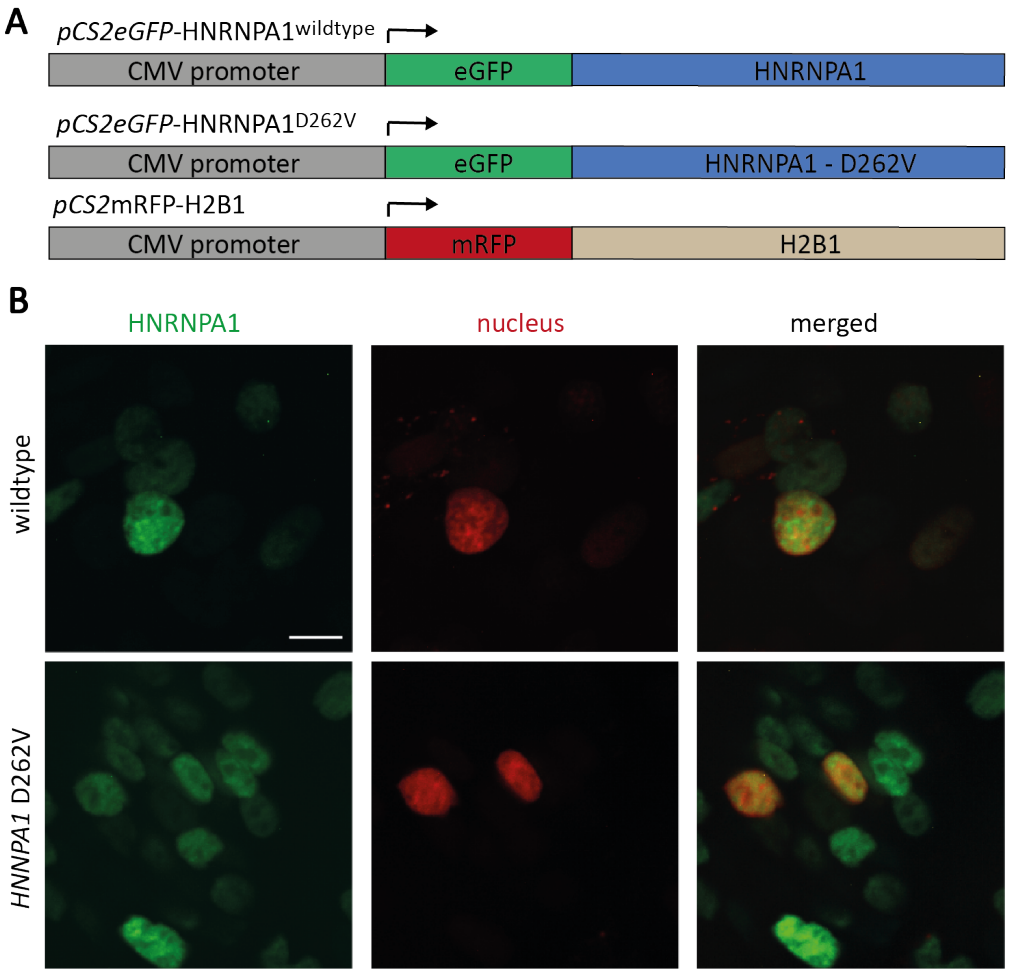


**Figure 3.8 - HNRNPA1$^{D262}$ does not mislocalize or aggregate *in vivo*. A:** Schematic illustration of HNRNPA1 expression constructs in neurons. HNRNPA1 coding sequences (blue) are fused to GFP (green) under the control of the CMV promoter (grey). H2B1 coding sequence (light brown) is fused to mRFP (red) under the control of the CMV promoter (grey). **B:** Representative images of HNRNPA1$^{wildtype}$ and HNRNPA1$^{D262V}$ protein expression and RFP nuclear labeling in 2 dpf zebrafish embryos. Scalebar=10 µm.

HNRNPA1$^{D262V}$ disease mutation is located in the PrLD of HNRNPA1 and is predicted to enhance aggregation propensity according to prion domain prediction algorithms [101].

To investigate whether the patient mutation affects nuclear transport of human HNRNPA1 protein resulting in HNRNPA1 redistribution to the cytosol and/or HNRNPA1 aggregation,

localization of HNRNPA1 wildtype and mutant protein was analyzed *in vivo*. Therefore, I cloned two reporter constructs fusing human HNRNPA1$^{wildtype}$ or HNRNPA1$^{D262V}$ to a GFP tag. Additionally, I cloned a reporter construct fusing H2B1 to a RFP tag, which stains the nuclei in red. All three constructs were under the control of a CMV promoter (see Figure 3.8A). These plasmids were injected in 1-cell stage zebrafish embryos resulting in a mosaic expression pattern and immunofluorescence staining was performed at 2 dpf. Stained cells were analyzed for HNRNPA1 localization changes or aggregation. From the staining it becomes evident that HNRNPA1$^{wildtype}$ and HNRNPA1$^{D262V}$ are both restricted to the nucleus in neurons (see Figure 3.8B) and do not differ in their subcellular localization.
It can be concluded that the D262V patient mutation does not seem to cause nuclear shuttle defects and HNRNPA1$^{D262V}$ expression is indistinguishable from HNRNPA1$^{wildtype}$.

## 3.3 Generation of *hnrnpa1a*, *hnrnpa1b*, *hnrnpa3* loss of function mutants

Mutations in *HNRNPA1* and *HNRNPA2B1* were identified in patients suffering from ALS and MSP, but the effect of these mutations on protein function is not clear [101]. In order to study their protein function in zebrafish, I generated *hnrnpa1a* and *hnrnpa1b* loss of function zebrafish. As another member of the HNRNPA protein family, HNRNPA3 was associated with ALS as it was found to aggregate in motoneurons of patients carrying *C9ORF72* repeats [70]. Hnrnpa3 is furthermore highly similar in structure to HNRNPA1 and HNRNPA2B1 and was shown to bind $G_4C_2$ repeats found in ALS patient's *C9ORF72* gene [70]. I therefore generated an additional zebrafish line that is deficient of Hnrnpa3. In this study I generate protein loss of function mutants by CRISPR/Cas9 genome editing, as these are stable and inherited so that studies can be also performed in adult zebrafish.

### 3.3.1 gRNAs targeting *hnrnpa1a*, *hnrnpa1b*, and *hnrnpa3*

To generate mutations, I targeted *hnrnpa1a*, *hnrnpa1b*, and *hnrnpa3* with a gRNA that was designed as described in section 2.2.6.3 and Cas9, and screened injected embryos for indel mutations by RFLP. I designed two gRNAs for each gene to target two different loci of each gene and to thereby create two independent loss of function lines for the *hnrnpa1a* and *hnrnpa1b*. An additional fish line was obtained from the Sanger center, which was N-ethyl-N-nitrosourea (ENU) mutagenized. It contains a point mutation in the *hnrnpa3* gene at aa 140 that is predicted to result in a premature termination codon (PTC).

For each gene one gRNA targets the 5' end of the ORF as frame shift mutations in this region are likely to result in loss of function as mutated mRNAs may be recognized by the NMD machinery leading to translation of a truncated protein. The second gRNA targets the gene close to the patient mutation site more towards the 3' end of the ORF and was initially designed to introduce patient mutations at this locus by targeted KI. By targeting the genes at two different loci at distinct ends of the gene (one at the 5' end and the other towards the 3' ed of the ORF) independent KO lines for the same genes were generated (see Figure 3.9). Two independently generated alleles reduce the probability of identical off-target effects. gRNAs

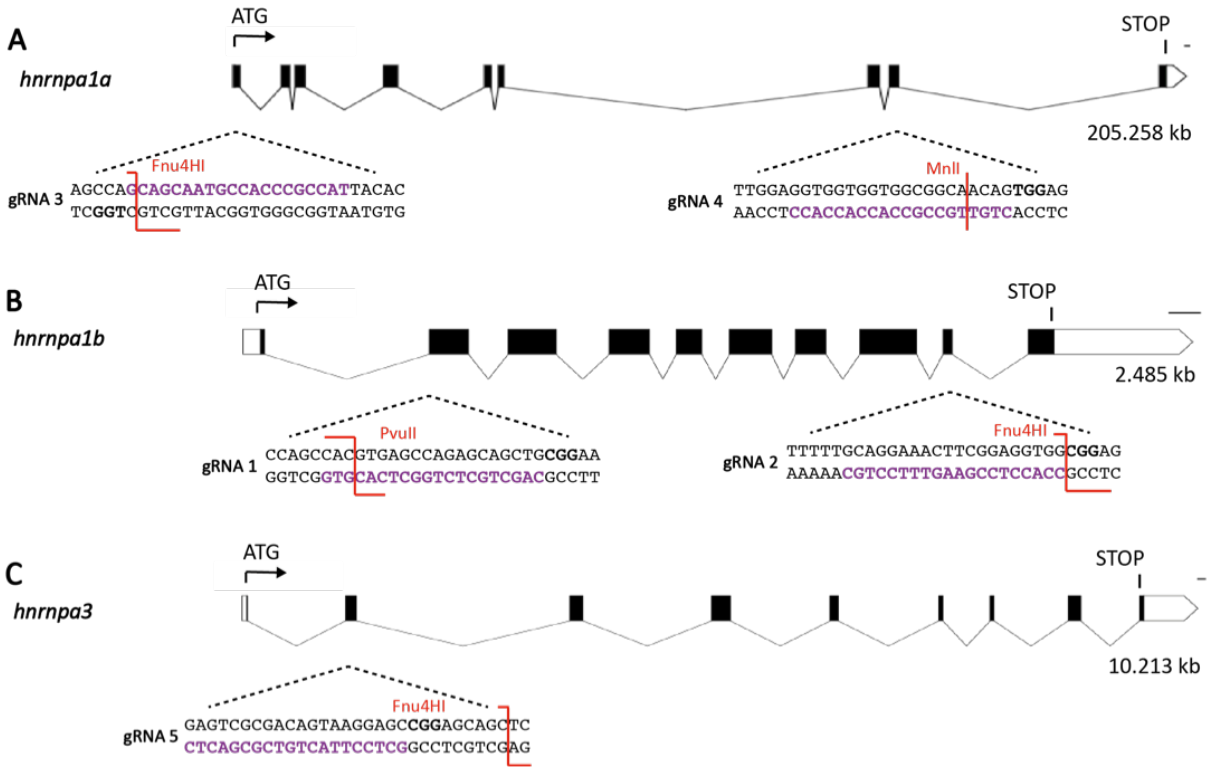


**Figure 3.9 - Localization of gRNA target sequences in *hnrnpa1a*, *hnrnpa1b*, and *hnrnpa3* A:** Schematic illustration of the *hnrnpa1a* genomic exon/intron structure. gRNA3 targets the first coding exon. Induced mutations are detected with the restriction endonuclease (RE) Fnu4HI. gRNA4 targets the ninth coding exon close to the patient mutation site and induced mutations are detected with the RE MnlI. **B:** Schematic illustration of the *hnrnpa1b* genomic exon/intron structure. gRNA1 targets the second coding exon and induced mutations are detected with the RE PvuII. gRNA2 targets the ninth coding exon close to the patient mutation site and induced mutations are detected with the RE Fnu4HI. **C:** Schematic illustration of the *hnrnpa3* genomic exon/intron structure. gRNA5 targets the second coding exon and induced mutations are detected with the RE Fnu4HI. Red lines: binding and cut sites of the RE. Purple: gRNA target sequence. Bold: PAM motif. Scale bar: 100 bp – Schematic illustrations were genered with http://wormweb.org/exonintron

were designed manually in CLC by choosing the target locus and designing the gRNA close to the next available PAM NGG motif. For later genetic screening purposes only those NGG

motifs were chosen that additionally have a RE cutting site close to them with the additional limitation that the chosen enzyme does only cut once in the region in such manner (approximately 150 bp up- and downstream of the NGG site) that the digested (wildtype unmodified allele) and undigested (modified KO allele) PCR product can be separated according to their length by gel electrophoresis). Selected gRNAs were then checked for their GC content using the online tool Multiple Primer Analyzer by Thermofischer and a GC content of 40 to 60% was considered suitable. Furthermore, the gRNA was tested for specificity in a BLAST search (http://blast.ncbi.nlm.nih.gov/blast.cgi). All the chosen gRNAs had off-target coverage below 70% upon Blast search against the zebrafish genome, thereby reducing the likelihood of off-target binding. As a next step the gRNAs were injected together with Cas9 protein by microinjection into the cell of zebrafish eggs at the 1-cell stage (see Figure 3.10).

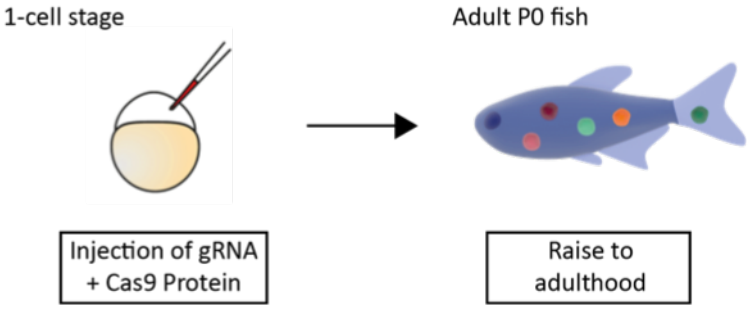


**Figure 3.10 - Schematic illustration of gRNA+Cas9 protein injection into zebrafish eggs.** Injection of *hnrnpa1a*, *hnrnpa1b*, or *hnrnpa3* targeting gRNAs with Cas9 protein and the resulting mosaic $P_0$ generation. Colored dots in $P_0$ fish indicate mosaic expression of different induced mutations.

### 3.3.2 Screening for *hnrnpa1a*, *hnrnpa1b*, and *hnrnpa3* mutations

For identification of successfully edited zebrafish eggs, screening assays were established that allow the detection of mutations that are induced by the cell`s error prone repair mechanism NHEJ after induction of a DSB. The screening assay not only functions as a read out of the gRNAs` efficiency can additionally be used for screening of edited alleles. Genomic DNA of 2 dpf old injected fish or finclip material of adult fish was amplified by PCR using primer that span the target site of the gRNA. Subsequently, the PCR product was digested with the respective RE (see Table 3.2) and separated on an agarose gel side by side to the undigested

| gRNA set | PCR product [bp] | RE | RE (No. of cut sites) | Band pattern in digested wt [bp] | Band pattern in digested mutant [bp] |
|---|---|---|---|---|---|
| gRNA1 | 346 | PvuII | 1 | 108+**238** | 346 |
| gRNA2 | 305 | Fnu4HI | 1 | 126+**179** | 305 |
| gRNA3 | 296 | Fnu4HI | 2 | **201**+7+88 | **289**+7 |
| gRNA4 $P_0$ | 396 | AciI | 1 | **297**+99 | 396 |
| gRNA4 $F_1$ | 396 | MnlI | 10 | 32+3+3+3+12+3+ **153**+65+7+21+90 | 32+3+3+3+12+3+**2** **18**+7+21+90 |
| gRNA5 | 232 | Fnu4HI | 1 | 98+**136** | 232 |

**Table 3.2 – PCR band pattern for screening CRISPR/Cas9 induced *hnrnpa* mutations.** For explanation see text.

PCR product. In the wildtype situation the PCR product that was treated with the respective RE is completely digested resulting in digested bands that run at a lower MW than the undigested PCR product. In case that the RE cuts once in the PCR product two bands are present in the digested PCR product (see Figure 3.11C+D+E), whereas more smaller bands are present in case that the enzyme cuts multiple times in the PCR product (see Table 3.2). Mutations altering the RE recognition motif prevent binding of the enzyme and the PCR product remains undigested. The amoung of undigested PCR product is proportional to the amount of edited alleles deleting the restriction recognition site. In embryos that were injected with gRNA3 **(**see Figure 3.11A**)** and gRNA 4 (see Figure 3.11B) targeting *hnrnpa1a,* the PCR band at 296 bp or 396 bp respectively was only partially digested showing successful induction of mutations in the $P_0$ generation in the *hnrnpa1a* gene. The PCR product at 346 bp and 305 bp is also only partially digested in embryos that were injected with gRNA1 and gRNA2, respectively, pointing towards successfully induced *hnrnpa1b* mutations in the $P_0$ generation (see Figure 3.11C+D). Additionally, in embryos injected with gRNA5, which targets *hnrnpa3,* the PCR band at 232 bp was only partially digested from which it can be concluded that some cells of the $P_0$ embryos carry mutations in the *hnrnpa3* gene (see Figure 3.11E).

Altogether, I established genotyping assays to introduce and screen for mutation. Moreover, I generated *hnrnpa1a, hnrnpa1b,* and *hnrnap3* mutations in injected $P_0$ fish. Next, these mutation carrier fish will be screened for successful germline transmission.

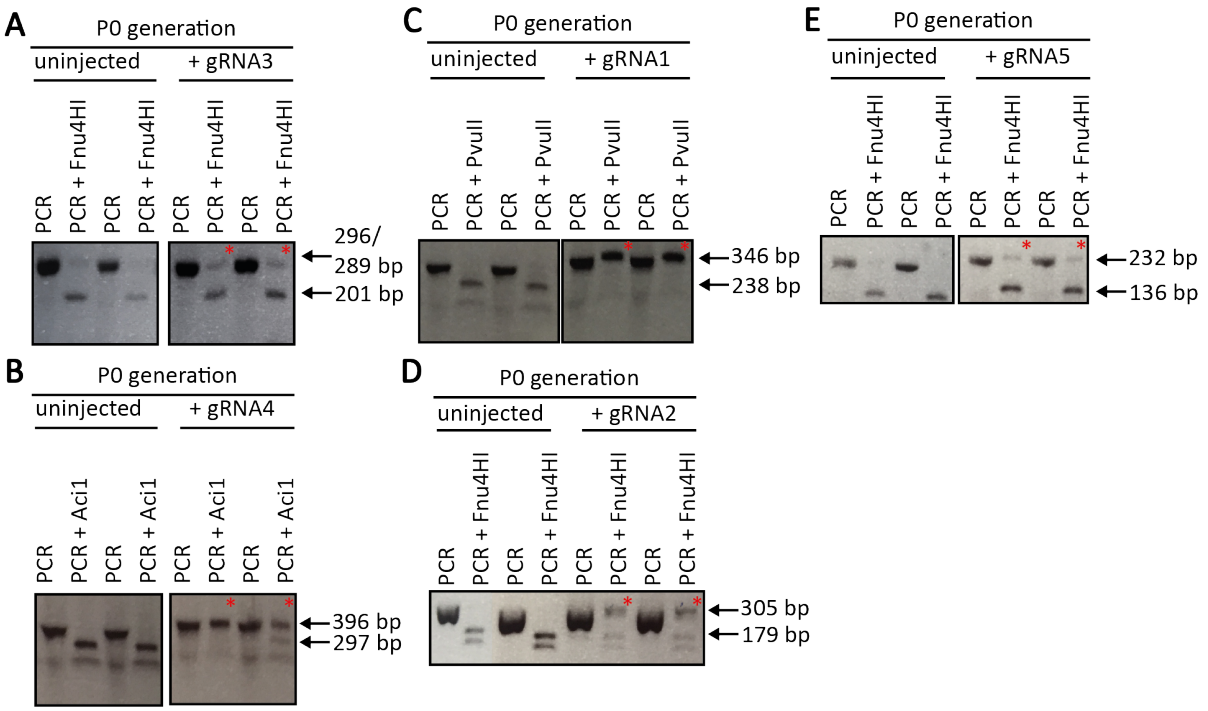


**Figure 3.11 - Screening assays for CRISPR/Cas9 $P_0$ induced *hnrnpa* mutations.** Uninjected and injected $P_0$ 2 dpf embryos were tested. PCR and corresponding RE-digested samples were separated on agarose gels **A:** Injection with *hnrnpa1a* gRNA3 targeting exon 1. RE: Fnu4HI. **B:** Injection with *hnrnpa1a* gRNA4 targeting exon 8. RE: AciI. **C:** Injection with *hnrnpa1b* gRNA1 targeting exon 1. RE: PvuII. **D:** Injection with *hnrnpa1b* gRNA 2 targeting exon 9. RE: Fnu4HI. **E:** Injection with *hnrnpa3* gRNA5 targeting exon 1. RE: Fnu4HI. The red asterisks (*) mark the band size in the RE-digested sampled that remained in gRNA injected samples only indicative of an undigested band due to an induced mutation by CRISPR/Cas9.

### 3.3.3 Screening for *hnrnpa1a*, *hnrnpa1b*, and *hnrnpa3* mutants

Genetically edited $P_0$ fish are mosaic, meaning that not every cell has the same mutation and/or that some cells have no mutation at all. In order to obtain a $F_2$ zebrafish that carries a single mutation in every cell the following screen (see Figure 3.12) was performed:

Having identified a mosaic $P_0$ fish using the RFLP assay after injection of *hnrnpa1a*, *hnrnpa1b* or *hnrnpa3* targeting gRNA and Cas9, this fish was outcrossed to a wildtype fish. The heterozygous $F_1$ generation was analyzed for successful germline transmission of mutations and the region around the target site of the mutant allele was sequenced to determine the introduced mutation. For each of the targeted loci frameshift mutations were identified resulting in mutations leading to either a PTC, deletion of the translation initiation codon ATG, or deletion of splice target sites.

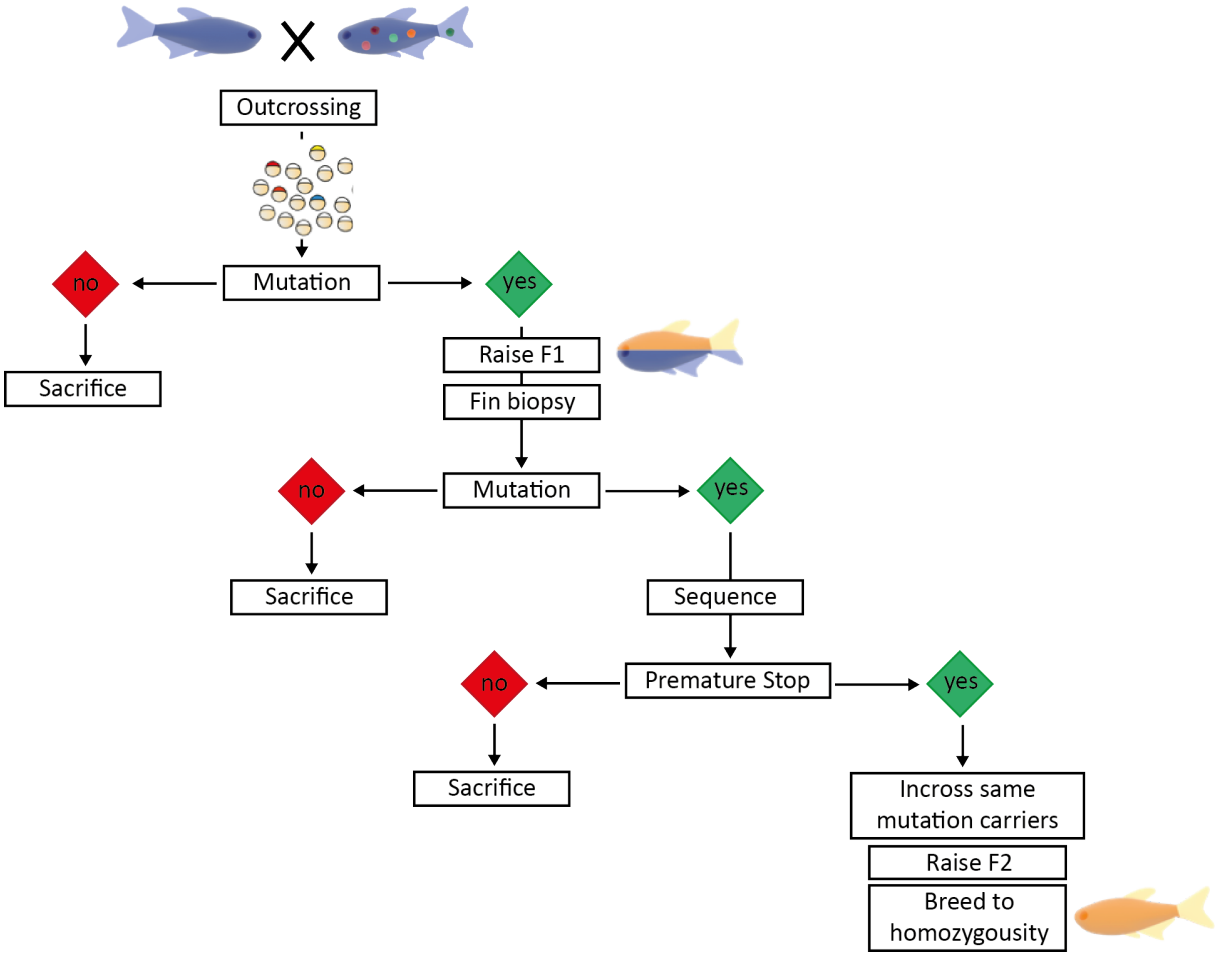


**Figure 3.12 - Schematic illustration of breeding $P_0$ mosaic mutation carrier to homozygousity.** The Figure shows the process of generating *hnrnpa1a*, *hnrnpa1b* and *hnrnpa3* homozygous mutation carriers from mosaic mutation carriers obtained by CRISPR/Cas9 genome editing in zebrafish.

The ratio of frameshift mutations in contrast to in frame mutations was quite variable for each locus (see Table 3.3). Upon identification of mosaic founder fish, these were outcrossed with a wildtype fish and the offspring was analyzed using finclip material for genotyping. *hnrnpa1a* exon 1 targeted founder fish resulted in 23 % mutation carrying offspring of which 67% had frameshift mutations. *hnrnpa1a* exon 8 targeted founder fish resulted in 14 % mutation carrying offspring of which only 40% had frameshift mutations. All offspring of *hnrnpa1b* exon 2 targeted founder fish had mutations (100 % germline efficiency), of which 60% caused frameshifts. The majority of offspring (79%) obtained from *hnrnpa1b* exon 9 targeted founder fish had mutations, which resulted in frameshift mutations in 67% of the fish. Only a small part (13%) of the offspring obtained from *hnrnpa3* exon 2 targeted founder fish showed mutations of which 67% caused a frameshift. With the assumption that the identified mutations will result in nonfunctional protein, zebrafish siblings carrying the same

mutation were incrossed to obtain a homozygous $F_2$ generation and outcrossed to wildtype fish to establish the line. For each gRNA target site one allele was chosen for further experiments (see Figure 3.13) and was bred to homozygosity. For these alleles genotyping assays were established, which are depicted in Figure 3.14. Primer flanking the mutation site are used for PCR amplification followed by an analytic RE digest. A wildtype allele becomes fully digested while a mutated allele stays undigested. The digestion pattern depicts homozygous wildtype (fully digested PCR product), heterozygous (50% digested PCR product), or homozygous KO (undigested PCR product).

| Gene (exon#) | # tested for mutation | # positive for mutation | % positive for mutation | % inframe alleles | % frameshift alleles |
|---|---|---|---|---|---|
| *hnrnpa1a (1)* | 291 | 68 | 23 | 33 | 67 |
| *hnrnpa1a (8)* | 257 | 37 | 14 | 60 | 40 |
| *hnrnpa1b (2)* | 94 | 94 | 100 | 40 | 60 |
| *hnrnpa1b (9)* | 48 | 38 | 79 | 33 | 67 |
| *hnrnpa3 (2)* | 120 | 15 | 13 | 33 | 67 |

**Table 3.3 - Allele frequencies in $F_1$ after targeting *hnrnpa* loci –** For explanation see text.

The genotypes were detected by the same readout used for detection of mutations in $P_0$ generation (see Table 3.3, Figure 3.14A+C+E+F). Two exceptions are mutants that carry mutations in exon 9 of *hnrnpa1* or mutations in exon 8 of *hnrnpa1b*. For these fish new screening assays were developed as either the mutation cannot be detected by the initial RE assay or the mutation induced such large deletion that can be already detected by a band shift in the PCR product (see Figure 3.18B+D). The genotype of *hnrnpa1a* exon 9 targeted zebrafish can be detected by mutation spanning PCR amplification resulting in a 396 bp PCR product. Upon digest of the PCR product with the RE MnlI a band is obtained at 218 bp and and some small digest products in the wildtype allele. In the homozygous allele one enzyme binding site is mutated resulting in a band at 218 bp and some small digest products (see Figure 3.14B). The genotype of *hnrnpa1b* exon 8 targeted zebrafish can be detected by mutation spanning primer that amplify the wildtype and mutated allele resulting in a 305 bp PCR product in the wildtype allele and a 252 bp PCR product in the mutated allele carrying a 53 bp deletion (see Figure 3.14D). The *hnrnpa3* allele obtained from the Sanger Center can be genotyped by mutation specific primer pairs, which specifically either amplify the wildtype or the mutated allele. Only in heterozygous samples each PCR reaction results in a PCR product,

whereas in homozygous mutation carriers or wildtype, only the mutation or wildtype specific PCR reaction results in a PCR product (see Figure 3.14F).

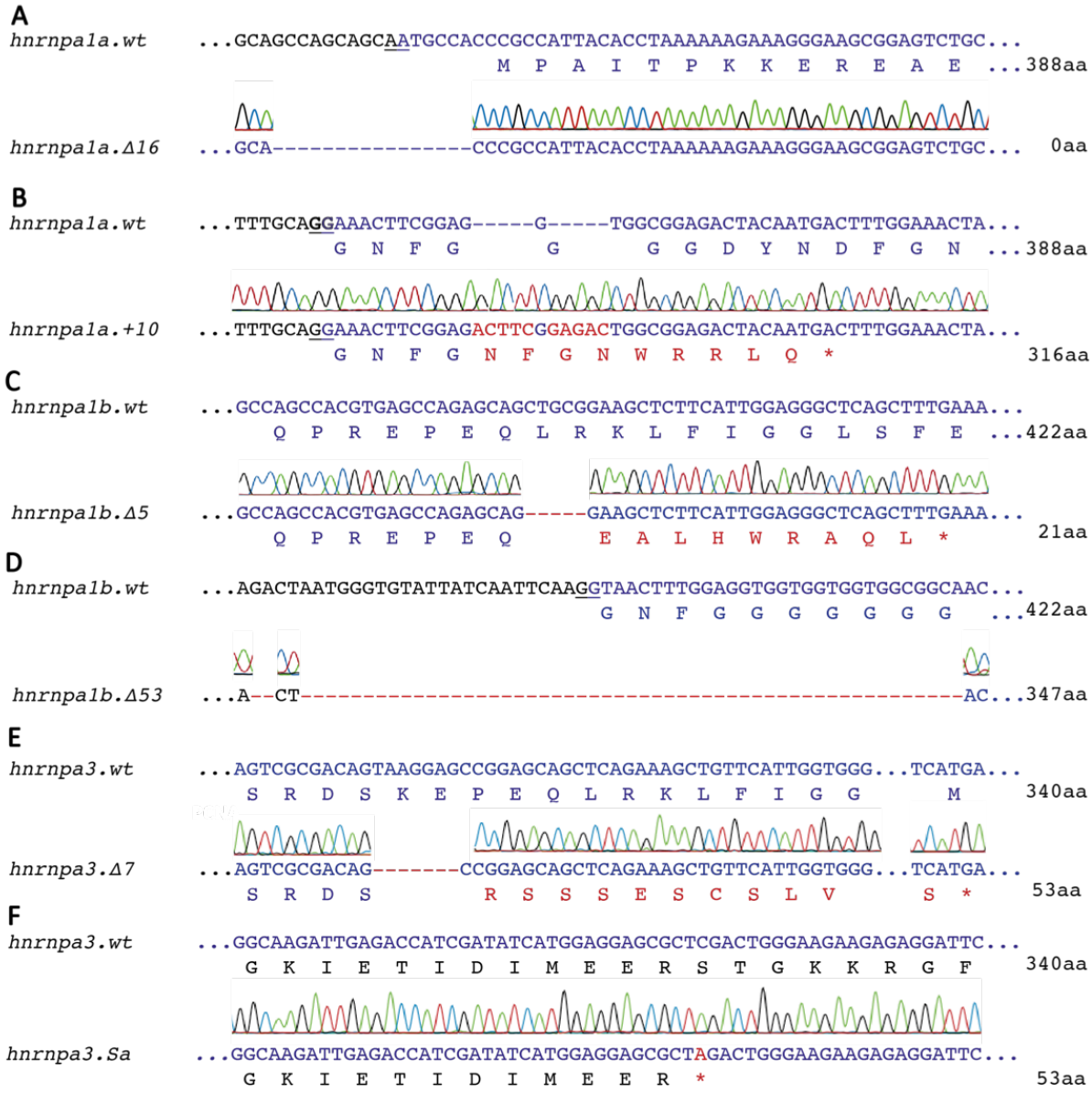


**Figure 3.13 - Genomic sequences of selected alleles. (A-F):** Top rows depict the wildtype nucleotide and aa sequence. The lower sequence depicts the respective mutant allele. **A:** *hnrnpa1a* wildtype exon 1 region and the mutated allele leading to ATG deletion **B:** *hnrnpa1a* wildtype exon 9 region and the mutated allele containing a 10 bp insertion **C:** *hnrnpa1b* wildtype exon 2 region and the mutated allele contains a 5 bp deletion. **D:** *hnrnpa1b* wildtype exon 9 region the mutant allele has a 53 bp deletion spanning an exon-intron site and leads to translation of the previous intron and a PTC stop. **E:** *hnrnpa3* wildtype exon 2 region the mutant allele contains a 7 bp deletion. **F:** *hnrnpa3* wildtype exon 4 region the sanger mutant containing point mutation that leads to a PTC codon. Blue: exonic sequence.. black: intronic sequence. Δ: deletion. +: insertion. Exon-intron boundary underlined. *: Stop.

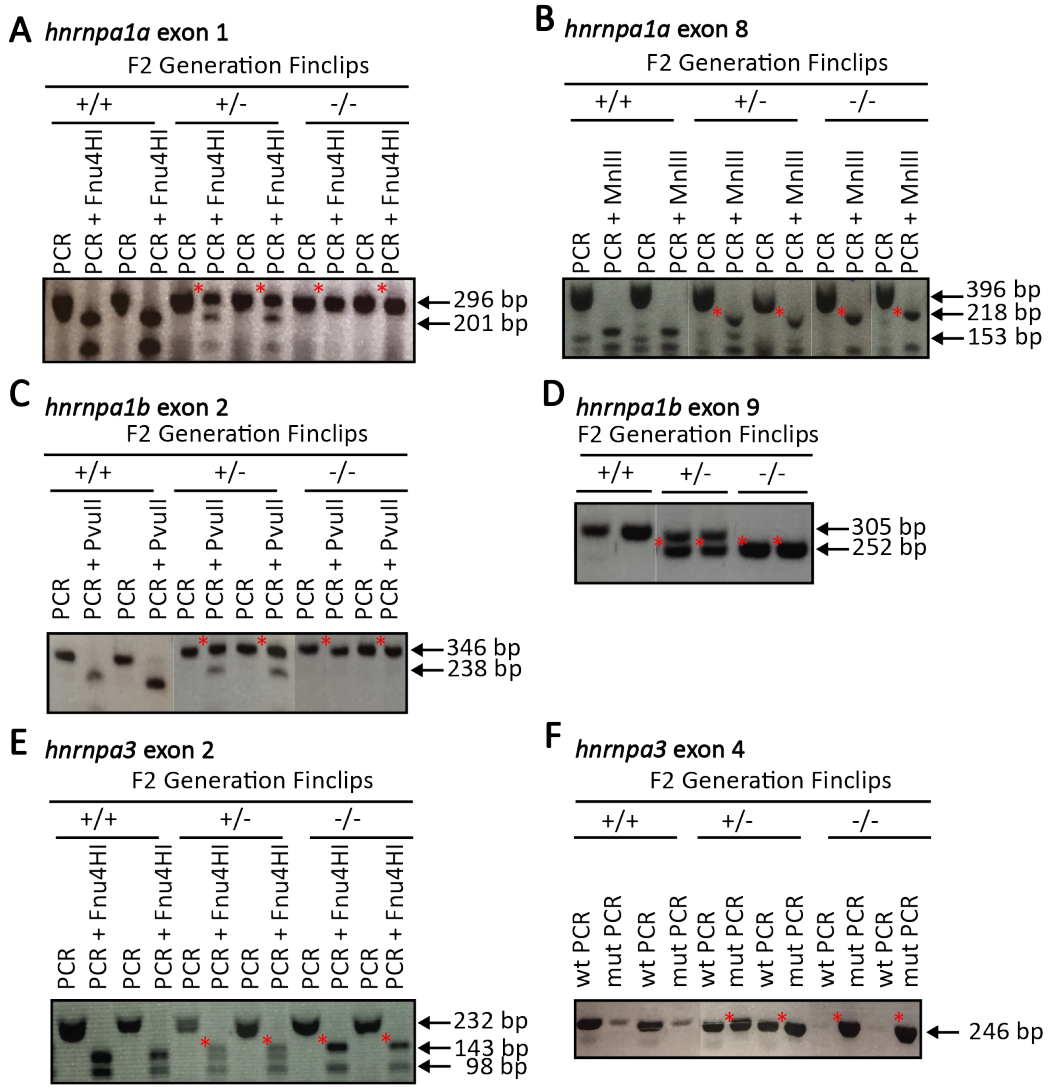


**Figure 3.14 - Genotyping assays in $F_2$ to discriminate between different genotypes. A:** *hnrnpa1a* edited exon 1 locus. Mutation spanning primer amplify the wildtype and mutated allele. Wildtype alleles are fully digested by the RE resulting in a fully digested PCR product. The mutation results in loss of the RE cutting site whereby an undigested PCR product remains. Heterozygous mutation carriers are recognized by a partially digested PCR product. RE: Fnu4HI**. B:** *hnrnpa1a* edited exon 8 locus. RE: MnlI. **C:** *hnrnpa1b* edited exon 2 locus. RE: PvuII. **D:** *hnrnpa1b* edited exon 9 locus. Mutation spanning primer allow to distinguish between the wildtype and mutated allele. The mutated allele carrying a 53 bp deletion can be detected by a band shift of 53 bp downwards on an agarose gel. **E:** *hnrnpa3* edited exon 2 locus. RE: Fnu4HI **F:** *hnrnpa3* edited exon 4 locus. Mutation specific primer either recognize the mutant or wildtype allele. For each sample two PCR reactions were performed. Only in heterozygous samples each PCR reaction results in a PCR product, whereas in homozygous mutation carriers or wildtype only the mutation or wildtype specific PCR reaction results in a PCR product, respectively. The red asterisks (*) mark the band that remains in the edited allele only.

In summary, gRNAs led to mutations in the germline, which are thereby transmitted to the next generation. Zebrafish carrying mutations that result in a frameshift or splice alterations leading to a PTC, or delete the translation initiation ATG codon, were identified using the

screening assay described in Table 3.2 and were bred to homozygousity. These mutations are likely to result in loss of protein function.

### 3.3.4 *hnrnpa1b* and *hnrnpa3* mutants are loss of function mutants

The generated KO lines required confirmation that they are loss of function alleles and that no functional protein is produced by the selected alleles. The mutant mRNA containing a PTC is likely to be degraded by NMD [209]. If mutant mRNA is targeted to NMD was assayed by qRT-PCR and loss of protein by immunoblot.

As no Hnrnpa1a specific antibody is available, mRNA levels of brains derived from *hnrnpa1a*$^{ins10-/-}$ brains were analysed by qRT-PCR, which revealed that *hnrnpa1a* mRNA levels are reduced to 30% compared to wildtype siblings, which is a significant decrease (see Figure 3.15A). The remaining 30% of *hnrnpa1a* mRNA point to partial degradation of *hnrnpa1a* mRNA by NMD. It has to be further confirmed whether the remaining *hnrnpa1a*

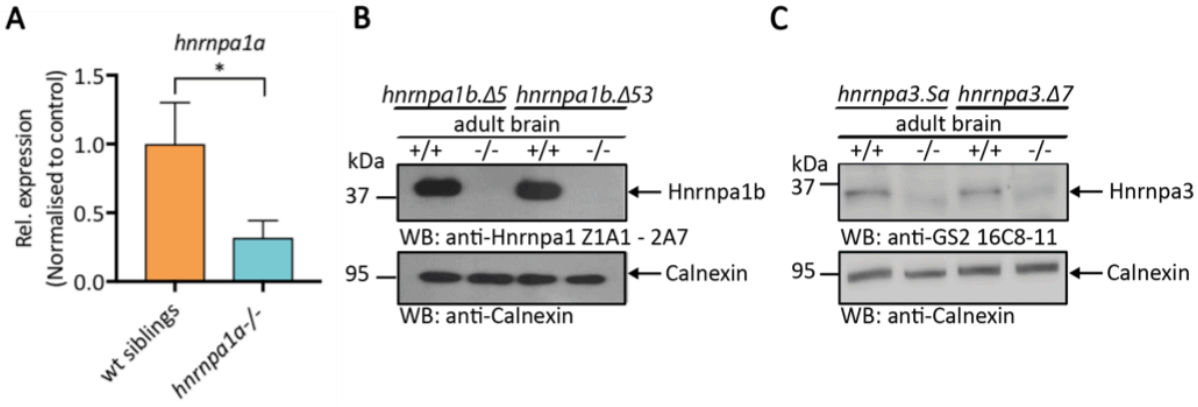


**Figure 3.15 - The selected *hnrnpa1a*, *hnrnpa1b*, and *hnrnpa3* alleles are loss of function alleles A:** *hnrnpa1a* mRNA levels were measured in *hnrnpa1a*$^{ins10-/-}$ mutants as no Hnrnpa1a specific antibody is available. *Hnrnpa1a* mRNA levels are significantly reduced in the brains of *hnrnpa1b*$^{-/-}$ mutants. (*$p$<0.02) n=4. Error bar indicates S.E.M. Normalized to *rflp13a* and *elf1a2*. Student's t-test. **B:** The Hnrnpa1b specific band is absent in all brain samples derived from *hnrnpa1b*$^{-/-}$ mutants, whereas an Hnrnpa1b specific signal was detected in brain samples of *hnrnpa1b*$^{+/+}$ siblings. **C:** The Hnrnpa3 specific band was absent in all brain samples derived from *hnrnpa3*$^{-/-}$ mutants, whereas an Hnrnpa3 specific signal was detected in brain samples of *hnrnpa3*$^{+/+}$ siblings.

mRNA levels are translated into a functional protein. Antibodies against Hnrnpa1b and Hnrnpa3 were used in Western blot analysis in order to confirm Hnrnpa1b absence in the *hnrnpa1b*$^{\Delta 5-/-}$ and *hnrnpa1b*$^{\Delta 53-/-}$ zebrafish and Hnrnpa3 absence in *hnrnpa3*$^{\Delta 7-/-}$ and *hnrnpa3*$^{Sa-/-}$ zebrafish brains, respectively. On immunoblots against Hnrnpa1b a band is present at 42.6 kDa in wildtype brain samples, which is not detectable in brain samples from *hnrnpa1b*$^{-/-}$ mutants. The Hnrnpa3 specific signal is present in wildtype brain samples at 35.6

kDa but not in *hnrnpa3*$^{-/-}$ mutant brain samples. Given the absence of the Hnrnpa1b and Hnrnpa3 specific band in brain samples of *hnrnpa1b*$^{-/-}$ and *hnrnpa3*$^{-/-}$ mutants it can be concluded that the respective proteins are no longer produced or degraded (see Figure 3.15B+C).

In summary, Hnrnpa1a loss of function could only be assessed on mRNA level and revealed a 70% decrease in *hnrnpa1a* mRNA levels compared to wildtype. All selected alleles for *hnrnpa1b* and *hnrnpa3* are loss of function alleles whereby the respective protein is no longer produced or degraed.

## 3.4 Basic characterization of single *hnrnpa1a*$^{-/-}$, *hnrnpa1b*$^{-/-}$ and *hnrnpa3*$^{-/-}$ mutants

The aim of this study was to establish stable KO lines for Hnrnpa1a, Hnrnpa1b and Hnrnpa3 to study the function of these proteins *in vivo*. Having generated these lines I next addressed the consequences of protein loss of function in single and double mutants. For further analysis only one allele of each gene was taken: *hnrnpa1a*$^{ins10}$*; hnrnpa1b*$^{\Delta 53}$, and *hnrnpa3*$^{Sa}$.

### 3.4.1 *hnrnpa*$^{-/-}$ single mutants are viable and fertile

Single *hnrnpa1a*$^{-/-}$, *hnrnpa1b*$^{-/-}$, and *hnrnpa3*$^{-/-}$ mutants were examined for viability from hatching until adulthood. For all in- and outbreedings natural occurring egg lay numbers were obtained with a majority of fertilized eggs. Among all the crosses, expected ratios of Mendelian inheritance were obtained (see Table 3.4). All embryos were raised to adulthood with an indistinguishable lifespan between mutants and wildtype siblings.

| **Incross of *hnrnpa1a*** $^{+/-}$, (n=302 | | | |
|---|---|---|---|
| Genotype | *hnrnpa1a* $^{+/+}$ | *hnrnpa1a* $^{+/-}$ | *hnrnpa1a* $^{-/-}$ |
| Examined Ratio | 24,42% ± 0.04 | 52,94% ± 0.04 | 22,64% ± 0.02 |
| Expected ratio | 25% | 50% | 25% |

| **Incross of *hnrnpa1b*** $^{+/-}$, (n=150) | | | |
|---|---|---|---|
| Genotype | *hnrnpa1b* $^{+/+}$ | *hnrnpa1b* $^{+/-}$ | *hnrnpa1b* $^{-/-}$ |
| Examined Ratio | 21.88% ± 0.02 | 48.25% ± 0.02 | 29.87% ± 0.03 |
| Expected ratio | 25% | 50% | 25% |

| **Incross of *hnrnpa3* $^{+/-}$**, (n=156) | | | |
|---|---|---|---|
| Genotype | *hnrnpa3* $^{+/+}$ | *hnrnpa3* $^{+/-}$ | *hnrnpa3* $^{-/-}$ |
| Examined Ratio | 23.96% ±0.01 | 48.89% ± 0.03 | 27.15% ± 0.02 |
| Expected ratio | 25% | 50% | 25% |

**Table 3.4 - Mendelian laws apply for incrosses of single *hnrnpa*$^{-/-}$ mutants -** for each clutch 40 eggs analyzed. n=number of embryos analyzed (obtained from at least 3 different clutches). ± : standard deviation.

To analyze the single mutants in further detail I examined them for obvious morphological changes. Thereby the body shape, body length, eye, brain and yolk were observed throughout the development from embryo stage up to adult hood. The analysis revealed no morphological differences among mutants and wildtype siblings. Representative images are depicted in Figure 3.16. In summary, *hnrnpa1a*$^{-/-}$, *hnrnpa1b*$^{-/-}$, and *hnrnpa3*$^{-/-}$ single mutants are hetero- and homozygous viable and fertile and have no obvious morphological phenotype.

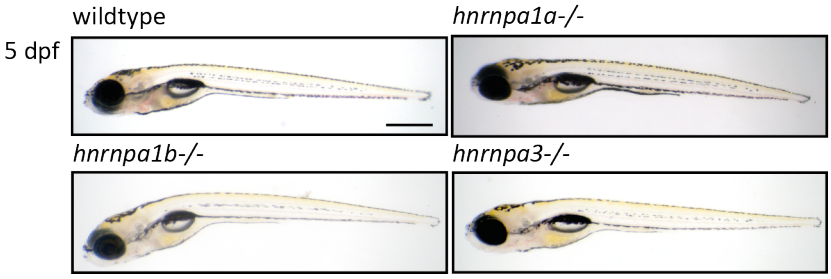


**Figure 3.16 - *hnrnpa*$^{-/-}$ single mutants show no obvious morphological phenotype.** Images of 5 dpf old wildtype, *hnrnpa1a*$^{-/-}$, *hnrnpa1b*$^{-/-}$ and *hnrnpa3*$^{-/-}$ mutants. Lateral view. Anterior to the left. Images were taken with Axio Scope A1. Scalebar represents 500 µm.

### 3.4.2 *hnrnpa*$^{-/-}$ single mutants have no morphological phenotype in ALS associated cells or tissues

One central characteristic for ALS is the degeneration of upper and lower motoneurons and subsequent muscle wasting [41]. As a first step *hnrnpa1a*$^{-/-}$, *hnrnpa1b*$^{-/-}$, and *hnrnpa3*$^{-/-}$ single mutants were therefore analyzed for changes in ALS related tissues, such as motoneurons and muscles. Maternal mRNA, provided to the eggs by the mother allows embryos to synthesize proteins before the onset of their own zygotic transcription. Therefore Hnrnpa1a, Hnrnpa1b, or Hnrnpa3 protein translation from maternal mRNA at the earliest stages of development could potentially preclude identification of early phenotypes [210]. To exclude maternal contribution embryos used for the analysis of ALS related phenotypes originate from incrosses of homozygous mutants.

### 3.4.2.1 *hnrnpa*$^{-/-}$ single mutants mutants have no motoneuron phenotype

The SpMN axon of the Cap motoneuron axon, which project ventrally from the spinal cord to innervate muscles, is frequently used as a neuron vulnerability readout in zebrafish. In the past a variety of zebrafish KO models were analyzed for SpMN axon morphology by quantifying the SpMN axonal outgrowth length and branching [211] [212] [12] [190].

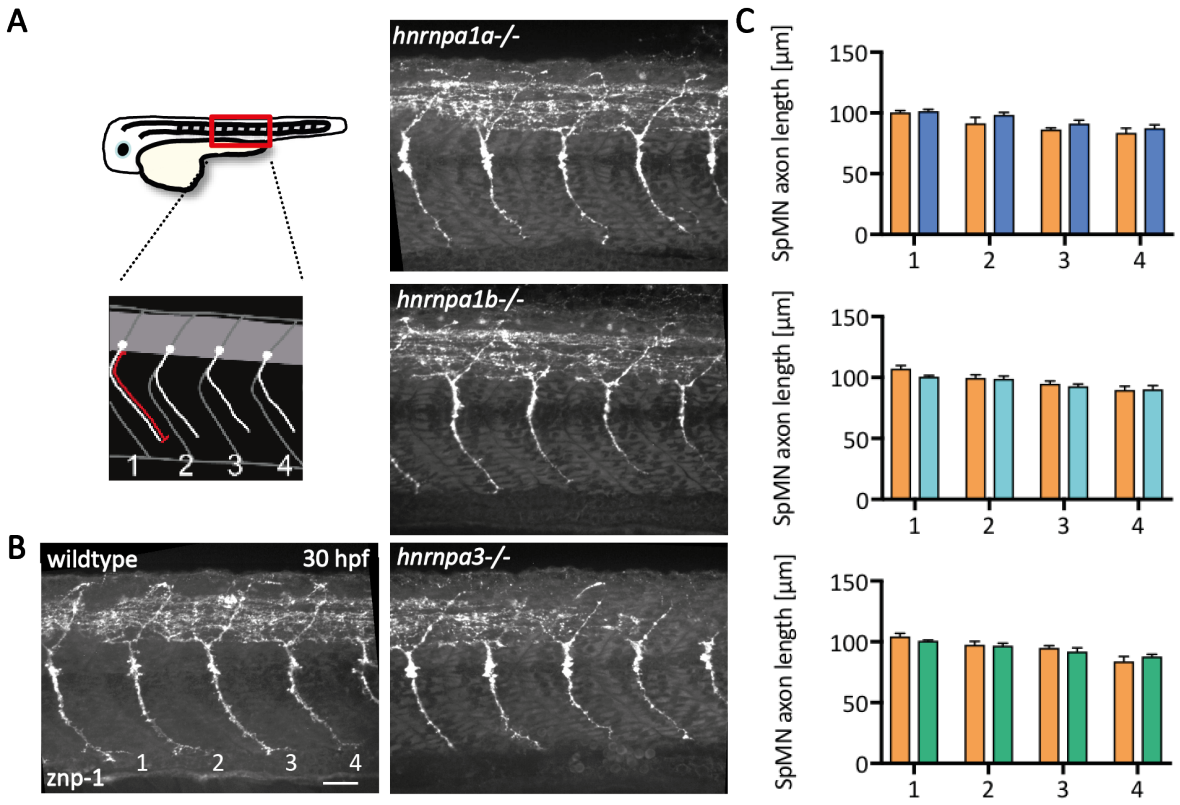


**Figure 3.17 - *hnrnpa*$^{-/-}$ single mutants show normal SpMN axon outgrowth. A:** Schematic illustration of a 30 hpf embryo with the analyzed region in detail (red box). SpMNs and their axons are illustrated in white and the red line marks the measured axon length for SpMN axon 1. Grey: spinal cord. **B:** Examples of whole-mount IF stainings of 30 hpf wildtype, *hnrnpa1a*$^{-/-}$, *hnrnpa1b*$^{-/-}$, and *hnrnpa3*$^{-/-}$ mutants stained with znp-1 antibody. The four SpMN axons anterior to the end of the yolk extension are shown. Images are taken with the spinning disk cell observer. Maximum intensity projection. Lateral view. Anterior to the left. Scale bar: 25 µm **C:** A comparison of the SpMN axon lengths of wildtype (orange), *hnrnpa1a*$^{-/-}$ (turquoise) ($p$(1-4)>0.34, n=7), *hnrnpa1b*$^{-/-}$ (blue) ($p$(1-4)>0.23, n=7), and *hnrnpa3*$^{-/-}$ (green) ($p$(1-4)>0.99, n=7) embryos at 30 hpf revealed no significant difference in the SpMN axon length when compared to wildtype. S.E.M. Two-way ANOVA. Bonferroni post-test.

SpMN were visualized by immunohistochemical staining of 30 hpf old PTU treated embryos using a znp-1 antibody. Quantification of the SpMN axon length of the Cap, which is defined as the length from the ventral side of the spinal cord to the end of the growth cone, revealed

no significant length difference in *hnrnpa1a*$^{-/-}$, *hnrnpa1b*$^{-/-}$ and *hnrnpa3*$^{-/-}$ mutants compared to age matched wildtypes (see Figure 3.17), indicating normal SpMN axon outgrowth in *hnrnpa1a*$^{-/-}$, *hnrnpa1b*$^{-/-}$ and *hnrnpa3*$^{-/-}$ mutants.

### 3.4.2.2 *hnrnpa*$^{-/-}$ single mutants mutants have no muscle defects

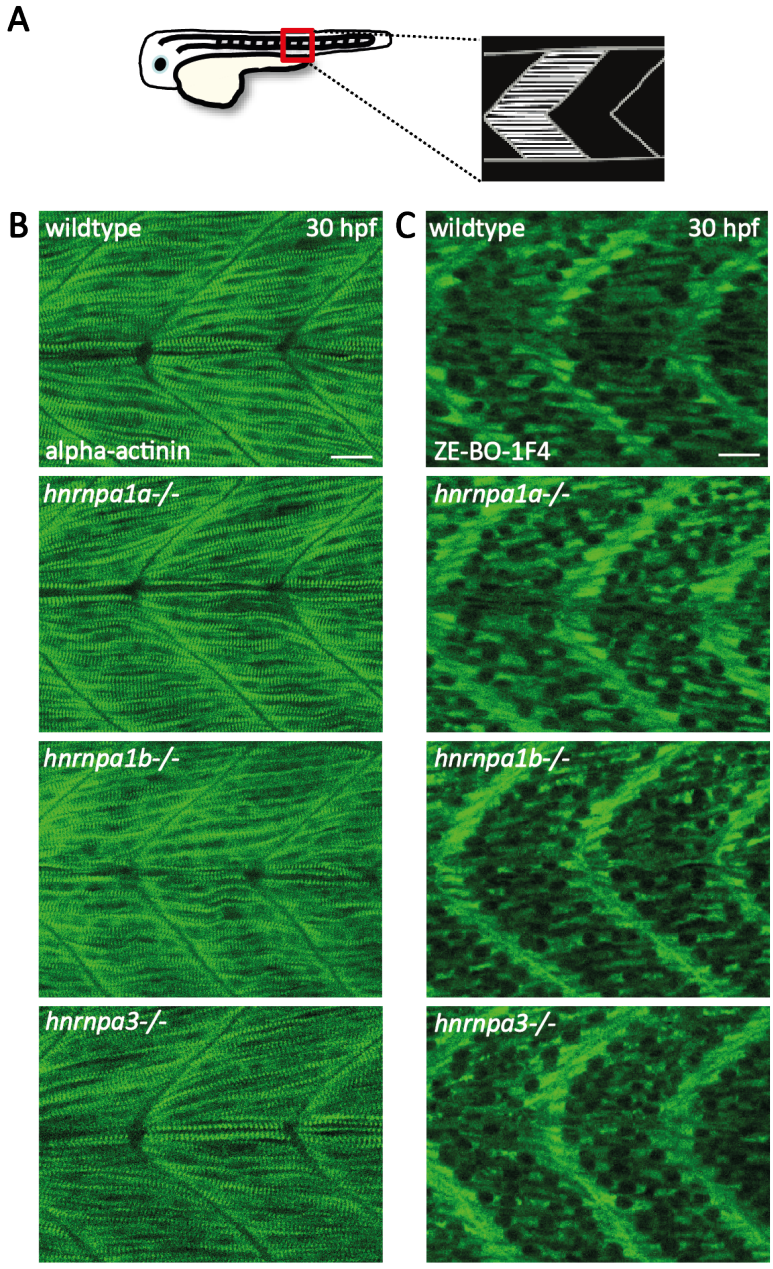


**Figure 3.18 - *hnrnpa*$^{-/-}$ single mutants show no morphological muscle defects A:** Schematic illustration of the assayed region (red box) **B:** Antibody staining of 30 hpf wildtype, *hnrnpa1a*$^{-/-}$, *hnrnpa1b*$_{-/-}$, and *hnrnpa3*$^{-/-}$ mutants with the Actinin specific antibody (green). **C:** Antibody staining of 30 hpf wildtype, *hnrnpa1a*$^{-/-}$, *hnrnpa1b*$^{-/-}$, and *hnrnpa3*$^{-/-}$ embryos with the myosin specific antibody ZE-BO-1F4 (green). **B and C:** Pictures taken by confocal laser scanning microscopy using the 488 nm laser. Lateral view. Anterior to the left. Scale bar represents 25 µm.

To visualize the muscle fibers I performed immunohistochemistry on 30 hpf old PTU treated *hnrnpa1a*$^{-/-}$*; hnrnpa1b*$^{-/-}$ *and hnrnpa3*$^{-/-}$ embryos using α-actinin and ZE-BO 1F4 antibodies. α-actinin is a marker for Z-discs, while ZE-BO 1F4 binds to smooth muscles, striated skeletal and heart muscles (fast-twitch muscle fibers) [213] [195]. *hnrnpa1a*$^{-/-}$*, hnrnpa1b*$^{-/-}$ and *hnrnpa3*$^{-/-}$ mutants showed no difference in muscle patterning using α-actinin (see Figure 3.18B) and ZE-BO 1F4 (Figure 3.18C) antibodies compared to age-matched wildtype embryos. These findings implicate normally developed Z-discs and fast-twitching muscle fibers and that the muscle is morphologically wildtype at 30 hpf in *hnrnpa1a*$^{-/-}$*, hnrnpa1b*$^{-/-}$ and *hnrnpa3*$^{-/-}$ mutants.

### 3.4.3 Tdp-43 variant protein levels are not changed in *hnrnpa*$^{-/-}$ single mutants

The lack of any obvious phenotype in single *hnrnpa1*$^{-/-}$, *hnrnpa1b*$^{-/-}$, and *hnrnpa3*$^{-/-}$ mutants prompted us to investigate potential crossregulation of HNRNP family members. Since TDP-43 is the key aggregating protein in ALS we asked if TDP-43 levels change upon depletion of

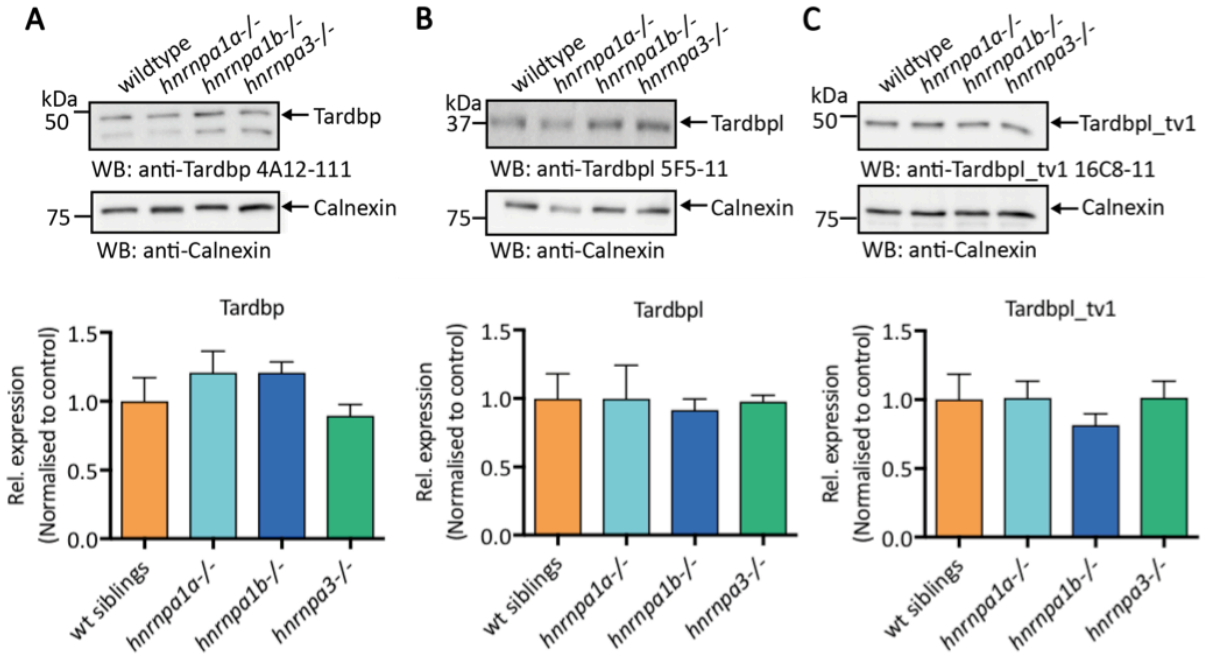


**Figure 3.19 – Tdp-43 variant levels are not changed in brains of *hnrnpa*$^{-/-}$ single mutants A:** Tardbp levels were not changed in *hnrnpa1a*$^{-/-}$ *(p>0.13, n=4)*, *hnrnpa1b*$^{-/-}$ *(p>0.52, n=8),* and *hnrnpa3*$^{-/-}$ *(p>0.51, n=4)* mutants. **B:** Tardbpl levels were not changed in *hnrnpa1a*$^{-/-}$ *(p>0.99, n=8)*, *hnrnpa1b*$^{-/-}$ *(p>0.57, n=4),* and *hnrnpa3*$^{-/-}$ *(p>0.76, n=8) mutants*. **C:** Tardbpl_tv1 levels were not changed in *hnrnpa1a*$^{-/-}$ *(p>0.90, n=8)*, *hnrnpa1b*$^{-/-}$ *(p>0.09; n=8),* and *hnrnpa3*$^{-/-}$ *(p>0.93; n=4)* mutants. Normalized to control. Student's t-test. Error bars indicate S.E.M. Calnexin served as a loading control.

HNRNPA proteins. In order to address this question Tdp-43 protein levels were examined in brain samples derived from *hnrnpa1a*$^{-/-}$, *hnrnpa1b*$^{-/-}$ and *hnrnpa3*$^{-/-}$ mutant zebrafish. In zebrafish two isoforms of TDP-43, named *tardbp* and *tardbpl*, are present. Furthermore, our group and others described another *tdp-43* transcript variant, named *tardbpl_tv1*, which is generated by alternative splicing of *tardbpl* upon tardbp depletion [12]. Our laboratory developed antibodies that specifically detect Tardbp, Tardbpl, and Tardbpl_tv1. Upon usage of these antibodies by immunoblotting no differences in Tardbp, Tardbpl or Tardbpl_tv1 protein levels were observed in *hnrnpa1a*$^{-/-}$, *hnrnpa1b*$^{-/-}$ or *hnrnpa3*$^{-/-}$ brain samples (see Figure 3.19).

It can be concluded that loss of Hnrnpa1a, Hnrnpa1b, or Hnrnpa3 protein function does not affect the protein levels of Tdp-43 in zebrafish.

### 3.4.4 Differentially expressed RNAs in single mutants

In order to identify differentially expressed genes in *hnrnpa1b*$^{-/-}$ and *hnrnpa3*$^{-/-}$ mutants an unbiased approach was chosen by sending *hnrnpa1b*$^{-/-}$ and *hnrnpa3*$^{-/-}$ brains (six months) for RNA sequencing (total RNA including small and noncoding RNAs, paired end, 35 Million reads/sample).

#### 3.4.4.1 Differentially expressed genes in *hnrnpa1b*$^{-/-}$ zebrafish brain

NGS revealed 45 genes with p-value smaller than 0.01 and a positive or negative fold change greater than one between mutants and wildtype siblings. Of these genes 26 were upregulated and 19 were downregulated. *hnrnpa1b* itself is downregulated by 1.23 (*p-adj*.=2.91E-41), supporting the successful KO of *hnrnpa1b* previously shown by Western blot. Interestingly, nine lincRNAs were identified with these settings whereby all of them were upregulated.

| Gene | Ensembl ID | Human Orthologue | $log_2$fold change | p-adjusted |
|---|---|---|---|---|
| *CU929061.1* | ENSDARG00000107933 | n.a. | 5.10 | 8.07E-4 |
| *si:dkey-240n22.3* | ENSDARG00000095013 | n.a. | 3.70 | 1.28E-6 |
| *si:ch211-196h24.2* | ENSDARG00000100341 | n.a. | 3.53 | 1.08E-3 |
| *si:dkey-165o8.1* | ENSDARG00000098369 | n.a. | 2.45 | 4.44E-3 |
| *si:ch211-227e10.1* | ENSDARG00000104968 | n.a. | 2.17 | 1.87E-5 |
| *si:ch211-205a14.1* | ENSDARG00000102713 | n.a. | 2.04 | 3.791E-7 |

| | | | | |
|---|---|---|---|---|
| *cyp2aa6* | ENSDARG00000103590 | n.a. | 1.68 | 4.00E-10 |
| *si:ch211-106j21.2* | ENSDARG00000102575 | n.a. | 1.52 | 4.74E-3 |
| *si:ch211-232d10.2* | ENSDARG00000100348 | n.a. | 1.49 | 1.70E-6 |
| *BX322575.1* | ENSDARG00000095595 | n.a. | 1.42 | 6.13E-3 |
| | | | | |
| *si:dkey-207l24.2* | ENSDARG00000101688 | n.a. | -7.70 | 3.48E-6 |
| *BX649431.1* | ENSDARG00000098522 | n.a. | -7.19 | 5.68E-5 |
| *BX004873.8* | ENSDARG00000108677 | n.a. | -2.91 | 5,38E-7 |
| *N.A.* | ENSDARG00000102102 | n.a. | -2.78 | 1.46E-3 |
| *rnf17* | ENSDARG00000056387 | *RNF17* | -2.50 | 4.85E-6 |
| *si:dkey-14o6.1* | ENSDARG00000098383 | n.a. | -2.44 | 8.90E-4 |
| *BX004873.5* | ENSDARG00000101310 | n.a. | -2.40 | 3.74E-3 |
| *si:dkey-16p6.1* | ENSDARG00000088245 | n.a. | -2.37 | 5.33E-3 |
| *si:dkey-16b10.1* | ENSDARG00000096139 | n.a. | -2.26 | 2.61E-3 |
| *znf1105* | ENSDARG00000104887 | n.a. | -2.09 | 1.78E-05 |

**Table 3.5 –** Top 10 differentially expressed genes and the respective human orthologues in *hnrnpa1b*$^{-/-}$ brains. For zebrafish genes lacking a human orthologue the abbreviation not available (n.a.) is used.

### 3.4.4.2 Differentially expressed genes in *hnrnpa3*$^{-/-}$ zebrafish brain

Upon Hnrnpa3 KO NGS revealed 343 differentially expressed genes with a p-value smaller than 0.01 and a upwards or downwards fold change greater than one between mutants and wildtype siblings. Of these genes 263 are upregulated and 80 downregulated. *hnrnpa3* itself is 1.86 fold downregulated (*p-adj.*=3,50E-29) supporting the successful KO of *hnrnpa1b* previously shown by Western blot. Interestingly, 16 linc RNAs are changed.

| **Gene** | **Ensembl ID** | **Human Orthologue** | **$log_2$fold change** | **p-adjusted** |
|---|---|---|---|---|
| *si:dkey-200c24.1* | ENSDARG00000104305 | n.a. | 9.02 | 2.15E-10 |
| *CR848784.1* | ENSDARG00000096895 | n.a. | 7.96 | 1.45E-7 |
| *myhc4* | ENSDARG00000035438 | MYH1 | 6.63 | 2.64E-3 |
| *CABZ01002522.1* | ENSDARG00000107775 | n.a. | 5.93 | 5.45E-3 |
| *zgc:175177* | ENSDARG00000102296 | n.a. | 3.27 | 2.63E-7 |
| *slc16a5b* | ENSDARG00000102668 | SLC16A5 | 3.21 | 7.31E-9 |

| | | | | |
|---|---|---|---|---|
| *hsp90aa1.1* | ENSDARG00000010478 | HSP90 | 3.03 | 1.56E-3 |
| *FO834829.1* | ENSDARG00000099605 | n.a. | 2.98 | 2.22E-5 |
| *hbaa2* | ENSDARG00000069735 | n.a. | 2.83 | 6.33E-5 |
| *slc6a5* | ENSDARG00000067964 | SLC6A | 2.74 | 2.18E-11 |
| | | | | |
| *N.A.* | ENSDARG00000102915 | HIN2 | -7.06 | 4.72E-6 |
| *BX000534.2* | ENSDARG00000102489 | n.a. | -3.44 | 2.28E-7 |
| *cryabb* | ENSDARG00000101380 | CRYABB | -3.41 | 5.89E-13 |
| *CU856343.1* | ENSDARG00000099073 | n.a. | -2.99 | 5.60E-3 |
| *sesn2* | ENSDARG00000070012 | SESN2 | -2.76 | 1.09E-3 |
| *si:rp71-80o10.4* | ENSDARG00000094316 | n.a. | -2.69 | 1.25E-4 |
| *BX649622.2* | ENSDARG00000105085 | n.a. | -2.54 | 6.41E-05 |
| *slc1a4* | ENSDARG00000000551 | SLC1A4 | -2.16 | 3.60E-3 |
| *mars* | ENSDARG00000034396 | MARS | -2.06 | 8.75E-3 |
| *asns* | ENSDARG00000016375 | ASNS | -2.03 | 3.75E-3 |

**Table 3.6 -** Top 10 differentially expressed genes and the respective human orthologues in *hnrnpa3*$^{-/-}$ brains

### 3.4.5 Hnrnpa1a and Hnrnpa1b compensate for each other loss of function, which is not compensated by Hnrnpa3

Since *hnrnpa1a* and *hnrnpa1b* are duplicated genes and both orthologues of human HNRNPA1 (see Figure 3.2), the lack of a phenotype in single *hnrnpa1a*$^{-/-}$ *and hnrnpa1b*$^{-/-}$ mutant zebrafish could be due to compensational mechanisms. Hnrnpa1b could take over the function of Hnrnpa1a upon Hnrnpa1a KO or vice versa. Alternatively, there could be functional compensation within the larger Hnrnpa family and Hnrnpa3 could take over the function of the Hnrnpa1 proteins. To investigate potential crossregulatory mechanisms, I performed immunoblotting of Hnrnpa1a and Hnrnpa3 on brain samples of the *hnrnpa1a*$^{-/-}$, *hnrnpa1b*$^{-/-}$ and *hnrnpa3*$^{-/-}$ mutants. Due to the lack of a Hnrnpa1a specific antibody, compensation of Hnrnpa1a protein in *hnrnpa1b*$^{-/-}$ and *hnrnpa3*$^{-/-}$ mutants could not be addressed. Instead, *hnrnpa1a* mRNA levels were measured in *hnrnpa1b*$^{-/-}$ and *hnrnpa3*$^{-/-}$ zebrafish brain samples by qRT-PCR. The analysis revealed significant upregulation of *hnrnpa1a* mRNA upon KO of Hnrnpa1b or Hnrnpa3 (see Figure 3.20A). Hnrnpa1b protein levels showed no change in Hnrnpa1a or Hnrnpa3 deficient zebrafish brain samples by immunoblotting (see Figure 3.20B). Interestingly, Hnrnpa1b levels were highly increased in brains derived from *hnrnpa1a*$^{-/-}$ mutants compared to age-matched wildtype (see Figure

3.20B). This upregulation was observed in two independent KO lines, *hnrnpa1a*$^{\Delta 16}$ and *hnrnpa1a*$^{ins10}$ pointing to the specificity of the upregulatory effect (see Figure 3.20B). Immunoblotting for Hnrnpa3 revealed no change in protein levels in brain samples of *hnrnpa1a*$^{-/-}$ or *hnrnpa1b*$^{-/-}$ mutants compared to age matched wildtype (see Figure 3.20C).

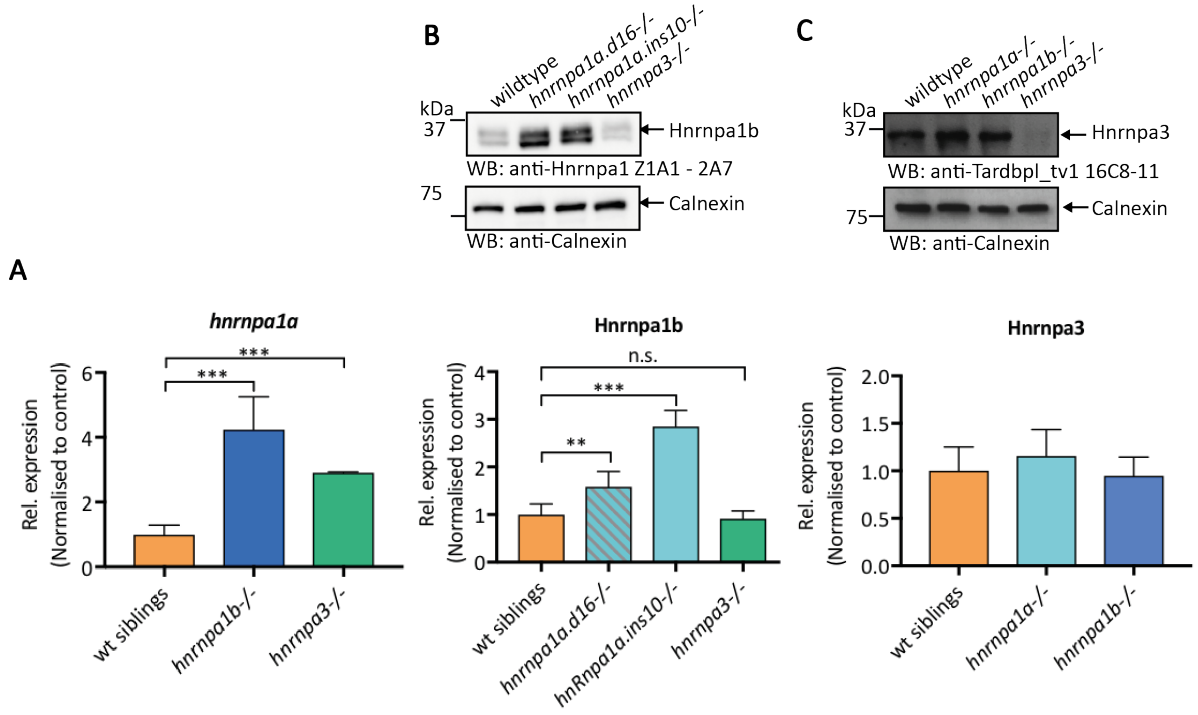


**Figure 3.20 – Hnrnpa1a and Hnrnpa1b compensate for each others loss of function, which is not compensated by Hnrnpa3. A:** mRNA levels of hnrnpa1a were significantly upregulated in brains of *hnrnpa1b*$^{-/-}$ (***$p$<0.001; n=4) and *hnrnpa3*$^{-/-}$ (***$p$<0.001; n=4) mutants. . Normalized to *rflp13a* and *elf1a2*. Error bar indicates SEM. Student's t-test. Results by qRT-PCR were reproduced twice using the same cDNA. **B:** Hnrnpa1b levels were significantly upregulated in brains of *hnrnpa1a* mutants (*hnrnpa1a*$^{\Delta 16-/-}$: ***$p$<0.0001, n=8; *hnrnpa1a*$^{ins10-/-}$: ***$p$<0.0001, n=8) and not changed in brains of *hnrnpa3*$^{-/-}$ mutants ($p$>0.69, n=4) compared to their wildtype siblings. **C:** Hnrnpa3 levels were not changed in brains of *hnrnpa1a*$^{-/-}$ mutants ($p$>1.1, n=8) and *hnrnpa1b*$^{-/-}$ mutants ($p$>0.64, n=8) compared to their wildtype siblings. Student's t-test. Error bars indicate S.E.M. Calnexin served as a loading control.

It can be concluded that Hnrnpa3 protein levels are not changed upon *hnrnpa1a* or *hnrnpa1b* KO. Upon KO of Hnrnpa1a a high increase in Hnrnpa1b protein was observed, which was confirmed in two independent hnrnpa1b KO lines. Vice versa, *hnrnpa1a* mRNA levels were upregulated upon *hnrnpa1b* KO. Moreover, slight *hnrnpa1a* mRNA upregulation was observed upon Hnrnpa3 KO.

## 3.5 Analysis of *hnrnpa1a*$^{-/-}$; *hnrnpa1b*$^{-/-}$ mutants

Hnrnpa1a, Hnrnpa1b, and Hnrnpa3 have multiple functions of which some are overlapping but others are specific to one particular protein. The previous analysis revealed crossregulation among Hnrnpas shown by upregulation of Hnrnpa1b upon loss of Hnrnpa1a protein and vice versa. While Hnrnpa3 protein levels were not changed upon Hnrnpa1a or Hnrnpa1b loss of function, Hnrnpa1b was slightly upregulated upon Hnrnpa3 loss of function. In order to address potential Hnrnpa redundancy and functional compensation in single KO, I generated double KO fish.

### 3.5.1 *hnrnpa1a*$^{-/-}$; *hnrnpa3*$^{-/-}$ and *hnrnpa1b*$^{-/-}$; *hnrnpa3*$^{-/-}$ mutants are viable

Double homozygous KO fish obtained from a homozygous *hnrnpa1a*$^{-/-}$; *hnrnpa3*$^{-/-}$ or *hnrnpa1b*$^{-/-}$; *hnrnpa3*$^{-/-}$ incross were viable and did not show any obvious morphological phenotype (see Figure 3.21). Also, these fish reached adulthood and showed Mendelian inheritance pattern (data not shown).

It can be concluded that combined loss of Hnrnpa1a or Hnrnpa1b and Hnrnpa3 protein function does not result in obvious morphological abnormalities in zebrafish. This result points to either non-essential functions of these proteins or further redundancy in the zebrafish genome.

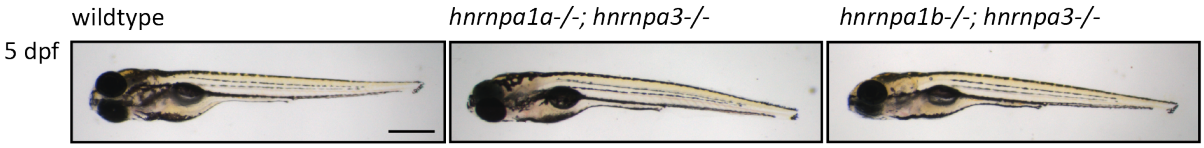


**Figure 3.21 - *hnrnpa1a*$^{-/-}$; *hnrnpa3*$^{-/-}$ and *hnrnpa1b*$^{-/-}$; *hnrnpa3*$^{-/-}$ mutants show no obvious morphological phenotype.** Representative images of 5 dpf old wildtype, *hnrnpa1a*$^{-/-}$; *hnrnpa3*$^{-/-}$, and *hnrnpa1b*$^{-/-}$; *hnrnpa3*$^{-/-}$ embryos. Lateral view. Anterior to the left. Images were taken Axio Scope A1. Scalebar represents 500 µm.

### 3.5.2 *hnrnpa1a*$^{-/-}$; *hnrnpa1b*$^{-/-}$ mutants are not viable

Interestingly, no adult *hnrnpa1a*$^{-/-}$; *hnrnpa1b*$^{-/-}$ fish were obtained from an incross of *hnrnpa1a*$^{+/-}$; *hnrnpa1b*$^{+/-}$ mutant fish. The Mendelian ratios obtained from genotyping adult offspring from this incross show that all possible genotypes are present in the expected ratio apart from *hnrnpa1a*$^{-/-}$; *hnrnpa1b*$^{-/-}$ fish, of which no fish was obtained (see Table 3.7). To address the question whether *hnrnpa1a*$^{-/-}$; *hnrnpa1b*$^{-/-}$ fish die while breeding them to adulthood, or as embryos until they are transferred to the breeding system at 5 dpf, or whether

| **Incross of *hnrnpa1a* $^{+/-}$; *hnrnpa1b* $^{+/-}$**, (n=4) | | | | | | | | | |
|---|---|---|---|---|---|---|---|---|---|
| Genotype | $a^{+/+}$ ; $b^{+/+}$ | $a^{+/-}$ ;$b^{+/+}$ | $a^{+/+}$; ;$b^{+/-}$ | $a^{+/-}$ ;$b^{+/-}$ | $a^{-/-}$ ;$b^{+/+}$ | $a^{+/+}$ ;$b^{-/-}$ | $a^{-/-}$ ;$b^{+/-}$ | $a^{+/-}$ ;$b^{-/-}$ | $a^{-/-}$ ;$b^{-/-}$ |
| Examined Ratio (%, s.d.) | 3.92 ± 0.01 | 13.30 ± 0.03 | 13.71 ± 0.03 | 33.38 ± 0.03 | 7.70 ±0.01 | 4.94 ± 0.02 | 10.33 ± 0.06 | 12.73 ± 0.05 | 0 |
| Expected ratio (%) | 6.25 | 12.5 | 12.5 | 25 | 6.25 | 6.25 | 12.5 | 12.5 | 6.25 |

**Table 3.7 - *hnrnpa1a*$^{-/-}$; *hnrnpa1b*$^{-/-}$ mutants do not reach adulthood.** Clutch number of minimum 40 eggs. n=number of clutches analyzed.

they are not even born, offspring obtained from a *hnrnpa1a*$^{+/-}$; *hnrnpa1b*$^{+/-}$ incross were genotyped at 2 dpf. At this point all genotypes were present in the expected ratios (data not shown) showing that *hnrnpa1a*$^{-/-}$; *hnrnpa1b*$^{-/-}$ mutants are born but die before reaching adulthood (see Table 3.7). Careful analysis of newborn embryos obtained from a *hnrnpa1a*$^{+/-}$; *hnrnpa1b*$^{+/-}$ incross from 0 hpf until 5 dpf showed that some embryos have reduced blood flow, a thinned yolk extension, cell death, and develop severe heart edema at 4 dpf until they die at around 5 dpf (see Figure 3.22). Those embryos were present at the expected ratio of around 6.25% pointing towards loss of both Hnrnpa1a and Hnrnpa1b causing the morphological abnormalities. This was confirmed by genotyping the phenotypic embryos from the clutch.

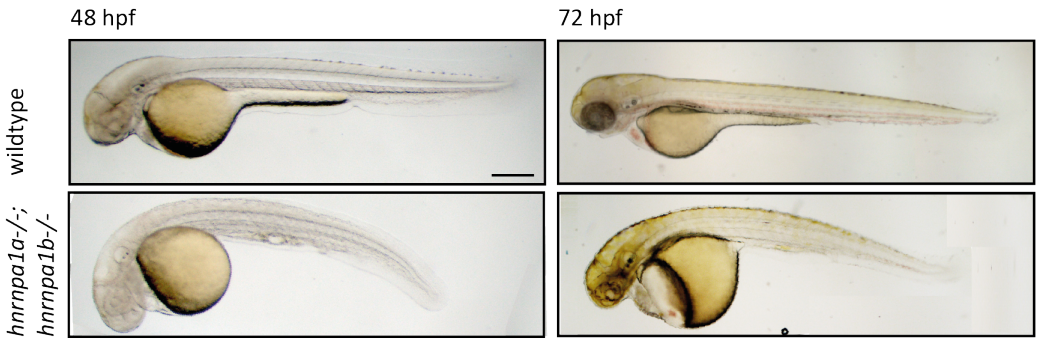


**Figure 3.22 - *hnrnpa1a*$^{-/-}$; hnrnpa1b$^{-/-}$ mutants are embryonically lethal and show blood circulation defects.** After 48 hpf *hnrnpa1a*$^{-/-}$; *hnrnpa1b*$^{-/-}$ mutants show reduced blood flow and a thinned yolk extension (left panel). After 72 hpf *hnrnpa1a*$^{-/-}$; *hnrnpa1b*$^{-/-}$ mutants develop severe heart edema (right panel). Scalebar represents 200 µm.

### 3.5.2.1 *hnrnpa1a*$^{-/-}$*; hnrnpa1b*$^{-/-}$ mutants are full loss of protein function mutants

While no antibody is available that specifically detects Hnrnpa1a, full protein loss of function in *hnrnpa1a*$^{-/-}$*; hrnnpa1b*$^{-/-}$ mutants was assessed by immunoblot with an antibody that detects

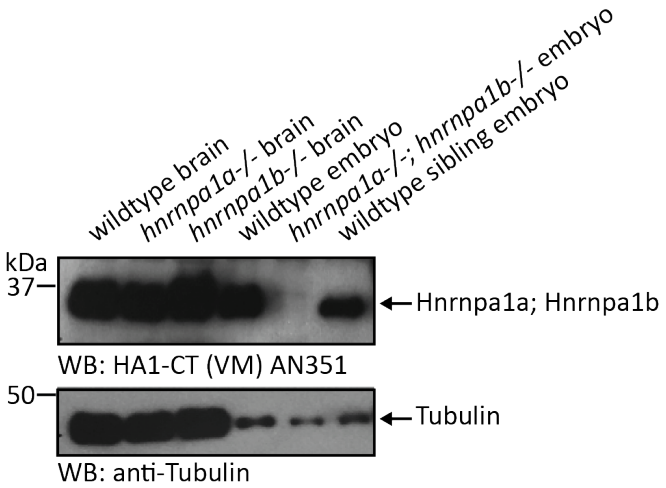


**Figure 3.23 - *hnrnpa1a*$^{-/-}$*; hnrnpa1b*$^{-/-}$ mutants are loss of protein mutants.** The antibody HA1-CT (VM) AN351 detects Hnrnpa1a and Hnrnpa1b since a band at the expected size of Hnrnpa1a and Hnrnpa1b appears in wildtype, *hnrnpa1a*$^{-/-}$ and *hnrnpa1b*$^{-/-}$ zebrafish brains. Slight upregulation of Hnrnpa1b in *hnrnpa1a*$^{-/-}$ mutants is also detected as previously observed. No band appears at the expected size in *hnrnpa1a*$^{-/-}$*, hnrnpa1b*$^{-/-}$ embryos. Tubulin serves as a loading control.

Hnrnpa1 and Hnrnpa1b (kind gift from Julia Nikolic, Douglas black lab). Immunoblotting showed a band at the expected size on brain samples obtained from Hnrnpa1a and Hnrnpa1b single KO showing that the antibody detects both proteins. Moreover, the antibody could detect Hnrnpa1a and Hnrnpa1b in 30 hpf wildtype embryos and can hence be used already in early developmental stages. No band was detected in *hnrnpa1a*$^{-/-}$*; hrnnpa1b*$^{-/-}$ whole embryo samples demonstrating loss of Hnrnpa1a and Hnrnpa1b protein in the double mutants (see Figure 3.23). Concluding, it was shown that *hnrnpa1a*$^{-/-}$*; hrnnpa1b*$^{-/-}$ mutants do not express Hnrnpa1a or Hnrnpa1b protein and are thereby full double protein loss of function mutants. In combination with the phenotypic analysis of these mutants, this finding further shows that loss of these two proteins leads to the observed phenotypes.

### 3.5.2.2 Further characterization of *hnrnpa1a*$^{-/-}$*; hnrnpa1b*$^{-/-}$ mutants

*hnrnpa1a*$^{-/-}$*; hnrnpa1b*$^{-/-}$ mutants are not viable and die around 5 dpf with a severe heart edema. The cellular abnormalities causing premature death are though unknown. For further analysis I focused on the difference of morphologically affected *hnrnpa1a*$^{-/-}$*; hnrnpa1b*$^{-/-}$

mutants and morphologically wildtype looking siblings, obtained from an *hnrnpa1a*$^{+/-}$; *hnrnpa1b*$^{-/-}$ incross. *hnrnpa1a*$^{-/-}$; *hnrnpa1b*$^{-/-}$ mutant embryos become first distinguishable from their wildtype looking siblings at 30 hpf. At this point wildtype looking embryos start to have blood flow, whereas *hnrnpa1a*$^{-/-}$; *hnrnpa1b*$^{-/-}$ mutants do not have developed blood flow yet (data not shown). Furthermore, *hnrnpa1a*$^{-/-}$; *hnrnpa1b*$^{-/-}$ mutants have a thinned yolk extension (see Figure 3.27A), whereas wildtype looking embryos have a healthy looking yolk extension with a roundish shape. Lastly, apoptotic tissue can be observed in the entire body in *hnrnpa1a*$^{-/-}$; *hnrnpa1b*$^{-/-}$ mutants (data not shown). The phenotype is progressive and accompanied by secondary effects due to advanced cell death (data not shown). In order to minimize secondary morphological and cellular phenotypes, the timepoint at 30 hpf when *hnrnpa1a*$^{-/-}$; *hnrnpa1b*$^{-/-}$ mutants can be firstly morphologically distinguished from their siblings, was chosen for further analysis. Three criteria were developed to reproducibly identify *hnrnpa1a*$^{-/-}$; *hnrnpa1b*$^{-/-}$ mutants and to minimize missorting. The criteria are the following: absence of blood flow, thinned yolk extension, and indication of cell death.

*3.5.2.2.1 hnrnpa1a*$^{-/-}$; *hnrnpa1b*$^{-/-}$ mutants are developmentally delayed

Several points of evidence suggest involvement of Hnrnpa1 in development [214] [162]. The developmental stage of the embryos was assessed using the head-trunk angle that was firstly described by Kimmel et al. [198]. The head trunk angle is assessed by drawing a line through the middle of the ear and the eye, and a second line from the middle of the ear to the point where the yolk extension grows out from the yolk (see Figure 3.24A). The head-trunk angle increases throughout development between 20 hpf and 70 hpf as a consequence of morphogenesis of the embryo. Upon identification of the head-trunk angle a specific developmental stage can be determined given that the embryos were kept at 28.5° [198]. At 30 hpf the head-trunk angle accounts 90° under normal conditions and was averaged at 86° in age matched wildtype, and 81° in *hnrnpa1a*$^{-/-}$; *hnrnpa1b*$^{-/-}$ mutants. At 48 hpf the head-trunk angle accounts 138° under normal conditions and was averaged at 139° in wildtype controls and 121° in *hnrnpa1a*$^{-/-}$; *hnrnpa1b*$^{-/-}$ mutants (see Figure 3.24B). At both time points the angle was significantly smaller *hnrnpa1a*$^{-/-}$; *hnrnpa1b*$^{-/-}$ mutants than in age matched controls pointing to developmental delay of *hnrnpa1a*$^{-/-}$; *hnrnpa1b*$^{-/-}$ mutants (see Figure 3.24D). Developmental delay in *hnrnpa1a*$^{-/-}$; *hnrnpa1b*$^{-/-}$ mutants is further evidenced by a delay in melanin pigmentation (see Figure 3.24B).

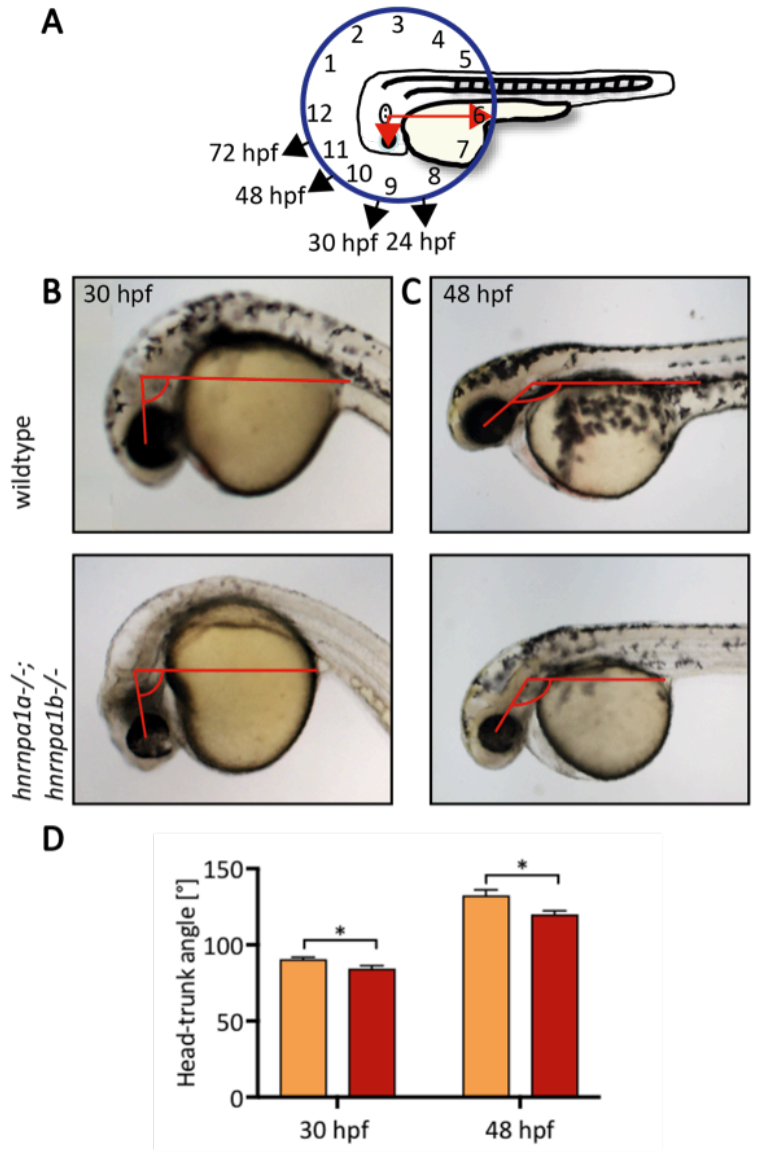


**Figure 3.24 - *hnrnpa1a*$^{-/-}$*; hnrnpa1b*$^{-/-}$ mutants are developmentally delayed. A:** Schematic illustration of the head-trunk angle and its dependency on developmental stage. **B:** At 30 hpf the head angle of wildtype embryos was measured at 86° and for *hnrnpa1a*$^{-/-}$*; hnrnpa1b*$^{-/-}$ mutants at 81°. The reference angle at 30 hpf is 90°. **C:** At 48 hpf the head angle of wildtype embryos was measured at 139° and for *hnrnpa1a*$^{-/-}$*; hnrnpa1b*$^{-/-}$ mutants at 121°. The reference angle at 48 hpf is 138°. Lateral view. Anterior to the left. Images taken by Axio Scope A1 microscope. **D:** The head trunk angle is significantly smaller in *hnrnpa1a*$^{-/-}$*; hnrnpa1b*$^{-/-}$ mutants at 30 hpf ($p$<0.02; n=6) and 48 hpf ($p$<0.02; n=6) compared to age matched wildtype. Student's t-test. Error bar indicates S.E.M.

### *3.5.2.2.2. hnrnpa1a*$^{-/-}$*; hnrnpa1b*$^{-/-}$ mutants have shortened SpMN axon length

SpMN of *hnrnpa1a*$^{-/-}$*; hnrnpa1b*$^{-/-}$ mutants were visualized as previously described for single KOs (see section 3.4.2.1). The SpMN axonal length was measured and quantification revealed that *hnrnpa1a*$^{-/-}$*; hnrnpa1b*$^{-/-}$ mutants have significantly shorter SpMN axons (see

Figure 3.25). However, no abnormal migration pattern or aberrant branching was observed in *hnrnpa1a*$^{-/-}$*; hnrnpa1b*$^{-/-}$ mutants.

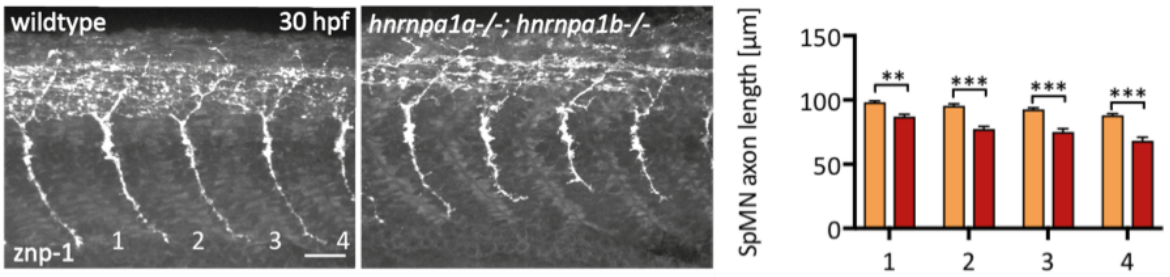


**Figure 3.25 - *hnrnpa1a*$^{-/-}$*; hnrnpa1b*$^{-/-}$ mutants show impaired SpMN axon outgrowth.** Examples of whole-mount IF stainings of 30 hpf wildtype and *hnrnpa1a*$^{-/-}$; *hnrnpa1b*$^{-/-}$ embryos stained with znp-1 antibody. The four SpMN axons anterior to the end of the yolk extension are shown. Images are taken with the spinning disk cell observer. Maximum intensity projection. Lateral view. Anterior to the left. Scale bar: 25 µm. A comparison of the SpMN axon lengths of wildtype (orange) and *hnrnpa1a*$^{-/-}$*; hnrnpa1b*$^{-/-}$ mutants (red) at 30 hpf revealed reduced SpMN axon outgrowth in *hnrnpa1a*$^{-/-}$*; hnrnpa1b*$^{-/-}$ mutants (***p*(1)<0.001; ****p*(2-4)<0.0001; n=16;. Error bar indicates S.E.M. Two-way ANOVA. Bonferroni post-test.

### *3.5.2.2.3 hnrnpa1a*$^{-/-}$*; hnrnpa1b*$^{-/-}$ mutants show muscle defects

Muscle integrity of *hnrnpa1a*$^{-/-}$*; hnrnpa1b*$^{-/-}$ embryos was analyzed since muscle degeneration is a pathological hallmark of ALS [40]. Muscle fibers of *hnrnpa1a*$^{-/-}$*; hnrnpa1b*$^{-/-}$ mutants

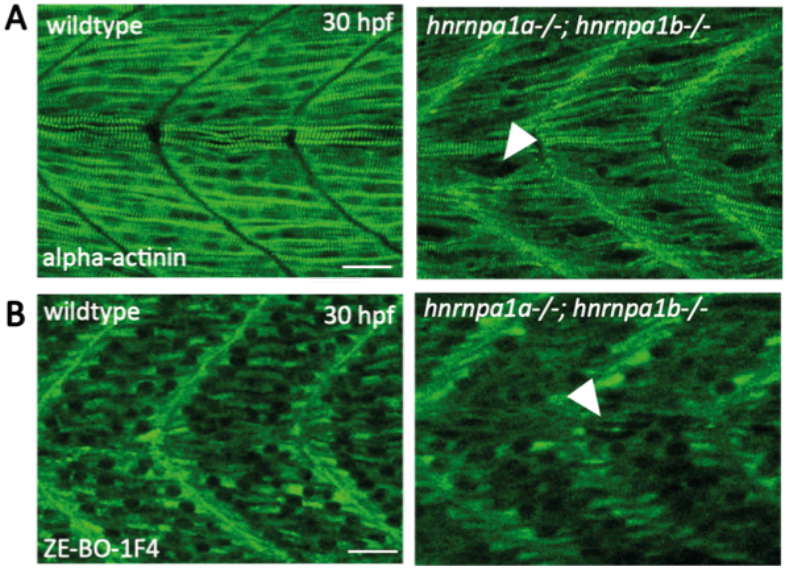


**Figure 3.26 - *hnrnpa1a*$^{-/-}$; *hnrnpa1b*$^{-/-}$ mutants show morphological muscle defects A:** Antibody staining of 30 hpf wildtype and *hnrnpa1a*$^{-/-}$; *hnrnpa1b*$_{-/-}$ mutants with the α-actinin specific antibody (green). **B:** Antibody staining of 30 hpf wildtype and *hnrnpa1a*$^{-/-}$; *hnrnpa1b*$^{-/-}$ mutants with the myosin specific antibody ZE-BO-1F4 (green). **A and B:** White arrow indicates areas that show loss of muscle integrity. Pictures taken by confocal laser-scanning microscopy using the 488 nm laser. Lateral view. Anterior to the left. Scale bar represents 25 µm.

were visualized as described in section 3.4.2.2. Loss of muscle integrity can be observed at 30 hpf at variable sites of the trunk. Immunohistochemical analysis with the α-actinin antibody and the myosin specific antibody ZE-BO-1F4 shows defects in muscle integrity (see Figure 3.26). From the actin staining it becomes evident that the thin filaments in fast muscle fibers are disorganized. Likewise the thick muscle filaments in fast muscle fibers stained by the myosin specific antibody are disarrayed.

*3.5.2.2.4 hnrnpa1a$^{-/-}$; hnrnpa1b$^{-/-}$* mutants have yolk extension and lipid uptake defects

A prominent feature of the *hnrnpa1a$^{-/-}$; hnrnpa1b$^{-/-}$* mutants is the abnormally thinning yolk extension during development This phenotype becomes first detectable at 24 hpf as the yolk

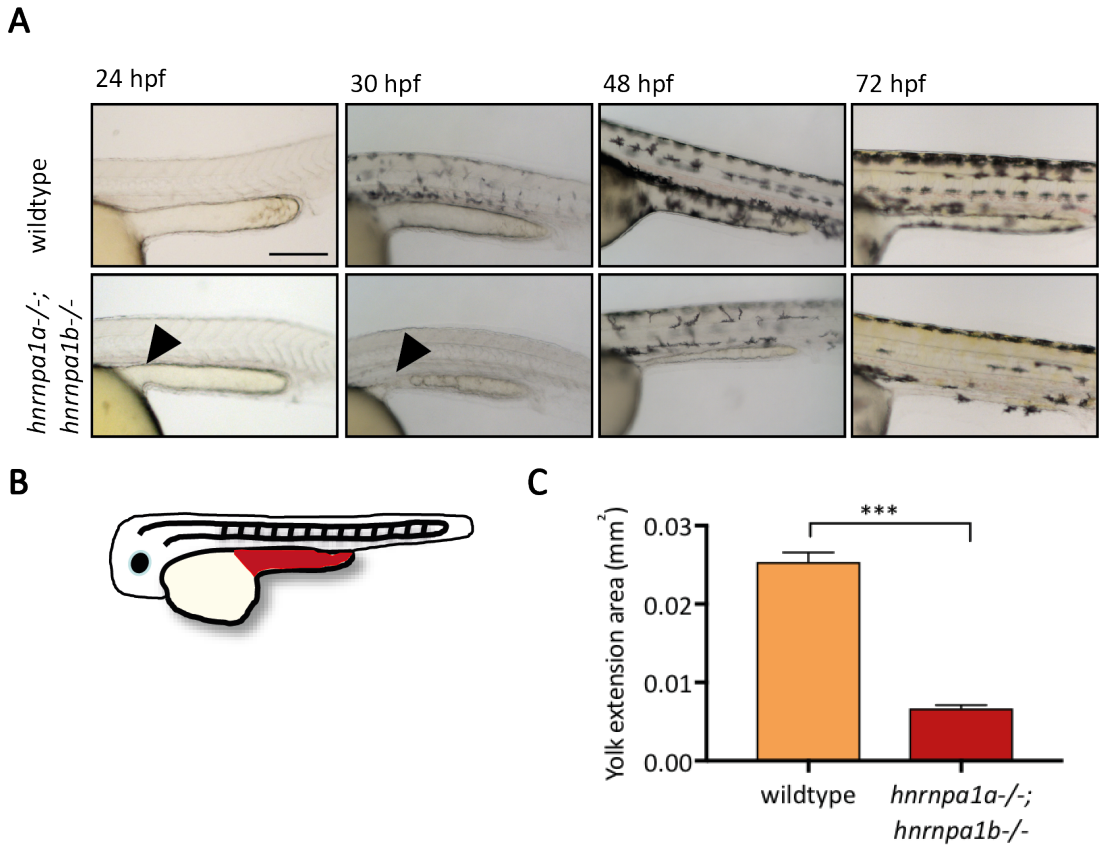


**Figure 3.27 - *hnrnpa1a$^{-/-}$; hnrnpa1b$^{-/-}$* mutants have a thinned yolk extension. A:** Images of wildtype (upper panel) and *hnrnpa1a$^{-/-}$; hnrnpa1b$^{-/-}$* (lower panel) mutants at 24 hpf, 30 hpf, and 48 hpf. At 24 hpf *hnrnpa1a$^{-/-}$; hnrnpa1b$^{-/-}$* mutants can be hardly distinguished from their wildtype siblings apart from a small bulge in the yolk extension. After 30 hpf the yolk extension of *hnrnpa1a$^{-/-}$; hnrnpa1b$^{-/-}$* embryos starts to thin, which becomes more severe over time resulting in an severely reduced yolk extension after 48 hpf up to 72 hpf. Lateral view. Anterior to the left. Images were taken with Axio Scope A1. Scalebar represents 200 µm. **B:** Schematic illustration of the measured area of the yolk extension (indicated in red) at 30 hpf. **C:** Quantification of the two-dimensional yolk extension area at 30 hpf shows significant reduction in yolk extension area in *hnrnpa1a$^{-/-}$; hnrnpa1b$^{-/-}$* mutants compared to wildtype. Student's t-test (n=13; ***p<0.0001). Error bars indicate S.E.M.

extension shows a small bulge at the site where it connects to the yolk. Over time (30 hpf to 48 hpf) the yolk extension becomes thinner until it is almost completely absent at 72 hpf (see Figure 3.27A). Quantification of two-dimensional area of the yolk extension (see Figure 3.27B) revealed a significant reduction in size in 30 hpf *hnrnpa1a*$^{-/-}$*; hnrnpa1b*$^{-/-}$ mutants (see Figure 3.27C). In order to assess a potential lipid phenotype in further detail ORO staining, which labels neutral lipids, was performed. Upon staining neutral fat distribution can be detected. ORO stain was detectable in the wildtype embryos in the yolk, the yolk extension, and the head. This lipid staining pattern correlates with previously reported ORO staining [215]. In contrast, in the *hnrnpa1a*$^{-/-}$*; hnrnpa1b*$^{-/-}$ mutants strikingly lower levels of lipid were detected in the yolk extension. Additionally, more neutral lipid staining appeared to be present in the embryo`s body (see Figure 3.28).

It can be concluded that loss of Hnrnpa1 leads to thinning of the yolk extension, which initiates at 24 hpf and becomes more severe during development. Also, neutral lipids are detected more prominently in the body compared to age matched wildtype embryos.

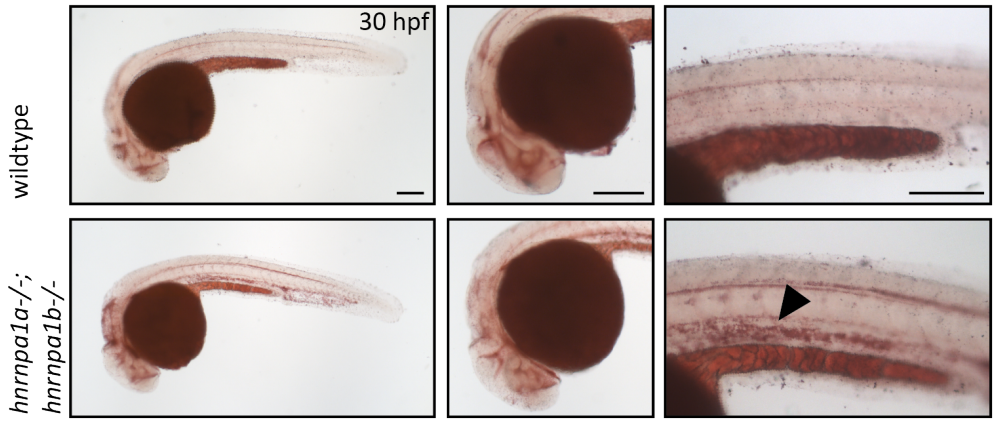


**Figure 3.28 - *hnrnpa1a*$^{-/-}$*; hnrnpa1b*$^{-/-}$ mutants show altered neutral lipid distribution.** ORO stained the head structures, the yolk, yolk extension and around the spinal cord. Reduced amounts of neutral lipids in the yolk extension are present in *hnrnpa1a*$^{-/-}$*; hnrnpa1b*$^{-/-}$ mutants at 30 hpf. Additionally, *hnrnpa1a*$^{-/-}$*; hnrnpa1b*$^{-/-}$ mutants show increased amounts of neutral lipid in the trunk (black arrow). Lateral view. Anterior to the left. Images were taken with Axio Scope A1 microscope. Scalebar represents 200 µm.

### *3.5.2.2.5 hnrnpa1a*$^{-/-}$*; hnrnpa1b*$^{-/-}$ mutants show no alteration in *pkma* splicing

The yolk sac extension thinning and the increased uptake of neutral lipids from the yolk extension to the zebrafish trunk point to misregulated metabolic pathways, such as fatty acid (FA) and amino acid metabolism. As a potential molecular candidate responsible for this phenotype we tested Pyruvate kinase muscle 2 (PKM2), which is a limiting glycolytic enzyme that catalyzes the final step in glycolysis. This protein is not only involved in tumor

metabolism and growth, which could explain the potential metabolic phenotype in *hnrnpa1a*$^{-/-}$ ; *hnrnpa1b*$^{-/-}$ mutants, but it was also previously shown that HNRNPA1 and HNRNPA2/B1 bind and control *PKM1* alternative splicing giving rise to *PKM1* and *PKM2* [216] [217].

In human *PKM1* is mainly expressed in adult tissues, while *PKM2* is expressed in embryonic and adult tissues and is also enriched in many cancers . PKM1 is predominantly active and expressed in terminally differentiated tissues, which require a large supply of ATP. In contrast, PKM2 is expressed in proliferating cells, which have anabolic function. In zebrafish two isoforms exist, *pkma202* and *pkma201*, which were identified to have high conservation in gene structure with human *PKM1* and *PKM2* isoforms, respectively [219]. The zebrafish *pkma202* and *pkma201* isoforms share the mutually exclusive exons 10 and 11 with the human *PKM1* and *PKM2*, which have mutually exclusive exons 9 and 10 (see Figure 3.29A). Semiquantitative PCR was performed on *hnrnpa1a*$^{-/-}$; *hnrnpa1b*$^{-/-}$ mutants and wildtype siblings to amplify *pkma* exon 202 and exon 203. No significant difference in expression of the two transcripts was detected upon Hnrnpa1 KO (see Figure 3.29B+C).

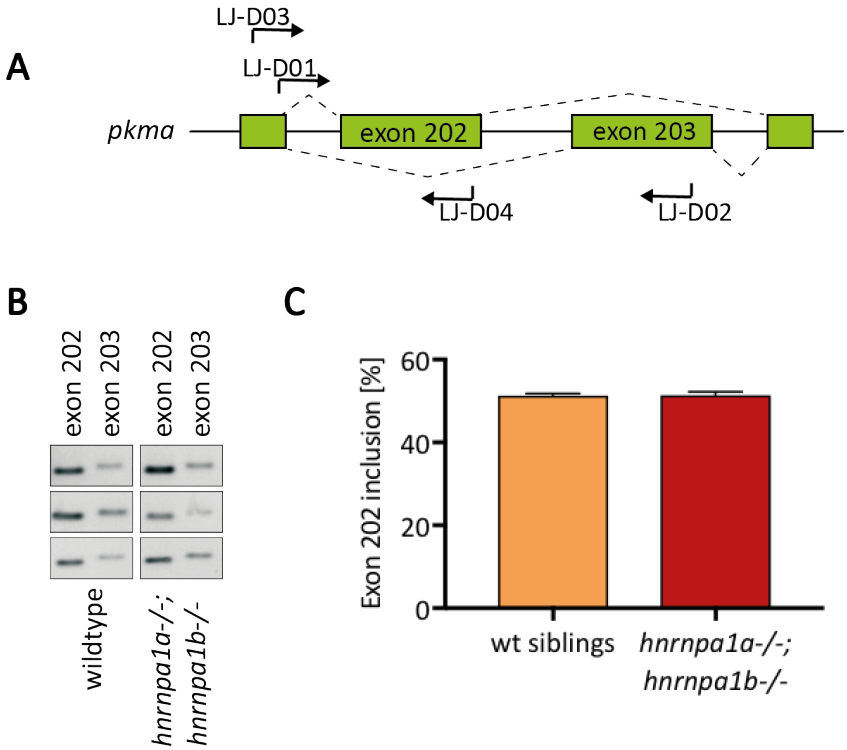


**Figure 3.29 - *hnrnpa1a*$^{-/-}$; *hnrnpa1b*$^{-/-}$ mutants show no alteration in *pkma* splicing. A:** Schematic illustration of alternative splicing pattern of *pkma* exon 202 (Primer pair: LJ-D03 + LJ-D04) and exon 203 (Primer pair: LJ-D01 + LJ-D02) usage. **B:** Semiquantitative PCR products produced by exon 202 and exon 203 specific primer on cDNA of 30 hpf *hnrnpa1a*$^{-/-}$; *hnrnpa1b*$^{-/-}$ mutants and wildtype siblings. **C:** *pkma* exon 202 inclusion was not changed in *hnrnpa1a*$^{-/-}$; *hnrnpa1b*$^{-/-}$ mutants compared to their wildtype siblings ($p$>0.78, n=4). Student's t-test. Error bars indicate S.E.M. Pools of 20 embryos of independent clutches at 30 hpf were used.

One can conclude that the mechanism whereby HNRNPA1 controls the splicing of *PKM1* is not conserved in zebrafish as depletion of Hnrnpa1 does not have an effect on the alternative splicing of *pkma* exon 10 or 11 of in zebrafish.

*3.5.2.2.6 hnrnpa1a$^{-/-}$; hnrnpa1b$^{-/-}$* mutants show increased cell death

Death of the upper and lower motoneurons is the ultimate cause for muscle wasting, muscle weakness, and aberrant motor unit activity in ALS patients [40]. Given the shortened SpMN axon length, the muscle impairment, and the lethality of the *hnrnpa1a$^{-/-}$; hnrnpa1b$^{-/-}$* mutants, I assayed for cell death via the incorporation of the DNA intercalating dye Acridine Orange, which marks apoptotic and necrotic cells and serves as a marker to detect cell death in zebrafish *in vivo* [202]. The dye was applied at 30 hpf. The spinal cord was imaged and the Acridine Orange positive cells in this region were counted using Fiji. Quantification identified a significantly increased number of Acridine Orange stained cells in *hnrnpa1a$^{-/-}$, hnrnpa1b$^{-/-}$* mutants compared to wildtype (see Figure 3.30).

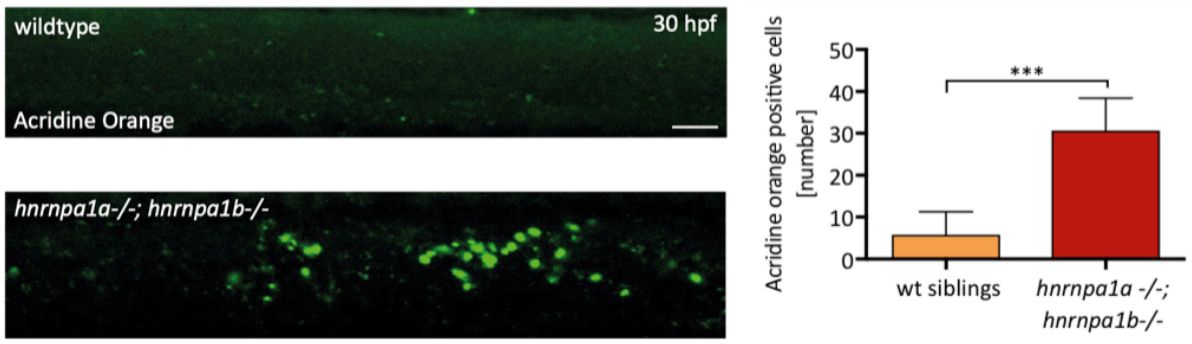


**Figure 3.30 - *hnrnpa1a$^{-/-}$; hnrnpa1b$^{-/-}$* mutants show increased cell death in the spinal cord.** Images of wildtype and *hnrnpa1a$^{-/-}$; hnrnpa1b$^{-/-}$* mutants stained with Acridine Orange (green), which is taken up by apoptotic and necrotic cells (only part of the spinal cord is shown). Lateral view. Anterior to the left. Maximum intensity projection of stacks of ten 0.9 µm images. Images were taken with laser scanning confocal microscope using the 488 nm laser. Quantification of Acridine Orange positive cells within the spinal cord of wildtype and *hnrnpa1a$^{-/-}$; hnrnpa1b$^{-/-}$* mutants. Number of Acridine Orange positive cells is significantly increased in *hnrnpa1a$^{-/-}$; hnrnpa1b$^{-/-}$* mutants. Error bars indicate S.E.M; n=9 embryos per experiment; ***p<0.0001; Student's-t-test. Scalebar represents 40 µm.

It can be concluded that loss of Hnrnpa1 increases cell death in the spinal cord illustrated by an increased number of Acridine Orange stained cells. This provides further evidence for neuronal cell death, which could explain the shortened SpMN axons in the *hnrnpa1a$^{-/-}$; hnrnpa1b$^{-/-}$* mutants. Furthermore, the high levels of cell death may be the cause of the ultimate lethality of the *hnrnpa1a$^{-/-}$; hnrnpa1b$^{-/-}$* mutants.

*3.5.2.2.7 hnrnpa1a$^{-/-}$; hnrnpa1b$^{-/-}$* mutants show vascular mispatterning

Some ALS patients were described to show signs of dysfunctional circulation effects like hypoperfusion [220] [221]. Moreover, *tardbp$^{-/-}$; tardbpl$^{-/-}$* mutants display vascular mispatterning.

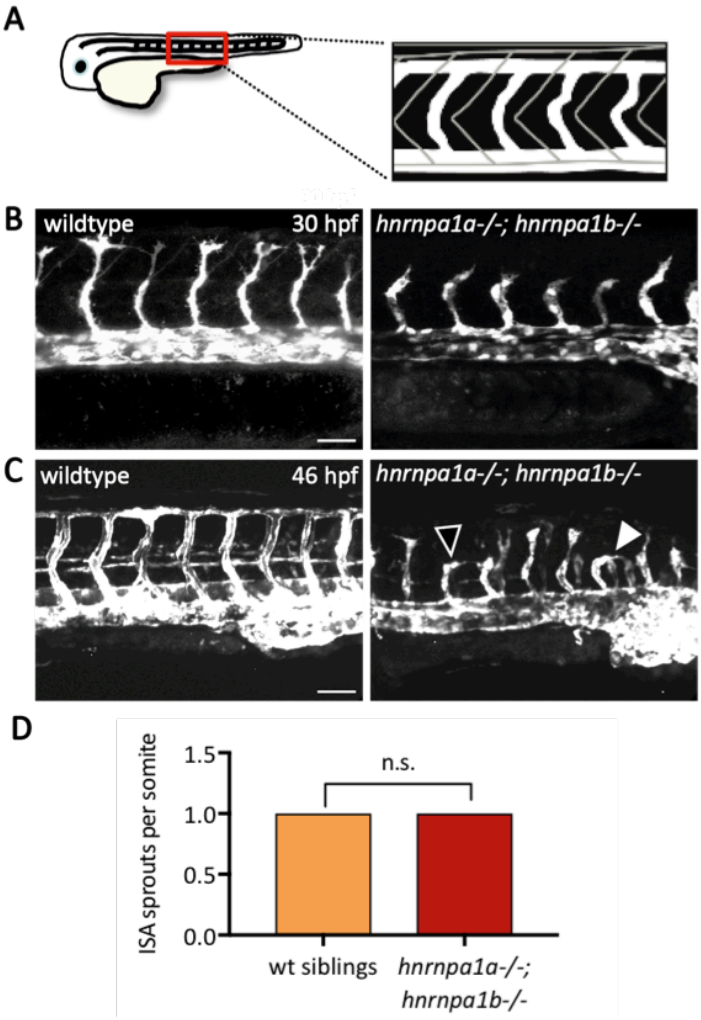


**Figure 3.31 - *hnrnpa1a$^{-/-}$; hnrnpa1b$^{-/-}$* mutants show vascular outgrowth delay and mispatterning.** Representative whole mount images of single wildtype and *hnrnpa1a$^{-/-}$; hnrnpa1b$^{-/-}$* mutants. The shown embryos are Tg(fli1a:EGFP) highlighting the vasculature. The area dorsal of the yolk sack extension is displayed. **A:** Schematic illustration of the assayed region (red box) **B:** At 30 hpf the *hnrnpa1a$^{-/-}$; hnrnpa1b$^{-/-}$* mutants display reduced length of intersomitic vessels compared to their wildtype siblings but the correct number of sprouts is formed. Scale bar represents 25 µm. Anterior to the left. Lateral view. Maximum intensity projection. Images were taken with cell observer spinning disc microscope **C:** At 46 hpf the *hnrnpa1a$^{-/-}$; hnrnpa1b$^{-/-}$* mutants display vascular mis-patterning reflected by intersomitic vessels that are misconnected (white arrow) or ISVs that are still unconnected (black arrow). Scale bar represents 25 µm. Anterior to the left. Lateral view. Maximum intensity projection. Images were taken by confocal laser scanning microscopy. **D:** Quantification of the number of sprouts that have formed per somite at 30 hpf in wildtype and *hnrnpa1a$^{-/-}$; hnrnpa1b$^{-/-}$* mutants. No difference in sprout number was observed. No statistical analysis was performed as always one sprout formed per somite in all analyzed embryos.

I therefore investigated vessel morphology in *hnrnpa1a*$^{-/-}$*; hnrnpa1b*$^{-/-}$ mutants by crossing them to the transgenic line Tg(fli1a:EGFP). In this line the blood vessels are visible as the line expresses GFP under the control of the blood vessel specific promoter fli1a [194]. *hnrnpa1a*$^{-/-}$*; hnrnpa1b*$^{-/-}$ mutants and their wildtype siblings were PFA fixed to keep the analysis time points among the embryos as similar as possible, and imaged at 30 hpf and 46 hpf. In contrast to *tardbp*$^{-/-}$*; tardbpl*$^{-/-}$ mutants, *hnrnpa1a*$^{-/-}$*; hnrnpa1b*$^{-/-}$ mutants form the correct number of sprouts per somite (see Figure 3.31D). However, growing sprouts extend lateral lamellipodia, which correctly form a lumen and expand, and are developmentally delayed resulting in reduced length of intersomitic vessels (ISV) compared to wildtype at 30 hpf (see Figure 3.31B). The growing sprouts occasionally fail to connect with their neighboring sprouts or misconnect to other sprouts (see Figure 3.31B+C). To better follow the vasculature development, age matched embryos obtained from a *hnrnpa1a*$^{-/-}$*; hnrnpa1b*$^{+/-}$ incross were recorded in a movie for 20 h starting at 24 hpf and were afterwards genotyped. The movie showed that endothelial sprouts follow their physiological path, but that this process is delayed, which becomes evident already at the beginning of the recording (24 hpf). Ultimately, the endothelial sprouts divert their physiological path and fail to connect or misconnect.

In summary, *hnrnpa1a*$^{-/-}$*; hnrnpa1b*$^{-/-}$ mutants and *tardbp*$^{-/-}$*; tardbpl*$^{-/-}$ mutants have distinct vascular mispatterning defects in early development. They share the vascular defect of mislead lamellipodia that ultimately misconnect or stay unconnected. However, the vascular phenotype is more severe in *tardbp*$^{-/-}$*; tardbpl*$^{-/-}$ mutants with the additional defect of increased endothelial sprouting from the dorsal aorta at the very early event of sprout formation.

*3.5.2.2.8 hnrnpa1a*$^{-/-}$*; hnrnpa1b*$^{-/-}$ and *tardbp*$^{-/-}$*; tardbpl*$^{-/-}$ mutants show significantly increased levels of *fn1b*

It was previously shown that vascular defects, represented by hypersprouting, in *tardbp*$^{-/-}$*; tardbpl*$^{-/-}$ mutants arise from increased levels of the extracellular matrix protein *fibronectin1b (fn1b)*. FN1A and Vascular cell adhesion molecule *1* (VCAM1) signal through the INTEGRIN ALPHA4 4 (ITGA4) receptor. Genes for these three proteins were identified to be highly upregulated upon TDP-43 KD in Human umbilical vein endothelial cells (HUVEC) [222]. I therefore tested whether a member of this ligand-receptor complex is also responsible for the vascular defects observed in *hnrnpa1a*$^{-/-}$*, hnrnpa1b*$^{-/-}$ mutants. To address changes in

mRNA levels of these genes I performed qRT-PCR on *hnrnpa1a*$^{-/-}$, *hnrnpa1b*$^{-/-}$ mutants using *fn1a*, *fn1b*, *itga4*, or *vcam1* specific primer pairs.

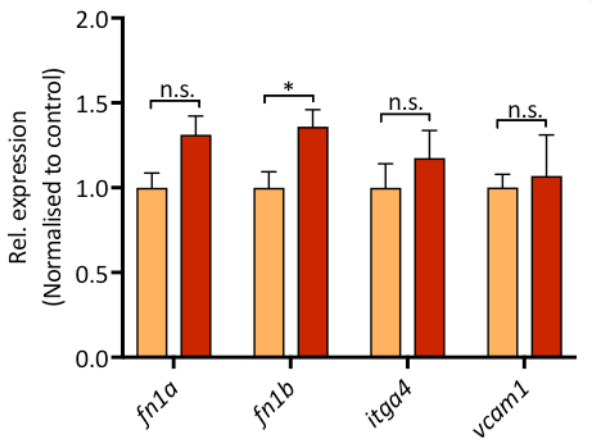


**Figure 3.32 - mRNA expression of *fn1b* is increased in *hnrnpa1a*$^{-/-}$; *hnrnpa1b*$^{-/-}$ mutants.** Relative mRNA expression of *fn1b* (*$p$<0.04; n=4), but not *fn1a* ($p$>0.06; n=4), *itg4* ($p$>0.44; n=4), or *vcam1* ($p$>0.79; n=4) is increased in *hnrnpa1a*$^{-/-}$; *hnrnpa1b*$^{-/-}$ embryos (red) compared to their wildtype siblings (orange). n=4 pools of embryos of independent clutches at 30 hpf, Student's t-test. Results by qRT-PCR were reproduced twice using the same cDNA. Error bars indicate S.E.M.

While *fn1a*, *itga4* and *vcam1* mRNA levels are not significantly changed in *hnrnpa1a*$^{-/-}$ *and* *hnrnpa1b*$^{-/-}$ mutants, *fn1b* levels are significantly upregulated (see Figure 3.32). The same result was previously obtained in *tardbp*$^{-/-}$; *tardbpl*$^{-/-}$ mutants [222]. It can be concluded that Hnrnpa1 and Tdp-43 both control *fn1b* mRNA levels and loss of Tdp-43 or Hnrnpa1 leads to increased *fn1b* mRNA levels.

### 3.5.2.3 Differentially expressed genes and proteins in *hnrnpa1a*$^{-/-}$; *hnrnpa1b*$^{-/-}$ mutants

In order to identify differentially expressed genes and proteins upon Hnrnpa1 deficiency, which potentially lead to the observed phenotype in *hnrnpa1a*$^{-/-}$; *hnrnpa1b*$^{-/-}$ mutants, two unbiased approaches were chosen. As *hnrnpa1a*$^{-/-}$; *hnrnpa1b*$^{-/-}$ mutants are not viable, 30 hpf old embryos were used for NGS and proteomic analysis. The mutant embryos were selected according to the criteria described in section 3.5.2.2.

3.5.2.3.1 Differentially expressed RNAs of *hnrnpa1a*$^{-/-}$; *hnrnpa1b*$^{-/-}$ mutants

NGS (total RNA, transcriptome sequencing, paired end, 35 Million reads/sample) revealed 615 differentially expressed genes of an adjusted p-value smaller than 0.01 and an up- or downregulated fold change greater than one. 235 of these genes were upregulated and 282 were downregulated. Genes of a p-value smaller than 0.001 and with a more than 2 fold

change in expression were analyzed in further detail. Functional annotation clustering using the annotation tool DAVID (david.ncifcrf.gov/home.jsp) revealed that many of the total 517 differentially expressed genes are involved in "cell cycle", "p53 signaling", "FoxO signaling", or "Notch signaling" (see Figure 3.33).

| Gene | Ensembl ID | Human Orthologue | $log_2$fold change | p-adjusted |
|---|---|---|---|---|
| *BX323459.3* | ENSDARG00000115555 | n.a. | 6.10 | 2,28E-06 |
| *drd6b* | ENSDARG00000040765 | n.a. | 5.26 | 1,07E-04 |
| *isg15* | ENSDARG00000086374 | *ISG15* | 4.58 | 1,08E-12 |
| *cdkn2a/b* | ENSDARG00000037262 | *CDKN2A* | 4.53 | 5,91E-23 |
| *ifit8* | ENSDARG00000057173 | *IFIT3* | 4.37 | 3,21E-13 |
| *btr07* | ENSDARG00000105558 | n.a. | 4.33 | 4,50E-06 |
| *cacna2d4b* | ENSDARG00000023886 | *CANA2D4* | 4.32 | 6,03E-19 |
| *si:dkey-145c18.3* | ENSDARG00000078738 | *NAMPT* | 4.06 | 5,74E-14 |
| *CT583625.5* | ENSDARG00000110288 | n.a. | 3.98 | 5,74E-05 |
| *si:ch211-132b12.8* | ENSDARG00000055250 | *CNTD2* | 3.72 | 8,42E-15 |
| | | | | |
| *si:ch211-256m1.8* | ENSDARG00000055172 | n.a. | -3.74 | 4.06E-18 |
| *lctla* | ENSDARG00000036139 | *LCTL* | -3.21 | 1.64E-10 |
| *apoda.1* | ENSDARG00000060345 | *APOD* | -3.16 | 2.24E-15 |
| *defbl1* | ENSDARG00000075161 | n.a. | -3.15 | 9.75E-11 |
| *crygm2d15* | ENSDARG00000069826 | n.a. | -3.11 | 1.40E-04 |
| *crygm2d2* | ENSDARG00000086917 | *CRYGD* | -2.98 | 3.25E-05 |
| *crygm2d16* | ENSDARG00000076790 | n.a. | -2.97 | 2.61E-06 |
| *cyb561a3b* | ENSDARG00000028257 | *CYB561A3* | -2.77 | 6.17E-10 |
| *cryaa* | ENSDARG00000053502 | *CRYAA* | -2.66 | 4.34E-15 |
| *cpa5* | ENSDARG00000021339 | *CPA1* | -2.62 | 2.40E-04 |

**Table 3.8 - Top 10 differentially expressed genes and the respective human orthologues in *hnrnpa1a*$^{-/-}$; *hnrnpa1b*$^{-/-}$ mutants**

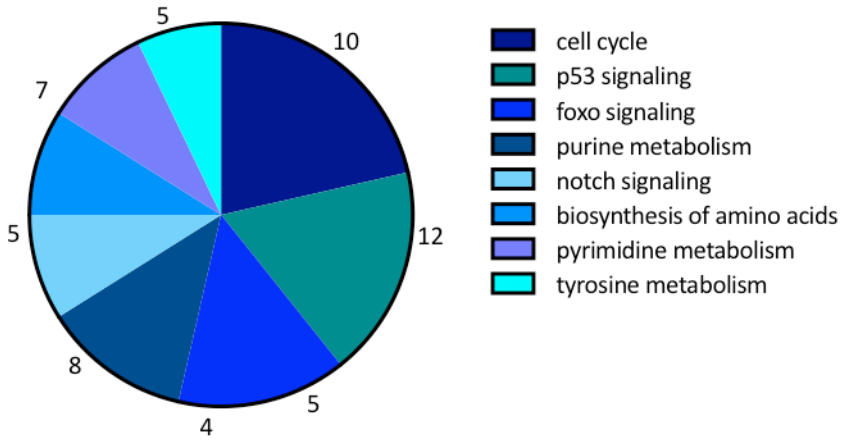


**Figure 3.33 – Top affected pathways based on RNA sequencing in *hnrnpa1a*$^{-/-}$; *hnrnpa1b*$^{-/-}$ mutants.** The numbers represent gene numbers involved in the process.

The top genes with interesting function and potential disease relevance were analyzed by qRT-PCR to confirm differential gene expression in *hnrnpa1a*$^{-/-}$; *hnrnpa1b*$^{-/-}$ mutants. Decreased expression of *apoda.1* (~6 % remaining *apoda.1)* and *glycoprotein nonmetastatic melanoma b (gpnmb)* was verified by qRT-PCR, while increased expression of *nampt* could not be reproduced by qRT-PCR (see Figure 3.34). *gpnmb* encodes Gpnmb ,which is a type I transmembrane protein and is involved in a variety of processes including osteoplast differentiation and function, and regulation of autoimmune responses [223]. GPNMB was shown to exert a neuroprotective role and was linked to ALS due to its higher expression levels in sporadic ALS patients [224].

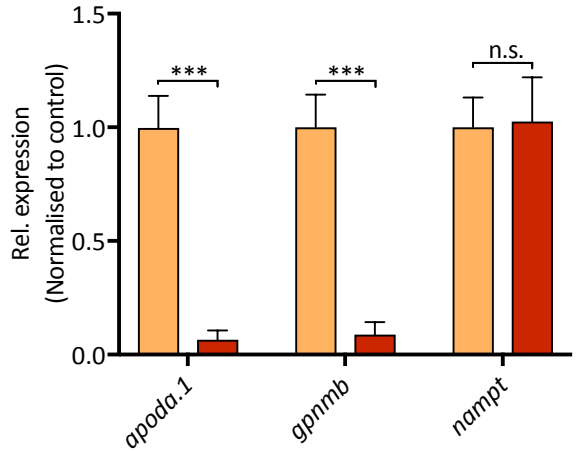


**Figure 3.34 - mRNA expression of *apoda.1* and *gpnmb* is decreased in *hnrnpa1a*$^{-/-}$; *hnrnpa1b*$^{-/-}$ mutants.** Relative mRNA expression of *apoda.1* (***$p$<0.0001) and *gpnmb* (***$p$<0.0001), is decreased in *hnrnpa1a*$^{-/-}$, *hnrnpa1b*$^{-/-}$ mutants (red) compared to their wildtype siblings (orange) while *nampt* ($p$>0.83) expression is not changed. n=4 pools of embryos of independent clutches at 30 hpf, Student's t-test. Results by qRT-PCR were reproduced twice using the same cDNA. Error bars indicate S.E.M.

The expression of genes linked to ALS and/or FTD were only mildly changed in *hnrnpa1a*$^{-/-}$, *hnrnpa1b*$^{-/-}$ mutants and were mostly not significant (see Table 3.9). *grn2* shows the largest change with a 4.23 fold decrease, which is though not significant. *fus* and *ccnf* show significant changes, though with a small fold change of approximately 0.7.

| Gene | Ensembl ID | $log_2$ fold change | p-adjusted |
|---|---|---|---|
| *c9orf72* | ENSDARG00000011837 | 0.32 | 0.21 |
| *ccnf* | ENSDARG00000105046 | -0.71 | 5.12E-5 |
| *ewsr1a* | ENSDARG00000113252 | n.a. | n.a. |
| *ewsr1b* | ENSDARG00000117011 | -0.53 | 0.35 |
| *grn1* | ENSDARG00000089362 | -0.31 | 0.88 |
| *grn2* | ENSDARG00000088641 | -4.23 | 0.69 |
| *fus* | ENSDARG00000037968 | -0.78 | 5.96E-9 |
| *sod1* | ENSDARG00000043848 | -0.30 | 0.08 |
| *taf15* | ENSDARG00000070019 | -0.33 | 0.015 |
| *tardbp* | ENSDARG00000040031 | -0.24 | 0.09 |
| *tardbpl* | ENSDARG00000004452 | -0.40 | 0.82 |
| *tia* | ENSDARG00000052536 | -0.46 | 0.01 |
| *vapb* | ENSDARG00000070435 | 0.07 | 0.78 |
| *vcp* | ENSDARG00000020008 | 0.13 | 0.50 |

**Table 3.9 - Expression of ALS and/or FTD related genes in *hnrnpa1a*$^{-/-}$*; hnrnpa1b*$^{-/-}$ mutants.**

3.5.2.3.2 Expression of the cell cycle regulators *cdk1a*, *cdk2a/b*, *gadd45, p53, and rbl2* is increased in *hnrnpa1a*$^{-/-}$*; hnrnpa1b*$^{-/-}$ mutants

RNA sequencing hits involved in cell cycle were reanalyzed by qRT-PCR. As depicted in Figure 3.35 the levels of *cdkn1a*, *cdkn2a/b*, *gadd45*, *p53* and *rbl2,* but not *ccne1*, were significantly increased in *hnrnpa1a*$^{-/-}$*; hnrnpa1b*$^{-/-}$ mutants compared to their wildtype siblings. It can be concluded that the majority of genes, which were found by RNA sequencing to be differentially expressed in *hnrnpa1a*$^{-/-}$*; hnrnpa1b*$^{-/-}$ mutants and are involved in cell cycle are upregulated. This finding makes it highly possible that cell cycle alterations contribute to the observed phenotypic abnormalities in *hnrnpa1a*$^{-/-}$*; hnrnpa1b*$^{-/-}$ mutants.

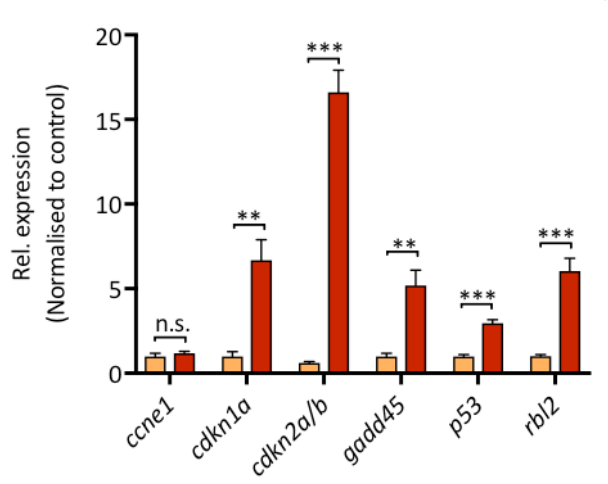


**Figure 3.35 - mRNA expression of *cdkn1a*, *cdkn2a/b*, *gadd45*, *p53*, and *rbl2* is increased in *hnrnpa1a*$^{-/-}$; *hnrnpa1b*$^{-/-}$ mutants.** Relative mRNA expression of *cdkn1a* (***p*<0.004), *cdkn2a/b* (****p*<0.0004), *gadd45* (***p*<0.005), *p53* (****p*<0.0003), and rbl2 (****p*<0.0007) but not *ccne* (*p*>0.40) is increased in *hnrnpa1a*$^{-/-}$, *hnrnpa1b*$^{-/-}$ embryos (red) compared to their wildtype siblings (orange). n=4 pools of embryos of independent clutches at 30 hpf. Student's-t-test. Results by qRT-PCR were reproduced twice using the same cDNA. Error bars indicate S.E.M.

#### 3.5.2.3.3 Splice analysis of *hnrnpa1a*$^{-/-}$; *hnrnpa1b*$^{-/-}$ mutants

A list of interesting potential splice targets of HNRNPA1 was analyzed for changes in splicing pattern in *hnrnpa1a*$^{-/-}$; *hnrnpa1b*$^{-/-}$ mutants. The splice analysis was performed by Özge Pelin, a PhD student from our group. No splicing differences were detected in cell cycle related genes, such as *ccne1*, *ccne2*, or *cdk2*. Also, splicing of *apod.a1*, *fn1b* or *pkma* was not affected in *hnrnpa1a*$^{-/-}$, *hnrnpa1b*$^{-/-}$ mutants (data not shown). While the splicing of *tardbp* was not affected, *tardbpl* was differentially spliced upon Hnrnpa1 KO. The analysis further revealed that one of the alternative 3'UTR of *apoeb* shows significantly higher expression levels in *hnrnpa1a*$^{-/-}$; *hnrnpa1b*$^{-/-}$ embryos leading to higher usage of a longer 3'UTR version (personal communication with Özge Pelin). Interestingly, HNRNPA1 KO was previously shown to regulate Apolipoprotein E (APOE) promoter activity, which is important in the development of AD [142].

### 3.5.2.4 Differentially expressed proteins of *hnrnpa1a*$^{-/-}$; *hnrnpa1b*$^{-/-}$ mutants

To identify altered protein expression in *hnrnpa1a*$^{-/-}$; *hnrnpa1b*$^{-/-}$ mutants quantitative mass spectrometry was performed. Due to the richness of yolk proteins, which may mask detection of other proteins at this early stage, the yolk was manually removed from the embryos.

| Protein | NCBI accession | log2 fold change | p-value |
|---|---|---|---|
| vitellogenin 4 precursor | NP_001038759 | 1.75 | 7.69E-3 |
| vitellogenin 1 precursor | NP_001038362 | 1.54 | 3.18E-3 |
| retinoic acid receptor RXR-beta-A isoform X9 | XP_009292301 | 0.65 | 4.00E-3 |
| ADP-ribosylation factor-like protein 3 isoform 2 | NP_001017827 | 0.58 | 5.75E-3 |
| tumor necrosis factor receptor type 1-associated DEATH domain protein | NP_571682 | 0.56 | 7.86E-3 |
| serine/threonine-protein kinase tousled-like 1 isoform X1 | XP_009302714 | 0.54 | 9.99E-3 |
| putative RNA-binding protein 15 | XP_001335820 | 0.53 | 5.53E-3 |
| N-lysine methyltransferase SMYD2-A | NP_001013568 | 0.46 | 9.57E-3 |
| tumor protein D52 | NP_001038486 | 0.41 | 4.65E-3 |
| S-formylglutathione hydrolase | NP_001017796 | 0.41 | 6.59E-3 |
| | | | |
| heterogeneous nuclear ribonucleoprotein A1 isoform X3 | XP_021335236.1 | -6.16 | 6.88E-7 |
| hemoglobin embryonic subunit alpha | XP_001333555.1 | -5.35 | 4.49E-6 |
| GTP cyclohydrolase 1 | NP_571742.1 | -3.37 | 4.26E-4 |
| immunoglobulin superfamily DCC subclass member 3-like | XP_009292645.2 | -5,94 | 1.15E-6 |

| | | | |
|---|---|---|---|
| wu:fc46h12 precursor | NP_001278276.1 | -2,16 | 6.89E-3 |
| proliferation marker protein Ki-67 isoform X1 | XP_021335806.1 | -2.09 | 8.18E-3 |
| hemoglobin beta embryonic-3 | NP_001015058.1 | -2.57 | 2.67E-3 |
| lymphoid-specific helicase | NP_001032178.1 | -2.60 | 2.53E-3 |
| 40S ribosomal protein S30 | NP_957031.1 | -2.76 | 1.74E-3 |
| ribonucleoside-diphosphate reductase subunit M2 | NP_571525.1 | -4.72 | 1.90E-5 |

**Table 3.10 - Top 10 differentially expressed proteins in *hnrnpa1a*$^{-/-}$; *hnrnpa1b*$^{-/-}$ mutants.**

Only those samples were considered for further analysis that had a minimum coverage of 4.000 proteins and had less than 10% remaining Hnrnpa1a protein. The p-value cut off was set to $p<0.05$ and only those values were included for further analysis that had an upwards or downwards fold change greater than one. The remaining 240 proteins met these criteria and were analyzed using the annotation tool DAVID (david.ncifcrf.gov/home.jsp), which revealed that most of the differentially expressed proteins are involved in the "ribosome",

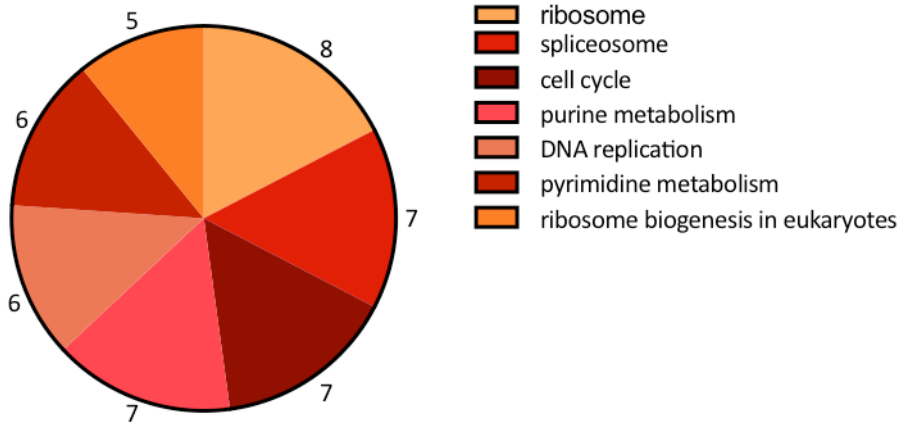


**Figure 3.36 - Top affected pathways based on proteomics in *hnrnpa1a*$^{-/-}$; *hnrnpa1b*$^{-/-}$ mutants.** The numbers represent protein numbers involved in the process.

"spliceosome", "cell cycle", or "purine metabolism" pathway (see Figure 3.36). Even though these top pathways highly overlap with those found by RNA sequencing, the comparison with

the RNA sequencing data revealed little overlap of the most significant targets, most likely because the top RNA sequencing hits were below protein detection level.

#### 3.5.2.5 *hnrnpa1a*$^{-/-}$*; hnrnpa1b*$^{-/-}$ mutants show no altered Pcna levels or distribution pattern

Several lines of evidence point to cell cycle misregulation in the $G_1$ to S-phase transition in *hnrnpa1a*$^{-/-}$*; hnrnpa1b*$^{-/-}$ mutants. First, The RNA sequencing revealed the cell cycle as the most affected pathway in *hnrnpa1a*$^{-/-}$*; hnrnpa1b*$^{-/-}$ mutants. I could further verify upregulation of the $G_1$/S-phase related genes *cdkn1a*, *cdkn2a/b*, *gadd45*, *p53*, and *rbl2* by qRT-PCR. Second, the proteome analysis of *hnrnpa1a*$^{-/-}$*; hnrnpa1b*$^{-/-}$ mutants revealed cell cycle as one of the main affected pathways. Third, a previous study identified cell cycle S-phase as one of the top 10 affected processes upon Hnrnpa1 KO in mice [162]. To address cell cycle progression the protein levels and distribution pattern of Pcna in *hnrnpa1a*$^{-/-}$*; hnrnpa1b*$^{-/-}$ mutants was investigated. PCNA is an evolutionary well-conserved protein, which is involved in many steps of cell division, such as processivity of DNA polymerase, chromatin remodeling, DNA replication control, and DNA repair. Furthermore, expression of the *PCNA* gene correlates with cell proliferation [225] [226] [227]. A decrease in Pcna in zebrafish mutants would thereby be an indicator of reduced cell proliferation [228]. Western blotting with a Pcna specific antibody on *hnrnpa1a*$^{-/-}$*; hnrnpa1b*$^{-/-}$ mutants revealed unchanged Pcna protein levels compared to wildtype (see Figure 3.37A). Moreover, PCNA staining is suitable to discriminate the cell cycle stages $G_1$ and S-phase. During $G_1$-phase PCNA is equally distributed over the whole nucleus. In S-phase PCNA accumulates to small, equally distributed foci, which are located at the nuclear periphery or the center of the nuclei depending whether it is mid S-phase or late S-phase, respectively [229]. Upon whole mount staining of 30 hpf *hnrnpa1a*$^{-/-}$*; hnrnpa1b*$^{-/-}$ mutants with Pcna, the embryos were imaged with the cell observer spinning disc microscope. The different Pcna staining patterns revealing the cell cycle stage ($G_1$ and S-phase) of the specific cells are visible. There was no difference detected in cells undergoing $G_1$ or S-phase between *hnrnpa1a*$^{-/-}$*; hnrnpa1b*$^{-/-}$ mutants and wildtype (see Figure 3.37C).

It can be concluded that Pcna protein levels are not changed upon Hnrnpa1 KO. Moreover, loss of Hnrnpa1 does not seem to alter the number of cells undergoing $G_1$ or S-phase.

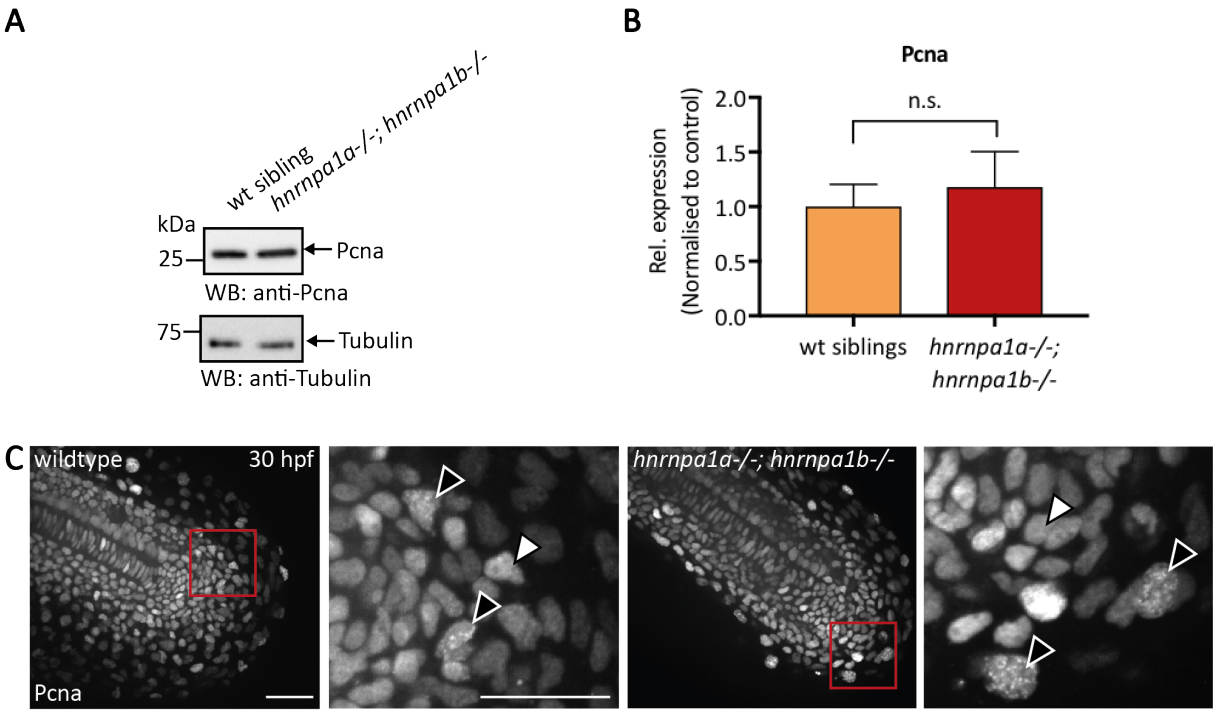


**Figure 3.37 - *hnrnpa1a*$^{-/-}$; *hnrnpa1b*$^{-/-}$ mutants show no change in Pcna levels or distribution pattern. A:** Immunoblotting of Pcna on *hnrnpa1a*$^{-/-}$; *hnrnpa1b*$^{-/-}$ mutants and wildtype embryos. Tubulin served as a loading control. **B:** Quantification revealed no significant differences in Pcna levels among *hnrnpa1a*$^{-/-}$; *hnrnpa1b*$^{-/-}$ mutants and wildtype embryos ($p$>0.20; n=8). Student's t-test. Error bars indicate S.E.M. **C:** Pcna whole mount staining in wildtype and *hnrnpa1a*$^{-/-}$; *hnrnpa1b*$^{-/-}$ mutants. In the enlarged view the cell stage can be detected by the Pcna pattern. Equally grey stained cells undergo $G_1$-phase (white arrowhead) and cells with white punctae are in S-phase (black arrowhead). Lateral view of the tail. Anterior to the left. Scalebar represents 50 µm. Images were taken by cell observer spinning disc microscope using the 488 nm laser.

### 3.5.2.6 Hnrnpa1 KO vs. Tdp-43 KO

TDP-43 and HNRNPA1 belong to the HNRNP protein family, share similar protein structure, and mutations in these proteins were associated with ALS. Interestingly, the phenotype of *hnrnpa1a*$^{-/-}$; *hnrnpa1b*$^{-/-}$ mutants is quite similar at first to that observed in *tardbp*$^{-/-}$, *tardbpl*$^{-/-}$ mutant embryos. [12]. I therefore asked myself whether loss of function of these proteins in zebrafish causes similar phenotypes and overlapping molecular signatures.

3.5.2.6.1 Phenotype analysis

*tardbp*$^{-/-}$; *tardbpl*$^{-/-}$ and *hnrnpa1a*$^{-/-}$; *hnrnpa1b*$^{-/-}$ mutants share some phenotypic overlap, such as lethality, development of heart edema, shortened SpMN axons, muscle defects, and vascular development defects [12] [222]. However, the vascular phenotype shows distinct characteristics in the two mutants. *hnrnpa1a*$^{-/-}$; *hnrnpa1b*$^{-/-}$ mutants develop lateral lamellopodia, diverting from their physiological migration path and misconnect, whereas ectopic sprouting from the dorsal aorta is characteristic for *tardbp*$^{-/-}$; *tardbpl*$^{-/-}$ mutants.

Moreover, *hnrnpa1a*$^{-/-}$*; hnrnpa1b*$^{-/-}$ mutants show a thinned yolk extension (see Figure 3.27), increased lipid uptake from the yolk extension to the trunk (see Figure 3.28), a higher number of dying cells in the spinal cord (see Figure 3.30) and developmental delay (see Figure 3.24) - all features that were so far not specifically addressed in *tardbp*$^{-/-}$*; tardbpl*$^{-/-}$ mutants.

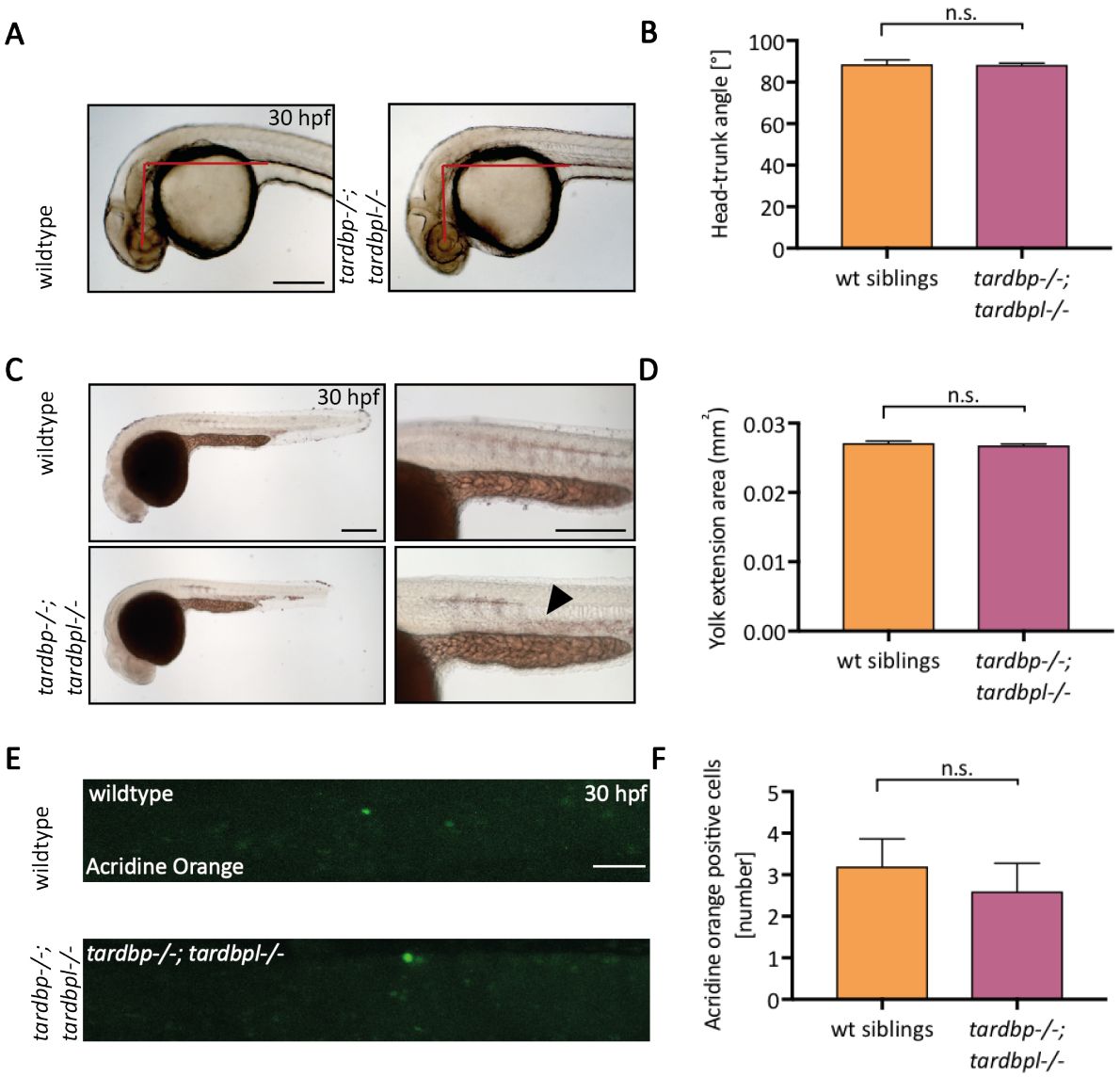


**Figure 3.38 - *tardbp*$^{-/-}$*; tardbpl*$^{-/-}$ mutants are not developmentally delayed, show no changed neutral lipid distribution or cell death. A:** Representative images of 30 hpf old wildtype and *tardbp*$^{-/-}$*; tardbpl*$^{-/-}$ mutants with head trunk angle measurement. Lateral view. Anterior to the left. Images taken by Axio Scope A1 microscope. Scalebar represents 200 µm. **B:** Quantification of head trunk angle of 30 hpf old wildtype (88°) and *tardbp*$^{-/-}$*; tardbpl*$^{-/-}$ (88°) embryos revealed no significant difference; n=8 embryos; p>0.91; Student's-t-test. Error bars indicate S.E.M. **C:** Representative images of 30 hpf wildtype and *tardbp*$^{-/-}$*; tardbpl*$^{-/-}$ mutants stained with ORO. Slightly increased neutral lipid uptake is observed in *tardbp*$^{-/-}$*; tardbpl*$^{-/-}$ mutants (black arrow) Lateral view. Anterior to the left. Scalebar represents 200 µm. **D:** Quantification of the 2-dimensional yolk extension area of wildtype and *tardbp*$^{-/-}$*; tardbpl*$^{-/-}$ mutants reveals no significant difference. n=10 embryos; p>0.41; Student's-t-test. Error bars indicate S.E.M. **E:** Representative images of 30 hpf wildtype and *tardbp*$^{-/-}$*; tardbpl*$^{-/-}$ mutants stained with Acridine Orange (green), which is taken up by apoptotic and necrotic cells (only part of the spinal cord is shown). Lateral view. Anterior to the left. Maximum intensity projection. Images were taken with laser scanning confocal microscope using the 488 nm laser. Scalebar represents 40 µm. **F:** Quantification of Acridine Orange positive cells is unchanged in *tardbp*$^{-/-}$*; tardbpl*$^{-/-}$ mutants. n=5 embryos per experiment; p>0.54; Student's-t-test. Error bars indicate S.E.M.

Assessment of the head trunk angle revealed no significant change pointing to no or very little developmental delay in *tardbp*$^{-/-}$; *tardbpl*$^{-/-}$ mutants (see Figure 3.38A+B). Upon staining of *tardbp*$^{-/-}$; *tardbpl*$^{-/-}$ mutants with ORO, it becomes evident that *tardbp*$^{-/-}$; *tardbpl*$^{-/-}$ mutants do neither have a thinned yolk extension nor do they show highly augmented neutral lipid uptake from the yolk extension to the body as depicted in *hnrnpa1a*$^{-/-}$; *hnrnpa1b*$^{-/-}$ embryos (see Figure 3.38C+D). The occurrence of cell death was addressed by staining 30 hpf *tardbp*$^{-/-}$; *tardbpl*$^{-/-}$ mutants with Acridine Orange. No increase in Acridine Orange positive cells was observed in *tardbp*$^{-/-}$; *tardbpl*$^{-/-}$ mutants (see Figure 3.38E+F).

3.5.2.6.2 Comparison between RNA sequencing datasets from *tardbp*$^{-/-}$; *tardbpl*$^{-/-}$ and *hnrnpa1a*$^{-/-}$; *hnrnpa1b*$^{-/-}$ mutants

In order to identify whether loss of Tdp-43 or Hnrnpa1 affect common downstream targets in zebrafish and to thereby determine whether they may act in similar pathways, I compared the RNA sequencing data obtained from *hnrnpa1a*$^{-/-}$; *hnrnpa1b*$^{-/-}$ mutants to RNA sequencing data of *tardbp*$^{-/-}$; *tardbpl*$^{-/-}$ mutants with bioinformatic help from Özge Pelin. The two data sets were analyzed in the same manner to allow for better comparison between the two data

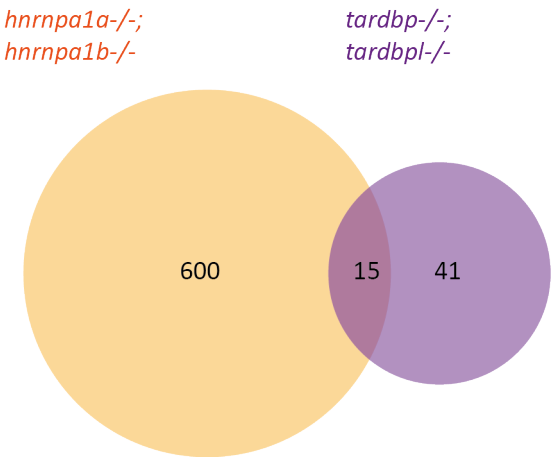


**Figure 3.39 - Venn diagram showing shared and distinct differentially expressed genes upon Hnrnpa1 or Tdp-43 KO.** 615 genes are differentially expressed in *hnrnpa1a*$^{-/-}$; *hnrnpa1b*$^{-/-}$ mutants compared to their wildtype siblings. 56 genes are differentially expressed in *tardbp*$^{-/-}$; *tardbpl*$^{-/-}$ mutants. 15 among these two data sets were found to overlap. p-value was adjusted to $p<0.01$.

sets. The p-value was adjusted to 0.01 as the Tdp-43 dataset did not contain as many hits as the Hnrnpa1 data, and only those values were included that have an up- or downward fold change greater than one. With these settings 615 genes were differentially expressed in *hnrnpa1a*$^{-/-}$; *hnrnpa1b*$^{-/-}$ mutants compared to wildtype. In *tardbp*$^{-/-}$; *tardbpl*$^{-/-}$ mutants 56 genes were differentially expressed compared to wildtype (see Figure 3.39). 15 genes were

changed in both datasets among which 8 genes were changed in the same direction (see Table 3.11).

| **Gene symbol** | **Human gene** | **log2 foldchange *hnrnpa1*** | **p-adj. *hnrnpa1*** | **log2 fold change *tardbp*** | **p-adj. *tardbp*** | **Same direction** |
|---|---|---|---|---|---|---|
| *ace* | *AC113554.1* | 0,61 | 6,69E-06 | -0,94 | 5,19E-04 | no |
| *ankrd1a* | *ANKRD1* | 0,69 | 4,54E-06 | 0,62 | 1,02E-4 | yes |
| *chrng* | *CHRNG* | -0,48 | 1,27E-04 | 1,16 | 5,29E-4 | no |
| *ctgfa* | *CTGF* | -2,50 | 1,16E-06 | -0,61 | 2,18E-05 | yes |
| *flnca* | *FLNC* | 0,65 | 3,05E-07 | 1,92 | 3,44E-10 | yes |
| *gli2b* | / | 1,63 | 3,62E-07 | -0,99 | 6,75E-10 | no |
| *hspb11* | / | 1,03 | 7,16E-08 | 2,03 | 1,94E-22 | yes |
| *mylpfb* | *MYLPF* | 0,79 | 1,72E-05 | 1,02 | 7,74E-17 | yes |
| *npr1a* | *NPR2* | -0,98 | 3,09E-04 | 1,18 | 2,64E-06 | no |
| *plxnb3* | *PLXNB3* | 0,63 | 6,29E-07 | 1,01 | 5,46E-06 | yes |
| *pvalb1* | / | 0,66 | 3,43E-04 | 1,12 | 9,77E-06 | yes |
| *rnf44* | *RNF44* | -4,32 | 3,67E-06 | 0,90 | 8,04E-05 | no |
| *tcap* | *TCAP* | -0,66 | 2,25E-05 | 1,24 | 4,33E-14 | no |
| *wfikkn1* | / | 0,34 | 9,55E-3 | -0,87 | 1,77E-03 | no |
| *zmp:0000 001082* | *ITGAX* | 0,62 | 1,08E-05 | 0,63 | 6,39E-04 | yes |

**Table 3.11 - Shared differentially expressed genes upon Hnrnpa1 or Tdp-43 KO.** For explanation see text.

## 3.6 KD of *apoda.1* phenocopies the observed yolk extension thinning observed in *hnrnpa1a*$^{-/-}$*; hnrnpa1b*$^{-/-}$ mutants in a dose-dependent manner

*apoda.1* was identified by RNA sequencing as one of the main downregulated genes in *hnrnpa1a*$^{-/-}$*; hnrnpa1b*$^{-/-}$ mutants. One of the most striking phenotypes in *hnrnpa1a*$^{-/-}$*; hnrnpa1b*$^{-/-}$ mutants is the thinned yolk extension and increased neutral lipid uptake, pointing to lipid metabolism defects. In order to test whether reduction in *apoda.1* is involved in causing the lipid phenotype, I knocked down *apoda.1* in AB wildtype fish using a splice site targeting MO as the KD efficiency can be easily assessed by PCR (see Figure 3.40A+B).

Binding of the *apoda.1* MO leads to inclusion of intron 2 resulting in a longer RNA. This was verified by sequence analysis (data not shown) of the resulting higher band appearing in *apoda.1* MO injected embryos at about 630 bp (see Figure 3.40B). Bands were cut, DNA

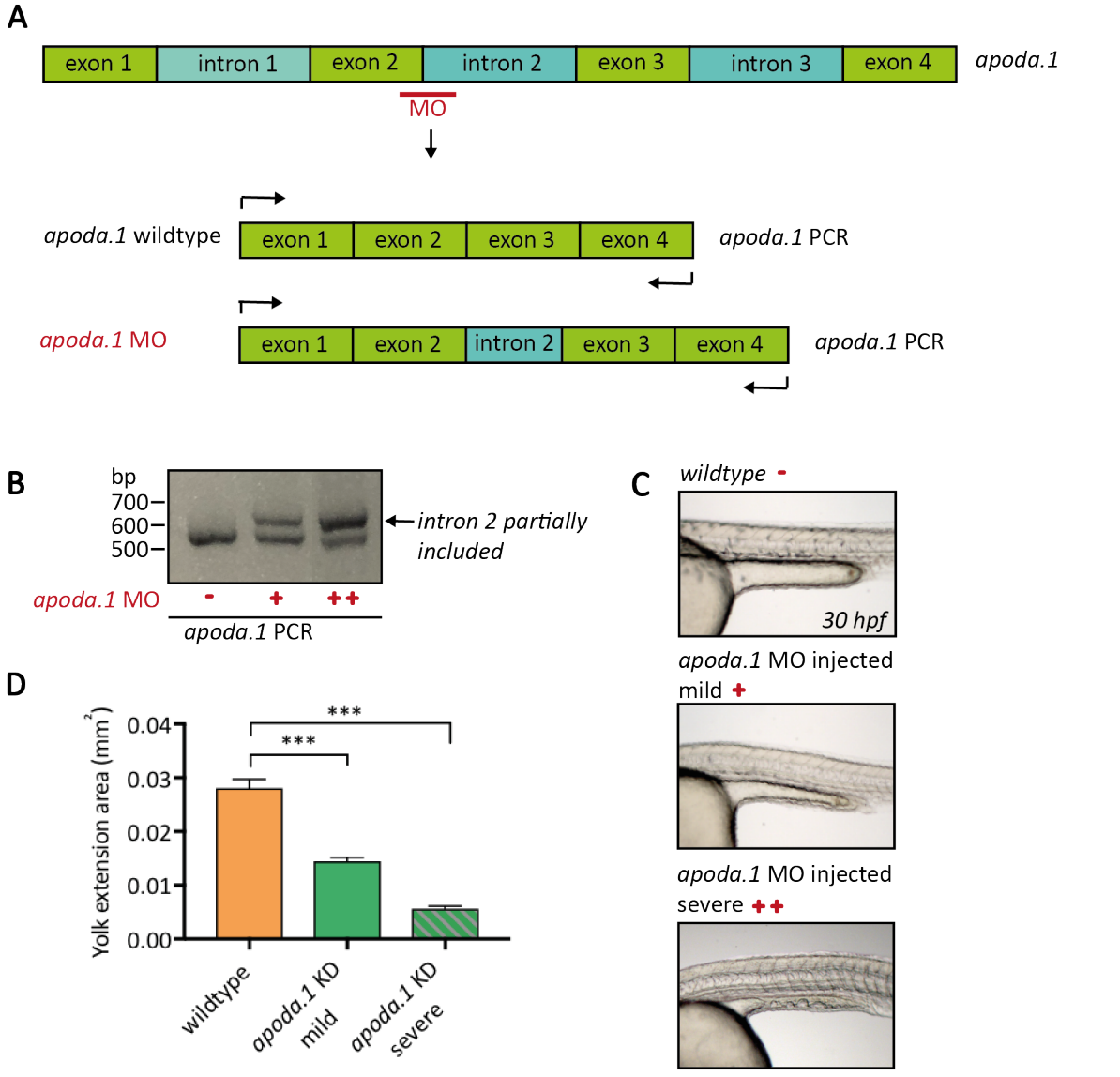


**Figure 3.40 – KD of *apoda.1* mimics the yolk extension thinning observed in *hnrnpa1a*$^{-/-}$; *hnrnpa1b*$^{-/-}$ mutants. A:** Schematic illustration the four exons and three introns of *apoda.1*. Binding of the *apoda.1* MO (indicated in red) leads to inclusion of intron 2 resulting in a longer RNA (see A). Primers used for amplification are indicated by black arrows. **B:** PCR products of cDNA from MO injected AB (+) embryos and uninjected siblings (-) shown in C. Injection of *apoda.1* MO leads to appearance of a second, higher migrating band representing *apoda.1* RNA with partial intron 2 inclusion. The lower band represents the normally spliced *apoda.1* RNA. **C:** Images show the thinned yolk extension of AB embryos injected with 1 µM *apoda.1* MO. Upper picture shows uninjected wildtype control with a normally developed roundish yolk extension. The middle picture shows an embryo with a mild phenotype showing little thinning of the yolk extension. The bottom picture shows an embryo with a severe phenotype characterized by a greatly thinned yolk extension. Lateral view. Anterior to the left. **D:** The two-dimensional yolk extension area is significantly reduced in embryos showing mild (n=11; ***$p$<0.0001) and severe (n=8; ***$p<0.0001$) thinning of the yolk extension caused by low and high KD levels of *apoda.1,* respectively. The analysis demonstrates that *apoda.1* reduction phenocopies the yolk extension thinning observed in *hnrnpa1a*$^{-/-}$; *hnrnpa1b*$^{-/-}$ mutants. Student's t-test. Error bars indicate S.E.M.

purified and sent for sequencing, revealing a frameshift resulting from partial intron inclusion leading to a PTC at 79 aa. To quantify the phenocopy effect of *apoda.1* KD in AB embryos, the average two-dimensional yolk area was measured at 30 hpf (see section 3.5.2.2.1). Strikingly, upon injection of the *apoda.1* MO into wildtype embryos the majority of injected embryos showed a thinned yolk extension. Since the severity of this phenotype was variable among the injected embryos, embryos were divided into two classes (mild and severe) depending on the severity of the yolk extension thinning. Both groups showed a significantly smaller two-dimensional yolk extension area than wildtype embryos. Moreover, the efficiency of the MO KD correlates to the severity of the lipid phenotype (mild: 50% remaining *apoda.1*; severe: 25 % remaining *apoda.1*; see Figure 3.40 B+C+D).

I conclude that reduction in *apoda.1* phenocopies the lipid phenotype observed in *hnrnpa1a*$^{-/-}$*; hnrnpa1b*$^{-/-}$ embryos in a dose dependent manner. This suggests that Apoda.1 reduction is causative for the lipid phenotype.

# 4 Discussion

## 4.1 Evolution of HNRNPA proteins

HNRNPA proteins are among the most abundant HNRNP proteins and are highly conserved across species [230]. In contrast to a single HNRNPA1 gene in mammals, two Hnrnpa1 orthologues are present in zebrafish named Hnrnpa1 and Hnrnpa1b. The shared synteny of *hnrnpa1a* and *hnrnpa1b* with *HNRNPA1* supports that these genes are orthologues. The presence of Hnrnpa1 and Hnrnpa1b can be explained by the TSD that lead to an additional round of WGD in zebrafish during evolution [231]. WGDs generates complexity by generating genes without preassigned essential function that can serve as genetic raw material for evolutionary innovation [232]. WGD-derived genes can undergo different fates: one of the duplicates may be lost (non-functionalization), both duplicates may acquire changes so that the ancestral gene's function is shared by the duplicates (subfunctionalization), or one of the duplicated genes may acquire a new function (neofunction) [231]. These events are not mutually exclusive and each of them was observed in the past. Two questions arise in this context: First, whether Hnrnpa1a and Hnrnpa1b share common functions and second, which one of them better resembles Human HNRNPA1. Interestingly, no orthologue of HNRNPA2 is described in zebrafish whereas it is found in lamprey and coelacanth. Since Hnrnpa1 is duplicated in zebrafish it is possible that Hnrnpa2 is lost due to functional redundancy [203] as it has been previously suggested that upon WGD many genes are deleted so that the gene content is only slightly increased [233]. Alternatively, Hnrnpa1a and/or Hnrnpa1b may have taken over HNRNPA2 functions.

Regarding the first question whether Hnrnpa1a and Hnrnpa1b share common functions, the lab of J. Trimarchi shed more light on Hnrnpa1a and Hnrnpa1b function by studying their expression pattern in zebrafish. They found *hnrnpa1a* and *hnrnpa1b* to be expressed mainly in the head with a fainter expression in the trunk and in the retina at 2 dpf, 3 dpf and 4 dpf. *hnrnpa1a* showed ubiquitous expression in the head, while *hnrnpa1b* was only expressed in a subset of cells at these development stages. *hnrnpa1a* was slightly detected in the trunk at 2 dpf and 3 dpf, while it was strongly expressed at 4 dpf. *hnrnpa1b* was absent at 2 dpf and was only faintly expressed in the trunk at 3 dpf and 4 dpf [234]. The *in situ* hybridization (ISH) expression pattern points to an important role of *hnrnpa1a* and *hnrnpa1b* in brain development [234]. The different temporal and spatial expression pattern of *hnrnpa1a* and

*hnrnpa1b* imply unique functions in zebrafish development, whereas the partial overlap in localization also suggests shared functions. The latter could speak in favor of compensatory mechanisms. Functional compensation is supported by the finding that Hnrnpa1b protein levels are significantly upregulated in *hnrnpa1a*$^{-/-}$ mutants. Correspondingly, *hnrnpa1a* mRNA levels were significantly upregulated in *hnrnpa1b*$^{-/-}$ mutants. These findings clearly show that Hnrnpa1a and Hnrnpa1b compensate for one another's function by upregulating their protein or mRNA levels, respectively. Similarly, the Hnrnp family member *tardbp* shows compensational mechanisms by alternative splicing of *tardbpl* upon KO of its paralog *tardbp* [12]. Moreover, HNRNPA1 was shown to compensate for HNRNPA2/B1 function in mouse spinal cord, and HNRNPA2/B1 upregulation was observed upon HNRNPA1 loss of function in HeLa cells but not mice [235] [102] [162]. This could be because regulation of HNRNPA2/B1 upon HNRNPA1 may be much more complicated in an animal than a cell. It seems that in the mouse HNRNPA1 has a unique function that cannot be compensated by HNRNPA2/B1. The compensation among Hnrnpa1a and Hnrnpa1b observed in zebrafish presents a different scenario as these genes are both orthologues and are likely to both possess HNRNPA1 related function and/or acquired new ones. As zebrafish lack the Hnrnpa2 orthologue compensation among Hnrnpa1 and Hnrnpa2 cannot be addressed. Furthermore, single *hnrnpa1a*$^{-/-}$ or *hnrnpa1b*$^{-/-}$ mutants lack any morphological abnormalities. More detailed analysis of ALS related phenotypes revealed neither a change in SpMN axon length nor muscle defects. Based on this finding it seems unlikely that one of these genes became nonfunctional as in this case the double KO would have been also phenotypically normal, but instead these mutants were embryonically lethal. We hypothesize that these genes became subject of subfunctionalization with each gene taking over essential functions in zebrafish development. The functions are though not fully complementary as in this scenario loss of either of them would result in a phenotype.

In order to address the second question, which *hnrnpa* zebrafish orthologue is more closely realted to human HNRNPA1, sequence homology analysis using UniProt was performed and revealed a higher sequence homology of Hnrnpa1a and Hnrnpa1b to HNRNPA1-B, which is the minor isoform, than to HNRNPA1-A. Moreover, the full-length gene sequence of *hnrnpa1a* shows greater similarity with *HNRNPA1-B* than with *hnrnpa1b*. These findings imply that rather *hnrnpa1a* correlates with HNRNPA1 on a structural basis, while no conclusions on the functional relation can be drawn.

Hnrnpa3 is highly identical to Human HNRNPA3 in its sequence and seems to be functionally more distinct from Hnrnpa1, based on the following observations. First, Hnrnpa3

RNA and protein levels in *hnrnpa1a*$^{-/-}$ and *hnrnpa1b*$^{-/-}$ single mutants are unchanged. Second, *hnrnpa1a*$^{-/-}$*; hnrnpa3*$^{-/-}$ and *hnrnpa1b*$^{-/-}$*; hnrnpa3*$^{-/-}$ double mutants were viable and did not show phenotypic abnormalities. Hnrnpa3's sequence differs more from Hnrnpa1a and Hnrnpa1b than Hnrnpa1a and Hnrnpa1b to each other. The function of Hnrnpa3 is not well characterized in the literature. However, there is some evidence that points to a distinct function of HNRNPA3 compared to HNRNPA1 and HNRNPA2B1. He et al. showed that the levels of HNRNPA1 and HNRNPA2B1, but not HNRNPA3 are modulated during cell cycle in Colo16 squamous carcinoma cells, suggesting that HNRNPA1 and HNRNPA2B1 are required at specific stages of the cell cycle, while HNRNPA3 functions in a more generalized manner [236]. While no KO or KD animal was generated so far and no study did address compensation by HNRNPA3 upon loss of another HNRNP family member, the finding that Hnrnpa3 KO fish are viable but not Hnrnpa1 deficient zebrafish, gives further evidence that Hnrnpa3 is functionally distinct from Hnrnpa1.

Taken together the expression pattern and sequence homology analysis shows that Hnrnpa1a and Hnrnpa1b have functional overlap while also having distinct roles. This suggests that subfunctionalization split the HNRNPA1 function to Hnrnpa1a and Hnrnpa1b. Hnrnpa1a and Hnrnpa1b have the greatest sequence similarity with the human minor form HNRNPA1-B. There is no HNRNPA2 homologue in zebrafish and only one HNRNPA3 homologue.

## 4.2 What underlying mechanisms may cause the different phenotypes observed upon Hnrnpa1 KO or KD?

KD studies are a powerful tool to study the physiological function of genes in zebrafish during development [237]. KD of *hnrnpa1b* by MO injection in zebrafish embryos was previously shown by Liu et al. to result in abnormalities of the dorsal axis and vessels, and development of heart edema. Upon usage of a higher MO concentration 77.7% of the *hnrnpab1* MO injected embyos were lethal before 24 hpf [162]. In contrast, MO induced *hnrnpa1b* KD in zebrafish described by Cartealy et al. resulted in three different classes of phenotypes: (I) small and underdeveloped embryos, (II) kinked body and disorganized somites, and (III) lack of midbrain-hindbrain boundary. From the diversity of observed phenotypes upon KD of the same gene using two different MOs (one against the ATG, the other targeting the 5'UTR) a high level of discrepancy is observed. Contrasting these KD studies, the KO of Hnrnpa1a or Hnrnpa1b by CRISPR/Cas9 did not result in any developmental abnormalities. Discrepancies among the observed KD or KO phenotypes were

also previously observed for other genes [238]. In the following the potential underlying reasons for the observation of different phenotypes upon *hnrnpa1b* KD or KO are discussed.

The usage of MOs to transiently KD genes has been highly criticized over the past years due to the high rate of divergent phenotypes upon KO of the same gene by genome editing. The high frequency of off-target effects makes it difficult to determine how much of an antisense mediated phenotype results from the KD of the actual gene of interest, and how much derives from the KD of other genes [237]. To validate MO specificity, Stanier et al. provided guidelines for the usage of MO in the generation of genetic KDs and recommended the following: Usage of multiple MOs, rescue experiments, control MOs, dose-response curves, comparison with existent mutant, loss of protein confirmation, and minimization of off-target effects.

Both *hnrnpa1b* KD studies used a translation blocking MO by either targeting the ATG directly or the 5'UTR. The gold standard to address efficient MO KD is the usage of a specific antibody [237]. Both MO *hnrnpa1b* KD studies lack a verification of Hnrnpa1b protein loss by Western blot using an antibody that specifically recognizes the protein of interest. Cartealy et al. used the approach of coinjecting a plasmid containing GFP tagged to 5'UTR including the target site of the MO and take the relative decrease in GFP signal as an indicator of the overall genetic MO KD efficiency [163]. This approach was determined to be of little value, as suppression of GFP expression was observed to be a general phenomenon [239]. Liu et al. performed qRT-PCR using *hnrnpa1b* specific primer to determine the *hnrnpa1b* MO KD efficiency and showed 50% reduction in *hnrnpa1b* mRNA [162]. To control for toxicity effects both studies used scrambled MO. However, none of the studies performed rescue experiments by which specificity of the MO could be determined.

Another possible explanation for the phenotype in MO induced KD of *hnrnpa1b* could be the simultaneous translation blocking of maternal RNA, whereas mutants derived from a heterozygous *hnrnpa1a* or *hnrnpa1b* incross contain remaining maternal RNA. As incrosses from homozygous KO mutants gave healthy offspring the possibility that maternal contribution rescues the early phenotype can be ruled out for single Hnrnpa1a or Hnrnpa1b KOs. Moreover, a study by Carla Neugebauers lab states that translation blocking MO usage is not applicable. Due to the large maternal contribution of Hnrnpa1a and Hnrnpa1b protein the maternally deposited Hnrnpa1a or Hnrnpa1b protein may still be sufficient carry out essential functions preventing sufficient KD efficiency [214]. Another explanation for the existence of a phenotype in *hnrnpa1b* morphants are off target effects. Both studies lack thorough analysis using an unbiased approach or analyzing educated guesses due to sequence

similarity, to identify off target effects. Due to the high sequence similarity of *hnrnpa1a* and *hnrnpa1b* the MO directed to *hnrnpa1b* could target *hnrnpa1a* as well, blocking the translation of both genes and leading to generation of a double KD. To clarify KD specificity and uncover compensatory mechanisms, it would have been interesting to see whether *hnrnpa1a* levels are reduced upon KD of *hnrnpa1b* and whether the *hnrnpa1b* morphant phenotype can be observed upon *hnrnpa1a* KD. Lastly, we cannot rule out that the lack of compensatory upregulation of *hnrnpa1a* upon KD of *hnrnpa1b* (as seen in the KO) and vice versa might be causing the discrepancy seen in KD vs. KO.

It can be concluded that zebrafish mutants provide several advantages over morphants, such as reduction of hitting off targets. Outcrossing can eliminate mutations introduced in other loci than the gene of interest. Furthermore, mutants possess complete long-lasting KO of a gene, compared to MO generated KD models, which are mostly only partial loss of function and restricted to the first days of development. Taken together the discrepancy among *hnrnpa1b* KD models and the lack of appropriate controls raises concerns about the specificity of the described MOs. The lack of any phenotypic abnormalities in the generated *hnrnpa1a*$^{-/-}$ and *hnrnpa1b*$^{-/-}$ mutants again confirms this. As *hnrnpa1a* and *hnrnpa1b* were targeted with two different gRNAs and several alleles were raised to homozygosity, which all lack a phenotype, this observation can be considered to be specific.

## 4.3 Is there evidence for ALS associated phenotypes in *hnrnpa1a*$^{-/-}$*; hnrnpa1b*$^{-/-}$ mutants?

Having identified compensatory mechanisms among Hnrnpa1a and Hnrnpa1b but not Hnrnpa3, and having observed lethality only upon Hnrnpa1a and Hnrnpa1b double KO, we focused our further analysis on *hnrnpa1a*$^{-/-}$*; hnrnpa1b*$^{-/-}$ mutants. Moreover, in contrast to HNRNPA3, HNRNPA1 was directly linked to ALS and MSP patients by mutations that are causative for these diseases. The identification of HNRNPA1 mutations and the associated HNRNPA1 cytoplasmic mislocalization in ALS and MSP patients suggest that animal models lacking HNRNPA1 might recapitulate ALS and MSP associated phenotypes, which I analyzed in the *hnrnpa1a*$^{-/-}$*; hnrnpa1b*$^{-/-}$ mutants. ALS is defined by the degeneration of upper and lower motoneuron, ultimately leading to muscle degeneration [38] [40] [40]. In some cases ALS patients were described to show signs of dysfunctional circulation effects like hypoperfusion [220] [221]. Muscle integrity is hereby particularly relevant as MSP patients suffer from myopathies and HNRNPA1 KO mice show a prominent muscle phenotype [162].

### 4.3.1 *hnrnpa1a*$^{-/-}$*; hnrnpa1b*$^{-/-}$ and *tardbp*$^{-/-}$*, tardbpl*$^{-/-}$ mutants show partially overlapping phenotypes

The identified phenotypes, such as shortened motoneuron axons, muscle defects, and to a limited extend vasculature mispatterning in *hnrnpa1a*$^{-/-}$*; hnrnpa1b*$^{-/-}$ mutants are similarly present in *tardbp*$^{-/-}$*; tardbpl*$^{-/-}$ mutants [12] and suggest common underlying mechanisms upon loss of these proteins. Both proteins belong to the HNRNP family, have similar structure, and were shown to functionally and physically interact with one another to regulate RNA metabolism [240] [149] [150]. Also, HNRNPA1 and HNRNPA2/B1 MSP patients show nuclear clearance and cytoplasmic inclusions of TDP-43 in muscle tissue next to HNRNPA1 or HNRNPA2/B1 pathology [101]. Therefore, we compared our Hnrnpa1 KO model to the previously established Tdp-43 KO zebrafish regarding their phenotypes and molecular signature.

#### 4.3.1.1 Shortened SpMN in *hnrnpa1a*$^{-/-}$*; hnrnpa1b*$^{-/-}$ mutants

The HNRNPA1 KO mouse was not analyzed for neurodegeneration phenotypes specifically. However, several findings suggest a role of HNRNPA1 in neuron development. The top affected process comparison based on differentially expressed genes between wildtype, homozygous and heterozygous HNRNPA1 KO mice revealed “developmental neurogenesis”, “axonal guidance”, “synaptogenesis”, “neurophysiological processes”, and “neurotransmission” among the top 10 affected pathways. Likewise, top 10 process network analysis based on alternative splicing genes of these mice revealed neurodevelopment specific pathways, such as “neurogenesis”, “neurohormone signaling”, “neuropeptide signaling”, and “axonal guidance” [162]. As HNRNPA1 has its highest expression levels in the mouse CNS, followed by the liver and placenta, HNRNPA1 seems to play a crucial role in neuronal processes. Likewise, a role for Hnrnpa1 in neurodevelopment in zebrafish is supported by the expression pattern analysis by J. Trimarchi, who found that *hnrnpa1a* and *hnrnpa1b* are mainly expressed in the zebrafish head. Also, Cartealy et al. previously showed that *hnrnpa1b* mRNA is mainly localized to the brain, the forebrain, midbrain, hindbrain, and spinal cord neurons at 24 hpf [163]. Moreover, *hnrnpa1a*$^{-/-}$*; hnrnpa1b*$^{-/-}$ mutants show vascular mispatterning accompanied by reduced blood flow, which leads us to the assumption that cerebral blood flow is similarly dysregulated. This finding is in line with the observation that hypoperfusion is present in ALS patients and models, which correlates with disease severity [241] [242] [243].

Our finding that *hnrnpa1a*$^{-/-}$*; hnrnpa1b*$^{-/-}$ mutants have shortened SpMN can be explained by the previously identified role of Hnrnpa1 in neurodevelopment, which seems to be conserved among zebrafish and mice. It remains though elusive at this point what mechanism underlies the neuronal impairment. Alternatively, the developmental delay observed in *hnrnpa1a*$^{-/-}$*; hnrnpa1b*$^{-/-}$ mutants could account for the reduced SpMN axon length.

#### 4.3.1.2 Loss of muscle integrity in *hnrnpa1a*$^{-/-}$*; hnrnpa1b*$^{-/-}$ mutants

HNRNPA1 heterozygous KO mice show muscle development defects, such as irregular tongue muscle, and diaphragm skeletal muscles with fibrous tissue infiltration. The muscle phenotype is further supported by global expression changes in genes related to muscle and an exon array study that identified muscle contraction as the second most affected process [162]. Moreover, alternative splicing pattern of muscle development-related genes was changed upon heterozygous KO of HNRNPA1 in mice. Likewise, *hnrnpa1a*$^{-/-}$*; hnrnpa1b*$^{-/-}$ zebrafish mutants show muscle disintegrity at 30 hpf pointing to a conserved role of Hnrnpa1 in muscle development. Altogether these findings point to a crucial role of HNRNPA1 in muscle development. An additional role of HNRNPA1 in muscle maintenance could contribute to muscle wasting later in life as observed in HNRNPA1 associated ALS patients due to loss of HNRNPA1 function.

From the observed neuronal impairment and loss of muscle integrity upon Hnrnpa1 and Tdp-43 KO paired with findings from previous studies, it seems plausible that these proteins play a vital role in neuronal and muscle development. Due to the drastic phenotype in both mutants leading to premature death after few days, these morphological abnormalities may though not be highly specific to Hnrnpa1 or Tdp-43 loss of function. The *hnrnpa1a*$^{-/-}$*; hnrnpa1b*$^{-/-}$ mutants shows high levels of cell death in the spinal cord at the time analyzed, which is not present in *tardbp*$^{-/-}$*; tardpl*$^{-/-}$ mutants. It is therefore difficult to say whether these developmental defects are a direct consequence of Hnrnpa1 loss of function or whether the apoptotic tissue environment disrupts the correct formation of muscles and neurons. Motoneuron shortening especially is a commonly observed phenotype upon KD of genes, and is in most cases accompanied by general atrophy in the developing embryo or a developmental delay due to toxicity [244] [245] [246] [247]. Our previous study in *tardbp*$^{-/-}$*; tardbpl*$^{-/-}$ mutants linked these phenotypes to upregulation of *Filamin C* (*FLNC)*, which codes for FLNC, an actin cross-linking protein that provides anchors for membrane proteins and structural components, has important signaling functions, and was linked to FTLD-TDP patients due to its upregulation in these patients' brains [12] [248]. Strikingly, *flnca*

upregulation was likewise found in *hnrnpa1a*$^{-/-}$*; hnrnpa1b*$^{-/-}$ mutants. The link between upregulated *flnca* upon TDP-43 or HNRNPA1 loss of function paired with *Filamin C* upregulation in ALS patients supports loss of function disease mechanisms and common pathomechanisms leading to HNRNPA1 and TDP-43 pathology. It will be relevant in the future to determine whether upregulated *Filamin C* levels are also found in HNRNPA1 associated ALS/MSP cases.

Concluding, *Filamin C* is a molecular link between Hnrnpa1 and Tdp-43 KO muscle phenotype and muscle deficits in ALS patients in line with a potential common pathomechanism.

#### 4.3.1.3 Vasculature abnormalities *hnrnpa1a*$^{-/-}$*; hnrnpa1b*$^{-/-}$ mutants

Vascular phenotypes were not investigated in HNRNPA1 KO mice, but the network analysis between wildtype and heterozygous or homozygous HNRNPA1 KO mice revealed regulation of angiogenesis and development of blood vessels among the top 10 affected processes. Moreover, recent research suggests a role of HNRNPA1 in vascular smooth muscle cell (VSMC) function by regulating VSMC-specific gene expression, proliferation, and migration [249]. Similarly, *hnrnpa1a*$^{-/-}$*; hnrnpa1b*$^{-/-}$ mutants show vascular mispatterning with impaired and delayed sprouting starting at 30 hpf. A vascular phenotype is also present in *tardbp*$^{-/-}$*; tardbpl*$^{-/-}$ mutants sharing certain commonalities and differences with *hnrnpa1a*$^{-/-}$*; hnrnpa1b*$^{-/-}$ mutants. Both mutants show vasculature misspatterning displayed by supernumerous sprouts that leave their physiological path, and ultimately misconnect or stay unconnected. However, in *hnrnpa1a*$^{-/-}$*; hnrnpa1b*$^{-/-}$ mutants this hypersprouting is restricted to the intersegmental vessels dorsal to the horizontal mypseptum and the correct number of one sprout from the dorsal aorta per somite ventral to the horizontal myoseptum is formed (see Figure 3.31D). In contrast, *tardbp*$^{-/-}$*; tardbpl*$^{-/-}$ mutants grow approximately 1.5 sprouts per somite and hypersprout also ventral to the horizontal myoseptum [222]. Moreover, the intersegmental sprouts of *hnrnpa1a*$^{-/-}$*; hnrnpa1b*$^{-/-}$ mutants that extend along their physiological path up to the horizontal myoseptum and form a lumen, while the sprouts of *tardbp*$^{-/-}$*; tardbpl*$^{-/-}$ mutants hyperbranch already ventral to the horizontal myoseptum show a thinned lumen restricting constant blood flow.

Sprouting blood vessels are formed by angiogenesis, a process that includes regulation of endothelial cells (EC) migration, proliferation, and adhesion. The leading cell senses stimuli that cause extension of one lamellipodium and several filopodia to the direction of migration. Thus, pro-angiogenic signaling cues have to be provided locally at the correct time and place

to ensure sprout growth along defined paths at distinct sites and developmental stages [250]. In *hnrnpa1a*$^{-/-}$*; hnrnpa1b*$^{-/-}$ mutants the high level of cell death may disrupt this highly specialized signaling pattern. Also, vascular sprouting starts later in development than in wildtype embryos since the mutants are generally developmentally delayed.

Concluding, the delay in vasculature formation and the mispatterning of ISV upon Hnrnpa1 KO are in accordance with previous findings that suggest an essential role for Hnrnpa1 in vasculature development. As the observed phenotype may be additionally influenced by cell death and developmental delay that is present in these mutants, we cannot determine whether the vascular phenotype is a primary or secondary effect. Lastly, the vascular phenotype is for the most part distinct to that observed in Tdp-43 deficient embryos, suggesting distinct underlying mechanisms leading to vascular mispatterning.

### *fn1b* upregulation: a potential link to vasculature defects observed upon Hnrnpa1 or TDP-43 KO

Endothelial hypersprouting in *tardbp*$^{-/-}$*; tardbpl*$^{-/-}$ mutants was linked to upregulation of *fn1b*, *vcam1 and itgα4/β1*. Likewise, *hnrnpa1a*$^{-/-}$*; hnrnpa1b*$^{-/-}$ mutants show increased *fn1b* levels potentially linking the commonalities of the vascular phenotype present in Hnrnpa1 and Tdp-43 deficient embryos. Interestingly, *vcam1 and itgα4/β* were not upregulated in *hnrnpa1a*$^{-/-}$*; hnrnpa1b*$^{-/-}$ mutants. FN1 is a high molecular weight glycoprotein of 250 kDa and is involved in cell adhesion, growth, and migration [251]. FN1 KO mice are embryonically lethal with heart defects in heart and blood vessel development, pointing to an essential role of FN1 during embryonic development [252] [253] [254]. Zebrafish have two FN1 genes, *fn1a* and *fn1b* [255], which were both shown to be required for somite boundary formation and maintenance [256]. While having overlapping functions, loss of *fn1a* or *fn1b* function point to distinct roles during zebrafish embryo development. *fn1a* deficiency results in mild somite boundary defects in the anterior somites, whereas *fn1b* KD zebrafish show normal somite formation but tail extension defects and disruption of the regular somite morphology by the 15-20 somite stage [257]. Correct formation of somite boundaries is particularly important during development [256]. Once the somites are formed, distinct areas of each somite are subregionalized in various tissues and cell types, which are important for bone, musculature, and nervous system development [258]. Any disruption of somite formation can hence result in anomalies affecting various tissues, such as vasculature or muscle.

Upregulation of *fn1b, vcam1 and itgα4/β1* in *tardbp*$^{-/-}$*; tardbpl*$^{-/-}$ mutants was causative for the vasculature hypersprouting, and increased FN1 expression was detected deposited around

ectopically sprouting EC. The contribution of *fn1b, vcam1 and itgα4/β1* to the phenotype could be further verified by a partial MO KD to wildtype levels in these mutants that were sufficient to rescue the phenotype. Moreover, FN1 was found among the top 30 bound transcripts by individual nucleotide resolution cross-linking immunoprecipitation-high-throughput sequencing (iCLIPs) [259]. Prominent binding of TDP-43 to the entire RNA of *FN1* suggests regulation of transcript stability or translation [260] [261]. It remains elusive how *fn1b* upregulation causes the vasculature mispatterning in *hnrnpa1a*$^{-/-}$*; hnrnpa1b*$^{-/-}$ mutants as the phenotype is different than that observed in *tardbp*$^{-/-}$*; tardbpl*$^{-/-}$ mutants, which additionally show hypersprouting ventral to the horizontal myoseptum. As Fn1b has a direct role in extracellular matrix (ECM) signalling and somite formation, Fn1b upregulation may contribute to common characteristics of the vascular phenotypes, such as hypersprouting dorsal to the horizontal myoseptum and mispatterning of ISV, in several ways. FN1 is secreted by EC, deposited in the ECM and functions in multiple aspects of EC behavior [262]. The ECM-EC interaction induces several signaling events, which are crucial for directed migration of EC during vascular development. Upon increased levels of *fn1b* the ECM-EC signaling may be impaired leading to impaired EC migration and sprout formation. Alternatively, somite boundaries, which are key for shaping the basic structure for later vasculature formation, may be disrupted due to FN1's importance in somite formation. As a consequence growing sprouts lack their guidance, divert from their physiological path, and misconnect.

It would be interesting to perform FN1 staining in these mutants as performed previously in *tardpb*$^{-/-}$*; tardbpl*$^{-/-}$ mutants to detect Fn1 expression pattern and determine potential differences observed in Tdp-43 and Hnrnpa1 KO zebrafish that could explain the distinct vascular phenotypes with common increase in *fn1b*. Moreover, a MO rescue approach could be performed to identify whether reduced *fn1b* is sufficient to restore normal vasculature development also in *hnrnpa1a*$^{-/-}$*; hnrnpa1b*$^{-/-}$ mutants. While no direct binding between FN1 and HNRNPA1 was described yet, it is possible that these two proteins either directly or indirectly interact via TDP-43, as HNRNPA1 and TDP-43 are direct interaction partners [149]. Alternatively, the different vascular phenotypes may arise from secondary effects as both HNRNPA1 and TDP-43 have hundreds of targets that may influence vasculature development.

One can conclude that Hnrnpa1 or Tdp-43 causes largely different vascular phenotypes but share the upregulation of *fn1b*, which could contribute to the few common aspects of the phenotype.

### 4.3.2 Shared genes that are differentially expressed genes in *hnrnpa1a*$^{-/-}$; *hnrnpa1b*$^{-/-}$ mutants

We wondered if besides *fn1b* and *flnca* there are more shared misregulated genes contributing to the partially overlapping phenotypes of *hnrnpa1a*$^{-/-}$; *hnrnpa1b*$^{-/-}$ *and tardpb*$^{-/-}$; *tardbpl*$^{-/-}$ mutants. We performed RNA sequencing of *hnrnpa1a*$^{-/-}$; *hnrnpa1b*$^{-/-}$ mutants and compared the dataset to the previously obtained RNA sequencing dataset of *tardpb*$^{-/-}$; *tardbpl*$^{-/-}$ mutants in order to identify potential overlap of differentially expressed genes upon KO of Hnrnpa1 or Tdp-43. The overlap analysis revealed 15 genes whose expression is changed in both datasets of which 8 genes are changed in the same direction. It has to be noted that RNA sequencing of *hnrnpa1a*$^{-/-}$; *hnrnpa1b*$^{-/-}$ mutants revealed far more differentially expressed genes (615 in total) with a more than one fold change and a p-value<0.01 than RNA sequencing data obtained from *tardpb*$^{-/-}$; *tardbpl*$^{-/-}$ mutants (56 in total). Interestingly, the majority of commonly differentially expressed genes encode proteins that are present in the ECM or encode membrane proteins pointing to overlapping differentially expressed genes related to structure. Other genes were related to muscle integrity, which links HNRNPA1 and TDP-43 loss of function with the muscle phenotype observed upon their KO and muscle deficits in ALS patients.

### 4.3.3 Regulation among Hnrnpas and Tdp-43

The overlapping findings of shared phenotypes and common differentially expressed genes upon Hnrnpa1 or Tdp-43 deficiency, prompted us to investigate whether protein levels of any of the three Tdp-43 zebrafish paralogues are changed upon Hnrnpa KO. Upon single loss of Hnrnpa1a, Hnrnpa1b, or Hnrnpa3 no differences in Tardbp, Tardbpl or Tardbpl_tv1 protein levels were detected. Similar results were obtained in *hnrnpa1a*$^{-/-}$; *hnrnpa1b*$^{-/-}$ mutants. Apart from TDP-43 and HNRNPA1 being well-known splicing factors that control the expression of many different target genes, and the finding that HNRNPA1 and TDP-43 control their own splicing and/or transcript levels in zebrafish [12], there is also evidence that they regulate the splicing of each other. It was previously shown that upon loss of nuclear TDP-43 the splicing pattern of HNRNPA1 is altered resulting in a longer and more aggregation prone HNRNPA1 isoform, named HNRNPA1-B [150]. We could further determine that upon loss of Hnrnpa1, *tardbpl* is alternatively spliced leading to the integration of a longer exon 6 isoform, most probably functioning as an alternative 3'UTR, which plays a crucial role in transcript stability, control of gene expression, or nuclear export [263]. Differentially used 3`UTRs

upon Hnrnpa1 KO may therefore have widespread effects and contribute to disease pathogenesis. The finding needs further research to determine whether the alternative 3' UTR usage is linked to increased expression of Tardbpl_tv1 or Tardbp protein. While the proteomic analysis revealed no difference in Tardbp or Tardbpl levels, the changes may be either too subtle to detect or be restricted to the Tardbpl_tv1 isoform, which was neither identified by mass spectrometry nor studied on Western blot. It will be of relevance to determine whether HNRNPA1 loss of function in ALS leads to such alterations in TDP-43 as it has been described vice versa.

One can conclude that Hnrnpa1 and Tdp-43 control their own splicing/transcription, which results in compensatory mechanisms among the different paralogues. Moreover, Hnrnpa1 and Tdp-43 influence each other by controlling each other's splicing and we could show here for the first time that loss of Hnrnpa1 has an effect on Tdp-43 splicing.

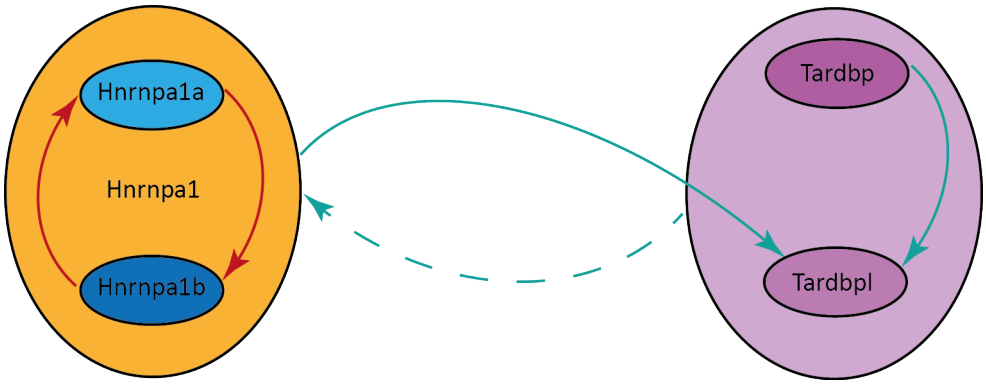


**Figure 4.1 - Schematic illustration of transcriptional and alternative splicing regulation between Hnrnpa1 and Tdp-43.** Hnrnpa1 (depicted in orange) has two different orthologues in zebrafish, Hnrnpa1a and Hnrnpa1b, that regulate each other on transcriptional level. Upon loss of Tardbp, *Tardbpl* is differentially spliced resulting in another transcript variant, *tardbpl_tv1*. Alternative splicing regulation among Hnrnpa1 and Tardbp in zebrafish and human could be also shown. Upon Loss of Hnrnpa1, *tardbpl* is differentially spliced resulting in expression of a variant possessing a longer exon 6, which likely resembles an alternative 3'UTR. Vice versa, upon TDP-43 depletion in human cells, *HNRNPA1* is differentially spliced causing inclusion of exon 8 that results in higher levels of the HNRNPA1-B isoform. Red indicates transcriptional regulation. Turquoise indicates alternative splicing regulation. Dashed line represents findings from human samples.

### 4.3.4 What causes the partial overlap in phenotype and differentially expressed genes upon Hnrnpa1 or Tdp-43 loss of function?

HNRNPA1 and TDP-43 both belong to the HNRNP family, are nuclear shuttle proteins, and are ubiquitously expressed. The high degree of complexity among HNRNPs and their splicing targets results in some combinations of HNRNPs that exhibit significant synergy while others

act antagonistically [264]. While having many overlapping features regarding structure and function, certain characteristics are unique to HNRNPA1 and TDP-43, respectively. HNRNPA1 does not contain a classical nuclear localization signal (NLS) as TDP-43, but a specialized M9 domain and a PY-NLS like FUS [265]. RNA specificity is particularly determined by the terminal region of the RMM and the variable regions of the loops that give structure to the beta strands [266]. Also the binding motif preferences of HNRNPA1 and TDP-43 are different. While HNRNPA1 binds preferentially to AU-rich sequences with its most prominent binding motif being UUAGGG, TDP-43 binds to UG repeats [267]. The binding of TDP-43 mostly occurs in introns and 3`UTRs [268, 269], while HNRNPA1 preferentially associates with exons and introns [270] [271]. Their binding in most cases leads to splicing repression, but no studies have compared the effect of HNRNPA1 or TDP-43 loss of function on their overall effect on their target genes to identify potential overlap and differences. While we could identify 15 commonly differentially upregulated genes upon Hnrnpa1 or Tdp-43 loss of function, it will be interesting to determine if and how these genes contribute to disease pathogenesis and whether some of these genes can be verified in other model systems to show conservation.

It can be concluded that the majority of the underlying mechanisms upon Hnrnpa1 or Tdp-43 deficiency are diverse while some overlap is present shown by some common differentially expressed genes.

## 4.4 Could metabolic impairment be the underlying cause of premature death of *hnrnpa1a*$^{-/-}$*; hnrnpa1b*$^{-/-}$ mutants

The most striking phenotype in *hnrnpa1a*$^{-/-}$*; hnrnpa1b*$^{-/-}$ mutants is the thinned yolk extension phenotype, which is not present in *tardbp*$^{-/-}$*; tardbpl*$^{-/-}$ mutants and points to a specific phenotype upon Hnrnpa1 KO. Paired with the significant developmental delay we hypothesize metabolic deficits upon Hnrnpa1 KO.

### 4.4.1 Developmental delay in *hnrnpa1a*$^{-/-}$*; hnrnpa1b*$^{-/-}$ mutants

Apart from being lethal after 5 dpf, *hnrnpa1a*$^{-/-}$*; hnrnpa1b*$^{-/-}$ mutants are developmentally delayed. Likewise, HNRNPA1 KO mice are partially embryonically lethal, which was shown by a reduced number of homozygous HNRNPA1 KO mice after incrossing HNRNPA1 heterozygous mice. Genotyping of E18.5 embryos showed that HNRNPA1 KO mice develop in the expected numbers but die before being born [162]. Early lethality of HNRNPA1 deficient mice and zebrafish points to a crucial role of HNRNPA1 in early development. The

lab of Karla Neugebauer performed a detailed study on the role of Hnrnpa1 (Hnrnpa1a and Hnrnpa1b) in early developing zebrafish as it was found among other nuclear pre-mRNA processing factors to be highly enriched before zygotic genome activation (ZGA). As embryos are transcriptionally silent at the preZGA state an unconventional function of Hnrnpa1 during this phase was suggested. Hnrrnpa1 plays a role in RNA metabolism during embryogenesis as is regulates poly(A) tail length before ZGA through 3' UTR binding and encourages translation of maternal transcripts [214]. Based on the finding of the Karla Neugebauer's lab one can assume that upon loss of Hnrnpa1 translation of maternal transcripts is decreased, which may have widespread consequences on general protein synthesis. Given the dependence of early embryos on RNA-based regulation of gene expression, major roles for RBPs in developmental transitions are anticipated. RBPs are of critical importance to regulate every step of RNA metabolism through their association with RNA sequences [261] [272]. Despic et. al further reported a developmentally essential nuclear function of Hnrnpa1 at ZGA. Hnrnpa1 was found to bind basal, single-stranded segments of pri-miR-430a and thereby regulates miR-430 biogenesis [214]. miR-430 comprises an evolutionary conserved miRNA family, whose absence results in disrupted neural tube formation and brain morphogenesis [273] [274].

It can be concluded that Hnrnpa1 plays a vital role already in very early development, especially before ZGA, which fits to our finding that *hnrnpa1a*$^{-/-}$*; hnrnpa1b*$^{-/-}$ mutants are developmentally delayed and die at larval stage. It remains to be determined whether embryos become developmentally delayed and go down the detrimental path already before ZGA due to lack of transcription of maternal RNAs or after ZGA. Moreover, it is not clear which precise mechanism leads to developmental delay, but a previous study could show that developmental delay may arise from slowed down cell cycle [275]. It may be therefore interesting to assess cell cycle progression in these mutants. This model may be further used to better identify the role of Hnrnpa1 in preZGA state and to thereby elucidate how Hnrnpa1 regulates poly(A) tail length and controls transcription.

### 4.4.2 Alterations in *pkma* splicing do not cause metabolic defects in *hnrnpa1a*$^{-/-}$*; hnrnpa1b*$^{-/-}$ mutants

A potential molecular candidate that links HNRNPA1 loss of function and metabolic defects is PKM. The two isoforms, PKM1 and PKM2, are generated by alternative splicing of the primary RNA transcript of the *PKM* gene, by differential usage of exon 9 and 10, respectively. The non-allosteric isoform PKM1 is constitutively active, and expressed in

terminally differentiated tissues, including the muscle and the brain, which require a large supply of ATP. PKM2 is expressed in tissues with anabolic functions, including proliferating cells and cancer cells. The OE of PKM2 in cancer cells is controlled by the oncoprotein c-Myc, which activates the transcription of HNRNPA1 and HNRNPA2/B1 [276]. Upon binding of these HNRNPA proteins to exon 9 of PKM1, the splicing of PKM1 mRNA is inhibited, which allows the synchronous expression of the PKM2 isoform [216] [217]. Upon loss of HNRNPA1 function splicing is no longer inhibited and less PKM2 is expressed. The effect of HNRNPA1 KD in HeLa cells was previously reported to result only in minor changes in PKM splicing pattern. In contrast, depletion of both HNRNPA1 and HNRNPA2/B1 resulted in an increase in *PKM1* mRNA from 2% to 29%, and a concomitant decrease in *PKM2* mRNA [277]. PKM2 is a limiting glycolytic enzyme that catalyzes the final step in glycolysis, which is key in growth. Reduced expression of PKM2 due to loss of HNRNPA1 could thereby explain the developmental delay observed in *hnrnpa1a*$^{-/-}$*; hrnnpa1b*$^{-/-}$ mutants. In zebrafish two PKM orthologues exist: Pkma and Pkmb. Of these *pkma* is alternative spliced resulting in different isoforms of which *pkma202* and *pkma201* were identified to have a high conservation in gene structure and sequence with human *PKM1* and *PKM2* isoforms, respectively [219].

We did not observe alternative splicing of *pkma* in zebrafish upon Hnrnpa1 KO, which indicates that this splice regulation is not conserved between human cells and zebrafish. The growth retardation seems therefore not result from changes in expression of *pkma201* and *pkma202*. Interestingly, upon generation of a liver tumor zebrafish model the *pkm2* isoform was found to be highly enriched and *hnrnpa1* (no information available whether this refers to *hnrnpa1a* or *hnrnpa1b* or both) was greatly upregulated [219]. Discrepancies between these findings can be explained in several ways: potentially, loss of Hnrnpa1 function is not enough to induce increased *pkm201* expression in zebrafish as only minor changes were observed in HeLa cells and the tumor zebrafish represents a quite aggressive model. Alternatively, gain and loss of Hnrnpa1 function might not simply have opposite function in zebrafish or *pkma* alternative splicing may highly depend on the developmental stage and may thus not occur at 30 hpf. Furthermore, increased PKM2 expression was only observed in HeLa cells after depletion of both HNRNPA1 and HNRNPA2/B1. Since zebrafish lack an HNRNPA2/B1 orthologue, other genes may be involved to control *pkma* splicing in zebrafish.

### 4.4.3 Identification of dysregulated candidate genes by NGS

Having excluded expression alterations in the candidate gene *pkma* as being responsible for the impaired metabolism phenotype in *hnrnpa1a*$^{-/-}$*; hnrnpa1b*$^{-/-}$ mutants, I aimed for an unbiased approach to identify differentially expressed genes involved in metabolism upon Hnrnpa1 KO. NGS revealed 615 differentially expressed genes with more than a two-fold change in differential expression and a p-value smaller than 0.01 in 30 hpf *hnrnpa1a*$^{-/-}$*; hnrnpa1b*$^{-/-}$ mutants. The only other RNA sequencing data available for HNRNPA1 KO comes from a mouse study. The number of genes with altered expression upon HNRNPA1 KO in mouse and zebrafish are quite different. While Liu et al. report 4355 upregulated genes and 4968 downregulated genes in HNRNPA1 KO mouse (foldchange>3; p-value<0.05), with the same settings only 121 genes were downregulated and 174 genes upregulated in *hnrnpa1a*$^{-/-}$*; hnrnpa1b*$^{-/-}$ mutants. HNRNPA1 dependent regulation of specific mRNAs seems to vary in different tissues, organisms, and stages of development. While differentially expressed genes upon HNRNPA1 KO were analyzed from the mouse heart, for the analysis of zebrafish genes the whole embryos were taken. Moreover, the mouse study compared heterozygous HNRNPA1 KO mice to wildtype, while we compared *hnrnpa1a*$^{-/-}$*; hnrnpa1b*$^{-/-}$ mutants to wildtype looking embryos, which are a mix of the genotypes of *hnrnpa1a*$^{+/-}$ *and* *hnrnpa1a*$^{+/+}$.

Functional annotation clustering revealed that the majority of the differentially expressed genes in zebrafish are involved in “cell cycle”, “p53 signaling pathway”, “FoXo signaling”, and “Notch signaling pathway”. As p53 signaling, FoXo signaling [278], and Notch signaling [279] all affect cell cycle progression, I focused on the cell cycle for further analysis.

### 4.4.4 Could impaired cell cycle at $G_1$/S-phase be responsible for the metabolic slow down in *hnrnpa1a*$^{-/-}$*; hnrnpa1b*$^{-/-}$ mutants?

RNA sequencing of *hnrnpa1a*$^{-/-}$*; hnrnpa1b*$^{-/-}$ mutants revealed cell cycle as one of the most altered processes based on differentially expressed genes. The differentially expressed genes involved in cell cycle are *ccne1*, *cdkn1a*, *cdkn2a/b*, *gadd45*, *p53*, and *rbl2*. Their increased mRNA expression could be verified by qRT-PCR, with the exception of *ccne*1, which was found to be unchanged. Interestingly, genetic profiling studies of ALS patients and ALS animal models revealed *gadd45*, *cdkn1a*, and *rb1* among the top upregulated genes, which were also detected in G86R SOD1 mice before symptom onset or motoneuron death [280] [281]. The corresponding proteins are all involved in $G_1$/S-phase transmission pointing to

impairment of this specific cell cycle step upon Hnrnpa1 KO. Impairment of the cell cycle is further supported by the developmental delay and the increased cell death observed in *hnrnpa1a*$^{-/-}$*; hnrnpa1b*$^{-/-}$ mutants. Moreover, additional lines of evidence support a role of Hnrnpa1 in cell cycle progression. First, Hnrnpa1 has been highly linked to cancer due to the finding of increased Hnrnpa1 levels in colorectal cancers and lymphoma [282]. Furthermore, one study reported cell cycle arrest at $G_2$/M stage [158], while others showed cell cycle arrest at $G_0/G_1$ phase upon HNRNPA1 KD [146]. Even though current studies reveal non-overlapping results, it can be agreed on that reduced HNRNPA1 levels are associated with low proliferating or resting cells [283].

The $G_1$/S transition is tightly controlled by the tumor suppressor protein RB and the E2F family of transcription factors. E2F family members bind cell cycle gene promoters and thereby control the temporal expression of genes required for the $G_1$/S transition. Phosphorylated RB results in the release of the transcription factor E2F and the transcription of target genes. In contrast, unmodified RB binds to the E2F transcription factor preventing the transcription of target genes [284]. The RBL2/E2F2 is controlled by the p53 pathway. During $G_1$/S-phase transition p53 levels are below the threshold that induces activation of Cdkn1a and Cdkn1b, which are potent inhibitors of the Ccne/Cdk2 complex. The active Ccne/Cdk2 complex phosphorylates Rbl2 upon which it dissociates from E2F2, which becomes free and shuttles into the cytoplasm where it binds promoters that initiate transcription of S-phase genes. Upon Hnrnpa1 KO, p53 levels are highly upregulated causing transcriptional enhancement of *cdkn1a* and *cdkn2b*, whose encoded proteins are active inhibitors of Cdk2. At the same time p53 directly regulates transcription of *gadd45*, which is a tumor suppressor gene, and induces upregulation that causes inhibition at $G_1$/S-phase by interaction with Cdkn1a and Cdkn2b [285]. The inhibition of Cdk2 activity prevents phosphorylation of Rbl2 and hence dissociation of E2F2. As a result, E2F2 does not shuttle to the cytoplasm to initiate transcription of its target genes and the cell remains in $G_1$ phase (see Figure 4.2) [286]. Reduced $G_1$/S-phase transition can occur in response to several initiators, such as cellular stress or DNA damage.

We addressed cell cycle progression of *hnrnpa1a*$^{-/-}$*; hnrnpa1b*$^{-/-}$ mutants by analyzing the protein levels of Pcna, which was previously reported to label actively dividing cells, and did not observe any difference between *hnrnpa1a*$^{-/-}$*; hnrnpa1b*$^{-/-}$ and wildtype looking siblings.

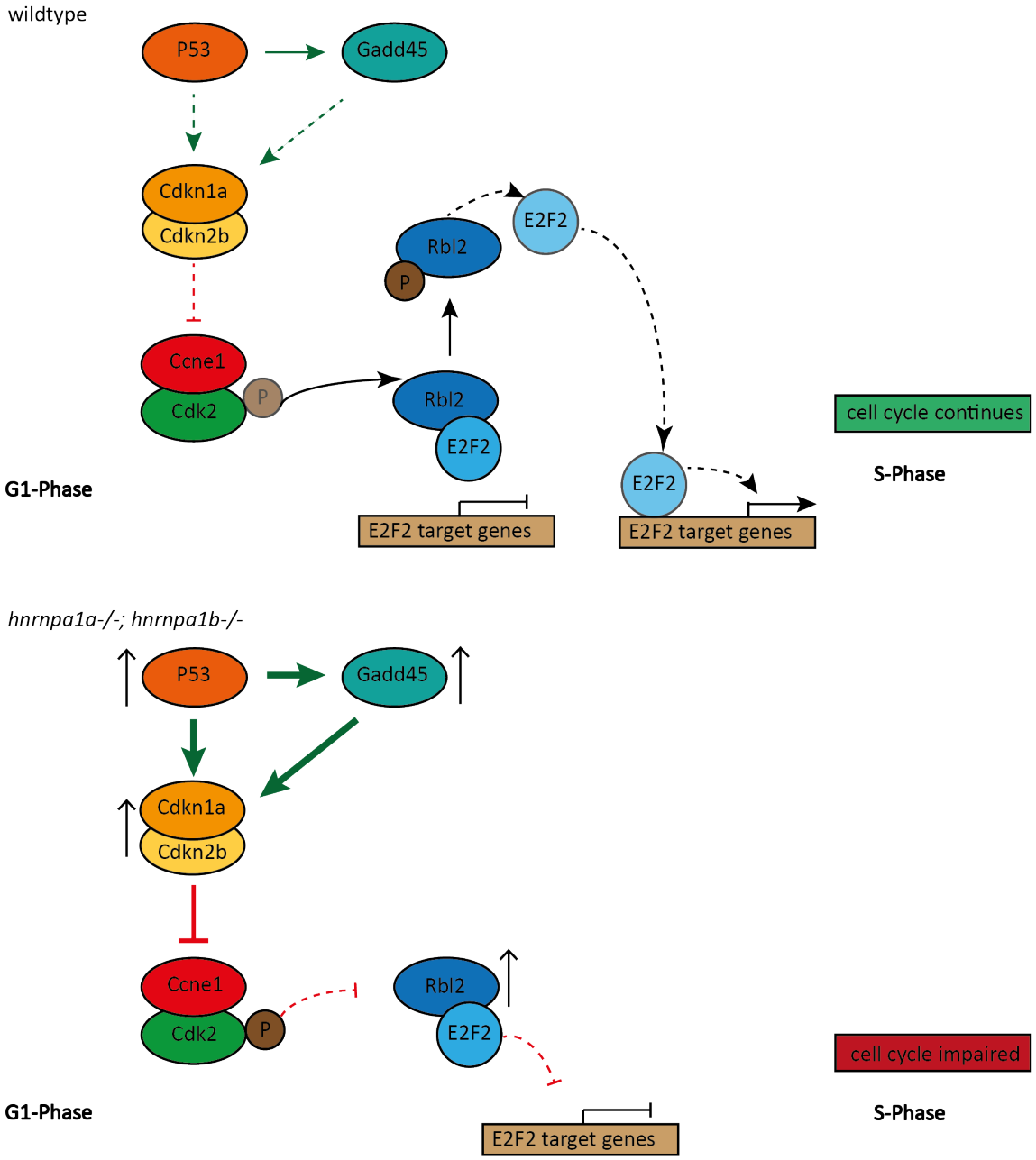


**Figure 4.2 - Scheme illustrating the hypothetical cell cycle impairment in $G_1$/S-phase transition in *hnrnpa1a*$^{-/-}$; *hnrnpa1b*$^{-/-}$ mutants.** For explanation see text.

Likewise, Western blotting with a Pcna specific antibody was not substantially altered in the mutants. However, for the analysis of Pcna protein levels the whole embryo was taken. Therefore, lower levels of Pcna in a specific region that may be affected by reduced proliferation could be masked by other region showing greater proliferation. The changes in cell proliferation may also be below detection limit and small changes in the size of the analyzed embryos may cover subtle changes in Pcna protein levels. The staining pattern of Pcna is not clear, as many cells cannot be assorted to a specific cell cycle phase according to their staining. Quantification of cells undergoing a specific cell cycle phase is therefore not possible and no conclusion can be drawn whether more cells remained in $G_1$ phase upon

Hnrnpa1 KO. For a more detailed and clear analysis, the transgenic Dual Fucci zebrafish carrying reporters that permit *in vivo* imaging of the cell cycle by labeling each cell cycle stage at a different fluorescence would be a more suitable model [287]. The finding of differentially expressed cell cycle associated genes upon Hnrnpa1 loss of function suggest a crucial role of Hnrnpa1 in controlling important mediators of the cell cycle, which is particularly important during development. However, functional impairment of the cell cycle in *hnrnpa1a*$^{-/-}$*; hnrnpa1b*$^{-/-}$ mutants could not be directly shown and would require further crossings to a transgenic reporter fish. The upregulation of some genes in cell cycle control upon Hnrnpa1 KO can also promote apoptotic pathways, which also plays an important role during normal development. It remains to be determined whether p53 activation is a direct effect of Hnrnpa1 loss of function. As a follow up one could examine when p53 activation starts by measuring *p53* RNA levels throughout embryo development at various time points earlier than the currently selected 30 hpf. Moreover, it would be interesting to examine if the expression of *p53* and its target genes is localized to specific regions in the *hnrnpa1a*$^{-/-}$*; hnrnpa1b*$^{-/-}$ mutants by performing an ISH and if MO mediated KO of *p53* rescues the developmental delay or apoptosis.

### 4.4.5 Lipid metabolism defects in *hnrnpa1a*$^{-/-}$*; hnrnpa1b*$^{-/-}$ mutants

While we could not pinpoint cell cycle defects to the observed metabolic deficits we aimed for other pathways that may be altered and ultimately lead to cell cycle impairment. The thinned yolk extension of *hnrnpa1a*$^{-/-}$*; hnrnpa1b*$^{-/-}$ mutants points to impaired lipid metabolism upon Hnrnpa1 KO. There is so far little evidence of involvement of HNRNPA1 in lipid metabolism and no alterations in lipid related genes were reported upon HNRNPA1 KO in mice [162]. One study revealed an indirect role of HNRNPA1 in metabolism as the liver of high-fat-diet fed mice contained decreased nuclear HNRNPA1 compared to the liver of standard-diet-fed mice. The authors propose endoplasmatic reticulum (ER) stress related HNRNPA1 translocation to the cytosol where it mediates the activation of the transcription factor SREBP-1, which modulates expression of several enzymes involved in lipid synthesis [288]. Due to the fact that dysregulated energy metabolism is frequently linked to ALS, we focused on the phenotype in more detail. Hyperlipidaemia in particular was proposed as one of the reasons for energy imbalance in ALS patients and current literature suggests that the lipid metabolism plays a crucial role in ALS progression. However, the findings are still controversial and the underlying mechanisms linking lipid metabolism defects and ALS remain unclear.

A standard approach to assess lipid expression in the developing zebrafish embryo is to perform ORO staining that labels the neutral lipids and triglycerides. Under healthy conditions ORO staining in the yolk gradually decreases over time, meaning that less neutral lipids are present in the yolk. The lipids were then either used up by the embryo or were stored in the embryo body. In *hnrnpa1a*$^{-/-}$*; hnrnpa1b*$^{-/-}$ mutants, ORO stain revealed lower amount of neutral lipids in the yolk extension and increased uptake from the yolk extension to the zebrafish trunk, suggesting that the yolk extension thinning arises from increased uptake of lipids. This finding implies an important role for Hnrnpa1 in lipid transport and metabolism during zebrafish development. The underlying mechanisms remain unclear raising the question how increased neutral lipid transport is mediated.

During the first four days of development, zebrafish are lecithotrophic and rely on their yolk sac for the nutrients needed to sustain growth and survival. The developing embryo receives vital fat-solube vitamins from the yolk, as well as triacylglyerol and cholesterol, which is an essential component of cell membranes. The yolk syncytial layer (YSL) is implicated in yolk lipid metabolism and lipoprotein biogenesis, to transport yolk nutrients to the developing embryos [289]. Upon formation of the circulatory system, lipoproteins transport the yolk lipids to their specific target site via the bloodstream [290]. Defective lipoprotein assembly during embryogenesis was demonstrated to result in unabsorbed yolk phenotype suggesting that yolk lipids are assembled into lipoproteins for transport to the developing embryo [291] [292] [293].

It is of particular interest to identify how lipids are being transported through the living embryo and at what point of development lipid usage becomes impaired in *hnrnpa1a*$^{-/-}$*; hnrnpa1b*$^{-/-}$ mutants. As a next step, to assess lipid absorption and metabolism during zebrafish development, one can inject BODIPY labeled fluorescent FA analogs that closely resemble native FAs.

### 4.4.6 Identification of a lipid transporter gene as the main hit

Analysis of differential expression of genes that may be responsible for lipid processing in *hnrnpa1a*$^{-/-}$*; hnrnpa1b*$^{-/-}$ mutants revealed the genes *apoda.1*, *nampt* and *gpnmb* as promising candidates. qRT-PCR confirmed downregulation of *gpnmb* and *apoda.1*, but not *nampt*. The reduction in *apoda.1* and *gpnmb* paired with their involvement in metabolism suggest that reduction the corresponding proteins could be responsible for the metabolic defects observed in *hnrnpa1a*$^{-/-}$*, hnrnpa1b*$^{-/-}$ mutants. Since Apoda.1 is a lipid processing protein and the *hnrnpa1a*$^{-/-}$*, hnrnpa1b*$^{-/-}$ mutants show striking lipid processing defects, I focused my further

analysis on Apoda.1. APOD belongs to the lipocalin family of glycoproteins, binds small hydrophobic ligands, and was associated with lipid metabolism and metabolic syndrome [294] [295] [296] [297]. These studies clearly indicate an important role of APOD in energy and lipid homeostasis. However, the precise role of APOD remains unclear. No splicing alteration of *apoda.1* mRNA was detected, indicating regulation of transcription itself or RNA degradation by Hnrnpa1.

## 4.5 Apoda.1 as a potential link of the distinct lipid phenotype in *hnrnpa1a*$^{-/-}$; *hnrnpa1b*$^{-/-}$ mutants

Apoda.1 is downregulated by 8.9 fold upon KO of HNRNPA1 in zebrafish and is involved in lipid transport. Due to the lack of a zebrafish specific antibody, the protein levels of Apoda.1 could not be analyzed. If decreased expression of *apoda.1* is responsible for the metabolic and lipid phenotype observed in *hnrnpa1a*$^{-/-}$*; hnrnpa1b*$^{-/-}$ mutants, KD of *apoda.1* in AB wildtype embryos should mimic the Hnrnpa1 associated loss of function phenotype. Upon MO KD we could not only identify a specific role for *apoda.1* to cause a similar lipid phenotype as upon Hnrnpa1 deficiency, but also determine a dosage dependent phenotype severity. Moreover, we could show that a certain threshold of at least 75% *apoda.1* reduction has to be reached in order to fully phenocopy the observed thinning of the yolk extension in *hnrnpa1a*$^{-/-}$*; hnrnpa1b*$^{-/-}$ mutants. For making the final link between the phenotype observed upon Hnrnpa1 KO and Apoda.1 loss of function it will be interesting to determine whether Apoda.1 overexpression can rescue the lipid phenotype in the *hnrnpa1a*$^{-/-}$*; hnrnpa1b*$^{-/-}$ mutants.

### 4.5.1 How could reduced Apoda.1 cause increased lipid transport across the YSL?

Having identified *apoda.1* as one of the most downregulated genes upon Hnrnpa1 KO the question remains whether and how *apoda.1* is involved in causing the observed lipid phenotype. APOD is a small glycoprotein of 29 kDa with a high degree of sequence conservation among different species. It is a soluble carrier protein and has many functions including protection from oxidative stress and lipid transport. Both the different structure of APOD compared to the other apolipoprotein family members, such as APOB and APOC, as well as its allocation to the lipocalin family suggest a distinct role of APOD in lipid transport. While the *APOD* gene has been thoroughly studied in humans and mice, linking its abnormal expression to human diseases, such as PD and AD, only little is known about the role of APOD in zebrafish [298] [299] [300]. In zebrafish there are three copies of the *apod* gene: a1, a2, and b2. *apoda.1* KD in AB wildtype embryos results in a thinned yolk extension, indicating that Apoda.1 is required for proper lipid processing in zebrafish. Moreover, KO

studies from mice demonstrated a correlation between APOD expression and healthy plasma lipid profiles. We can only speculate about its role in the developing embryo based on our findings and other previous animal studies. The *hnrnpa1a*$^{-/-}$*; hnrnpa1b*$^{-/-}$ mutants show increased neutral lipid transport from the yolk extension to the trunk combined with highly decreased levels of Apoda.1. A direct role for Apoda.1 in YSL mediated lipid transport seems therefore unlikely as one would expect decreased YSL transport upon Apoda.1 loss of function as observed in mutants for typical apolipoproteins, such as ApoB and ApoC [301] [302]. The KO zebrafish mutant *stalactite,* lacking the gene encoding microsomal triglyeride transfer protein *(mtp)*, which is involved in biosynthesis of apolipoproteinB (ApoB)-containing lipoproteins, shows defects in yolk absorption pointing to decreased neutral lipid transport (characterized by retention of yolk volume and a reduction in neutral lipids in the body) and dies after approximately 6 dpf. A similar phenotype is observed upon KD of *apoc2* in zebrafish. No difference in these genes was found in *hnrnpa1a*$^{-/-}$*; hnrnpa1b*$^{-/-}$ mutants, implying that lipid transport across the YSL is not directly impaired. It remains though unclear whether other proteins are similarly involved in this process. It should be noted at this point that the *stalactite* and *apoc2* mutant show, apart from their delay in yolk consumption, also an underdeveloped vasculature or ectopic hypersprouting through up- or downregulation of vasculature endothelial growth factor (vegf), respectively. These mutants provide a link between the lipid impairment and vasculature mispatterning, as observed in *hnrnpa1a*$^{-/-}$*; hnrnpa1b*$^{-/-}$ mutants. In contrast, Ear et al. developed a MO KD of the ribosomal protein L11 (RPL11) that shows a similar thinned yolk extension as *hnrnpa1a*$^{-/-}$*; hnrnpa1b*$^{-/-}$ mutants and developmental delay through an increased p53 dependent apoptotic response [303]. It is not clear how reduction of RPL11 leads to increased lipid uptake. It is though plausible that due to the function of RPL11 in ribosome biogenesis, a process, which is a key component in cellular growth [304], RPL11 indirectly regulates the p53 pathway leading to impairment of cell cycle progression and metabolic processes, hence providing a phenotypic overlap to the *hnrnpa1a*$^{-/-}$*; hnrnpa1b*$^{-/-}$ mutants. The levels of *rpl11* are not changed in *hnrnpa1a*$^{-/-}$*; hnrnpa1b*$^{-/-}$ mutants, suggesting another link to the p53 pathway activation. Alternatively, RPL11 expression may be changed due to alternative splicing or posttranslational modifications, both features that were not addressed in our analysis.

Increased lipid transport and cell cycle impairment may be connected in the following way: During embryonic development the yolk, containing mainly lipids, serves as an energy source to support growth by keeping the cell cycle going once they are transported to the zebrafish body. As a cell divides it undergoes a highly energy demanding transformation, which it will

only continue in the presence of the required nutrients, such as lipids that provide the basis for membranes. We could show that neutral lipids are effectively transported to the embryo body, but we speculate that due to Apoda.1 downregulation these are not being metabolized or transported to their target locations and thus accumulate leading to cell cycle progression impairment. Lipids are taken up as triglycerides from the yolk, are transported through the body, and need to be broken down to FAs for further processing. In case that Apoda.1 is required for transport through the body, triglycerides that are taken up from the yolk will remain at the YSL where they cannot be further processed. Alternatively, the lipid processing itself may be impaired leading to successful lipid transport through the body but ineffective break down to FAs. A previous study showed increased peroxisome proliferator-activated gamma (PPARγ) mRNA levels, which is a key regulator of lipid metabolism [305], in mice overexpressing APOD. The interaction between PPARγ and APOD is directly mediated by arachidonic acid (AA), the main ligand of APOD [306]. Likewise, we can assume that upon KD of APOD, PPARγ activity is reduced leading to a slow down of lipid metabolism and reduced FA uptake and/or processing. The inability of efficient nutrient usage upon APOD loss of function is further supported by an APOD KO mouse that shows augmented food intake without increase in body weight pointing to enhanced energy expenditure [307]. We assume that a similar phenomenon is present in *hnrnpa1a*$^{-/-}$*; hnrnpa1b*$^{-/-}$ mutants. In order to compensate the nutrient deficiency more lipids are transported to the zebrafish body from the yolk and the embryo uses up its yolk nutrient reservoir ultimately starving to death. Lastly, it may be possible that a higher rate of beta-oxidation and usage of fats as a primary energy source is present resulting in increased lipid mobilization from the yolk to the trunk. The detected increase in neutral lipids in the trunk may reflect the lipids being transported to their sites of further processing. The ability of Apoda.1 deficient embryos/larvae to grow and survive to 5 dpf suggests that some lipid must be successfully transported to their target sites and are effectively used or that other nutrient sources keep the metabolism going at a reduced rate.

We can conclude that Apoda.1 seems to play a distinct role in lipid metabolism compared to other apolipoproteins and seems to be not involved in yolk to body lipid transport directly but potentially in transporting lipids through the body to the organs. In this scenario, loss of Apod function may lead to cells lacking essential nutrients in form of lipids leading to increased lipid uptake from to embryonic yolk and ultimate starvation of the embryo.

### 4.5.2 Possible effects of dysregulated APOD in HNRNPA1 ALS/MSP patients

*apoda.1* is downregulated upon loss of Hnrnpa1 and seems to be indirectly causative for increased lipid transport from the yolk extension to the zebrafish trunk. A loss of HNRNPA1 function disease mechanism in HNRNPA1 associated ALS is supported by several lines of evidence. First, HNRNPA1 essentiality was shown by the lethality of previous loss of function animal models. Second, HNRNPA1 has widespread functions by regulating various RNAs, and third, HNRNPA1 is cleared from nuclei in cells of HNRNPA1 ALS mutation carriers. Likewise, misregulation of *apoda.1* may also contribute to disease causing mechanisms. The resulting possible effects in the context of neurodegeneration are discussed below. APOD is the most robust age dependent upregulated gene in the brain and several lines of evidence support a highly neuroprotective role, such as decrease in the number of cortex neurons in APOD KO mice [308]. Moreover, APOD is among the top 10 most significantly upregulated proteins in CSF obtained from AD, HD, and PD patients [309]. Due to its involvement in a variety of cellular functions, APOD may be neuroprotective on several levels, e.g. protecting from reactive oxygen species, sustaining lipid transport to neurons, and, maintaining astrocyte health.

First, APOD was shown to protect the aging brain from OS, which is supported by studies in mice and flies demonstrating APOD's ability to decrease lipid peroxides, which are a major source of OS, in membranes. Likewise, KO of the APOD drosophila or plant homologue results in higher sensitivity to OS [310]. McCarthy et al. could further show a brain specific acute APOD upregulation in mice after induction of OS related neurodegeneration [311], suggesting a specific function of APOD in the response of the nervous system to oxidative injury [312]. These findings clearly support the hypothesis that APOD is an acute response protein with a protective function against physiological and pathological OS. Interestingly, OS is evident in sALS and fALS [313] [314], and often resembles an early contributor to pathology that promotes tissue damage ultimately leading to motoneuron degeneration.

Second, APOD has a well-established function in transport and modification of lipids, which play a critical role in CNS structure, particularly at the cell membrane as lipids control membrane fluidity, improve transmission of electric signals, and stabilize synapses [315]. As membrane fluidity is directly determined by enrichment of sphingolipids and cholesterol, which are known transport targets of APOD, reduced APOD levels are linked to impaired membrane integrity [316], a characteristic that was shown to precede ALS disease onset in G93A SOD1 mice [317]. Lipid transport becomes particularly important upon exposure to

OS, as damaged peroxidized lipids need to be removed from neurons and be transported to astrocytes that can oxidize these and generate energy [318].

Third, APOD was shown to control astrocytes' reactivity upon stress since lack of APOD renders astrocytes more vulnerable to OS [319] and APOD KO mice have higher levels of reactive astrogliosis in the cortex [320]. These data suggest that APOD is important to maintain astrocyte health, particularly upon exposure to OS, possibly by promoting removal of peroxidized lipids. Protecting astrocytes against OS is important as OS triggers astrocyte reactivity, lowering neuronal protection over time [321] [319]. In ALS astrocytes change their shape and molecular expression pattern indicating a reactive astrocyte state, and interaction between motoneurons and astrocytes was shown to be impaired (reviewed in [322]). The involvement of APOD in astrogliosis paired with reactive astrocytes in ALS provides a direct link between APOD loss of function and motoneuron degeneration by impaired astrocytic support.

Taken together, APOD loss of function is linked to aging, degeneration, and injury of the nervous system, all features that are present in ALS patient brains. Due to its neuroprotective function APOD plays a vital role in maintaining brain metabolism and loss of APOD function may resemble a very early event in disease pathology leading to impaired lipid transport and membrane integrity, which over time causes motoneuron degeneration in ALS. Owing to the high evolutionary conservation of APOD and its neuroprotective effects, the downregulation of APOD upon HNRNPA1 KO may resemble the failure of HNRNPA1 deficient brains to protect themselves against age-dependent challenges. It is unlikely that APOD loss of function alone causes ALS, but that other environmental or pathological events contribute to disease progression. As previously proposed by Dorman et al. as the "two hit model" one pathogenic event may not be enough to cause the disease even in the presence of a disease associated mutation [323]. In HNRNPA1 ALS cases, the combinatory effect of loss of HNRNPA1 function due to mislocalization and aggregation in the cytoplasm resulting in loss of neuroprotective APOD function and increased OS may provide the detrimental combination leading to ALS pathogenic process initiation. Currently, the late diagnosis allows disease mechanism to override regenerative mechanisms leading to accelerated motoneuron death.

Like APOD, the AD associated APOE protein, is a member of the apolipoprotein family, and highly expressed in the mammalian system. [324]. As lipid transporters are considered to play a role in the nervous system metabolic homeostasis, our findings prompted us to think whether APOD may play a similarly important role in ALS as APOE does in AD. In humans

three allelic variants of APOE are present, of which the APOE4 allele is the most common AD susceptibility locus [325], while APOE2 is considered to be neuroprotective as it decreases an individual's risk for developing AD [326]. While APOD neuroprotection is dependent on its expression levels, the presence of one or the other APOE variant determines neuroprotective effects in AD patients. Overall, APOD seems to mostly resemble APOE2 function in AD, since both proteins are beneficial through neuroprotection.

### 4.5.3 Therapy

In this study we could identify APOD, which was previously found to have neuroprotective capacity, as an interesting highly downregulated gene upon Hnrnpa1 loss of function. The identification of the underlying pathogenic mechanisms in ALS, will provide essential support in developing effective therapies against this devastating disease. In case that decreased APOD levels are an early cause of mutated HNRNPA1 one can design therapies much earlier and support regenerative mechanisms. In order to abolish one of the two hits, therapeutic approaches could on the one hand aim to reduce OS either by increasing endogenous levels of antioxidants or by lowering the generation of OS by stabilizing mitochondrial energy production [327]. On the other hand compensation of the lipid metabolism defects by providing nutritional support could prevent onset of or at least alleviate ALS symptoms. The second approach has been previously realized by providing high caloric diet to ALS patients and animal models leading to delayed disease onset and extended survival [328] [329] [330].

Moreover, restoring APOD function seems to be a realistic approach. An interesting link between APOD and clozapine, which binds to multiple neurotransmitter receptors and is currently used in Schizophrenia treatment, was found [331]. Upon clozapine treatment of mice, APOD increased both at the mRNA and protein level in the mouse brain [332]. In the case that, as we propose, HNRNPA1 ALS/MSP patients lack APOD upregulation as a neuroprotective effect, it will be interesting to determine whether clozapine can restore endogenous or increase APOD levels to enhance neuroprotective mechanisms. As a first step, we could perform a drug screen in the *hnrnpa1a*$^{-/-}$*; hnrnpa1b*$^{-/-}$ mutants and determine whether decreased APOD levels can be upregulated resulting in rescue of the loss of function phenotypes of these mutants.

# 5 Conclusion and Outlook

Currently suggested disease pathomechanisms for HNRNPA1 related ALS and MSP include loss of HNRNPA1 function due to nuclear clearance or gain of function by HNRNPA1 deposits that are neurotoxic in ALS and MSP patients. Resolving that question is of fundamental importance for understanding the underlying cellular mechanisms of ALS and MSP, but also to better develop future therapeutic strategies. My findings demonstrate that Hnrnpa1 plays an important role in zebrafish development. We identify a crucial physiological requirement of Hnrnpa1 in vessel patterning, muscle maintenance, and motoneuron integrity, ultimately leading to premature death if missing. This is in line with previous HNRNPA1 KO models in mice and flies, which also showed early lethality or reduction in life span, respectively [162] [333]. Due to the early lethality of the HNRNPA1 KO mouse the consequences of HNRNPA1 loss of function in mammalian development is difficult to address. The wide range of cells affected in different HNRNPA1 KO animal models associated with cellular toxicity is consistent with a loss of function pathomechanism. It will be therefore interesting to determine whether HNRNPA1 patient mutations cause a full or partial loss of protein function, or lead to toxic gain of function as previously shown for HNRNPA2B1 mutations [102]. The next step will be to rescue the mutant phenotype with either wildtype or mutant HNRNPA1 to determine whether mutant HNRNPA1 is sufficient to carry out essential functions in zebrafish development. Furthermore, novel animal models with KI of the patient mutations need to be developed to additionally address the possibility of (toxic) gain of function mechanisms. Alternatively, a combination of loss and gain of function could synergistically lead to disease.

The most striking finding is that Hnrnpa1 regulates lipid transport from the yolk extension to the trunk in zebrafish. The direct or indirect mediator of this function is Apoda.1, which is an important transporter of lipids and is among the top 10 downregulated genes upon Hnrnpa1 KO. Interestingly, APOD is highly upregulated upon injury and is greatly expressed in ALS and AD patients suggesting a neuroprotective role. It will be interesting to find out whether HNRNPA1 directly binds to *APOD* to regulate its expression levels or which alternative pathway connects Hnrnpa1 loss of function to *apoda.1* downregulation. To examine whether lack of APOD induced neuroprotection is involved in the disease mechanism of ALS/MSP, the following questions need to be addressed. First, do HNRNPA1 ALS/MSP lack the APOD neuroprotection observed in other neurodegenerative diseases such as AD? Second, are the

identified HNRNPA1 targets also differentially expressed in HNRNPA1 ALS patients? So far only few HNRNPA1 ALS/MSP cases were identified making it difficult to obtain patient material and to address whether they show increased levels of ROS, impaired membrane integrity, or defects in their lipid metabolism. The second question can be answered by the examination of APOD expression levels and expression pattern of neurons derived from HNRNPA1 ALS/MSP patients. Alternatively, one can perform RNA sequencing on HNRNPA1 ALS/MSP derived spinal cord/brain tissue or iPSC derived motoneurons to determine whether the identified HNRNPA1 targets are also up- or downregulated upon HNRNPA1 induced pathology [334]. With the advanced technology it would further be possible to utilize cells from healthy individuals and induce HNRNPA1 patient mutations by CRISPR/Cas9 technology. These experiments will reveal a potential involvement of APOD in HNRNPA1 associated ALS/MSP disease pathomechanisms and provide a new step for the ultimate goal of developing a drug for HNRNPA1 specific ALS and potentially sALS.

# References


[1] UNITED NATIONS, D. O. E. A. S. A., POPULATION DIVISION 2015. World population aging.

[2] ARTHUR, K. C., CALVO, A., PRICE, T. R., GEIGER, J. T., CHIÒ, A. & TRAYNOR, B. J. 2016. Projected increase in amyotrophic lateral sclerosis from 2015 to 2040. *Nature Communications,* 7**,** 12408.

[3] AGUZZI, A. & HAASS, C. 2003. Games played by rogue proteins in prion disorders and Alzheimer's disease. *Science,* 302**,** 814-8.

[4] HAASS, C. & SELKOE, D. J. 2007. Soluble protein oligomers in neurodegeneration: lessons from the Alzheimer's amyloid beta-peptide. *Nat Rev Mol Cell Biol,* 8**,** 101-12.

[5] OSKARSSON, B., HORTON, D. K. & MITSUMOTO, H. 2015. Potential Environmental Factors in Amyotrophic Lateral Sclerosis. *Neurol Clin,* 33**,** 877-88.

[6] BOILLEE, S., VANDE VELDE, C. & CLEVELAND, D. W. 2006. ALS: a disease of motor neurons and their nonneuronal neighbors. *Neuron,* 52**,** 39-59.

[7] RAMANAN, V. K. & SAYKIN, A. J. 2013. Pathways to neurodegeneration: mechanistic insights from GWAS in Alzheimer's disease, Parkinson's disease, and related disorders. *American journal of neurodegenerative disease,* 2**,** 145-175.

[8] TURNER, M. R., HARDIMAN, O., BENATAR, M., BROOKS, B. R., CHIO, A., DE CARVALHO, M., INCE, P. G., LIN, C., MILLER, R. G., MITSUMOTO, H., NICHOLSON, G., RAVITS, J., SHAW, P. J., SWASH, M., TALBOT, K., TRAYNOR, B. J., DEN BERG, L. H. V., VELDINK, J. H., VUCIC, S. & KIERNAN, M. C. 2013. Controversies and priorities in amyotrophic lateral sclerosis. *The Lancet. Neurology,* 12**,** 310-322.

[9] KIM, H. J., KIM, N. C., WANG, Y.-D., SCARBOROUGH, E. A., MOORE, J., DIAZ, Z., MACLEA, K. S., FREIBAUM, B., LI, S., MOLLIEX, A., KANAGARAJ, A. P., CARTER, R., BOYLAN, K. B., WOJTAS, A. M., RADEMAKERS, R., PINKUS, J. L., GREENBERG, S. A., TROJANOWSKI, J. Q., TRAYNOR, B. J., SMITH, B. N., TOPP, S., GKAZI, A.-S., MILLER, J., SHAW, C. E., KOTTLORS, M., KIRSCHNER, J., PESTRONK, A., LI, Y. R., FORD, A. F., GITLER, A. D., BENATAR, M., KING, O. D., KIMONIS, V. E., ROSS, E. D., WEIHL, C. C., SHORTER, J. & TAYLOR, J. P. 2013. Mutations in prion-like domains in hnRNPA2B1 and hnRNPA1 cause multisystem proteinopathy and ALS. *Nature.*

[10] FIFITA, J. A., ZHANG, K. Y., GALPER, J., WILLIAMS, K. L., MCCANN, E. P., HOGAN, A. L., SAUNDERS, N., BAUER, D., TARR, I. S., PAMPHLETT, R., NICHOLSON, G. A., ROWE, D., YANG, S. & BLAIR, I. P. 2017. Genetic and Pathological Assessment of hnRNPA1, hnRNPA2/B1, and hnRNPA3 in Familial and Sporadic Amyotrophic Lateral Sclerosis. *Neurodegener Dis,* 17**,** 304-312.

[11] MORI, K., NIHEI, Y., ARZBERGER, T., ZHOU, Q., MACKENZIE, I. R., HERMANN, A., HANISCH, F., KAMP, F., NUSCHER, B., OROZCO, D., EDBAUER, D. & HAASS, C. 2016. Reduced hnRNPA3 increases C9orf72 repeat RNA levels and dipeptide-repeat protein deposition. *EMBO Rep,* 17**,** 1314-25.

[12] SCHMID, B., HRUSCHA, A., HOGL, S., BANZHAF-STRATHMANN, J., STRECKER, K., VAN DER ZEE, J., TEUCKE, M., EIMER, S., HEGERMANN, J., KITTELMANN, M., KREMMER, E., CRUTS, M., SOLCHENBERGER, B., HASENKAMP, L., VAN BEBBER, F., VAN BROECKHOVEN, C.,

EDBAUER, D., LICHTENTHALER, S. F. & HAASS, C. 2013. Loss of ALS-associated TDP-43 in zebrafish causes muscle degeneration, vascular dysfunction, and reduced motor neuron axon outgrowth. *Proc Natl Acad Sci U S A,* 110**,** 4986-91.

[13] TAYLOR, J. P., BROWN, R. H., JR. & CLEVELAND, D. W. 2016. Decoding ALS: from genes to mechanism. *Nature,* 539**,** 197-206.

[14] SATHASIVAM, S. 2010. Motor neurone disease: clinical features, diagnosis, diagnostic pitfalls and prognostic markers. *Singapore Med J,* 51**,** 367-72; quiz 373.

[15] COURATIER, P., CORCIA, P., LAUTRETTE, G., NICOL, M. & MARIN, B. 2017. ALS and frontotemporal dementia belong to a common disease spectrum. *Rev Neurol (Paris),* 173**,** 273-279.

[16] FERRARI, R., KAPOGIANNIS, D., HUEY, E. D. & MOMENI, P. 2011. FTD and ALS: a tale of two diseases. *Current Alzheimer research,* 8**,** 273-294.

[17] VAN LANGENHOVE, T., VAN DER ZEE, J. & VAN BROECKHOVEN, C. 2012. The molecular basis of the frontotemporal lobar degeneration-amyotrophic lateral sclerosis spectrum. *Annals of medicine,* 44**,** 817-828.

[18] GORNO-TEMPINI, M. L., HILLIS, A. E., WEINTRAUB, S., KERTESZ, A., MENDEZ, M., CAPPA, S. F., OGAR, J. M., ROHRER, J. D., BLACK, S., BOEVE, B. F., MANES, F., DRONKERS, N. F., VANDENBERGHE, R., RASCOVSKY, K., PATTERSON, K., MILLER, B. L., KNOPMAN, D. S., HODGES, J. R., MESULAM, M. M. & GROSSMAN, M. 2011. Classification of primary progressive aphasia and its variants. *Neurology,* 76**,** 1006-14.

[19] LING, S.-C., POLYMENIDOU, M. & CLEVELAND, D. W. 2013. Converging mechanisms in ALS and FTD: disrupted RNA and protein homeostasis. *Neuron,* 79**,** 416-438.

[20] MACKENZIE, I. R., NEUMANN, M., BIGIO, E. H., CAIRNS, N. J., ALAFUZOFF, I., KRIL, J., KOVACS, G. G., GHETTI, B., HALLIDAY, G., HOLM, I. E., INCE, P. G., KAMPHORST, W., REVESZ, T., ROZEMULLER, A. J., KUMAR-SINGH, S., AKIYAMA, H., BABORIE, A., SPINA, S., DICKSON, D. W., TROJANOWSKI, J. Q. & MANN, D. M. 2010. Nomenclature and nosology for neuropathologic subtypes of frontotemporal lobar degeneration: an update. *Acta Neuropathol,* 119**,** 1-4.

[21] DEJESUS-HERNANDEZ, M., MACKENZIE, I. R., BOEVE, B. F., BOXER, A. L., BAKER, M., RUTHERFORD, N. J., NICHOLSON, A. M., FINCH, N. A., FLYNN, H., ADAMSON, J., KOURI, N., WOJTAS, A., SENGDY, P., HSIUNG, G. Y., KARYDAS, A., SEELEY, W. W., JOSEPHS, K. A., COPPOLA, G., GESCHWIND, D. H., WSZOLEK, Z. K., FELDMAN, H., KNOPMAN, D. S., PETERSEN, R. C., MILLER, B. L., DICKSON, D. W., BOYLAN, K. B., GRAFF-RADFORD, N. R. & RADEMAKERS, R. 2011. Expanded GGGGCC hexanucleotide repeat in noncoding region of C9ORF72 causes chromosome 9p-linked FTD and ALS. *Neuron,* 72**,** 245-56.

[22] RENTON, A. E., MAJOUNIE, E., WAITE, A., SIMON-SANCHEZ, J., ROLLINSON, S., GIBBS, J. R., SCHYMICK, J. C., LAAKSOVIRTA, H., VAN SWIETEN, J. C., MYLLYKANGAS, L., KALIMO, H., PAETAU, A., ABRAMZON, Y., REMES, A. M., KAGANOVICH, A., SCHOLZ, S. W., DUCKWORTH, J., DING, J., HARMER, D. W., HERNANDEZ, D. G., JOHNSON, J. O., MOK, K., RYTEN, M., TRABZUNI, D., GUERREIRO, R. J., ORRELL, R. W., NEAL, J., MURRAY, A., PEARSON, J., JANSEN, I. E., SONDERVAN, D., SEELAAR, H., BLAKE, D., YOUNG, K., HALLIWELL, N., CALLISTER, J. B., TOULSON, G., RICHARDSON, A., GERHARD, A., SNOWDEN, J., MANN, D., NEARY, D., NALLS, M. A., PEURALINNA, T., JANSSON, L.,

ISOVIITA, V. M., KAIVORINNE, A. L., HOLTTA-VUORI, M., IKONEN, E., SULKAVA, R., BENATAR, M., WUU, J., CHIO, A., RESTAGNO, G., BORGHERO, G., SABATELLI, M., HECKERMAN, D., ROGAEVA, E., ZINMAN, L., ROTHSTEIN, J. D., SENDTNER, M., DREPPER, C., EICHLER, E. E., ALKAN, C., ABDULLAEV, Z., PACK, S. D., DUTRA, A., PAK, E., HARDY, J., SINGLETON, A., WILLIAMS, N. M., HEUTINK, P., PICKERING-BROWN, S., MORRIS, H. R., TIENARI, P. J. & TRAYNOR, B. J. 2011. A hexanucleotide repeat expansion in C9ORF72 is the cause of chromosome 9p21-linked ALS-FTD. *Neuron,* 72**,** 257-68.

[23] SWINNEN, B. & ROBBERECHT, W. 2014. The phenotypic variability of amyotrophic lateral sclerosis. *Nat Rev Neurol,* 10**,** 661-70.

[24] RINGHOLZ, G. M., APPEL, S. H., BRADSHAW, M., COOKE, N. A., MOSNIK, D. M. & SCHULZ, P. E. 2005. Prevalence and patterns of cognitive impairment in sporadic ALS. *Neurology,* 65**,** 586-90.

[25] BAK, T. H. 2010. Motor neuron disease and frontotemporal dementia: One, two, or three diseases? *Annals of Indian Academy of Neurology,* 13**,** S81-S88.

[26] COOPER-KNOCK, J., KIRBY, J., HIGHLEY, R. & SHAW, P. J. 2015. The Spectrum of C9orf72-mediated Neurodegeneration and Amyotrophic Lateral Sclerosis. *Neurotherapeutics,* 12**,** 326-39.

[27] RADEMAKERS, R., CRUTS, M. & VAN BROECKHOVEN, C. 2004. The role of tau (MAPT) in frontotemporal dementia and related tauopathies. *Hum Mutat,* 24**,** 277-95.

[28] POORKAJ, P., BIRD, T. D., WIJSMAN, E., NEMENS, E., GARRUTO, R. M., ANDERSON, L., ANDREADIS, A., WIEDERHOLT, W. C., RASKIND, M. & SCHELLENBERG, G. D. 1998. Tau is a candidate gene for chromosome 17 frontotemporal dementia. *Ann Neurol,* 43**,** 815-25.

[29] TAKAZAWA, T., IKEDA, K., HIRAYAMA, T., KAWABE, K., NAKAMURA, Y., ITO, H., KANO, O., YOSHII, Y., TANAKA, F., SOBUE, G. & IWASAKI, Y. 2010. Familial amyotrophic lateral sclerosis with a novel G85S mutation of superoxide dismutase 1 gene: clinical features of lower motor neuron disease. *Intern Med,* 49**,** 183-6.

[30] TAYLOR, J. P. 2015. Multisystem proteinopathy: intersecting genetics in muscle, bone, and brain degeneration. *Neurology,* 85**,** 658-60.

[31] JOHNSON, J. O., MANDRIOLI, J., BENATAR, M., ABRAMZON, Y., VAN DEERLIN, V. M., TROJANOWSKI, J. Q., GIBBS, J. R., BRUNETTI, M., GRONKA, S., WUU, J., DING, J., MCCLUSKEY, L., MARTINEZ-LAGE, M., FALCONE, D., HERNANDEZ, D. G., AREPALLI, S., CHONG, S., SCHYMICK, J. C., ROTHSTEIN, J., LANDI, F., WANG, Y. D., CALVO, A., MORA, G., SABATELLI, M., MONSURRO, M. R., BATTISTINI, S., SALVI, F., SPATARO, R., SOLA, P., BORGHERO, G., GALASSI, G., SCHOLZ, S. W., TAYLOR, J. P., RESTAGNO, G., CHIO, A. & TRAYNOR, B. J. 2010. Exome sequencing reveals VCP mutations as a cause of familial ALS. *Neuron,* 68**,** 857-64.

[32] WONG, T. H., POTTIER, C., HONDIUS, D. C., MEETER, L. H. H., VAN ROOIJ, J. G. J., MELHEM, S., VAN MINKELEN, R., VAN DUIJN, C. M., ROZEMULLER, A. J. M., SEELAAR, H., RADEMAKERS, R. & VAN SWIETEN, J. C. 2018. Three VCP Mutations in Patients with Frontotemporal Dementia. *J Alzheimers Dis,* 65**,** 1139-1146.

[33] KOPPERS, M., VAN BLITTERSWIJK, M. M., VLAM, L., ROWICKA, P. A., VAN VUGHT, P. W., GROEN, E. J., SPLIET, W. G., ENGELEN-LEE, J., SCHELHAAS, H. J., DE VISSER, M., VAN DER KOOI, A. J., VAN DER POL, W. L., PASTERKAMP, R. J., VELDINK, J. H. & VAN DEN BERG, L.

H. 2012. VCP mutations in familial and sporadic amyotrophic lateral sclerosis. *Neurobiol Aging,* 33**,** 837.e7-13.

[34] TEYSSOU, E., TAKEDA, T., LEBON, V., BOILLEE, S., DOUKOURE, B., BATAILLON, G., SAZDOVITCH, V., CAZENEUVE, C., MEININGER, V., LEGUERN, E., SALACHAS, F., SEILHEAN, D. & MILLECAMPS, S. 2013. Mutations in SQSTM1 encoding p62 in amyotrophic lateral sclerosis: genetics and neuropathology. *Acta Neuropathol,* 125**,** 511-22.

[35] WEIHL, C. C., TEMIZ, P., MILLER, S. E., WATTS, G., SMITH, C., FORMAN, M., HANSON, P. I., KIMONIS, V. & PESTRONK, A. 2008. TDP-43 accumulation in inclusion body myopathy muscle suggests a common pathogenic mechanism with frontotemporal dementia. *J Neurol Neurosurg Psychiatry,* 79**,** 1186-9.

[36] SALAJEGHEH, M., PINKUS, J. L., TAYLOR, J. P., AMATO, A. A., NAZARENO, R., BALOH, R. H. & GREENBERG, S. A. 2009. Sarcoplasmic redistribution of nuclear TDP-43 in inclusion body myositis. *Muscle Nerve,* 40**,** 19-31.

[37] PINKUS, J. L., AMATO, A. A., TAYLOR, P. J. & GREENBERG, S. A. 2014. Abnormal distribution of heterogeneous nuclear ribonucleoproteins in sporadic inclusion body myositis. *Neuromuscular Disorders,* 24**,** 611-616.

[38] ROWLAND, L. P. & SHNEIDER, N. A. 2001. Amyotrophic lateral sclerosis. *N Engl J Med,* 344**,** 1688-700.

[39] KIERNAN, M. C., VUCIC, S., CHEAH, B. C., TURNER, M. R., EISEN, A., HARDIMAN, O., BURRELL, J. R. & ZOING, M. C. 2011. Amyotrophic lateral sclerosis. *The Lancet,* 377**,** 942-955.

[40] KIERNAN, M. C., VUCIC, S., CHEAH, B. C., TURNER, M. R., EISEN, A., HARDIMAN, O., BURRELL, J. R. & ZOING, M. C. 2011. Amyotrophic lateral sclerosis. *Lancet,* 377**,** 942-55.

[41] MILLER, R. G., MUNSAT, T. L., SWASH, M. & BROOKS, B. R. 1999. Consensus guidelines for the design and implementation of clinical trials in ALS. World Federation of Neurology committee on Research. *J Neurol Sci,* 169**,** 2-12.

[42] BROOKS, B. R. 1994. El Escorial World Federation of Neurology criteria for the diagnosis of amyotrophic lateral sclerosis. Subcommittee on Motor Neuron Diseases/Amyotrophic Lateral Sclerosis of the World Federation of Neurology Research Group on Neuromuscular Diseases and the El Escorial "Clinical limits of amyotrophic lateral sclerosis" workshop contributors. *J Neurol Sci,* 124 Suppl**,** 96-107.

[43] WILBOURN, A. J. 1998. Clinical neurophysiology in the diagnosis of amyotrophic lateral sclerosis: the Lambert and the El Escorial criteria. *J Neurol Sci,* 160 Suppl 1**,** S25-9.

[44] ANDERSEN, P. M., BORASIO, G. D., DENGLER, R., HARDIMAN, O., KOLLEWE, K., LEIGH, P. N., PRADAT, P. F., SILANI, V. & TOMIK, B. 2007. Good practice in the management of amyotrophic lateral sclerosis: clinical guidelines. An evidence-based review with good practice points. EALSC Working Group. *Amyotroph Lateral Scler,* 8**,** 195-213.

[45] MILLER, R. G., MITCHELL, J. D., LYON, M. & MOORE, D. H. 2002. Riluzole for amyotrophic lateral sclerosis (ALS)/motor neuron disease (MND). *Cochrane Database Syst Rev***,** Cd001447.

[46] LEIGH, P. N., WHITWELL, H., GAROFALO, O., BULLER, J., SWASH, M., MARTIN, J. E., GALLO, J. M., WELLER, R. O. & ANDERTON, B. H. 1991. Ubiquitin-immunoreactive intraneuronal inclusions in amyotrophic lateral sclerosis. Morphology, distribution, and specificity. *Brain,* 114 ( Pt 2)**,** 775-88.

[47] ARAI, T., HASEGAWA, M., AKIYAMA, H., IKEDA, K., NONAKA, T., MORI, H., MANN, D., TSUCHIYA, K., YOSHIDA, M., HASHIZUME, Y. & ODA, T. 2006. TDP-43 is a component of ubiquitin-positive tau-negative inclusions in frontotemporal lobar degeneration and amyotrophic lateral sclerosis. *Biochem Biophys Res Commun,* 351**,** 602-11.

[48] DORMANN, D. & HAASS, C. 2013. Fused in sarcoma (FUS): an oncogene goes awry in neurodegeneration. *Mol Cell Neurosci,* 56**,** 475-86.

[49] AL-CHALABI, A., JONES, A., TROAKES, C., KING, A., AL-SARRAJ, S. & VAN DEN BERG, L. H. 2012. The genetics and neuropathology of amyotrophic lateral sclerosis. *Acta Neuropathol,* 124**,** 339-52.

[50] ROSEN, D. R., SIDDIQUE, T., PATTERSON, D., FIGLEWICZ, D. A., SAPP, P., HENTATI, A., DONALDSON, D., GOTO, J., O'REGAN, J. P., DENG, H. X. & ET AL. 1993. Mutations in Cu/Zn superoxide dismutase gene are associated with familial amyotrophic lateral sclerosis. *Nature,* 362**,** 59-62.

[51] ROBERTSON, J., SANELLI, T., XIAO, S., YANG, W., HORNE, P., HAMMOND, R., PIORO, E. P. & STRONG, M. J. 2007. Lack of TDP-43 abnormalities in mutant SOD1 transgenic mice shows disparity with ALS. *Neurosci Lett,* 420**,** 128-32.

[52] URWIN, H., JOSEPHS, K. A., ROHRER, J. D., MACKENZIE, I. R., NEUMANN, M., AUTHIER, A., SEELAAR, H., VAN SWIETEN, J. C., BROWN, J. M., JOHANNSEN, P., NIELSEN, J. E., HOLM, I. E., DICKSON, D. W., RADEMAKERS, R., GRAFF-RADFORD, N. R., PARISI, J. E., PETERSEN, R. C., HATANPAA, K. J., WHITE, C. L., 3RD, WEINER, M. F., GESER, F., VAN DEERLIN, V. M., TROJANOWSKI, J. Q., MILLER, B. L., SEELEY, W. W., VAN DER ZEE, J., KUMAR-SINGH, S., ENGELBORGHS, S., DE DEYN, P. P., VAN BROECKHOVEN, C., BIGIO, E. H., DENG, H. X., HALLIDAY, G. M., KRIL, J. J., MUNOZ, D. G., MANN, D. M., PICKERING-BROWN, S. M., DOODEMAN, V., ADAMSON, G., GHAZI-NOORI, S., FISHER, E. M., HOLTON, J. L., REVESZ, T., ROSSOR, M. N., COLLINGE, J., MEAD, S. & ISAACS, A. M. 2010. FUS pathology defines the majority of tau- and TDP-43-negative frontotemporal lobar degeneration. *Acta Neuropathol,* 120**,** 33-41.

[53] KWIATKOWSKI, T. J., JR., BOSCO, D. A., LECLERC, A. L., TAMRAZIAN, E., VANDERBURG, C. R., RUSS, C., DAVIS, A., GILCHRIST, J., KASARSKIS, E. J., MUNSAT, T., VALDMANIS, P., ROULEAU, G. A., HOSLER, B. A., CORTELLI, P., DE JONG, P. J., YOSHINAGA, Y., HAINES, J. L., PERICAK-VANCE, M. A., YAN, J., TICOZZI, N., SIDDIQUE, T., MCKENNA-YASEK, D., SAPP, P. C., HORVITZ, H. R., LANDERS, J. E. & BROWN, R. H., JR. 2009. Mutations in the FUS/TLS gene on chromosome 16 cause familial amyotrophic lateral sclerosis. *Science,* 323**,** 1205-8.

[54] FECTO, F., YAN, J., VEMULA, S. P., LIU, E., YANG, Y., CHEN, W., ZHENG, J. G., SHI, Y., SIDDIQUE, N., ARRAT, H., DONKERVOORT, S., AJROUD-DRISS, S., SUFIT, R. L., HELLER, S. L., DENG, H. X. & SIDDIQUE, T. 2011. SQSTM1 mutations in familial and sporadic amyotrophic lateral sclerosis. *Arch Neurol,* 68**,** 1440-6.

[55] MARUYAMA, H., MORINO, H., ITO, H., IZUMI, Y., KATO, H., WATANABE, Y., KINOSHITA, Y., KAMADA, M., NODERA, H., SUZUKI, H., KOMURE, O., MATSUURA, S., KOBATAKE, K., MORIMOTO, N., ABE, K., SUZUKI, N., AOKI, M., KAWATA, A., HIRAI, T., KATO, T.,

OGASAWARA, K., HIRANO, A., TAKUMI, T., KUSAKA, H., HAGIWARA, K., KAJI, R. & KAWAKAMI, H. 2010. Mutations of optineurin in amyotrophic lateral sclerosis. *Nature,* 465**,** 223-6.

[56] DENG, H. X., CHEN, W., HONG, S. T., BOYCOTT, K. M., GORRIE, G. H., SIDDIQUE, N., YANG, Y., FECTO, F., SHI, Y., ZHAI, H., JIANG, H., HIRANO, M., RAMPERSAUD, E., JANSEN, G. H., DONKERVOORT, S., BIGIO, E. H., BROOKS, B. R., AJROUD, K., SUFIT, R. L., HAINES, J. L., MUGNAINI, E., PERICAK-VANCE, M. A. & SIDDIQUE, T. 2011. Mutations in UBQLN2 cause dominant X-linked juvenile and adult-onset ALS and ALS/dementia. *Nature,* 477**,** 211-5.

[57] WILLIAMS, K. L., TOPP, S., YANG, S., SMITH, B., FIFITA, J. A., WARRAICH, S. T., ZHANG, K. Y., FARRAWELL, N., VANCE, C., HU, X., CHESI, A., LEBLOND, C. S., LEE, A., RAYNER, S. L., SUNDARAMOORTHY, V., DOBSON-STONE, C., MOLLOY, M. P., VAN BLITTERSWIJK, M., DICKSON, D. W., PETERSEN, R. C., GRAFF-RADFORD, N. R., BOEVE, B. F., MURRAY, M. E., POTTIER, C., DON, E., WINNICK, C., MCCANN, E. P., HOGAN, A., DAOUD, H., LEVERT, A., DION, P. A., MITSUI, J., ISHIURA, H., TAKAHASHI, Y., GOTO, J., KOST, J., GELLERA, C., GKAZI, A. S., MILLER, J., STOCKTON, J., BROOKS, W. S., BOUNDY, K., POLAK, M., MUNOZ-BLANCO, J. L., ESTEBAN-PEREZ, J., RABANO, A., HARDIMAN, O., MORRISON, K. E., TICOZZI, N., SILANI, V., DE BELLEROCHE, J., GLASS, J. D., KWOK, J. B., GUILLEMIN, G. J., CHUNG, R. S., TSUJI, S., BROWN, R. H., JR., GARCIA-REDONDO, A., RADEMAKERS, R., LANDERS, J. E., GITLER, A. D., ROULEAU, G. A., COLE, N. J., YERBURY, J. J., ATKIN, J. D., SHAW, C. E., NICHOLSON, G. A. & BLAIR, I. P. 2016. CCNF mutations in amyotrophic lateral sclerosis and frontotemporal dementia. *Nat Commun,* 7**,** 11253.

[58] RENTON, A. E., CHIÒ, A. & TRAYNOR, B. J. 2013. State of play in amyotrophic lateral sclerosis genetics. *Nature Neuroscience,* 17**,** 17-23.

[59] CRUTS, M., GIJSELINCK, I., VAN LANGENHOVE, T., VAN DER ZEE, J. & VAN BROECKHOVEN, C. 2013. Current insights into the C9orf72 repeat expansion diseases of the FTLD/ALS spectrum. *Trends Neurosci,* 36**,** 450-9.

[60] YANG, M., LIANG, C., SWAMINATHAN, K., HERRLINGER, S., LAI, F., SHIEKHATTAR, R. & CHEN, J. F. 2016. A C9ORF72/SMCR8-containing complex regulates ULK1 and plays a dual role in autophagy. *Sci Adv,* 2**,** e1601167.

[61] MAHARJAN, N., KUNZLI, C., BUTHEY, K. & SAXENA, S. 2017. C9ORF72 Regulates Stress Granule Formation and Its Deficiency Impairs Stress Granule Assembly, Hypersensitizing Cells to Stress. *Mol Neurobiol,* 54**,** 3062-3077.

[62] MORI, K., ARZBERGER, T., GRASSER, F. A., GIJSELINCK, I., MAY, S., RENTZSCH, K., WENG, S. M., SCHLUDI, M. H., VAN DER ZEE, J., CRUTS, M., VAN BROECKHOVEN, C., KREMMER, E., KRETZSCHMAR, H. A., HAASS, C. & EDBAUER, D. 2013. Bidirectional transcripts of the expanded C9orf72 hexanucleotide repeat are translated into aggregating dipeptide repeat proteins. *Acta Neuropathol,* 126**,** 881-93.

[63] CHITIPROLU, M., JAGOW, C., TREMBLAY, V., BONDY-CHORNEY, E., PARIS, G., SAVARD, A., PALIDWOR, G., BARRY, F. A., ZINMAN, L., KEITH, J., ROGAEVA, E., ROBERTSON, J., LAVALLEE-ADAM, M., WOULFE, J., COUTURE, J. F., COTE, J. & GIBBINGS, D. 2018. A complex of C9ORF72 and p62 uses arginine methylation to eliminate stress granules by autophagy. *Nat Commun,* 9**,** 2794.

[64] O'ROURKE, J. G., BOGDANIK, L., YANEZ, A., LALL, D., WOLF, A. J., MUHAMMAD, A. K., HO, R., CARMONA, S., VIT, J. P., ZARROW, J., KIM, K. J., BELL, S., HARMS, M. B., MILLER, T. M., DANGLER, C. A., UNDERHILL, D. M., GOODRIDGE, H. S., LUTZ, C. M. & BALOH, R. H. 2016. C9orf72 is required for proper macrophage and microglial function in mice. *Science,* 351**,** 1324-9.

[65] KOPPERS, M., BLOKHUIS, A. M., WESTENENG, H. J., TERPSTRA, M. L., ZUNDEL, C. A., VIEIRA DE SA, R., SCHELLEVIS, R. D., WAITE, A. J., BLAKE, D. J., VELDINK, J. H., VAN DEN BERG, L. H. & PASTERKAMP, R. J. 2015. C9orf72 ablation in mice does not cause motor neuron degeneration or motor deficits. *Ann Neurol,* 78**,** 426-38.

[66] ASH, P. E., BIENIEK, K. F., GENDRON, T. F., CAULFIELD, T., LIN, W. L., DEJESUS-HERNANDEZ, M., VAN BLITTERSWIJK, M. M., JANSEN-WEST, K., PAUL, J. W., 3RD, RADEMAKERS, R., BOYLAN, K. B., DICKSON, D. W. & PETRUCELLI, L. 2013. Unconventional translation of C9ORF72 GGGGCC expansion generates insoluble polypeptides specific to c9FTD/ALS. *Neuron,* 77**,** 639-46.

[67] MORI, K., WENG, S. M., ARZBERGER, T., MAY, S., RENTZSCH, K., KREMMER, E., SCHMID, B., KRETZSCHMAR, H. A., CRUTS, M., VAN BROECKHOVEN, C., HAASS, C. & EDBAUER, D. 2013. The C9orf72 GGGGCC repeat is translated into aggregating dipeptide-repeat proteins in FTLD/ALS. *Science,* 339**,** 1335-8.

[68] MAY, S., HORNBURG, D., SCHLUDI, M. H., ARZBERGER, T., RENTZSCH, K., SCHWENK, B. M., GRASSER, F. A., MORI, K., KREMMER, E., BANZHAF-STRATHMANN, J., MANN, M., MEISSNER, F. & EDBAUER, D. 2014. C9orf72 FTLD/ALS-associated Gly-Ala dipeptide repeat proteins cause neuronal toxicity and Unc119 sequestration. *Acta Neuropathol,* 128**,** 485-503.

[69] LEE, Y. B., CHEN, H. J., PERES, J. N., GOMEZ-DEZA, J., ATTIG, J., STALEKAR, M., TROAKES, C., NISHIMURA, A. L., SCOTTER, E. L., VANCE, C., ADACHI, Y., SARDONE, V., MILLER, J. W., SMITH, B. N., GALLO, J. M., ULE, J., HIRTH, F., ROGELJ, B., HOUART, C. & SHAW, C. E. 2013. Hexanucleotide repeats in ALS/FTD form length-dependent RNA foci, sequester RNA binding proteins, and are neurotoxic. *Cell Rep,* 5**,** 1178-86.

[70] MORI, K., LAMMICH, S., MACKENZIE, I. R. A., FORNÉ, I., ZILOW, S., KRETZSCHMAR, H., EDBAUER, D., JANSSENS, J., KLEINBERGER, G., CRUTS, M., HERMS, J., NEUMANN, M., BROECKHOVEN, C., ARZBERGER, T. & HAASS, C. 2013. hnRNP A3 binds to GGGGCC repeats and is a constituent of p62-positive/TDP43-negative inclusions in the hippocampus of patients with C9orf72 mutations. *Acta Neuropathologica,* 125**,** 413-423.

[71] COOPER-KNOCK, J., HIGGINBOTTOM, A., STOPFORD, M. J., HIGHLEY, J. R., INCE, P. G., WHARTON, S. B., PICKERING-BROWN, S., KIRBY, J., HAUTBERGUE, G. M. & SHAW, P. J. 2015. Antisense RNA foci in the motor neurons of C9ORF72-ALS patients are associated with TDP-43 proteinopathy. *Acta Neuropathol,* 130**,** 63-75.

[72] GUO, Q., LEHMER, C., MARTÍNEZ-SÁNCHEZ, A., RUDACK, T., BECK, F., HARTMANN, H., PÉREZ-BERLANGA, M., FROTTIN, F., HIPP, M. S., HARTL, F. U., EDBAUER, D., BAUMEISTER, W. & FERNÁNDEZ-BUSNADIEGO, R. 2018. In Situ Structure of Neuronal C9orf72 Poly-GA Aggregates Reveals Proteasome Recruitment. *Cell,* 172**,** 696-705.e12.

[73] FREIBAUM, B. D. & TAYLOR, J. P. 2017. The Role of Dipeptide Repeats in C9ORF72-Related ALS-FTD. *Frontiers in molecular neuroscience,* 10**,** 35-35.

[74] NONAKA, T., MASUDA-SUZUKAKE, M., HOSOKAWA, M., SHIMOZAWA, A., HIRAI, S., OKADO, H. & HASEGAWA, M. 2018. C9ORF72 dipeptide repeat poly-GA inclusions promote: intracellular aggregation of phosphorylated TDP-43. *Hum Mol Genet*.

[75] TICOZZI, N., VANCE, C., LECLERC, A. L., KEAGLE, P., GLASS, J. D., MCKENNA-YASEK, D., SAPP, P. C., SILANI, V., BOSCO, D. A., SHAW, C. E., BROWN, R. H., JR. & LANDERS, J. E. 2011. Mutational analysis reveals the FUS homolog TAF15 as a candidate gene for familial amyotrophic lateral sclerosis. *Am J Med Genet B Neuropsychiatr Genet,* 156b**,** 285-90.

[76] NEUMANN, M., BENTMANN, E., DORMANN, D., JAWAID, A., DEJESUS-HERNANDEZ, M., ANSORGE, O., ROEBER, S., KRETZSCHMAR, H. A., MUNOZ, D. G., KUSAKA, H., YOKOTA, O., ANG, L. C., BILBAO, J., RADEMAKERS, R., HAASS, C. & MACKENZIE, I. R. 2011. FET proteins TAF15 and EWS are selective markers that distinguish FTLD with FUS pathology from amyotrophic lateral sclerosis with FUS mutations. *Brain,* 134**,** 2595-609.

[77] JOHNSON, J. O., PIORO, E. P., BOEHRINGER, A., CHIA, R., FEIT, H., RENTON, A. E., PLINER, H. A., ABRAMZON, Y., MARANGI, G., WINBORN, B. J., GIBBS, J. R., NALLS, M. A., MORGAN, S., SHOAI, M., HARDY, J., PITTMAN, A., ORRELL, R. W., MALASPINA, A., SIDLE, K. C., FRATTA, P., HARMS, M. B., BALOH, R. H., PESTRONK, A., WEIHL, C. C., ROGAEVA, E., ZINMAN, L., DRORY, V. E., BORGHERO, G., MORA, G., CALVO, A., ROTHSTEIN, J. D., DREPPER, C., SENDTNER, M., SINGLETON, A. B., TAYLOR, J. P., COOKSON, M. R., RESTAGNO, G., SABATELLI, M., BOWSER, R., CHIO, A. & TRAYNOR, B. J. 2014. Mutations in the Matrin 3 gene cause familial amyotrophic lateral sclerosis. *Nat Neurosci,* 17**,** 664-666.

[78] COUTHOUIS, J., HART, M. P., ERION, R., KING, O. D., DIAZ, Z., NAKAYA, T., IBRAHIM, F., KIM, H. J., MOJSILOVIC-PETROVIC, J., PANOSSIAN, S., KIM, C. E., FRACKELTON, E. C., SOLSKI, J. A., WILLIAMS, K. L., CLAY-FALCONE, D., ELMAN, L., MCCLUSKEY, L., GREENE, R., HAKONARSON, H., KALB, R. G., LEE, V. M., TROJANOWSKI, J. Q., NICHOLSON, G. A., BLAIR, I. P., BONINI, N. M., VAN DEERLIN, V. M., MOURELATOS, Z., SHORTER, J. & GITLER, A. D. 2012. Evaluating the role of the FUS/TLS-related gene EWSR1 in amyotrophic lateral sclerosis. *Hum Mol Genet,* 21**,** 2899-911.

[79] KOLB, S. J., SUTTON, S. & SCHOENBERG, D. R. 2010. RNA processing defects associated with diseases of the motor neuron. *Muscle Nerve,* 41**,** 5-17.

[80] BARALLE, M., BURATTI, E. & BARALLE, F. E. 2013. The role of TDP-43 in the pathogenesis of ALS and FTLD. *Biochem Soc Trans,* 41**,** 1536-40.

[81] POLYMENIDOU, M., LAGIER-TOURENNE, C., HUTT, K. R., HUELGA, S. C., MORAN, J., LIANG, T. Y., LING, S. C., SUN, E., WANCEWICZ, E., MAZUR, C., KORDASIEWICZ, H., SEDAGHAT, Y., DONOHUE, J. P., SHIUE, L., BENNETT, C. F., YEO, G. W. & CLEVELAND, D. W. 2011. Long pre-mRNA depletion and RNA missplicing contribute to neuronal vulnerability from loss of TDP-43. *Nat Neurosci,* 14**,** 459-68.

[82] TOLLERVEY, J. R., CURK, T., ROGELJ, B., BRIESE, M., CEREDA, M., KAYIKCI, M., KONIG, J., HORTOBAGYI, T., NISHIMURA, A. L., ZUPUNSKI, V., PATANI, R., CHANDRAN, S., ROT, G.,

ZUPAN, B., SHAW, C. E. & ULE, J. 2011. Characterizing the RNA targets and position-dependent splicing regulation by TDP-43. *Nat Neurosci,* 14**,** 452-8.

[83] AVENDANO-VAZQUEZ, S. E., DHIR, A., BEMBICH, S., BURATTI, E., PROUDFOOT, N. & BARALLE, F. E. 2012. Autoregulation of TDP-43 mRNA levels involves interplay between transcription, splicing, and alternative polyA site selection. *Genes Dev,* 26**,** 1679-84.

[84] AYALA, Y. M., DE CONTI, L., AVENDANO-VAZQUEZ, S. E., DHIR, A., ROMANO, M., D'AMBROGIO, A., TOLLERVEY, J., ULE, J., BARALLE, M., BURATTI, E. & BARALLE, F. E. 2011. TDP-43 regulates its mRNA levels through a negative feedback loop. *Embo j,* 30**,** 277-88.

[85] BURATTI, E. 2018. TDP-43 post-translational modifications in health and disease. *Expert Opin Ther Targets,* 22**,** 279-293.

[86] LAGIER-TOURENNE, C., POLYMENIDOU, M. & CLEVELAND, D. W. 2010. TDP-43 and FUS/TLS: emerging roles in RNA processing and neurodegeneration. *Hum Mol Genet,* 19**,** R46-64.

[87] VANDEN BROECK, L., CALLAERTS, P. & DERMAUT, B. 2014. TDP-43-mediated neurodegeneration: towards a loss-of-function hypothesis? *Trends Mol Med,* 20**,** 66-71.

[88] LOPEZ DE SILANES, I., GALBAN, S., MARTINDALE, J. L., YANG, X., MAZAN-MAMCZARZ, K., INDIG, F. E., FALCO, G., ZHAN, M. & GOROSPE, M. 2005. Identification and functional outcome of mRNAs associated with RNA-binding protein TIA-1. *Mol Cell Biol,* 25**,** 9520-31.

[89] WARIS, S., WILCE, M. C. & WILCE, J. A. 2014. RNA recognition and stress granule formation by TIA proteins. *Int J Mol Sci,* 15**,** 23377-88.

[90] GILKS, N., KEDERSHA, N., AYODELE, M., SHEN, L., STOECKLIN, G., DEMBER, L. M. & ANDERSON, P. 2004. Stress granule assembly is mediated by prion-like aggregation of TIA-1. *Mol Biol Cell,* 15**,** 5383-98.

[91] ITO, D., HATANO, M. & SUZUKI, N. 2017. RNA binding proteins and the pathological cascade in ALS/FTD neurodegeneration. *Sci Transl Med,* 9.

[92] MACKENZIE, I. R., NICHOLSON, A. M., SARKAR, M., MESSING, J., PURICE, M. D., POTTIER, C., ANNU, K., BAKER, M., PERKERSON, R. B., KURTI, A., MATCHETT, B. J., MITTAG, T., TEMIROV, J., HSIUNG, G. R., KRIEGER, C., MURRAY, M. E., KATO, M., FRYER, J. D., PETRUCELLI, L., ZINMAN, L., WEINTRAUB, S., MESULAM, M., KEITH, J., ZIVKOVIC, S. A., HIRSCH-REINSHAGEN, V., ROOS, R. P., ZUCHNER, S., GRAFF-RADFORD, N. R., PETERSEN, R. C., CASELLI, R. J., WSZOLEK, Z. K., FINGER, E., LIPPA, C., LACOMIS, D., STEWART, H., DICKSON, D. W., KIM, H. J., ROGAEVA, E., BIGIO, E., BOYLAN, K. B., TAYLOR, J. P. & RADEMAKERS, R. 2017. TIA1 Mutations in Amyotrophic Lateral Sclerosis and Frontotemporal Dementia Promote Phase Separation and Alter Stress Granule Dynamics. *Neuron,* 95**,** 808-816.e9.

[93] HIRSCH-REINSHAGEN, V., POTTIER, C., NICHOLSON, A. M., BAKER, M., HSIUNG, G. R., KRIEGER, C., SENGDY, P., BOYLAN, K. B., DICKSON, D. W., MESULAM, M., WEINTRAUB, S., BIGIO, E., ZINMAN, L., KEITH, J., ROGAEVA, E., ZIVKOVIC, S. A., LACOMIS, D., TAYLOR, J. P., RADEMAKERS, R. & MACKENZIE, I. R. A. 2017. Clinical and neuropathological features of ALS/FTD with TIA1 mutations. *Acta Neuropathol Commun,* 5**,** 96.

[94] TAN, A. Y. & MANLEY, J. L. 2009. The TET family of proteins: functions and roles in disease. *J Mol Cell Biol,* 1**,** 82-92.

[95] RADEMAKERS, R., NEUMANN, M. & R MACKENZIE, I. 2012. *Advances in understanding the molecular basis of frontotemporal dementia*.

[96] DENG, H., GAO, K. & JANKOVIC, J. 2014. The role of FUS gene variants in neurodegenerative diseases. *Nat Rev Neurol,* 10**,** 337-48.

[97] DORMANN, D., RODDE, R., EDBAUER, D., BENTMANN, E., FISCHER, I., HRUSCHA, A., THAN, M. E., MACKENZIE, I. R., CAPELL, A., SCHMID, B., NEUMANN, M. & HAASS, C. 2010. ALS-associated fused in sarcoma (FUS) mutations disrupt Transportin-mediated nuclear import. *Embo j,* 29**,** 2841-57.

[98] ANDERSON, P. & KEDERSHA, N. 2008. Stress granules: the Tao of RNA triage. *Trends Biochem Sci,* 33**,** 141-50.

[99] LIU, Q., SHU, S., WANG, R. R., LIU, F., CUI, B., GUO, X. N., LU, C. X., LI, X. G., LIU, M. S., PENG, B., CUI, L. Y. & ZHANG, X. 2016. Whole-exome sequencing identifies a missense mutation in hnRNPA1 in a family with flail arm ALS. *Neurology,* 87**,** 1763-1769.

[100] SHORTER, J. & TAYLOR, J. P. 2013. Disease mutations in the prion-like domains of hnRNPA1 and hnRNPA2/B1 introduce potent steric zippers that drive excess RNP granule assembly. *Rare Diseases,* 1**,** e25200.

[101] KIM, H. J., KIM, N. C., WANG, Y. D., SCARBOROUGH, E. A., MOORE, J., DIAZ, Z., MACLEA, K. S., FREIBAUM, B., LI, S., MOLLIEX, A., KANAGARAJ, A. P., CARTER, R., BOYLAN, K. B., WOJTAS, A. M., RADEMAKERS, R., PINKUS, J. L., GREENBERG, S. A., TROJANOWSKI, J. Q., TRAYNOR, B. J., SMITH, B. N., TOPP, S., GKAZI, A. S., MILLER, J., SHAW, C. E., KOTTLORS, M., KIRSCHNER, J., PESTRONK, A., LI, Y. R., FORD, A. F., GITLER, A. D., BENATAR, M., KING, O. D., KIMONIS, V. E., ROSS, E. D., WEIHL, C. C., SHORTER, J. & TAYLOR, J. P. 2013. Mutations in prion-like domains in hnRNPA2B1 and hnRNPA1 cause multisystem proteinopathy and ALS. *Nature,* 495**,** 467-73.

[102] MARTINEZ, F. J., PRATT, G. A., VAN NOSTRAND, E. L., BATRA, R., HUELGA, S. C., KAPELI, K., FREESE, P., CHUN, S. J., LING, K., GELBOIN-BURKHART, C., FIJANY, L., WANG, H. C., NUSSBACHER, J. K., BROSKI, S. M., KIM, H. J., LARDELLI, R., SUNDARARAMAN, B., DONOHUE, J. P., JAVAHERIAN, A., LYKKE-ANDERSEN, J., FINKBEINER, S., BENNETT, C. F., ARES, M., JR., BURGE, C. B., TAYLOR, J. P., RIGO, F. & YEO, G. W. 2016. Protein-RNA Networks Regulated by Normal and ALS-Associated Mutant HNRNPA2B1 in the Nervous System. *Neuron,* 92**,** 780-795.

[103] MOHAGHEGHI, F., PRUDENCIO, M., STUANI, C., COOK, C., JANSEN-WEST, K., DICKSON, D. W., PETRUCELLI, L. & BURATTI, E. 2016. TDP-43 functions within a network of hnRNP proteins to inhibit the production of a truncated human SORT1 receptor. *Hum Mol Genet,* 25**,** 534-45.

[104] GILPIN, K. M., CHANG, L. & MONTEIRO, M. J. 2015. ALS-linked mutations in ubiquilin-2 or hnRNPA1 reduce interaction between ubiquilin-2 and hnRNPA1. *Hum Mol Genet,* 24**,** 2565-77.

[105] RITSON, G. P., CUSTER, S. K., FREIBAUM, B. D., GUINTO, J. B., GEFFEL, D., MOORE, J., TANG, W., WINTON, M. J., NEUMANN, M., TROJANOWSKI, J. Q., LEE, V. M., FORMAN, M. S. & TAYLOR, J. P. 2010. TDP-43 mediates degeneration in a novel Drosophila model of disease caused by mutations in VCP/p97. *J Neurosci,* 30**,** 7729-39.

[106] MOLLIEX, A., TEMIROV, J., LEE, J., COUGHLIN, M., KANAGARAJ, A. P., KIM, H. J., MITTAG, T. & TAYLOR, J. P. 2015. Phase separation by low complexity domains promotes stress granule assembly and drives pathological fibrillization. *Cell,* 163**,** 123-133.

[107] HU, M. T. M., ELLIS, C. M., AL-CHALABI, A., LEIGH, P. N. & SHAW, C. E. 1998. Flail arm syndrome: a distinctive variant of amyotrophic lateral sclerosis. *Journal of Neurology, Neurosurgery & Psychiatry,* 65**,** 950.

[108] LE BER, I., VAN BORTEL, I., NICOLAS, G., BOUYA-AHMED, K., CAMUZAT, A., WALLON, D., DE SEPTENVILLE, A., LATOUCHE, M., LATTANTE, S., KABASHI, E., JORNEA, L., HANNEQUIN, D. & BRICE, A. 2014. hnRNPA2B1 and hnRNPA1 mutations are rare in patients with "multisystem proteinopathy" and frontotemporal lobar degeneration phenotypes. *Neurobiol Aging,* 35**,** 934.e5-6.

[109] KAPELI, K., MARTINEZ, F. J. & YEO, G. W. 2017. Genetic mutations in RNA-binding proteins and their roles in ALS. *Human Genetics,* 136**,** 1193-1214.

[110] HOFWEBER, M., HUTTEN, S., BOURGEOIS, B., SPREITZER, E., NIEDNER-BOBLENZ, A., SCHIFFERER, M., RUEPP, M. D., SIMONS, M., NIESSING, D., MADL, T. & DORMANN, D. 2018. Phase Separation of FUS Is Suppressed by Its Nuclear Import Receptor and Arginine Methylation. *Cell,* 173**,** 706-719.e13.

[111] PATEL, A., LEE, H. O., JAWERTH, L., MAHARANA, S., JAHNEL, M., HEIN, M. Y., STOYNOV, S., MAHAMID, J., SAHA, S., FRANZMANN, T. M., POZNIAKOVSKI, A., POSER, I., MAGHELLI, N., ROYER, L. A., WEIGERT, M., MYERS, E. W., GRILL, S., DRECHSEL, D., HYMAN, A. A. & ALBERTI, S. 2015. A Liquid-to-Solid Phase Transition of the ALS Protein FUS Accelerated by Disease Mutation. *Cell,* 162**,** 1066-77.

[112] PAUL, K. R., MOLLIEX, A., CASCARINA, S., BONCELLA, A. E., TAYLOR, J. P. & ROSS, E. D. 2017. Effects of Mutations on the Aggregation Propensity of the Human Prion-Like Protein hnRNPA2B1. *Mol Cell Biol,* 37.

[113] LI, H. R., CHIANG, W. C., CHOU, P. C., WANG, W. J. & HUANG, J. R. 2018. TAR DNA-binding protein 43 (TDP-43) liquid-liquid phase separation is mediated by just a few aromatic residues. *J Biol Chem,* 293**,** 6090-6098.

[114] KING, O. D., GITLER, A. D. & SHORTER, J. 2012. The tip of the iceberg: RNA-binding proteins with prion-like domains in neurodegenerative disease. *Brain Res,* 1462**,** 61-80.

[115] MURAKAMI, T., QAMAR, S., LIN, J. Q., SCHIERLE, G. S., REES, E., MIYASHITA, A., COSTA, A. R., DODD, R. B., CHAN, F. T., MICHEL, C. H., KRONENBERG-VERSTEEG, D., LI, Y., YANG, S. P., WAKUTANI, Y., MEADOWS, W., FERRY, R. R., DONG, L., TARTAGLIA, G. G., FAVRIN, G., LIN, W. L., DICKSON, D. W., ZHEN, M., RON, D., SCHMITT-ULMS, G., FRASER, P. E., SHNEIDER, N. A., HOLT, C., VENDRUSCOLO, M., KAMINSKI, C. F. & ST GEORGE-HYSLOP, P. 2015. ALS/FTD Mutation-Induced Phase Transition of FUS Liquid Droplets and Reversible Hydrogels into Irreversible Hydrogels Impairs RNP Granule Function. *Neuron,* 88**,** 678-90.

[116] GITLER, A. D. & SHORTER, J. 2011. RNA-binding proteins with prion-like domains in ALS and FTLD-U. *Prion,* 5**,** 179-87.

[117] LI, Y. R., KING, O. D., SHORTER, J. & GITLER, A. D. 2013. Stress granules as crucibles of ALS pathogenesis. *J Cell Biol,* 201**,** 361-72.

[118] PURICE, M. D. & TAYLOR, P. J. 2018. Linking hnRNP Function to ALS and FTD Pathology. *Frontiers in Neuroscience,* 12**,** 326.

[119] DREYFUSS, G., MATUNIS, M. J., PINOL-ROMA, S. & BURD, C. G. 1993. hnRNP proteins and the biogenesis of mRNA. *Annu Rev Biochem,* 62**,** 289-321.

[120] HE, Y. & SMITH, R. 2009. Nuclear functions of heterogeneous nuclear ribonucleoproteins A/B. *Cell Mol Life Sci,* 66**,** 1239-56.

[121] PINOL-ROMA, S., CHOI, Y. D., MATUNIS, M. J. & DREYFUSS, G. 1988. Immunopurification of heterogeneous nuclear ribonucleoprotein particles reveals an assortment of RNA-binding proteins. *Genes Dev,* 2**,** 215-27.

[122] GÖRLACH, M., WITTEKIND, M., BECKMAN, R. A., MUELLER, L. & DREYFUSS, G. 1992. Interaction of the RNA-binding domain of the hnRNP C proteins with RNA. *The EMBO Journal,* 11**,** 3289-3295.

[123] GEUENS, T., BOUHY, D. & TIMMERMAN, V. 2016. The hnRNP family: insights into their role in health and disease. *Human genetics,* 135**,** 851-867.

[124] DANGLI, A., GUIALIS, A., VRETOU, E. & SEKERIS, C. E. 1988. Autoantibodies to the core proteins of hnRNPs. *FEBS Lett,* 231**,** 118-24.

[125] KAMMA, H., HORIGUCHI, H., WAN, L., MATSUI, M., FUJIWARA, M., FUJIMOTO, M., YAZAWA, T. & DREYFUSS, G. 1999. Molecular characterization of the hnRNP A2/B1 proteins: tissue-specific expression and novel isoforms. *Exp Cell Res,* 246**,** 399-411.

[126] MARIS, C., DOMINGUEZ, C. & ALLAIN, F. H. 2005. The RNA recognition motif, a plastic RNA-binding platform to regulate post-transcriptional gene expression. *Febs j,* 272**,** 2118-31.

[127] VENABLES, J. P., KOH, C. S., FROEHLICH, U., LAPOINTE, E., COUTURE, S., INKEL, L., BRAMARD, A., PAQUET, E. R., WATIER, V., DURAND, M., LUCIER, J. F., GERVAIS-BIRD, J., TREMBLAY, K., PRINOS, P., KLINCK, R., ELELA, S. A. & CHABOT, B. 2008. Multiple and specific mRNA processing targets for the major human hnRNP proteins. *Mol Cell Biol,* 28**,** 6033-43.

[128] MARTINEZ-CONTRERAS, R., CLOUTIER, P., SHKRETA, L., FISETTE, J. F., REVIL, T. & CHABOT, B. 2007. hnRNP proteins and splicing control. *Adv Exp Med Biol,* 623**,** 123-47.

[129] PINOL-ROMA, S. & DREYFUSS, G. 1992. Shuttling of pre-mRNA binding proteins between nucleus and cytoplasm. *Nature,* 355**,** 730-2.

[130] SIOMI, M. C., EDER, P. S., KATAOKA, N., WAN, L., LIU, Q. & DREYFUSS, G. 1997. Transportin-mediated nuclear import of heterogeneous nuclear RNP proteins. *J Cell Biol,* 138**,** 1181-92.

[131] SUZUKI, H. & MATSUOKA, M. 2017. hnRNPA1 autoregulates its own mRNA expression to remain non-cytotoxic. *Molecular and Cellular Biochemistry,* 427**,** 123-131.

[132] GUIL, S., LONG, J. C. & CACERES, J. F. 2006. hnRNP A1 relocalization to the stress granules reflects a role in the stress response. *Mol Cell Biol,* 26**,** 5744-58.

[133] CAMMAS, A., PILEUR, F., BONNAL, S., LEWIS, S. M., LEVEQUE, N., HOLCIK, M. & VAGNER, S. 2007. Cytoplasmic relocalization of heterogeneous nuclear ribonucleoprotein A1 controls translation initiation of specific mRNAs. *Mol Biol Cell,* 18**,** 5048-59.

[134] RAJU, C. S., FUKUDA, N., LOPEZ-IGLESIAS, C., GORITZ, C., VISA, N. & PERCIPALLE, P. 2011. In neurons, activity-dependent association of dendritically transported mRNA transcripts with the transacting factor CBF-A is mediated by A2RE/RTS elements. *Mol Biol Cell,* 22**,** 1864-77.

[135] SHAN, J., MORAN-JONES, K., MUNRO, T. P., KIDD, G. J., WINZOR, D. J., HOEK, K. S. & SMITH, R. 2000. Binding of an RNA trafficking response element to heterogeneous nuclear ribonucleoproteins A1 and A2. *J Biol Chem,* 275**,** 38286-95.

[136] MA, A. S., MORAN-JONES, K., SHAN, J., MUNRO, T. P., SNEE, M. J., HOEK, K. S. & SMITH, R. 2002. Heterogeneous nuclear ribonucleoprotein A3, a novel RNA trafficking response element-binding protein. *J Biol Chem,* 277**,** 18010-20.

[137] DING, J., HAYASHI, M. K., ZHANG, Y., MANCHE, L., KRAINER, A. R. & XU, R. M. 1999. Crystal structure of the two-RRM domain of hnRNP A1 (UP1) complexed with single-stranded telomeric DNA. *Genes Dev,* 13**,** 1102-15.

[138] LABRANCHE, H., DUPUIS, S., BEN-DAVID, Y., BANI, M. R., WELLINGER, R. J. & CHABOT, B. 1998. Telomere elongation by hnRNP A1 and a derivative that interacts with telomeric repeats and telomerase. *Nat Genet,* 19**,** 199-202.

[139] TANAKA, E., FUKUDA, H., NAKASHIMA, K., TSUCHIYA, N., SEIMIYA, H. & NAKAGAMA, H. 2007. HnRNP A3 binds to and protects mammalian telomeric repeats in vitro. *Biochem Biophys Res Commun,* 358**,** 608-14.

[140] MORAN-JONES, K., WAYMAN, L., KENNEDY, D. D., REDDEL, R. R., SARA, S., SNEE, M. J. & SMITH, R. 2005. hnRNP A2, a potential ssDNA/RNA molecular adapter at the telomere. *Nucleic Acids Res,* 33**,** 486-96.

[141] DOUGLAS, J. N., GARDNER, L. A., SALAPA, H. E., LALOR, S. J., LEE, S., SEGAL, B. M., SAWCHENKO, P. E. & LEVIN, M. C. 2016. Antibodies to the RNA-binding protein hnRNP A1 contribute to neurodegeneration in a model of central nervous system autoimmune inflammatory disease. *J Neuroinflammation,* 13**,** 178.

[142] CAMPILLOS, M., LAMAS, J. R., GARCIA, M. A., BULLIDO, M. J., VALDIVIESO, F. & VAZQUEZ, J. 2003. Specific interaction of heterogeneous nuclear ribonucleoprotein A1 with the -219T allelic form modulates APOE promoter activity. *Nucleic Acids Res,* 31**,** 3063-70.

[143] BERSON, A., BARBASH, S., SHALTIEL, G., GOLL, Y., HANIN, G., GREENBERG, D. S., KETZEF, M., BECKER, A. J., FRIEDMAN, A. & SOREQ, H. 2012. Cholinergic-associated loss of hnRNP-A/B in Alzheimer's disease impairs cortical splicing and cognitive function in mice. *EMBO Mol Med,* 4**,** 730-42.

[144] DONEV, R., NEWALL, A., THOME, J. & SHEER, D. 2007. A role for SC35 and hnRNPA1 in the determination of amyloid precursor protein isoforms. *Mol Psychiatry,* 12**,** 681-90.

[145] CARPENTER, B., MACKAY, C., ALNABULSI, A., MACKAY, M., TELFER, C., MELVIN, W. T. & MURRAY, G. I. 2006. The roles of heterogeneous nuclear ribonucleoproteins in tumour development and progression. *Biochim Biophys Acta,* 1765**,** 85-100.

[146] LIU, X., ZHOU, Y., LOU, Y. & ZHONG, H. 2016. Knockdown of HNRNPA1 inhibits lung adenocarcinoma cell proliferation through cell cycle arrest at G0/G1 phase. *Gene,* 576**,** 791-7.

[147] JEAN-PHILIPPE, J., PAZ, S. & CAPUTI, M. 2013. hnRNP A1: the Swiss army knife of gene expression. *Int J Mol Sci,* 14**,** 18999-9024.

[148] HU, Y., SUN, Z., DENG, J., HU, B., YAN, W., WEI, H. & JIANG, J. 2017. Splicing factor hnRNPA2B1 contributes to tumorigenic potential of breast cancer cells through STAT3 and ERK1/2 signaling pathway. *Tumor Biology,* 39**,** 1010428317694318.

[149] BURATTI, E., BRINDISI, A., GIOMBI, M., TISMINETZKY, S., AYALA, Y. M. & BARALLE, F. E. 2005. TDP-43 binds heterogeneous nuclear ribonucleoprotein A/B through its C-terminal tail: an important region for the inhibition of cystic fibrosis transmembrane conductance regulator exon 9 splicing. *J Biol Chem,* 280**,** 37572-84.

[150] DESHAIES, J. E., SHKRETA, L., MOSZCZYNSKI, A. J., SIDIBE, H., SEMMLER, S., FOUILLEN, A., BENNETT, E. R., BEKENSTEIN, U., DESTROISMAISONS, L., TOUTANT, J., DELMOTTE, Q., VOLKENING, K., STABILE, S., AULAS, A., KHALFALLAH, Y., SOREQ, H., NANCI, A., STRONG, M. J., CHABOT, B. & VANDE VELDE, C. 2018. TDP-43 regulates the alternative splicing of hnRNP A1 to yield an aggregation-prone variant in amyotrophic lateral sclerosis. *Brain,* 141**,** 1320-1333.

[151] HONDA, H., HAMASAKI, H., WAKAMIYA, T., KOYAMA, S., SUZUKI, S. O., FUJII, N. & IWAKI, T. 2015. Loss of hnRNPA1 in ALS spinal cord motor neurons with TDP-43-positive inclusions. *Neuropathology.*

[152] KABASHI, E., VALDMANIS, P. N., DION, P., SPIEGELMAN, D., MCCONKEY, B. J., VANDE VELDE, C., BOUCHARD, J. P., LACOMBLEZ, L., POCHIGAEVA, K., SALACHAS, F., PRADAT, P. F., CAMU, W., MEININGER, V., DUPRE, N. & ROULEAU, G. A. 2008. TARDBP mutations in individuals with sporadic and familial amyotrophic lateral sclerosis. *Nat Genet,* 40**,** 572-4.

[153] BERTOLI, C., SKOTHEIM, J. M. & DE BRUIN, R. A. M. 2013. Control of cell cycle transcription during G1 and S phases. *Nature reviews. Molecular cell biology,* 14**,** 518-528.

[154] MCSHEA, A., WAHL, A. F. & SMITH, M. A. 1999. Re-entry into the cell cycle: a mechanism for neurodegeneration in Alzheimer disease. *Med Hypotheses,* 52**,** 525-7.

[155] GRANA, X. & REDDY, E. P. 1995. Cell cycle control in mammalian cells: role of cyclins, cyclin dependent kinases (CDKs), growth suppressor genes and cyclin-dependent kinase inhibitors (CKIs). *Oncogene,* 11**,** 211-9.

[156] SHERR, C. J. 1994. G1 phase progression: cycling on cue. *Cell,* 79**,** 551-5.

[157] MEIKRANTZ, W. & SCHLEGEL, R. 1995. Apoptosis and the cell cycle. *J Cell Biochem,* 58**,** 160-74.

[158] YU, C., GUO, J., LIU, Y., JIA, J., JIA, R. & FAN, M. 2015. Oral squamous cancer cell exploits hnRNP A1 to regulate cell cycle and proliferation. *J Cell Physiol,* 230**,** 2252-61.

[159] ZHANG, Q.-S., MANCHE, L., XU, R.-M. & KRAINER, A. R. 2006. hnRNP A1 associates with telomere ends and stimulates telomerase activity. *RNA (New York, N.Y.),* 12**,** 1116-1128.

[160] BALDWIN, A. S., JR. 1996. The NF-kappa B and I kappa B proteins: new discoveries and insights. *Annu Rev Immunol,* 14**,** 649-83.

[161] SINGH, A. K. & LAKHOTIA, S. C. 2012. The hnRNP A1 homolog Hrp36 is essential for normal development, female fecundity, omega speckle formation and stress tolerance in Drosophila melanogaster. *J Biosci,* 37**,** 659-78.

[162] LIU, T.-Y., CHEN, Y.-C., JONG, Y.-J., TSAI, H.-J., LEE, C.-C., CHANG, Y.-S., CHANG, J.-G. & CHANG, Y.-F. 2017. Muscle developmental defects in heterogeneous nuclear Ribonucleoprotein A1 knockout mice. *Open Biology,* 7**,** 160303.

[163] CARTEALY, I. 2008. *Characterization and knockdown of zebrafish Hnrnpa1.* Master of Philosophy, University of Queensland.

[164] GRUNWALD, D. J. & STREISINGER, G. 1992. Induction of recessive lethal and specific locus mutations in the zebrafish with ethyl nitrosourea. *Genet Res,* 59**,** 103-16.

[165] STREISINGER, G., WALKER, C., DOWER, N., KNAUBER, D. & SINGER, F. 1981. Production of clones of homozygous diploid zebra fish (Brachydanio rerio). *Nature,* 291**,** 293-6.

[166] HOWE, K., CLARK, M. D., TORROJA, C. F., TORRANCE, J., BERTHELOT, C., MUFFATO, M., COLLINS, J. E., HUMPHRAY, S., MCLAREN, K., MATTHEWS, L., MCLAREN, S., SEALY, I., CACCAMO, M., CHURCHER, C., SCOTT, C., BARRETT, J. C., KOCH, R., RAUCH, G.-J., WHITE, S., CHOW, W., KILIAN, B., QUINTAIS, L. T., GUERRA-ASSUNÇÃO, J. A., ZHOU, Y., GU, Y., YEN, J., VOGEL, J.-H., EYRE, T., REDMOND, S., BANERJEE, R., CHI, J., FU, B., LANGLEY, E., MAGUIRE, S. F., LAIRD, G. K., LLOYD, D., KENYON, E., DONALDSON, S., SEHRA, H., ALMEIDA-KING, J., LOVELAND, J., TREVANION, S., JONES, M., QUAIL, M., WILLEY, D., HUNT, A., BURTON, J., SIMS, S., MCLAY, K., PLUMB, B., DAVIS, J., CLEE, C., OLIVER, K., CLARK, R., RIDDLE, C., ELLIOTT, D., THREADGOLD, G., HARDEN, G., WARE, D., BEGUM, S., MORTIMORE, B., KERRY, G., HEATH, P., PHILLIMORE, B., TRACEY, A., CORBY, N., DUNN, M., JOHNSON, C., WOOD, J., CLARK, S., PELAN, S., GRIFFITHS, G., SMITH, M., GLITHERO, R., HOWDEN, P., BARKER, N., LLOYD, C., STEVENS, C., HARLEY, J., HOLT, K., PANAGIOTIDIS, G., LOVELL, J., BEASLEY, H., HENDERSON, C., GORDON, D., AUGER, K., WRIGHT, D., COLLINS, J., RAISEN, C., DYER, L., LEUNG, K., ROBERTSON, L., AMBRIDGE, K., LEONGAMORNLERT, D., MCGUIRE, S., GILDERTHORP, R., GRIFFITHS, C., MANTHRAVADI, D., NICHOL, S., BARKER, G., et al. 2013. The zebrafish reference genome sequence and its relationship to the human genome. *Nature,* 496**,** 498.

[167] HOWE, K., CLARK, M. D., TORROJA, C. F., TORRANCE, J., BERTHELOT, C., MUFFATO, M., COLLINS, J. E., HUMPHRAY, S., MCLAREN, K., MATTHEWS, L., MCLAREN, S., SEALY, I., CACCAMO, M., CHURCHER, C., SCOTT, C., BARRETT, J. C., KOCH, R., RAUCH, G. J., WHITE, S., CHOW, W., KILIAN, B., QUINTAIS, L. T., GUERRA-ASSUNCAO, J. A., ZHOU, Y., GU, Y., YEN, J., VOGEL, J. H., EYRE, T., REDMOND, S., BANERJEE, R., CHI, J., FU, B., LANGLEY, E., MAGUIRE, S. F., LAIRD, G. K., LLOYD, D., KENYON, E., DONALDSON, S., SEHRA, H., ALMEIDA-KING, J., LOVELAND, J., TREVANION, S., JONES, M., QUAIL, M., WILLEY, D., HUNT, A., BURTON, J., SIMS, S., MCLAY, K., PLUMB, B., DAVIS, J., CLEE, C., OLIVER, K., CLARK, R., RIDDLE, C., ELLIOT, D., THREADGOLD, G., HARDEN, G., WARE, D., BEGUM, S., MORTIMORE, B., KERRY, G., HEATH, P., PHILLIMORE, B., TRACEY, A., CORBY, N., DUNN, M., JOHNSON, C., WOOD, J., CLARK, S., PELAN, S., GRIFFITHS, G., SMITH, M., GLITHERO, R., HOWDEN, P., BARKER, N., LLOYD, C., STEVENS, C., HARLEY, J., HOLT, K., PANAGIOTIDIS, G., LOVELL, J., BEASLEY, H., HENDERSON, C., GORDON, D., AUGER, K., WRIGHT, D., COLLINS, J., RAISEN, C., DYER, L., LEUNG, K., ROBERTSON, L., AMBRIDGE, K., LEONGAMORNLERT, D., MCGUIRE, S., GILDERTHORP, R., GRIFFITHS, C., MANTHRAVADI, D., NICHOL, S., BARKER, G., et al. 2013. The zebrafish reference genome sequence and its relationship to the human genome. *Nature,* 496**,** 498-503.

[168] BEIS, D. & STAINIER, D. Y. 2006. In vivo cell biology: following the zebrafish trend. *Trends Cell Biol,* 16**,** 105-12.

[169] TAN, J. L. & ZON, L. I. 2011. Chapter 21 - Chemical Screening in Zebrafish for Novel Biological and Therapeutic Discovery. *In:* DETRICH, H. W., WESTERFIELD, M. & ZON, L. I. (eds.) *Methods in Cell Biology.* Academic Press.

[170] XI, Y., NOBLE, S. & EKKER, M. 2011. Modeling neurodegeneration in zebrafish. *Current neurology and neuroscience reports,* 11**,** 274-282.

[171] DOYON, Y., MCCAMMON, J. M., MILLER, J. C., FARAJI, F., NGO, C., KATIBAH, G. E., AMORA, R., HOCKING, T. D., ZHANG, L., REBAR, E. J., GREGORY, P. D., URNOV, F. D. & AMACHER, S. L. 2008. Heritable targeted gene disruption in zebrafish using designed zinc-finger nucleases. *Nat Biotechnol,* 26**,** 702-8.

[172] HUANG, P., XIAO, A., ZHOU, M., ZHU, Z., LIN, S. & ZHANG, B. 2011. Heritable gene targeting in zebrafish using customized TALENs. *Nat Biotechnol,* 29**,** 699-700.

[173] JAO, L. E., WENTE, S. R. & CHEN, W. 2013. Efficient multiplex biallelic zebrafish genome editing using a CRISPR nuclease system. *Proc Natl Acad Sci U S A,* 110**,** 13904-9.

[174] AUER, T. O., DUROURE, K., DE CIAN, A., CONCORDET, J. P. & DEL BENE, F. 2014. Highly efficient CRISPR/Cas9-mediated knock-in in zebrafish by homology-independent DNA repair. *Genome Res,* 24**,** 142-53.

[175] LI, J., ZHANG, B.-B., REN, Y.-G., GU, S.-Y., XIANG, Y.-H., HUANG, C. & DU, J.-L. 2015. Intron targeting-mediated and endogenous gene integrity-maintaining knockin in zebrafish using the CRISPR/Cas9 system. *Cell Research,* 25**,** 634.

[176] DEVEAU, H., GARNEAU, J. E. & MOINEAU, S. 2010. CRISPR/Cas system and its role in phage-bacteria interactions. *Annu Rev Microbiol,* 64**,** 475-93.

[177] HORVATH, P. & BARRANGOU, R. 2010. CRISPR/Cas, the immune system of bacteria and archaea. *Science,* 327**,** 167-70.

[178] WRIGHT, A. V., NUNEZ, J. K. & DOUDNA, J. A. 2016. Biology and Applications of CRISPR Systems: Harnessing Nature's Toolbox for Genome Engineering. *Cell,* 164**,** 29-44.

[179] JANSEN, R., EMBDEN, J. D., GAASTRA, W. & SCHOULS, L. M. 2002. Identification of genes that are associated with DNA repeats in prokaryotes. *Mol Microbiol,* 43**,** 1565-75.

[180] DELTCHEVA, E., CHYLINSKI, K., SHARMA, C. M., GONZALES, K., CHAO, Y., PIRZADA, Z. A., ECKERT, M. R., VOGEL, J. & CHARPENTIER, E. 2011. CRISPR RNA maturation by trans-encoded small RNA and host factor RNase III. *Nature,* 471**,** 602-607.

[181] JINEK, M., CHYLINSKI, K., FONFARA, I., HAUER, M., DOUDNA, J. A. & CHARPENTIER, E. 2012. A programmable dual-RNA-guided DNA endonuclease in adaptive bacterial immunity. *Science,* 337**,** 816-21.

[182] MOJICA, F. J., DIEZ-VILLASENOR, C., GARCIA-MARTINEZ, J. & ALMENDROS, C. 2009. Short motif sequences determine the targets of the prokaryotic CRISPR defence system. *Microbiology,* 155**,** 733-40.

[183] RAMESH, T., LYON, A. N., PINEDA, R. H., WANG, C., JANSSEN, P. M. L., CANAN, B. D., BURGHES, A. H. M. & BEATTIE, C. E. 2010. A genetic model of amyotrophic lateral sclerosis in zebrafish displays phenotypic hallmarks of motoneuron disease. *Disease Models & Mechanisms,* 3**,** 652-662.

[184] DA COSTA, M. M. J., ALLEN, C. E., HIGGINBOTTOM, A., RAMESH, T., SHAW, P. J. & MCDERMOTT, C. J. 2014. A new zebrafish model produced by TILLING of SOD1-related amyotrophic lateral sclerosis replicates key features of the disease and represents a tool for <em>in vivo</em> therapeutic screening. *Disease Models & Mechanisms,* 7**,** 73.

[185] KABASHI, E., BERCIER, V., LISSOUBA, A., LIAO, M., BRUSTEIN, E., ROULEAU, G. A. & DRAPEAU, P. 2011. FUS and TARDBP but not SOD1 interact in genetic models of amyotrophic lateral sclerosis. *PLoS Genet,* 7**,** e1002214.

[186] HASENKAMP, L. 2015. ALS and FTLD associated FUS in zebra □ sh - investigating disease mechanisms in vivo. *PhD thesis,* Munich.

[187] KABASHI, E., LIN, L., TRADEWELL, M. L., DION, P. A., BERCIER, V., BOURGOUIN, P., ROCHEFORT, D., BEL HADJ, S., DURHAM, H. D., VANDE VELDE, C., ROULEAU, G. A. & DRAPEAU, P. 2010. Gain and loss of function of ALS-related mutations of TARDBP (TDP-43) cause motor deficits in vivo. *Hum Mol Genet,* 19**,** 671-83.

[188] KABASHI, E., LIN, L., TRADEWELL, M. L., DION, P. A., BERCIER, V., BOURGOUIN, P., ROCHEFORT, D., HADJ, S., DURHAM, H. D., VELDE, C., ROULEAU, G. A. & DRAPEAU, P. 2010. Gain and loss of function of ALS-related mutations of TARDBP (TDP-43) cause motor deficits in vivo. *Human Molecular Genetics,* 19**,** 671-683.

[189] CORRADI, L. 2016. Functional analysis of the ALS/FTD-related C9orf72 gene in zebrafish *PhD thesis,* Munich.

[190] SOLCHENBERGER, B., RUSSELL, C., KREMMER, E., HAASS, C. & SCHMID, B. 2015. Granulin knock out zebrafish lack frontotemporal lobar degeneration and neuronal ceroid lipofuscinosis pathology. *PLoS One,* 10**,** e0118956.

[191] LI, Y.-H., CHEN, H.-Y., LI, Y.-W., WU, S.-Y., WANGTA, L., LIN, G.-H., HU, S.-Y., CHANG, Z.-K., GONG, H.-Y., LIAO, C.-H., CHIANG, K.-Y., HUANG, C.-W. & WU, J.-L. 2013. Progranulin regulates zebrafish muscle growth and regeneration through maintaining the pool of myogenic progenitor cells. *Scientific reports,* 3**,** 1176-1176.

[192] ROSSI, A., KONTARAKIS, Z., GERRI, C., NOLTE, H., HÖLPER, S., KRÜGER, M. & STAINIER, D. Y. R. 2015. Genetic compensation induced by deleterious mutations but not gene knockdowns. *Nature,* 524**,** 230.

[193] STAINIER, D. Y. R., RAZ, E., LAWSON, N. D., EKKER, S. C., BURDINE, R. D., EISEN, J. S., INGHAM, P. W., SCHULTE-MERKER, S., YELON, D., WEINSTEIN, B. M., MULLINS, M. C., WILSON, S. W., RAMAKRISHNAN, L., AMACHER, S. L., NEUHAUSS, S. C. F., MENG, A., MOCHIZUKI, N., PANULA, P. & MOENS, C. B. 2017. Guidelines for morpholino use in zebrafish. *PLoS Genet,* 13**,** e1007000.

[194] LAWSON, N. D. & WEINSTEIN, B. M. 2002. In vivo imaging of embryonic vascular development using transgenic zebrafish. *Dev Biol,* 248**,** 307-18.

[195] PRENGEL Jan. 2000. Entwicklung und immunmorphologische Charakterisierung monoklonaler Antikörper gegen Proteine des Zebrabärblings (Danio rerio). *PhD thesis,* Munich.

[196] TREVARROW, B., MARKS, D. L. & KIMMEL, C. B. 1990. Organization of hindbrain segments in the zebrafish embryo. *Neuron,* 4**,** 669-79.

[197] MULLINS, M. C., HAMMERSCHMIDT, M., HAFFTER, P. & NUSSLEIN-VOLHARD, C. 1994. Large-scale mutagenesis in the zebrafish: in search of genes controlling development in a vertebrate. *Curr Biol,* 4**,** 189-202.

[198] KIMMEL, C. B., BALLARD, W. W., KIMMEL, S. R., ULLMANN, B. & SCHILLING, T. F. 1995. Stages of embryonic development of the zebrafish. *Dev Dyn,* 203**,** 253-310.

[199] KARLSSON, J., VON HOFSTEN, J. & OLSSON, P. E. 2001. Generating transparent zebrafish: a refined method to improve detection of gene expression during embryonic development. *Mar Biotechnol (NY),* 3**,** 522-7.

[200] TIMME-LARAGY, A. R., KARCHNER, S. I. & HAHN, M. E. 2012. Gene knockdown by morpholino-modified oligonucleotides in the zebrafish (Danio rerio) model: applications for developmental toxicology. *Methods in molecular biology (Clifton, N.J.),* 889**,** 51-71.

[201] SIELAFF, M., KUHAREV, J., BOHN, T., HAHLBROCK, J., BOPP, T., TENZER, S. & DISTLER, U. 2017. Evaluation of FASP, SP3, and iST Protocols for Proteomic Sample Preparation in the Low Microgram Range. *J Proteome Res,* 16**,** 4060-4072.

[202] PAQUET, D., BHAT, R., SYDOW, A., MANDELKOW, E. M., BERG, S., HELLBERG, S., FALTING, J., DISTEL, M., KOSTER, R. W., SCHMID, B. & HAASS, C. 2009. A zebrafish model of tauopathy allows in vivo imaging of neuronal cell death and drug evaluation. *J Clin Invest,* 119**,** 1382-95.

[203] MEYER, A. & SCHARTL, M. 1999. Gene and genome duplications in vertebrates: the one-to-four (-to-eight in fish) rule and the evolution of novel gene functions. *Curr Opin Cell Biol,* 11**,** 699-704.

[204] VILELLA, A. J., SEVERIN, J., URETA-VIDAL, A., HENG, L., DURBIN, R. & BIRNEY, E. 2009. EnsemblCompara GeneTrees: Complete, duplication-aware phylogenetic trees in vertebrates. *Genome Res,* 19**,** 327-35.

[205] DURAN, C., EDWARDS, D. & BATLEY, J. 2009. Genetic maps and the use of synteny. *Methods Mol Biol,* 513**,** 41-55.

[206] MILSTEIN, C. 1999. The hybridoma revolution: an offshoot of basic research. *Bioessays,* 21**,** 966-73.

[207] PIÑOL-ROMA, S. & DREYFUSS, G. 1992. Shuttling of pre-mRNA binding proteins between nucleus and cytoplasm. *Nature,* 355**,** 730.

[208] SHORTER, J. & TAYLOR, J. P. 2013. Disease mutations in the prion-like domains of hnRNPA1 and hnRNPA2/B1 introduce potent steric zippers that drive excess RNP granule assembly. *Rare Dis,* 1**,** e25200.

[209] ISKEN, O. & MAQUAT, L. E. 2007. Quality control of eukaryotic mRNA: safeguarding cells from abnormal mRNA function. *Genes Dev,* 21**,** 1833-56.

[210] PELEGRI, F. 2003. Maternal factors in zebrafish development. *Dev Dyn,* 228**,** 535-54.

[211] LAIRD, A. S., VAN HOECKE, A., DE MUYNCK, L., TIMMERS, M., VAN DEN BOSCH, L., VAN DAMME, P. & ROBBERECHT, W. 2010. Progranulin is neurotrophic in vivo and protects against a mutant TDP-43 induced axonopathy. *PLoS One,* 5**,** e13368.

[212] PAQUET, D., BHAT, R., SYDOW, A., MANDELKOW, E.-M., BERG, S., HELLBERG, S., FÄLTING, J., DISTEL, M., KÖSTER, R. W., SCHMID, B. & HAASS, C. 2009. A zebrafish model of tauopathy allows in vivo imaging of neuronal cell death and drug evaluation. *The Journal of Clinical Investigation,* 119**,** 1382-1395.

[213] ZHANG, R., YANG, J., ZHU, J. & XU, X. 2009. Depletion of zebrafish Tcap leads to muscular dystrophy via disrupting sarcomere-membrane interaction, not sarcomere assembly. *Hum Mol Genet,* 18**,** 4130-40.

[214] DESPIC, V., DEJUNG, M., GU, M., KRISHNAN, J., ZHANG, J., HERZEL, L., STRAUBE, K., GERSTEIN, M. B., BUTTER, F. & NEUGEBAUER, K. M. 2017. Dynamic RNA–protein interactions underlie the zebrafish maternal-to-zygotic transition. *Genome Research,* 27**,** 1184-1194.

[215] FRAHER, D., ELLIS, M. K., MORRISON, S., MCGEE, S. L., WARD, A. C., WALDER, K. & GIBERT, Y. 2015. Lipid Abundance in Zebrafish Embryos Is Regulated by Complementary Actions of the Endocannabinoid System and Retinoic Acid Pathway. *Endocrinology,* 156**,** 3596-609.

[216] ALTENBERG, B. & GREULICH, K. O. 2004. Genes of glycolysis are ubiquitously overexpressed in 24 cancer classes. *Genomics,* 84**,** 1014-20.

[217] DAVID, C. J., CHEN, M., ASSANAH, M., CANOLL, P. & MANLEY, J. L. 2010. HnRNP proteins controlled by c-Myc deregulate pyruvate kinase mRNA splicing in cancer. *Nature,* 463**,** 364-8.

[218] BONNAL, S., VIGEVANI, L. & VALCARCEL, J. 2012. The spliceosome as a target of novel antitumour drugs. *Nat Rev Drug Discov,* 11**,** 847-59.

[219] LI, Z., ZHENG, W., LI, H., LI, C. & GONG, Z. 2015. Synergistic Induction of Potential Warburg Effect in Zebrafish Hepatocellular Carcinoma by Co-Transgenic Expression of Myc and xmrk Oncogenes. *PLoS One,* 10**,** e0132319.

[220] ISHIKAWA, T., MORITA, M. & NAKANO, I. 2007. Constant blood flow reduction in premotor frontal lobe regions in ALS with dementia - a SPECT study with 3D-SSP. *Acta Neurol Scand,* 116**,** 340-4.

[221] TANAKA, M., KONDO, S., HIRAI, S., SUN, X., YAMAGISHI, T. & OKAMOTO, K. 1993. Cerebral blood flow and oxygen metabolism in progressive dementia associated with amyotrophic lateral sclerosis. *J Neurol Sci,* 120**,** 22-8.

[222] STRECKER, K. 2015. *Linking Neurodegeneration to Vascular Dysfunction – Loss of ALS/FTD-Associated TDP-43 causes angiogenic defects.* PhD thesis.

[223] ABDELMAGID, S. M., SONDAG, G. R., MOUSSA, F. M., BELCHER, J. Y., YU, B., STINNETT, H., NOVAK, K., MBIMBA, T., KHOL, M., HANKENSON, K. D., MALCUIT, C. & SAFADI, F. F. 2015. Mutation in Osteoactivin Promotes Receptor Activator of NF $\kappa$ B Ligand (RANKL)-mediated Osteoclast Differentiation and Survival but Inhibits Osteoclast Function. *The Journal of Biological Chemistry,* 290**,** 20128-20146.

[224] TANAKA, H., SHIMAZAWA, M., KIMURA, M., TAKATA, M., TSURUMA, K., YAMADA, M., TAKAHASHI, H., HOZUMI, I., NIWA, J., IGUCHI, Y., NIKAWA, T., SOBUE, G., INUZUKA, T. & HARA, H. 2012. The potential of GPNMB as novel neuroprotective factor in amyotrophic lateral sclerosis. *Sci Rep,* 2**,** 573.

[225] MAGA, G. & HUBSCHER, U. 2003. Proliferating cell nuclear antigen (PCNA): a dancer with many partners. *J Cell Sci,* 116**,** 3051-60.

[226] BRAVO, R., FRANK, R., BLUNDELL, P. A. & MACDONALD-BRAVO, H. 1987. Cyclin/PCNA is the auxiliary protein of DNA polymerase-delta. *Nature,* 326**,** 515-7.

[227] TAN, C. K., CASTILLO, C., SO, A. G. & DOWNEY, K. M. 1986. An auxiliary protein for DNA polymerase-delta from fetal calf thymus. *J Biol Chem,* 261**,** 12310-6.

[228] STRZALKA, W. & ZIEMIENOWICZ, A. 2011. Proliferating cell nuclear antigen (PCNA): a key factor in DNA replication and cell cycle regulation. *Annals of Botany,* 107**,** 1127-1140.

[229] SCHÖNENBERGER, F., DEUTZMANN, A., FERRANDO-MAY, E. & MERHOF, D. 2015. Discrimination of cell cycle phases in PCNA-immunolabeled cells. *BMC Bioinformatics,* 16**,** 180.

[230] HAN, S. P., TANG, Y. H. & SMITH, R. 2010. Functional diversity of the hnRNPs: past, present and perspectives. *Biochem J,* 430**,** 379-92.

[231] GLASAUER, S. M. & NEUHAUSS, S. C. 2014. Whole-genome duplication in teleost fishes and its evolutionary consequences. *Mol Genet Genomics,* 289**,** 1045-60.

[232] OHNO, S. 1970a. *Evolution by gene duplication*, Springer, New York.

[233] JAILLON, O., AURY, J. M., BRUNET, F., PETIT, J. L., STANGE-THOMANN, N., MAUCELI, E., BOUNEAU, L., FISCHER, C., OZOUF-COSTAZ, C., BERNOT, A., NICAUD, S., JAFFE, D., FISHER, S., LUTFALLA, G., DOSSAT, C., SEGURENS, B., DASILVA, C., SALANOUBAT, M., LEVY, M., BOUDET, N., CASTELLANO, S., ANTHOUARD, V., JUBIN, C., CASTELLI, V., KATINKA, M., VACHERIE, B., BIEMONT, C., SKALLI, Z., CATTOLICO, L., POULAIN, J., DE BERARDINIS, V., CRUAUD, C., DUPRAT, S., BROTTIER, P., COUTANCEAU, J. P., GOUZY, J., PARRA, G., LARDIER, G., CHAPPLE, C., MCKERNAN, K. J., MCEWAN, P., BOSAK, S., KELLIS, M., VOLFF, J. N., GUIGO, R., ZODY, M. C., MESIROV, J., LINDBLAD-TOH, K., BIRREN, B., NUSBAUM, C., KAHN, D., ROBINSON-RECHAVI, M., LAUDET, V., SCHACHTER, V., QUETIER, F., SAURIN, W., SCARPELLI, C., WINCKER, P., LANDER, E. S., WEISSENBACH, J. & ROEST CROLLIUS, H. 2004. Genome duplication in the teleost fish Tetraodon nigroviridis reveals the early vertebrate proto-karyotype. *Nature,* 431**,** 946-57.

[234] LABOISSONNIERE, L. A., SMITH, C. L., MESENBRINK, J., CHOWDHURY, R., BURNEY, A., LANG, M., SIERRA, M., STARK, A., MALDONADO-CASALDUC, G., MULLER, M. & TRIMARCHI, J. M. 2018. ALS-associated genes display CNS expression in the developing zebrafish. *Gene Expression Patterns*.

[235] HUTCHISON, S., LEBEL, C., BLANCHETTE, M. & CHABOT, B. 2002. Distinct sets of adjacent heterogeneous nuclear ribonucleoprotein (hnRNP) A1/A2 binding sites control 5' splice site selection in the hnRNP A1 mRNA precursor. *J Biol Chem,* 277**,** 29745-52.

[236] HE, Y., BROWN, M. A., ROTHNAGEL, J. A., SAUNDERS, N. A. & SMITH, R. 2005. Roles of heterogeneous nuclear ribonucleoproteins A and B in cell proliferation. *Journal of Cell Science,* 118**,** 3173.

[237] EISEN, J. S. & SMITH, J. C. 2008. Controlling morpholino experiments: don't stop making antisense. *Development,* 135**,** 1735-43.

[238] SCHMID, B. & HAASS, C. 2013. Genomic editing opens new avenues for zebrafish as a model for neurodegeneration. *Journal of Neurochemistry,* 127**,** 461-470.

[239] STAINIER, D. Y. R., RAZ, E., LAWSON, N. D., EKKER, S. C., BURDINE, R. D., EISEN, J. S., INGHAM, P. W., SCHULTE-MERKER, S., YELON, D., WEINSTEIN, B. M., MULLINS, M. C., WILSON, S. W., RAMAKRISHNAN, L., AMACHER, S. L., NEUHAUSS, S. C. F., MENG, A., MOCHIZUKI, N., PANULA, P. & MOENS, C. B. 2017. Guidelines for morpholino use in zebrafish. *PLOS Genetics,* 13.

[240] MIKULA, M., DZWONEK, A., KARCZMARSKI, J., RUBEL, T., DADLEZ, M., WYRWICZ, L. S., BOMSZTYK, K. & OSTROWSKI, J. 2006. Landscape of the hnRNP K protein-protein interactome. *Proteomics,* 6**,** 2395-406.

[241] RULE, R. R., SCHUFF, N., MILLER, R. G. & WEINER, M. W. 2010. Gray matter perfusion correlates with disease severity in ALS. *Neurology,* 74**,** 821-827.

[242] ISHIKAWA, T., MORITA, M. & NAKANO, I. 2007. Constant blood flow reduction in premotor frontal lobe regions in ALS with dementia – a SPECT study with 3D-SSP. *Acta Neurologica Scandinavica,* 116**,** 340-344.

[243] ZHONG, Z., DEANE, R., ALI, Z., PARISI, M., SHAPOVALOV, Y., O'BANION, M. K., STOJANOVIC, K., SAGARE, A., BOILLEE, S., CLEVELAND, D. W. & ZLOKOVIC, B. V. 2008. ALS-causing SOD1 mutants generate vascular changes prior to motor neuron degeneration. *Nat Neurosci,* 11**,** 420-2.

[244] CIURA, S., LATTANTE, S., LE BER, I., LATOUCHE, M., TOSTIVINT, H., BRICE, A. & KABASHI, E. 2013. Loss of function of C9orf72 causes motor deficits in a zebrafish model of amyotrophic lateral sclerosis. *Annals of Neurology,* 74**,** 180-187.

[245] KABASHI, E., BERCIER, V., LISSOUBA, A., LIAO, M., BRUSTEIN, E., ROULEAU, G. A. & DRAPEAU, P. 2011. FUS and TARDBP but Not SOD1 Interact in Genetic Models of Amyotrophic Lateral Sclerosis. *PLOS Genetics,* 7**,** e1002214.

[246] KABASHI, E., LIN, L., TRADEWELL, M. L., DION, P. A., BERCIER, V., BOURGOUIN, P., ROCHEFORT, D., BEL HADJ, S., DURHAM, H. D., VELDE, C. V., ROULEAU, G. A. & DRAPEAU, P. 2010. Gain and loss of function of ALS-related mutations of TARDBP (TDP-43) cause motor deficits in vivo. *Human Molecular Genetics,* 19**,** 671-683.

[247] LATTANTE, S., DE CALBIAC, H., LE BER, I., BRICE, A., CIURA, S. & KABASHI, E. 2015. Sqstm1 knock-down causes a locomotor phenotype ameliorated by rapamycin in a zebrafish model of ALS/FTLD. *Human Molecular Genetics,* 24**,** 1682-1690.

[248] FENG, Y. & WALSH, C. A. 2004. The many faces of filamin: a versatile molecular scaffold for cell motility and signalling. *Nat Cell Biol,* 6**,** 1034-8.

[249] ZHANG, L., CHEN, Q., AN, W., YANG, F., MAGUIRE, E. M., CHEN, D., ZHANG, C., WEN, G., YANG, M., DAI, B., LUONG, L. A., ZHU, J., XU, Q. & XIAO, Q. 2017. Novel Pathological Role of hnRNPA1 (Heterogeneous Nuclear Ribonucleoprotein A1) in Vascular Smooth Muscle Cell Function and Neointima Hyperplasia. *Arterioscler Thromb Vasc Biol,* 37**,** 2182-2194.

[250] GERHARDT, H., GOLDING, M., FRUTTIGER, M., RUHRBERG, C., LUNDKVIST, A., ABRAMSSON, A., JELTSCH, M., MITCHELL, C., ALITALO, K., SHIMA, D. & BETSHOLTZ, C. 2003. VEGF guides angiogenic sprouting utilizing endothelial tip cell filopodia. *J Cell Biol,* 161**,** 1163-77.

[251] PROCTOR, R. A. 1987. Fibronectin: a brief overview of its structure, function, and physiology. *Rev Infect Dis,* 9 Suppl 4**,** S317-21.

[252] GEORGE, E. L., GEORGES-LABOUESSE, E. N., PATEL-KING, R. S., RAYBURN, H. & HYNES, R. O. 1993. Defects in mesoderm, neural tube and vascular development in mouse embryos lacking fibronectin. *Development,* 119**,** 1079-91.

[253] GEORGES-LABOUESSE, E. N., GEORGE, E. L., RAYBURN, H. & HYNES, R. O. 1996. Mesodermal development in mouse embryos mutant for fibronectin. *Dev Dyn,* 207**,** 145-56.

[254] GEORGE, E. L., BALDWIN, H. S. & HYNES, R. O. 1997. Fibronectins are essential for heart and blood vessel morphogenesis but are dispensable for initial specification of precursor cells. *Blood,* 90**,** 3073-81.

[255] ZHAO, Q., LIU, X. & COLLODI, P. 2001. Identification and characterization of a novel fibronectin in zebrafish. *Exp Cell Res,* 268**,** 211-9.

[256] KOSHIDA, S., KISHIMOTO, Y., USTUMI, H., SHIMIZU, T., FURUTANI-SEIKI, M., KONDOH, H. & TAKADA, S. 2005. Integrinalpha5-dependent fibronectin accumulation for maintenance of somite boundaries in zebrafish embryos. *Dev Cell,* 8**,** 587-98.

[257] JULICH, D., GEISLER, R. & HOLLEY, S. A. 2005. Integrinalpha5 and delta/notch signaling have complementary spatiotemporal requirements during zebrafish somitogenesis. *Dev Cell,* 8**,** 575-86.

[258] DERUITER, C. 2010. Somites: formation and role in developing the body plan. *Embryo Project Encyclopedia.* Arizona State University. School of Life Sciences.

[259] KATRIN HIPKE, B. P., ALEXANDER HRUSCHA, MIHA MODIC, VIKAS BANSAL, SEBASTIAN A. LEWANDOWSKI, DENISE OROCZCO, DIETER EDBAUER, STEFAN BONN, CHRISTIAN HAASS, ULRICH POHL, ELOI MONTANEZ, BETTINA SCHMID 2018. Loss of TDP-43 causes ectopic endothelial sprouting and migration defects through increased fn 1, vcam 1 and itg $\alpha 4/\beta 1$ DZNE Munich.

[260] COSTESSI, L., PORRO, F., IACONCIG, A. & MURO, A. F. 2014. TDP-43 regulates beta-adducin (Add2) transcript stability. *RNA Biol,* 11**,** 1280-90.

[261] GLISOVIC, T., BACHORIK, J. L., YONG, J. & DREYFUSS, G. 2008. RNA-binding proteins and post-transcriptional gene regulation. *FEBS Lett,* 582**,** 1977-86.

[262] MAGNUSSON, M. K. & MOSHER, D. F. 1998. Fibronectin: structure, assembly, and cardiovascular implications. *Arterioscler Thromb Vasc Biol,* 18**,** 1363-70.

[263] BRAY, N. 2018. The power of 3′ UTRs. *Nature Reviews Neuroscience,* 19**,** 319-319.

[264] HUELGA, S. C., VU, A. Q., ARNOLD, J. D., LIANG, T. Y., LIU, P. P., YAN, B. Y., DONOHUE, J. P., SHIUE, L., HOON, S., BRENNER, S., ARES, M., JR. & YEO, G. W. 2012. Integrative genome-wide analysis reveals cooperative regulation of alternative splicing by hnRNP proteins. *Cell reports,* 1**,** 167-178.

[265] GAMA-CARVALHO, M. & CARMO-FONSECA, M. 2001. The rules and roles of nucleocytoplasmic shuttling proteins. *FEBS Lett,* 498**,** 157-63.

[266] GORLACH, M., WITTEKIND, M., BECKMAN, R. A., MUELLER, L. & DREYFUSS, G. 1992. Interaction of the RNA-binding domain of the hnRNP C proteins with RNA. *Embo j,* 11**,** 3289-95.

[267] AYALA, Y. M., PANTANO, S., D'AMBROGIO, A., BURATTI, E., BRINDISI, A., MARCHETTI, C., ROMANO, M. & BARALLE, F. E. 2005. Human, Drosophila, and C.elegans TDP43: Nucleic Acid Binding Properties and Splicing Regulatory Function. *Journal of Molecular Biology,* 348**,** 575-588.

[268] PASSONI, M., DE CONTI, L., BARALLE, M. & BURATTI, E. 2012. UG repeats/TDP-43 interactions near 5' splice sites exert unpredictable effects on splicing modulation. *J Mol Biol,* 415**,** 46-60.

[269] BURATTI, E. & BARALLE, F. E. 2001. Characterization and functional implications of the RNA binding properties of nuclear factor TDP-43, a novel splicing regulator of CFTR exon 9. *J Biol Chem,* 276**,** 36337-43.

[270] BLANCHETTE, M. & CHABOT, B. 1999. Modulation of exon skipping by high-affinity hnRNP A1-binding sites and by intron elements that repress splice site utilization. *Embo j,* 18**,** 1939-52.

[271] NASIM, F. U., HUTCHISON, S., CORDEAU, M. & CHABOT, B. 2002. High-affinity hnRNP A1 binding sites and duplex-forming inverted repeats have similar effects on 5' splice site selection in support of a common looping out and repression mechanism. *Rna,* 8**,** 1078-89.

[272] JANKOWSKY, E. & HARRIS, M. E. 2015. Specificity and nonspecificity in RNA-protein interactions. *Nat Rev Mol Cell Biol,* 16**,** 533-44.

[273] TAKACS, C. M. & GIRALDEZ, A. J. 2016. miR-430 regulates oriented cell division during neural tube development in zebrafish. *Dev Biol,* 409**,** 442-50.

[274] GIRALDEZ, A. J., CINALLI, R. M., GLASNER, M. E., ENRIGHT, A. J., THOMSON, J. M., BASKERVILLE, S., HAMMOND, S. M., BARTEL, D. P. & SCHIER, A. F. 2005. MicroRNAs regulate brain morphogenesis in zebrafish. *Science,* 308**,** 833-8.

[275] DHANRAJ, S., RAO GUNJA, S. M., DEVEAU, A. P., NISSBECK, M., BOONYAWAT, B., COOMBS, A. J., RENIERI, A., MUCCIOLO, M., MAROZZA, A., BUONI, S., TURNER, L., LI, H., JARRAR, A., SABANAYAGAM, M., KIRBY, M., SHAGO, M., PINTO, D., BERMAN, J. N., SCHERER, S. W., VIRTANEN, A. & DROR, Y. 2015. Bone Marrow Failure and Developmental Delay Caused By Mutations in Poly(A)-Specific Ribonuclease. *Blood,* 126**,** 2404.

[276] DONG, G., MAO, Q., XIA, W., XU, Y., WANG, J., XU, L. & JIANG, F. 2016. PKM2 and cancer: The function of PKM2 beyond glycolysis. *Oncology letters,* 11**,** 1980-1986.

[277] CHEN, M. 2011. *Regulation of alternative splicing and its connections to cancer.* Columbia University.

[278] FURUKAWA-HIBI, Y., KOBAYASHI, Y., CHEN, C. & MOTOYAMA, N. 2005. FOXO transcription factors in cell-cycle regulation and the response to oxidative stress. *Antioxid Redox Signal,* 7**,** 752-60.

[279] JOSHI, I., MINTER, L. M., TELFER, J., DEMAREST, R. M., CAPOBIANCO, A. J., ASTER, J. C., SICINSKI, P., FAUQ, A., GOLDE, T. E. & OSBORNE, B. A. 2009. Notch signaling mediates G1/S cell-cycle progression in T cells via cyclin D3 and its dependent kinases. *Blood,* 113**,** 1689-1698.

[280] GONZALEZ DE AGUILAR, J. L., NIEDERHAUSER-WIEDERKEHR, C., HALTER, B., DE TAPIA, M., DI SCALA, F., DEMOUGIN, P., DUPUIS, L., PRIMIG, M., MEININGER, V. & LOEFFLER, J. P. 2008. Gene profiling of skeletal muscle in an amyotrophic lateral sclerosis mouse model. *Physiol Genomics,* 32**,** 207-18.

[281] SHTILBANS, A., CHOI, S. G., FOWKES, M. E., KHITROV, G., SHAHBAZI, M., TING, J., ZHANG, W., SUN, Y., SEALFON, S. C. & LANGE, D. J. 2011. Differential gene expression in patients with amyotrophic lateral sclerosis. *Amyotroph Lateral Scler,* 12**,** 250-6.

[282] USHIGOME, M., UBAGAI, T., FUKUDA, H., TSUCHIYA, N., SUGIMURA, T., TAKATSUKA, J. & NAKAGAMA, H. 2005. Up-regulation of hnRNP A1 gene in sporadic human colorectal cancers. *Int J Oncol,* 26**,** 635-40.

[283] LESTOURGEON, W. M., BEYER, A. L., CHRISTENSEN, M. E., WALKER, B. W., POUPORE, S. M. & DANIELS, L. P. 1978. The packaging proteins of core hnRNP particles and the maintenance of proliferative cell states. *Cold Spring Harb Symp Quant Biol,* 42 Pt 2**,** 885-98.

[284] SUN, A., BAGELLA, L., TUTTON, S., ROMANO, G. & GIORDANO, A. 2007. From G0 to S phase: a view of the roles played by the retinoblastoma (Rb) family members in the Rb-E2F pathway. *J Cell Biochem,* 102**,** 1400-4.

[285] SALVADOR, J. M., BROWN-CLAY, J. D. & FORNACE, A. J., JR. 2013. Gadd45 in stress signaling, cell cycle control, and apoptosis. *Adv Exp Med Biol,* 793**,** 1-19.

[286] ISRAELS, E. D. & ISRAELS, L. G. 2000. The cell cycle. *Oncologist,* 5**,** 510-3.

[287] BOULDIN, C. M. & KIMELMAN, D. 2014. Dual fucci: a new transgenic line for studying the cell cycle from embryos to adults. *Zebrafish,* 11**,** 182-3.

[288] DAMIANO, F., ROCHIRA, A., TOCCI, R., ALEMANNO, S., GNONI, A. & SICULELLA, L. 2013. hnRNP A1 mediates the activation of the IRES-dependent SREBP-1a mRNA translation in response to endoplasmic reticulum stress. *Biochem J,* 449**,** 543-53.

[289] CARVALHO, L. & HEISENBERG, C. P. 2010. The yolk syncytial layer in early zebrafish development. *Trends Cell Biol,* 20**,** 586-92.

[290] YOGANANTHARJAH, P., BYREDDY, A. R., FRAHER, D., PURI, M. & GIBERT, Y. 2017. Rapid quantification of neutral lipids and triglycerides during zebrafish embryogenesis. *Int J Dev Biol,* 61**,** 105-111.

[291] SCHLEGEL, A. & STAINIER, D. Y. 2006. Microsomal triglyceride transfer protein is required for yolk lipid utilization and absorption of dietary lipids in zebrafish larvae. *Biochemistry,* 45**,** 15179-87.

[292] BABIN, P. J., THISSE, C., DURLIAT, M., ANDRE, M., AKIMENKO, M. A. & THISSE, B. 1997. Both apolipoprotein E and A-I genes are present in a nonmammalian vertebrate and are highly expressed during embryonic development. *Proc Natl Acad Sci U S A,* 94**,** 8622-7.

[293] PICKART, M. A., KLEE, E. W., NIELSEN, A. L., SIVASUBBU, S., MENDENHALL, E. M., BILL, B. R., CHEN, E., ECKFELDT, C. E., KNOWLTON, M., ROBU, M. E., LARSON, J. D., DENG, Y., SCHIMMENTI, L. A., ELLIS, L. B., VERFAILLIE, C. M., HAMMERSCHMIDT, M., FARBER, S. A. & EKKER, S. C. 2006. Genome-wide reverse genetics framework to identify novel functions of the vertebrate secretome. *PLoS One,* 1**,** e104.

[294] RASSART, E., BEDIRIAN, A., DO CARMO, S., GUINARD, O., SIROIS, J., TERRISSE, L. & MILNE, R. 2000. Apolipoprotein D. *Biochim Biophys Acta,* 1482**,** 185-98.

[295] PERDOMO, G. & DONG, H. H. 2009. Apolipoprotein D in Lipid Metabolism and Its Functional Implication in Atherosclerosis and Aging. *Aging (Albany NY),* 1**,** 17-27.

[296] PERDOMO, G., KIM, D. H., ZHANG, T., QU, S., THOMAS, E. A., TOLEDO, F. G. S., SLUSHER, S., FAN, Y., KELLEY, D. E. & DONG, H. H. 2010. A role of apolipoprotein D in triglyceride metabolism. *Journal of Lipid Research,* 51**,** 1298-1311.

[297] VIJAYARAGHAVAN, S., HITMAN, G. A. & KOPELMAN, P. G. 1994. Apolipoprotein-D polymorphism: a genetic marker for obesity and hyperinsulinemia. *J Clin Endocrinol Metab,* 79**,** 568-70.

[298] CHEN, Y., JIA, L., WEI, C., WANG, F., LV, H. & JIA, J. 2008. Association between polymorphisms in the apolipoprotein D gene and sporadic Alzheimer's disease. *Brain Res,* 1233**,** 196-202.

[299] WALDNER, A., DASSATI, S., REDL, B., SMANIA, N. & GANDOLFI, M. 2018. Apolipoprotein D Concentration in Human Plasma during Aging and in Parkinson's Disease: A Cross-Sectional Study. *Parkinsons Dis,* 2018**,** 3751516.

[300] HELISALMI, S., HILTUNEN, M., VEPSALAINEN, S., IIVONEN, S., CORDER, E. H., LEHTOVIRTA, M., MANNERMAA, A., KOIVISTO, A. M. & SOININEN, H. 2004. Genetic variation in apolipoprotein D and Alzheimer's disease. *J Neurol,* 251**,** 951-7.

[301] AVRAHAM-DAVIDI, I., ELY, Y., PHAM, V. N., CASTRANOVA, D., GRUNSPAN, M., MALKINSON, G., GIBBS-BAR, L., MAYSELESS, O., ALLMOG, G., LO, B., WARREN, C. M.,

CHEN, T. T., UNGOS, J., KIDD, K., SHAW, K., ROGACHEV, I., WAN, W., MURPHY, P. M., FARBER, S. A., CARMEL, L., SHELNESS, G. S., IRUELA-ARISPE, M. L., WEINSTEIN, B. M. & YANIV, K. 2012. ApoB-containing lipoproteins regulate angiogenesis by modulating expression of VEGF receptor 1. *Nat Med,* 18**,** 967-73.

[302] QUINLIVAN, V. H. & FARBER, S. A. 2017. Lipid Uptake, Metabolism, and Transport in the Larval Zebrafish. *Front Endocrinol (Lausanne),* 8**,** 319.

[303] EAR, J., HUANG, H., WILSON, T., TEHRANI, Z., LINDGREN, A., SUNG, V., LAADEM, A., DANIEL, T. O., CHOPRA, R. & LIN, S. 2015. RAP-011 improves erythropoiesis in zebrafish model of Diamond-Blackfan anemia through antagonizing lefty1. *Blood,* 126**,** 880-90.

[304] DEISENROTH, C. & ZHANG, Y. 2011. The Ribosomal Protein-Mdm2-p53 Pathway and Energy Metabolism: Bridging the Gap between Feast and Famine. *Genes & cancer,* 2**,** 392-403.

[305] SCHOONJANS, K., PEINADO-ONSURBE, J., LEFEBVRE, A. M., HEYMAN, R. A., BRIGGS, M., DEEB, S., STAELS, B. & AUWERX, J. 1996. PPARalpha and PPARgamma activators direct a distinct tissue-specific transcriptional response via a PPRE in the lipoprotein lipase gene. *Embo j,* 15**,** 5336-48.

[306] LABRIE, M., LALONDE, S., NAJYB, O., THIERY, M., DANEAULT, C., DES ROSIERS, C., RASSART, E. & MOUNIER, C. 2015. Apolipoprotein D Transgenic Mice Develop Hepatic Steatosis through Activation of PPAR $\gamma$ and Fatty Acid Uptake. *PLOS ONE,* 10**,** e0130230.

[307] JIMENEZ-PALOMARES, M., COZAR-CASTELLANO, I., GANFORNINA, M. D., SANCHEZ, D. & PERDOMO, G. 2011. Genetic deficiency of apolipoprotein D in the mouse is associated with nonfasting hypertriglyceridemia and hyperinsulinemia. *Metabolism,* 60**,** 1767-74.

[308] DASSATI, S., WALDNER, A. & SCHWEIGREITER, R. 2014. Apolipoprotein D takes center stage in the stress response of the aging and degenerative brain. *Neurobiology of Aging,* 35**,** 1632-1642.

[309] BEREMAN, M. S., BERI, J., ENDERS, J. R. & NASH, T. 2018. Machine Learning Reveals Protein Signatures in CSF and Plasma Fluids of Clinical Value for ALS. *Scientific Reports,* 8**,** 16334.

[310] SANCHEZ, D., LOPEZ-ARIAS, B., TORROJA, L., CANAL, I., WANG, X., BASTIANI, M. J. & GANFORNINA, M. D. 2006. Loss of glial lazarillo, a homolog of apolipoprotein D, reduces lifespan and stress resistance in Drosophila. *Curr Biol,* 16**,** 680-6.

[311] MCCARTHY, S., SOMAYAJULU, M., SIKORSKA, M., BOROWY-BOROWSKI, H. & PANDEY, S. 2004. Paraquat induces oxidative stress and neuronal cell death; neuroprotection by water-soluble Coenzyme Q10. *Toxicol Appl Pharmacol,* 201**,** 21-31.

[312] GANFORNINA, M. D., DO CARMO, S., LORA, J. M., TORRES-SCHUMANN, S., VOGEL, M., ALLHORN, M., GONZALEZ, C., BASTIANI, M. J., RASSART, E. & SANCHEZ, D. 2008. Apolipoprotein D is involved in the mechanisms regulating protection from oxidative stress. *Aging Cell,* 7**,** 506-15.

[313] SHAW, P. J., INCE, P. G., FALKOUS, G. & MANTLE, D. 1995. Oxidative damage to protein in sporadic motor neuron disease spinal cord. *Ann Neurol,* 38**,** 691-5.

[314] FERRANTE, R. J., BROWNE, S. E., SHINOBU, L. A., BOWLING, A. C., BAIK, M. J., MACGARVEY, U., KOWALL, N. W., BROWN, R. H., JR. & BEAL, M. F. 1997. Evidence of increased oxidative damage in both sporadic and familial amyotrophic lateral sclerosis. *J Neurochem,* 69**,** 2064-74.

[315] SCHMITT, F., HUSSAIN, G., DUPUIS, L., LOEFFLER, J. P. & HENRIQUES, A. 2014. A plural role for lipids in motor neuron diseases: energy, signaling and structure. *Front Cell Neurosci,* 8**,** 25.

[316] COOPER, R. A. 1978. Influence of increased membrane cholesterol on membrane fluidity and cell function in human red blood cells. *J Supramol Struct,* 8**,** 413-30.

[317] MIANA-MENA, F. J., PIEDRAFITA, E., GONZALEZ-MINGOT, C., LARRODE, P., MUNOZ, M. J., MARTINEZ-BALLARIN, E., REITER, R. J., OSTA, R. & GARCIA, J. J. 2011. Levels of membrane fluidity in the spinal cord and the brain in an animal model of amyotrophic lateral sclerosis. *J Bioenerg Biomembr,* 43**,** 181-6.

[318] AUESTAD, N., KORSAK, R. A., MORROW, J. W. & EDMOND, J. 1991. Fatty acid oxidation and ketogenesis by astrocytes in primary culture. *J Neurochem,* 56**,** 1376-86.

[319] BAJO-GRANERAS, R., GANFORNINA, M. D., MARTIN-TEJEDOR, E. & SANCHEZ, D. 2011. Apolipoprotein D mediates autocrine protection of astrocytes and controls their reactivity level, contributing to the functional maintenance of paraquat-challenged dopaminergic systems. *Glia,* 59**,** 1551-66.

[320] SANCHEZ, D., BAJO-GRANERAS, R., DEL CANO-ESPINEL, M., GARCIA-CENTENO, R., GARCIA-MATEO, N., PASCUA-MAESTRO, R. & GANFORNINA, M. D. 2015. Aging without Apolipoprotein D: Molecular and cellular modifications in the hippocampus and cortex. *Exp Gerontol,* 67**,** 19-47.

[321] WATTS, L. T., RATHINAM, M. L., SCHENKER, S. & HENDERSON, G. I. 2005. Astrocytes protect neurons from ethanol-induced oxidative stress and apoptotic death. *J Neurosci Res,* 80**,** 655-66.

[322] YAMANAKA, K. & KOMINE, O. 2018. The multi-dimensional roles of astrocytes in ALS. *Neurosci Res,* 126**,** 31-38.

[323] BENTMANN, E., HAASS, C. & DORMANN, D. 2013. Stress granules in neurodegeneration – lessons learnt from TAR DNA binding protein of 43 kDa and fused in sarcoma. *The FEBS Journal,* 280**,** 4348-4370.

[324] UHLEN, M., FAGERBERG, L., HALLSTROM, B. M., LINDSKOG, C., OKSVOLD, P., MARDINOGLU, A., SIVERTSSON, A., KAMPF, C., SJOSTEDT, E., ASPLUND, A., OLSSON, I., EDLUND, K., LUNDBERG, E., NAVANI, S., SZIGYARTO, C. A., ODEBERG, J., DJUREINOVIC, D., TAKANEN, J. O., HOBER, S., ALM, T., EDQVIST, P. H., BERLING, H., TEGEL, H., MULDER, J., ROCKBERG, J., NILSSON, P., SCHWENK, J. M., HAMSTEN, M., VON FEILITZEN, K., FORSBERG, M., PERSSON, L., JOHANSSON, F., ZWAHLEN, M., VON HEIJNE, G., NIELSEN, J. & PONTEN, F. 2015. Proteomics. Tissue-based map of the human proteome. *Science,* 347**,** 1260419.

[325] MAHLEY, R. W., WEISGRABER, K. H. & HUANG, Y. 2006. Apolipoprotein E4: a causative factor and therapeutic target in neuropathology, including Alzheimer's disease. *Proc Natl Acad Sci U S A,* 103**,** 5644-51.

[326] CONEJERO-GOLDBERG, C., GOMAR, J. J., BOBES-BASCARAN, T., HYDE, T. M., KLEINMAN, J. E., HERMAN, M. M., CHEN, S., DAVIES, P. & GOLDBERG, T. E. 2014. APOE2 enhances neuroprotection against Alzheimer's disease through multiple molecular mechanisms. *Mol Psychiatry,* 19**,** 1243-50.

[327] POLJSAK, B. 2011. Strategies for reducing or preventing the generation of oxidative stress. *Oxidative medicine and cellular longevity,* 2011**,** 194586-194586.

[328] DUPUIS, L., OUDART, H., RENE, F., GONZALEZ DE AGUILAR, J. L. & LOEFFLER, J. P. 2004. Evidence for defective energy homeostasis in amyotrophic lateral sclerosis: benefit of a high-energy diet in a transgenic mouse model. *Proc Natl Acad Sci U S A,* 101**,** 11159-64.

[329] COUGHLAN, K. S., HALANG, L., WOODS, I. & PREHN, J. H. M. 2016. A high-fat jelly diet restores bioenergetic balance and extends lifespan in the presence of motor dysfunction and lumbar spinal cord motor neuron loss in TDP-43(A315T) mutant C57BL6/J mice. *Disease Models & Mechanisms,* 9**,** 1029-1037.

[330] PATEL, B. P., SAFDAR, A., RAHA, S., TARNOPOLSKY, M. A. & HAMADEH, M. J. 2010. Caloric restriction shortens lifespan through an increase in lipid peroxidation, inflammation and apoptosis in the G93A mouse, an animal model of ALS. *PLoS One,* 5**,** e9386.

[331] CIAPPARELLI, A., DELL'OSSO, L., PINI, S., CHIAVACCI, M. C., FENZI, M. & CASSANO, G. B. 2000. Clozapine for treatment-refractory schizophrenia, schizoaffective disorder, and psychotic bipolar disorder: a 24-month naturalistic study. *J Clin Psychiatry,* 61**,** 329-34.

[332] THOMAS, E. A., DANIELSON, P. E., NELSON, P. A., PRIBYL, T. M., HILBUSH, B. S., HASEL, K. W. & SUTCLIFFE, J. G. 2008. Clozapine increases apolipoprotein D expression in rodent brain: towards a mechanism for neuroleptic pharmacotherapy. *Journal of Neurochemistry,* 76**,** 789-796.

[333] SINGH, A. K. & LAKHOTIA, S. C. 2012. The hnRNP A1 homolog Hrp36 is essential for normal development, female fecundity, omega speckle formation and stress tolerance in Drosophila melanogaster. *Journal of Biosciences,* 37**,** 659-678.

[334] FUJIMORI, K., ISHIKAWA, M., OTOMO, A., ATSUTA, N., NAKAMURA, R., AKIYAMA, T., HADANO, S., AOKI, M., SAYA, H., SOBUE, G. & OKANO, H. 2018. Modeling sporadic ALS in iPSC-derived motor neurons identifies a potential therapeutic agent. *Nature Medicine,* 24**,** 1579-1589.

# List of Figures

# List of tables

# List of Abbreviations

| | |
|---|---|
| +/+ | wildtype |
| +/- | heterozygous |
| -/- | homozygous |
| A2RE | A2 response element |
| AA | arachidonic acid |
| aa | amino acid |
| AD | Alzheimer`s Disease |
| ALS | amyotrophic lateral sclerosis |
| APS | ammonium persulfate |
| ASO | antisense oligonucleotide |
| BCA | bicinchoninic acid |
| BMI | body mass index |
| Bp | base pair |
| CaP | Caudal primary motoneuron |
| Cas9 | CRISPR-associated 9 |
| CDK | Cycling dependant kinase |
| cDNA | Complementary DNA |
| CMV | cytomegalovirus |
| CNS | central nervous system |
| CRISPR | clustered regularly interspaced short palindromic repeats |
| cRNA | complementary RNA |
| crRNA | CRISPR RNA |
| CS | Cutsmart buffer |
| CSF | cerebrospinal fluid |
| dATP | deoxyadenosine triphosphate |
| dCTP | deoxycytosine triphosphate |
| DENN | differentially expressed in normal and neoplastic cells |
| DEPC | diethylpyrocarbonate |
| dGTP | deoxyguanosine triphosphate |
| DLAV | dorsal longitudinal anastomotic vessel |
| DNA | deoxyribonucleic acid |
| dNTP | deoxynucleoside triphosphates |

| | |
|---|---|
| DPR | dipeptide repeat protein |
| DSB | double strand break |
| dsDNA | double stranded DNA |
| DTT | dithiothreitol |
| dTTP | desoxythymidintriphosphat |
| dpf | days post fertilization |
| DSB | double strand break |
| EC | endothelial cells |
| ECM | extracellular matrix |
| e.g. | exempli gratia |
| ELISA | enzyme-linked immunosorbent assay |
| ENU | N-ethyl-N-nitrosourea |
| ER | endoplasmatic reticulum |
| FA | fatty acid |
| FCS | fetal calve serum |
| GFP | green fluorescent protein |
| GTP | guanosine triphosphate |
| gRNA | guide RNA |
| HDR | homology directed repair |
| HNRNP | heterogeneous nuclear ribonucleoprotein |
| Hnrnpa | zebrafish Hnrnpa1a, Hnrnpa1b, Hnrnpa3 |
| $H_2O$ | water |
| hpf | hours post fertilization |
| HRP | horseradish peroxidase |
| HUVEC | human umbilical vein endothelial cells |
| IHC | immunohistochemistry |
| Indels | insertions and deletions |
| iPSCs | induced pluripotent stem cells |
| ISH | *in situ* hybridisierung |
| kDa | kilo-Dalton |
| KD | knockdown |
| KI | knockin |
| KO | knockout |
| liq. $N_2$ | liquid nitrogen |

| | |
|---|---|
| LCD | low complexity domain |
| lincRNA | long non coding RNA |
| LMN | lower motoneuron |
| mAb | monoclonal antibody |
| miRNA | microRNA |
| mRNA | messenger RNA |
| MW | molecular weight |
| MND | motoneuron disease |
| MO | morpholino |
| MSP | Multisystem proteinopathy |
| MZT | maternal to zygotic transition |
| n.a. | not available |
| NCS | newborn calf serum |
| ND | neurodegenerative disease |
| NGS | next generation sequencing |
| NHEJ | non homologous end joining |
| NLS | nuclear localization signal |
| NMD | nonsense-mediated mRNA Decay |
| Nt | nucleotide |
| o/n | overnight |
| ORO | oil red O |
| OS | oxidative stress |
| OVA | ovalbumin |
| PAGE | polyacrylamide gel electrophoresis |
| PAM | protospacer-adjacent motif |
| PB | phosphate buffer |
| PBS | phosphate buffered saline |
| PCNA | proliferating cellular nuclear antigen |
| PCR | polymerase chain reaction |
| PTC | premature termination codon |
| PFA | paraformaldehyd |
| PI | proteinase inhibitor |
| PTU | phenylthiourea |
| PrLD | prion like domain |

| | |
|---|---|
| qRT-PCR | quantitative Realtime- PCR |
| RAN | repeat-associated non-ATG |
| RBD | RNA binding domain |
| RBP | RNA binding protein |
| RE | restriction endonuclease |
| RFLP | restriction fragment length polymorphism |
| RGG | arginine-glycine-glycine |
| RIPA | radioimmunoprecipitation assay buffer |
| RNA | ribonucleic acid |
| ROS | reactive oxygen species |
| RRM | RNA recognition motif |
| RT | room temperature |
| sALS | sporadic ALS |
| SD | standard deviation |
| SDS | sodium dodecyl sulfate |
| S.E.M. | standard error of the mean |
| SG | stress granules |
| SNP | single nucleotide polymorphism |
| SpCas9 | *Streptococcus pyogenes* Cas9 |
| SpMN | spinal motoneuron |
| SZ | Schizophrenia |
| TALEN | transcription activator-like effector nucleases |
| TARDBP | TAR-DNA-binding protein (human gene name) |
| Tardbp | zebrafish TAR-DNA-binding protein (zebrafish orthologue) |
| Tardbpl | zebrafish TAR-DNA-binding protein like (zebrafish orthologue) |
| TDP-43 | TAR-DNA-binding protein of 43kDa (used here for human protein) |
| Tdp-43 | TAR-DNA-binding protein of 43kDa (used here for zebrafish protein) |
| TEMED | tetramethylethylenediamine |
| TILLING | targeted induced local lesions in genomes |
| tracRNA | trans-activating cRNA |
| TSD | teleost specific duplication |
| UAS | upstream activation sequence |
| UMN | upper motoneuron |
| UTR | untranslated region |

| | |
|---|---|
| wt | wildtype |
| YSL | yolk syncytial layer |
| zf-Hnrnpas | Zebrafish Hnrnpas (Hnrnpa1a, Hnrnpa1b, Hnrnpa3) |
| ZFN | zinc-finger nucleases |
| ZGA | zygotic genome activation |

The herein listed abbreviations of genes and proteins are modified throughout the thesis according to the nomenclature guidelines of the respective species (http://www.genenames.org, http://www.informatics.jax.org, http://www.zfin.org)

# Acknowledgements

Very special thanks to...

...Prof. Christian Haass for scientifically supervising my thesis and your everlasting motivating enthusiasm.

...Dr. Bettina Schmid for your thoughtful supervision and your richness of ideas. Thank you for always keeping me going and all the opportunities you provided during my doctoral thesis.

...Dr. Dorothee Dormann und Dr. Dierk Nissing for being such great TAC members providing me with new scientific input and being curious about my study.

...my collaboration partners Elisabeth Kremmer for the zebrafish antibodies and Stephan Müller for the proteomic analysis.

...Sabine und Marcel for being so quick and reliable for ordering everything that I needed to finish this thesis.

...Thierry Latran Foundation for financial support of the project and my visits to the ENCALS meetings.

...the zebrafish group for making my time so enjoyable making it an unforgettable memory. Thank you Frauke for your amazing proofreading of this thesis, you endless expertise on PCRs and Western Blot, and for providing our group with delicious baking treats. Bella Laura, grazie per avermi insegnato di suonare come una vera italiana. Non sei sola una college stupenda ma anche un'amica meravigliosa. Thank you Özge for all the sweetness from Nutella sticks and of course your expertise for the RNAsequencing analysis. Roberto und Biene, danke für eure großartige Hilfe mit den Fischen und alles was dazugehört. Roberto, so viel wofür ich dir danke, vor allem für die beste kolumbianische Essensversorgung und täglich erfrischende Unterhaltung.

...the third floor for a always happy mood, amazing work atmosphere, the BBQ parties, and all the early morning coffee wisdoms.

# Appendix


A
hnrnpa1a.wt ...CACGTGACCTGACGTCGTGCAGCCAGCAGCAATGCCACCCGCCATTACACCTAAAAAAGAAAGGGAAGCGGAGTCTGCTGTTAGTC...
hnrnpa1a.Δ16 ...CACGTGACCTGACGTCGTGCA----------CCCGCCATTACACCTAAAAAAGAAAGGGAAGCGGAGTCTGCTGTTAGTC...
hnrnpa1a.Δ15 ...CACGTGACCTGACGTCGT----------GCCACCCGCCATTACACCTAAAAAAGAAAGGGAAGCGGAGTCTGCTGTTAGTC...
hnrnpa1a.Δ23 ...CACGTGACCTG----------CCACCCGCCATTACACCTAAAAAAGAAAGGGAAGCGGAGTCTGCTGTTAGTC...
hnrnpa1a.Δ4 ...CACGTGACCTGACGTCGTGCAGCCAGC----ATGCCACCCGCCATTACACCTAAAAAAGAAAGGGAAGCGGAGTCTGCTGTTAGTC...
hnrnpa1a.Δ3 ...CACGTGACCTGACGTCGTGCAGCCAGCA---ATGCCACCCGCCATTACACCTAAAAAAGAAAGGGAAGCGGAGTCTGCTGTTAGTC...
hnrnpa1a.Δ6 ...CACGTGACCTGACGTCGTGCAGCCA------ATGCCACCCGCCATTACACCTAAAAAAGAAAGGGAAGCGGAGTCTGCTGTTAGTC...
hnrnpa1a.Δ2 ...CACGTGACCTGACGTCGTGCAGCCA--AGCAATGCCACCCGCCATTACACCTAAAAAAGAAAGGGAAGCGGAGTCTGCTGTTAGTC...
hnrnpa1a.Δ12 ...CACGTGACCTGACGTCGTGCAGCCA----------CCCGCCATTACACCTAAAAAAGAAAGGGAAGCGGAGTCTGCTGTTAGTC...
hnrnpa1a.Δ7 ...CACGTGACCTGACGTCGTGCAGCCA-------TGCCACCCGCCATTACACCTAAAAAAGAAAGGGAAGCGGAGTCTGCTGTTAGTC...
B
hnrnpa1a wt ...GAGTTTAAAGAATTACTGAATTTTTGCAGGAAACTTCGGAG-----G-----T--GGCGGAGACTACAATGACTTTGGAAACTACA...
hnrnpa1a.Δ6 ...GAGTTTAAAGAATTACTGAATTTTTGCAGGAAACTTCGGA----------GGAGACTACAATGACTTTGGAAACTACA...
hnrnpa1a.Δ9 ...GAGTTTAAAGAATTACTGAATTTTTGCAGGAAACTT----------CGGAGACTACAATGACTTTGGAAACTACA...
hnrnpa1a.Δ7 ...GAGTTTAAAGAATTACTGAATTTTTGCAGGAAACTTCGG----------GGAGACTACAATGACTTTGGAAACTACA...
hnrnpa1a.+10 ...GAGTTTAAAGAATTGCTGAATTTTTGCAGGAAACTTCGGAGACTTCGGAGACT--GGCGGAGACTACAATGACTTTGGAAACTACA...
hnrnpa1.+2Δ3 ...GAGTTTAAAGAATTACTGAATTTTTGCAGGAAACTTCGGAG-----G-----TAT---GGAGACTACAATGACTTTGGAAACTACA...
C
hnrnpa1b.wt ...TGTTATTTCCAGGGCCAGCCACGTGAGCCAGAGCAG----CTGCGGAAGCTCTTCATTGGAGGGCTCAGCTTTGAGACCACAGACG...
hnrnpa1b.Δ5 ...TGTTATTTCCAGGGCCAGCCACGTGAGCCAGAGCAG---------GAAGCTCTTCATTGGAGGGCTCAGCTTTGAGACCACAGACG...
hnrnpa1b.Δ23 ...TGTTATTTCC-G----------AG----CTGCGGAAGCTCTTCATTGGAGGGCTCAGCTTTGAGACCACAGACG...
hnrnpa1b.+4Δ2 ...TGTTATTTCCAGGGCCAGCCACGTGAGCCAGAGCAGAAGA--GCGGAAGCTCTTCATTGGAGGGCTCAGCTTTGAGACCACAGACG...
hnrnpa1b.Δ12 ...TGTTATTTCCAGGGCCAGCCACGTGAGCCAG----------AGCTCTTCATTGGAGGGCTCAGCTTTGAGACCACAGACG...
hnrnpa1b.Δ52 ...TGTTATTTCC-G----------AGCTTTGAGACCACAGACG...
D
hnrnpa1b.wt ...CTATAACTATAGAGACTAATGGGTGTATTATCAATTCAAGGTAACTTTGGAGGTGGTGGTGGT---GGCGGCAACAGTGGAGGAGG...
hnrnpa1b.Δ53 ...CTATAACTATAGA--CT----------ACAGTGGAGGAGG...
hnrnpa1b.Δ43 ...CTATAACTATAGA--CTAATGGGTGTA----------ACAGTGGAGGAGG...
hnrnpa1b.+3 ...CTATAACTATAGAGACTAATGGGTGTATTATCAATTCAAGGTAACTTTGGAGGTGGTGGTGGTGGTGGCGGCAACAGTGGAGGAGG...


**Figure 5.1- Sequences of CRISPR/Cas9 induced mutations that were detected in the $F_1$ generation. A:** Offspring from founder fish injected with gRNA targeting hnrnpa1a exon1 9 different mutations were identified. **B:** Offspring from founder fish injected with gRNA targeting hnrnpa1a exon9 resulted in 5 different mutations **C:** In offspring from founder fish injected with gRNA targeting hnrnpa1b exon2 5 different mutations were identified **D:** Offspring from founder fish injected with gRNA targeting hnrnpa1b exon9 3 different mutations were identified **E:** Offspring from founder fish injected with gRNA targeting hnrnpa3 exon2 4 different mutations were identified +: deletion, + insertion, green: ATG start codon, red: mutations (deletion/insertion), blue: ORF

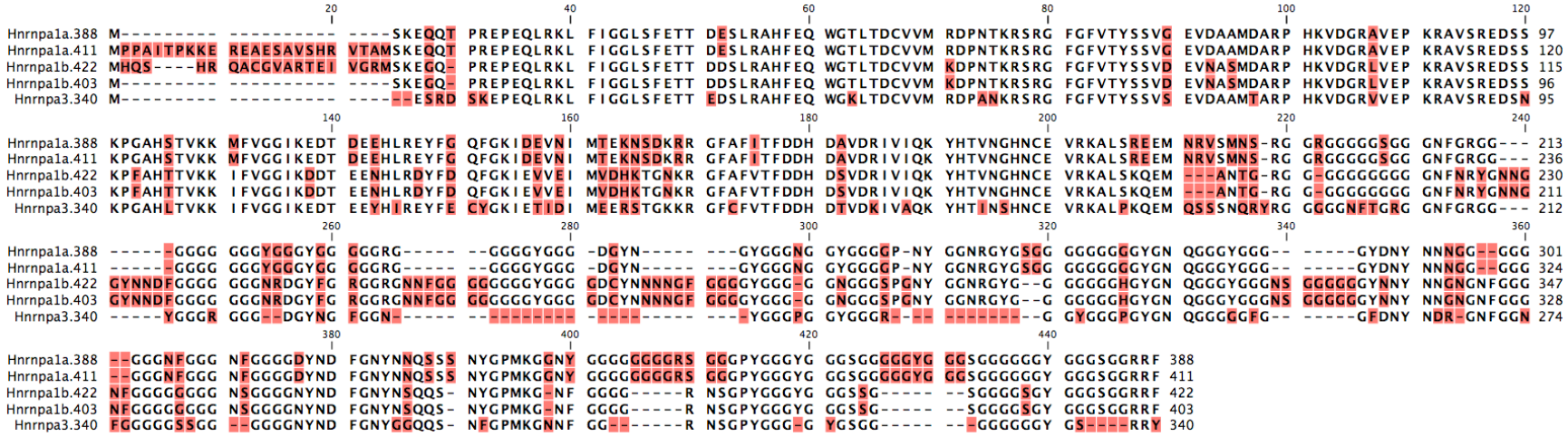


**Figure 5.2 – Alignement of Hnrnpa1a, Hnrnpa1b and Hnrnpa3.** Hnrnpa1a$^{388}$ (ENSDART00000018131.8), Hnrnpa1a$^{411}$ (NP_001349307.1), Hnrnpa1b$^{422}$ (ZFIN:ZDB-GENE-030912-14), Hnrnpa1b$^{403}$ (ENSDART00000053267.6), and Hnrnpa3$^{340}$ (ENSDART00000102934.4) were aligned with CLC Main Workbench. Red highlighted letters: aa that are different.